Patterned and switchable surfaces for biomaterial applications

Andrew Leslie Hook Bsc (Hons)

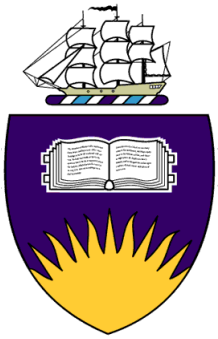

Flinders University, School of Chemistry, Physics and Earth Sciences.

Commonwealth Science and Industrial Research Organisation, Molecular and Health Technologies.

Submitted October 2008.

"*If at first, the idea is not absurd, then there is no hope for it.*"

Albert Einstein

"Science is not formal logic–it needs the free play of the mind in as great a degree as any other creative art."

Max Born

"One had to be a Newton to notice that the moon is falling, when everyone sees that it doesn't fall."

Paul Valéry

TABLE OF CONTENTS

SUMMARY

The interactions of biomolecules and cells at solid-liquid interfaces play a pivotal role in a range of biomedical applications and have hence been studied in detail. An improved understanding of these interactions results in the ability to manipulate biomolecules and concurrently cells spatially and temporally at surfaces with high precision. Spatial control can be achieved using patterned surface chemistries whilst temporal control is achieved by switchable surfaces. The combination of these two surface properties offers unprecedented control over the behaviour of biomolecules and cells at the solid-liquid interface. This is particularly relevant for cell microarray applications, where a range of biological processes must be duly controlled in order to maximise the efficiency and throughput of these devices. Of particular interest are transfected cell microarrays (TCMs), which significantly widen the scope of microarray genomic analysis by enabling the high-throughput analysis of gene function within living cells

Initially, this thesis focuses on the spatially controlled, electro-stimulated adsorption and desorption of DNA. Surface modification of a silicon chip with an allylamine plasma polymer (ALAPP) layer resulted in a surface that supported DNA adsorption and sustained cell attachment. Subsequent high density grafting of poly(ethylene glycol) (PEG) formed a layer resistant to biomolecule adsorption and cell attachment. PEG grafted surfaces also showed significantly reduced attachment of DNA with an equilibrium binding constant of 23 ml/mg as compared with 1600 ml/mg for ALAPP modified surfaces. Moreover, both hydrophobic and electrostatic interactions were shown to contribute to the binding of DNA to ALAPP. Spatial control over the surface chemistry was achieved using excimer laser ablation of the PEG coating which enabled the production of patterns of re-exposed ALAPP with

high resolution. Preferential electro-stimulated adsorption of DNA to the ALAPP regions and subsequent desorption by the application of a negative bias was observed. Furthermore, this approach was investigated for TCM applications. Cell culture experiments demonstrated efficient and controlled transfection of cells. Electro-stimulated desorption of DNA was shown to yield enhanced solid phase transfection efficiencies with values of up to 30%. The ability to spatially control DNA adsorption combined with the ability to control the binding and release of DNA by application of a controlled voltage enables an advanced level of control over DNA bioactivity on solid substrates and lends itself to biochip applications.

As an alternative approach to surface patterning, the fabrication and characterisation of chemical patterns using a technique that can be readily integrated with methods currently used for the formation of microarrays is also presented. Here, phenylazide modified polymers were printed onto low fouling ALAPP-PEG modified surfaces. UV irradiation of these polymer arrays resulted in the crosslinking of the polymer spots and their covalent attachment to the surface. Cell attachment was shown to follow the patterned surface chemistry. Due to the use of a microarray contact printer it was easily possible to deposit DNA on top of the polymer microarray spots. A transfected cell microarray was generated in this way, demonstrating the ability to limit cell attachment to specific regions and the suitability of this approach for high density cell assays. In order to allow for the high-throughput characterisation of the resultant polymer microarrays, surface plasmon resonance imaging was utilised to study the adsorption and desorption of bovine serum albumin, collagen and fibronectin. This analysis enabled insights into the underlying mechanisms of cell attachment to the polymers studied. For the system analysed here, electrostatic interactions were shown to dominate cellular behaviour.

DECLARATION

I certify that this thesis does not incorporate without acknowledgment any material previously submitted for a degree or diploma in any university; and that to the best of my knowledge and belief it does not contain any material previously published or written by another person except where due reference is made in the text.

Andrew Leslie Hook

ACKNOWLEDGEMENTS

Any large undertaking simply cannot be completed without the assistance of many different people, which is particularly true for this PhD thesis. Firstly, I would like to extend a very big thanks to my two supervisors who have become my biggest scientific influences. Professor Nicolas Voelcker and Dr. Helmut Thissen, thank you both so very much for your kind support, advice, time, encouragement, patience and wisdom that your have continually extended throughout my postgraduate study. I have greatly appreciated the friendship we have been able to enjoy. Thank you for opening your scientific expertise and also your homes to me.

The many colleagues I have shared ideas, laboratory space, skills and chemicals with have all made important contributions to my PhD. Many thanks to Dr. Endre Szili. You really have taught me just about everything I know about cell culture. The skills you spent the time to teach me right back at the start of Honours have been extremely important for the overall success of my PhD. Thanks to Dr. Sue Low. Anything I didn't learn about cell culture from Endre I learnt from you. Thank you for the time you gave to answer my questions, give your advice and draw on the white board. We really did create some masterpieces. Thank you also to Dr. Dusan Losic for your assistance with AFM.

Thanks to Steve McInnes, Martin Cole and Matthew Nussio. Our friendship goes right back to the start of uni. We are the first fledglings of the Nanotech phenomenon here at Flinders. Long may we continue to make the world a nano place. Thanks Steve for your friendship and all the squash games. I look forward to many more, and maybe one day we will beat Nico. Thank you Martin for your friendship, the surfing experience, touring Europe with me and for providing the PNIPAAm. I'm glad you taught me Aarhus is in Denmark.

Thank you to Yamini Akkamsetty, Noni Creasy and Michael Olbrich for your contribution to this project.

Thank you to Dr. Jamie Quinton and Dr. Joe Shapter for the use of your laboratory space, equipment and the corresponding support and advice here at Flinders. Your willingness to help has helped made things much easier and is greatly appreciated.

Thank you to the many faces at CSIRO that have supported and befriended me when I've visited Melbourne. The welcome and advice you continually give makes working at CSIRO so much more enjoyable and worthwhile. In particular, I would like to thank Dr. Keith McLean, Dr. Thomas Gengenbach, Dr. Paul Pasic, Dr. Ben Muir and Dr. Anna Tarasova.

Many thanks to Jason Hayes for time and assistance with laser ablation.

Thank you to Krasimir Vasilev for your time, support and advice with SPR imaging. Thanks also to Tim Burland from GWC technologies for your advice in regard to the tricky problems encountered with the SPR imager.

Thank you to Dr. Bandaru Murthy for showing me India. Thank you to Associate Prof. N. Jayaraman and Prof. Dipankar Chatterji for your advice and laboratory space whilst in India.

Thank you to Dr. Ken Short for your advice and assistance with force measurements.

Thank you Dr. Daniel Jardine and Dominic Reppucci for your assistance with SPR measurements.

Thank you to Flinders University, CSIRO, Australian Research Council and Australian Institute of Nuclear Science and Engineering for funding and the opportunity to conduct this project.

Many, many thanks for the love and support of my family. Thank you to Auntie Trish and Uncle John for opening your home to my in Melbourne. To me beloved wife Cindy, I cannot imagine life without you. There are no words to express my gratitude.

And finally, thank you to my Lord and Saviour Jesus Christ.

LIST OF PUBLICATIONS

Papers arising from Chapter 1

1. Hook, A.L., N. Voelcker, and H. Thissen, *Patterned and switchable surfaces for biomolecular manipulation.* Progress in Surface Science, **2008**, *In Press*.
2. Hook, A.L., N. Voelcker, and H. Thissen, *Surface manipulation of biomolecules for cell microarray applications.* TRENDS in Biotechnology, **2006**, *24(10)*, 471-477.

Papers arising from Chapter 2

3. Hook, A.L., H. Thissen, J.P. Hayes, and N.H. Voelcker, *Spatially controlled electro-stimulated DNA adsorption and desorption for biochip applications.* Biosensors and Bioelectronics, **2005**, *21(11)*, 2137-2145.
4. Hook, A.L., H. Thissen, J.P. Hayes, and N. Voelcker, *A platform for the advanced spatial and temporal control of biomolecules.* Proceedings of SPIE, **2006**, *6413(64130C)*, 1-11.
5. Hook, A.L., H. Thissen, J.P. Hayes, and N.H. Voelcker, *Development of an electro-responsive platform for the controlled transfection of mammalian cells* Proceedings of SPIE, **2005**, *5651*, 418-426.
6. Hook, A.L., H. Thissen, J.P. Hayes, and N. Voelcker, *Microstructured surfaces by laser ablation for formation of cell arrays.* Bio-medical materials and engineering, **2008**, *In press*.

Papers arising from Chapter 3

7. Hook, A.L., H. Thissen, J. Quinton, and N.H. Voelcker, *Comparison of the binding mode of plasmid DNA to allylamine plasma polymer and poly(ethylene glycol) surfaces.* Surface Science, **2008**, *602(10)*, 1883-1891.

Papers arising from Chapter 4

8. Hook, A.L., H. Thissen, and N.H. Voelcker, *Advanced substrate fabrication for cell microarrays.* Biomacromolecules, **2008**, *Under review*.
9. Hook, A.L., H. Thissen, and N.H. Voelcker, *Using the BioOdyssey Calligrapher Microarrayer to form a polymer array for studying cell-surface interactions.* BioRAD Technote, **2007**, *Bulletin 5577*.

Other papers

10. Creasey, R., A.L. Hook, H. Thissen, and N.H. Voelcker, *Enhancement of reverse transfection efficiency by combining stimulated DNA surface desorption and electroporation* Proceedings of SPIE, **2007**, *6799(67991D)*, 1-10.
11. Akkamsetty, Y., A.L. Hook, H. Thissen, J.P. Hayes, and N.H. Voelcker, *Application of nanostructured biochips for efficient cell transfection microarrays.* Proceedings of SPIE, **2006**, *6413(64130R)*, 1-9.

I

CHAPTER 1. INTRODUCTION

The content of this chapter is based upon references [1, 2].

Advanced biodevices that are able to control the behaviour of biomolecules at surfaces in both space and time are promising tools for elucidating solutions to many biologically based problems and are of particular interest to combat physiological disorders. Biomolecules of interest include proteins and shorter peptide chains, deoxyribonucleic acid (DNA), ribonucleic acid (RNA), oligonucleotides (oligonucleotides are short (2-50) bp of typically single stranded DNA), lipids and polysaccharides, as well as larger assemblies of these biomolecules, in particular living cells. Examples of such devices can be found in microarray technology, in 'smart' drug delivery, biosensing, bioelectronics and tissue engineering [3-8]. The development of a number of high-resolution two dimensional (2D) and three dimensional (3D) patterning techniques coupled with functional surface chemistry has enabled the formation of surfaces that offer stringent control over the adsorption of biomolecules and cells in space. Furthermore, the development of switchable surfaces that are able to respond to a particular signal to switch between disparate properties, such as hydrophobic/hydrophilic, positive/negative or swollen/collapsed, has added a new dimension to biomolecule manipulation. Individually, these processes have enabled the production of a number of advanced biodevices. Recently, these processes have been combined, producing devices that are able to control biomolecules and cells in both space and time, offering an unprecedented ability to manipulate biomolecular behaviour.

In order to manipulate biomolecules at surfaces, a thorough understanding of their behaviour at solid-liquid interfaces is required. Biomolecules differ substantially

from their synthetically produced polymeric counterparts of similar molecular weight due to the narrow dispersity in structure and size for the former. This results in unique and predictable adsorption behaviour, providing a unique opportunity for highly resolved control over these biomolecules at an interface. Indeed, in biological systems highly resolved spatial and temporal control of biomolecules is a critical requirement for the phenomenon of life. The thermodynamic and kinetic driving forces to permit this control are programmed into the sequence and 3D structure of biomolecules. An ability to better understand these driving forces would permit an increased capability to mimic *in vivo* biomolecular manipulation.

This chapter summarises the current knowledge on the underlying principles governing both DNA and protein adsorption to surfaces and how protein adsorption can be applied to manipulating cells at surfaces. Furthermore, the manner by which these principles have been applied in recent years to pattern biomolecules on surfaces and also to control their adsorption and desorption in time is discussed. The chapter also includes an outline of the various techniques used to form patterned and switchable surfaces. The particular focus here has been on cases where truly advanced biomolecule manipulation is achieved in both space and time.

1.1. Surface manipulation of biomolecules and cells

The ability to manipulate biomolecules at the solid/liquid interface requires a sound knowledge of how biomolecules behave in such an environment. The manipulation of biomolecules is significantly different from the manipulation of smaller molecules or synthetic polymers. Weak forces such as hydrophobic interactions are able to play a significant role given the ability of these biomolecules to form multivalent interactions. The size of these molecules also plays a

considerable role in regard to their behaviour at surfaces. For example, larger molecules tend to have a lower rate of surface adsorption when compared with smaller molecules which adsorb, desorb and diffuse more readily from and to the surface [9]. Both DNA and proteins have distinct characteristics that must be understood in order to effectively manipulate these molecules on surfaces. Cell-surface interactions can also be controlled effectively via the control of biomolecule-surface interactions since most cell-surface interactions are mediated by protein adsorbed on surfaces.

1.1.1. Principles of surface-biomolecular interactions

Although distinctive properties of specific biomolecules greatly influence their surface adsorption events, generally, hydrophobic interactions and the multivalent effect are key factors that govern the adsorption behaviour of many biomolecules at surfaces. Understanding these principles can concurrently lead to explanations of biomolecule-surface interactions.

1.1.1.1. The hydrophobic interaction

One of the key interactions for all biomolecule surface adsorption is the hydrophobic interaction. This results when hydrophobic domains or moieties are present on both the surface and the biomolecule of interest. Thermodynamically, the driving force for the adsorption of biomolecules through formation of hydrophobic interactions is entropic gain due to the disordering of hydrophilic solvent molecules that must otherwise become ordered at a hydrophilic/hydrophobic interface. Thus, the solvent has a vital role in the formation of these interactions and in the presence of a hydrophobic solvent, where there is no entropic gain in forming a hydrophobic interaction, these interactions are strongly reduced [10]. In water, any biomolecules

less polar than water or containing regions less polar than water will be driven to adsorb to hydrophobic surfaces by hydrophobic interactions [11].

1.1.1.2. The multivalent effect

Generally, interactions of biomolecules with surfaces are based upon weak forces. Thus, a key factor to ensure that any biomolecule remains adsorbed to the surface is the multivalent effect, whereupon many small bonds form and the combination of these many bonds leads to the formation of an overall strong interaction. The multivalent effect is thermodynamically favourable due to the increase in entropy introduced when a single large molecule adsorbs to the surface, displacing multiple smaller molecules. This effect pertains particularly to biomolecules due to their larger size. It is on the basis of the multivalent effect that surface diffusion can be explained. As any biomolecule is held to the surface by a number of weak interactions, at any time some of these bonds can break and reform at another location, however, provided enough bonds remain intact the molecule itself will not break from the surface. In such a manner the biomolecule is able to 'roll' along the surface where the molecule only partially adsorbs and desorbs [12]. The introduction of stronger biomolecule-surface interactions would, thus, also decrease the rate of surface diffusion due to a decreased rate of bond breakage [13].

1.1.2. Surface manipulation of DNA

In applications such as DNA microarrays, DNA based-biosensors and transfected cell microarrays (TCMs) [1, 14-17], the adsorption or desorption of DNA to or from a surface is required. The adsorption of DNA to a surface is governed by two forces associated with the functional groups of DNA; electrostatic forces associated with the negative charge of the phosphate groups and hydrophobic forces associated with

interactions of the DNA base pairs [18, 19], although hydrogen bond formation also plays a certain role in DNA surface interactions in aqueous conditions [20]. Unlike synthetic polyelectrolytes, which generally adopt a loop-train conformation when adsorbed to a surface due to their flexible 'thread-like' nature [21], double-stranded DNA (dsDNA) can be considered as a rigid rod (Figure 1.1B) with a nitrogenous core and a phosphate and pentose sugar exterior (Figure 1.1A) such that it generally lies flat to a surface upon adsorption [22]. Conversely, although more ordered and rigid than synthetic polyelectrolytes, single-stranded DNA (ssDNA) can be considered as a flexible thread, not nearly as rigid as dsDNA, with the nitrogenous bases readily exposed (Figure 1.1C). Thus, hydrophobic interactions play a more significant role with the adsorption of ssDNA as compared with dsDNA [22].

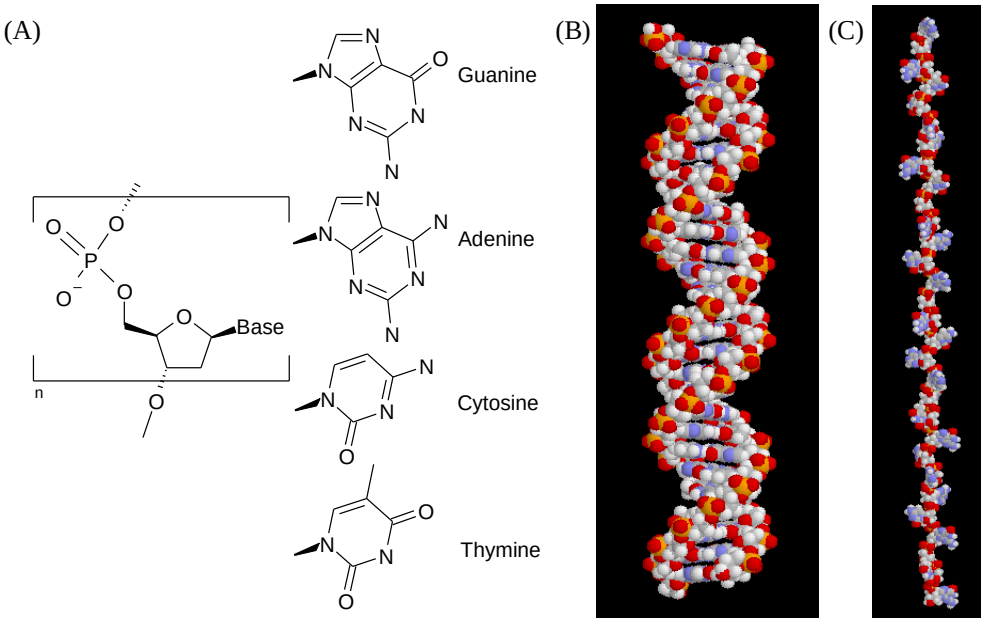

Figure 1.1. *Structure of DNA. (A) The chemical structure of DNA nucleotides, (B) three dimensional space filling model of B-type helical dsDNA, (C) three dimensional space filling model of ssDNA.*

In general, higher salt concentrations and lower pH increase the propensity for DNA adsorption and likewise, low salt concentration and high pH both increase the propensity for DNA desorption [20, 23, 24]. This is a result of two effects. First, under high salt concentration or low pH the strength of the DNA-surface electrostatic interactions can be increased by enhancing the cationic character of a surface and dampening the anionic character of DNA, which allows the DNA to proceed close enough to the surface for hydrophobic interactions to occur. Second, and more commonly observed with the use of cationic ions with a high valency of typically +3 or more, individual DNA strands are compacted due to neutralisation of repulsive electrostatic forces between adjacent phosphate groups, resulting in more compact DNA molecules and, therefore, the scope for higher surface coverage of DNA (Γ^{DNA}) [25, 26].

Electrostatic interactions with DNA have been the primary focus in studies where the adsorption of DNA and its manipulation was desired. The formation of positively charged surfaces is often employed for DNA adsorption experiments. This is commonly achieved by the production of amine rich surfaces, which are typically protonated at neutral pH, and have been shown to increase the Γ^{DNA} [27]. The ease of formation of strong DNA-surface interactions using aminated surfaces where hybridisation can still proceed [28] makes this an attractive approach for microarray applications as opposed to covalently immobilising DNA. A common strategy for the formation of aminated surfaces is silanisation of glass [9, 24, 28-30]. Aminated surfaces have also been produced by the adsorption of cationic molecules such as poly(ethyleneimine) (PEI) [31] or poly(L-lysine) (PLL) [32] and plasma polymerisation [33-37]. For a comprehensive review of plasma polymerisation see reference [38]. Interestingly, Saoudi et al., [27] reported the adsorption of DNA to

aminated polypyrrole silica particles, which had a near-zero surface charge despite the presence of protonated amine groups. The positive charges are compensated by anionic silanol groups. This study suggests that isolated positively charged groups and not a net positive surface charge are sufficient to stimulate DNA adsorption. Lemeshko et al., [28] investigated simplifying DNA microarray formation by adsorbing DNA probes to a surface utilising the electronegative nature of DNA for formation of electrostatic interactions with a positively charged 3-aminopropyltrimethoxysilane modified surface instead of by covalent linkage. A densely packed single-stranded oligonucleotide layer was successfully adsorbed to this surface, where the ssDNA oligomers were adsorbed side-on on the surface, and was used for subsequent hybridisation experiments that confirmed the accessibility of the adsorbed DNA probes for the formation of base pairs with complementary target DNA strand. Interestingly, asymmetric dissociation and DNAse digestion was observed for dsDNA formed in the manner described, whereupon, the hybridised target DNA strands dissociated quicker and were more heavily digested than the initial electrostatically bound probes. This suggests that a typical DNA helix is not formed between these two strands upon hybridisation.

More recently, the polyelectrolytic nature of DNA has been utilised for formation of multilayered films consisting of alternating layers of DNA and cationic polyelectrolytes [32, 39-41]. One polycation commonly used is PEI, which has been used to allow the adsorption of plasmid DNA to poly(lactic acid) (PLA) particles [42]. Yamauchi et al., [41] utilised this strategy to attain a very high Γ^{DNA} for TCM applications. Layer-by-layer assembly of PEI and plasmid DNA was utilised for formation of an electrode with a Γ^{DNA} of 0.6 $\mu g/cm^2$ that was subsequently used for the transfection of cells adherent on the electrode.

For some applications it has been desirable to adsorb DNA to negatively charged surfaces. This has been the case for atomic force microscopy (AFM) experiments with DNA, which commonly require adsorption of DNA to atomically flat, hydrophilic mica and also for adsorption to silica, which is an important and ubiquitous material for many biodevices [20]. The electrostatic repulsion between DNA and mica or other negatively charged surfaces or particles can be overcome, enabling DNA adsorption, in the presence of a divalent cation such as Mg^{2+}, which can act as bridging cations [20, 23, 43]. Generally, trivalent cations are more effective than divalent cations, which in turn are more effective than monovalent cations at enabling DNA adsorption. Hansma et al., [44] used AFM to study the effect of the type of divalent cation on binding of dsDNA of lengths from 79-1057 bp to mica. High amounts of DNA adsorbed to mica in the presence of Ni, Co and Zn ions, however, weak adsorption was seen with Mn, Hg and Cd ions. This effect was explained in terms of the structure of mica and how each type of ion interacted with the mica as opposed to a specific ion-DNA interaction, suggesting that the type of ion most suitable at enhancing DNA adsorption is dependant on the particular substratum surface.

1.1.3. Surface manipulation of proteins and cells

Many biodevice applications, including tissue engineering, cell microarrays and implants [4, 45-47], require the ability to manipulate proteins, and concurrently cells, at interfaces. The fundamental nature of how proteins behave at surfaces depends largely upon their primary structure, that is, the sequence of amino acids making up the protein. There are four main properties of amino acids that influence the behaviour of proteins; polar, non-polar, negatively charged and positively charged. It

is no surprise then that the main two interactions of proteins with surfaces, like in the case of DNA, are electrostatic and hydrophobic interactions.

As proteins function predominantly within aqueous environments, with the exception of membrane bound proteins, proteins try to minimise the entropic penalty of interactions with water with hydrophobic domains by shielding as many hydrophobic amino acids within the protein core whilst arranging the hydrophilic amino acids on the protein surface. However, this 'phase separation' is not always complete, particularly within smaller proteins that have a larger surface area to volume ratio. Thus, hydrophobic domains often exist on the surface of proteins, and those readily adsorb to hydrophobic surfaces even in the presence of electrostatic repulsion due to the large increase in entropy associated with surface de-solvation and the minimisation of polar/non-polar interfaces [11]. This thermodynamically favourable process is the driving force for protein adsorption. However, adsorption to a surface, particularly a hydrophobic surface, can lead to a rearrangement of hydrophobic domains within the centre of proteins to enable the formation of hydrophobic contacts between those domains and the surface. Thus, although highly hydrophilic surfaces will generally reduce protein adsorption, hydrophobic surfaces or hydrophobic patches on otherwise hydrophilic surfaces can cause the rearrangement of proteins resulting in their denaturation and exposure of previously buried hydrophobic residues. This protein rearrangement upon surface adsorption is driven by an increase in entropy due to the destabilisation of ordered protein domains, such as α-helices and β-sheets [11].

Elwing et al., [48] investigated the adsorption of human γ-globulin, human fibrinogen and lysozyme onto a surface with a wettability gradient. This surface was prepared using silanes onto doped silicon to form a wettability gradient with contact

angles ranging from 20-80˚. Significantly, for all proteins a higher surface coverage ($\Gamma^{protein}$) was attained at the hydrophobic end [48]. However, significant amounts of protein adsorption were still observed towards the hydrophilic end of the gradient, suggesting that although surface wettability plays a significant role in protein adsorption it is still not the only force at play. As a variant of this work, Tilton et al., [10] investigated the adsorption of ribonuclease A onto polystyrene (PS) in different alcohol co-solvents of different polarity. Decreasing adsorption propensity was demonstrated in solvents of decreasing polarity, which can be explained in terms of the minimisation of the driving force of protein adsorption [10].

As proteins are usually not geometrically symmetric, the orientation of adsorbed protein can impact upon its $\Gamma^{protein}$. For example, if a protein had an oblong shape such that there was a significant difference between the projected areas of the side-on and end-on orientation, then if all proteins were able to adsorb in an end-on orientation, a greater $\Gamma^{protein}$ would be attained as compared with an all side-on attachment [10]. The orientation of adsorbed proteins impacts not only upon $\Gamma^{protein}$. Surface orientation is of even greater importance for protein activity. Even if a high $\Gamma^{protein}$ is attained, most applications for protein adsorption are not viable if the adsorbed protein is not bioactive. For this reason, various approaches have been developed to control the orientation of adsorbed proteins. This is often achieved by modifying proteins at specific points on the protein exterior with molecular tethers or tags. Common approaches include the use of poly-histidine tagged protein, which forms a complex with surface bound nickel ions [49] and biotin labelled proteins that can form a strong biotin-avidin bridge with avidin functionalised surfaces [50]. A comprehensive review of methods to control protein orientation is available to the interested reader [51].

Living cells exist in nature within the extracellular matrix (ECM), which is a network of biomolecules forming the framework that cells attach to and are supported by. This matrix is composed largely of polysaccharides and various proteins; and it is these proteins, in particular collagen, fibronectin and vitronectin, that cells use to attach to the ECM. Thus, the adhesion of cells to a tissue is mediated by proteins that are already present on that tissue or that the cell produces itself. The same is true *in vitro* and, therefore, the mechanisms used to control protein adsorption, which have been discussed, can equally be applied to cell attachment.

Manipulating cell attachment has attracted much interest and is important for a wide range of biodevice applications. Research has been focussed on producing surfaces that support or resist cell growth, and more specifically, surfaces that either switch between an adherent and a non-adherent surface on demand or have the ability to direct cell growth to localised areas.

One of the most effective methods for promoting cell attachment is the use of extracellular proteins and in particular the Arg-Gly-Asp (RGD) integrin binding peptide based on a cell adhesion mediating site of fibronectin [33, 52-54]. This method is very effective as it utilises the mechanisms by which cells attach to surfaces within natural systems. Various other materials and surface chemistries, such as tissue culture PS and polyurethane, support cell attachment but the use of ECM proteins is unrivalled in its ability to actively promote cell attachment.

As well as chemically initiated cell attachment, the effects of topographical cues to initiate and control the attachment, proliferation, orientation and migration of cells and tissue samples on surfaces has been investigated [47, 55-62]. The ability of substratum topography to influence cell outgrowth suggests that the ECM may present both chemical and topographical signals to cells and is noteworthy in terms

of understanding phenomena like embryo development and wound healing and for the improvement of implant compatibility. Significantly, substrates with aligned grooves have been shown to orient cell growth parallel to the direction of the grooves whilst also improving cell attachment as compared with flat surfaces [57-59], enabling the formation of patterned cell growth. Of interest are studies that demonstrate the ability of micro- and nanostructures on surfaces that are smaller than the typical cell dimensions (≈ 20 μm) to influence the behaviour of cells [57, 58]. Use of cliffs, pillars and islands on surfaces have also been shown to influence cell outgrowth [60]. The mechanism behind this effect is not fully understood. In some cases, improved attachment may be due to the increased surface area of the surface. Recently, Wan et al., [63] investigated cell attachment of osteoblast-like cells (OCT-1) on microfabricated PS and PLA surfaces with hemispherical bump and pit surface features. These features had a bimodal distribution of sizes with an average diameter of 2.2 and 0.45 μm. The behaviour of the OCT-1 cells on the pit-patterned PS surface was most notable (Figure 1.2). Three interesting behavioural characteristics of cells were observed; first, cells showed the ability to be able to stride over both the 2.2 μm pits (Figure 1.2A) and the 0.45 μm pits (Figure 1.2B). Second, the more flexible pseudopods of the cells were able to enter into and grow along the walls of the 2.2 μm pits but not the 0.45 μm pits, which were evidently too small. Third, the filopodia of cells tended to grow along the ridge at the wall of the pits and as a result instigated a morphological change that allowed them to follow the curvature of the ridge (Figure 1.2C). This contact guidance phenomenon has also been observed in many other studies [57-59].

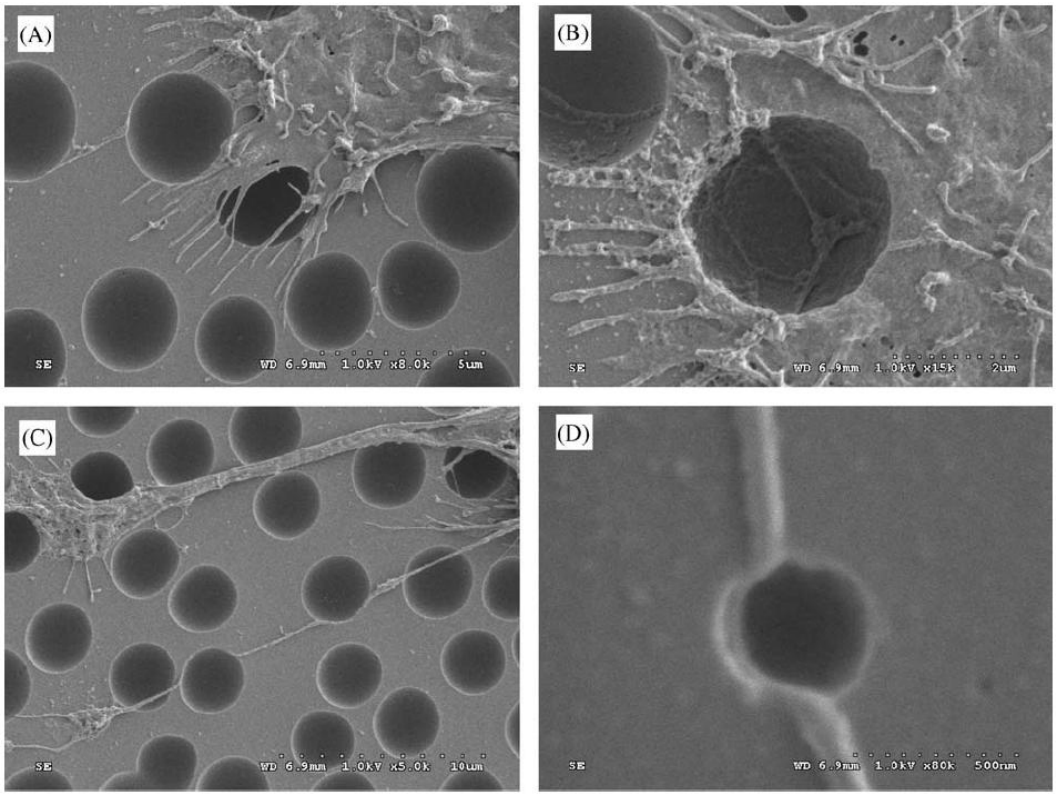

Figure 1.2. *SEM images of OCT-1 osteoblasts on different pits-patterned PS surface. (A) on micro-scale (2.2 μm) pits PS (8000x mag.) cells were observed to be able to stride over pits; (B) on micro-scale (2.2 μm) pits PS (15000x mag.) pseudopods of the cells were observed to enter into the pits and grow along the ridge at the wall of the pits instigating contact guidance of the attached cell; (C) on micro-scale (2.2 μm) pits PS (5000x mag.) filopodia of attached cells grew along the ridge at the wall of the pits instigating contact guidance of the attached cell and altering cell morphology; (D) on nano-scale pits (0.45 μm) PS (80000x mag.) cells tended to stride over these smaller features. From [63].*

Several strategies have demonstrated the ability to produce ‘low-fouling’ surfaces that resist non-specific protein adsorption, including the surface immobilisation of carbohydrates, dextrans or hydrogels [64]. However, the most common and the most effective method utilises the hydrophilic poly(ethylene glycol) (PEG) molecule either immobilised or polymerised onto the surface or other polymers or biomaterials functionalised with PEG. Three primary factors contribute to PEG’s low-fouling properties. Firstly, the hydrophilic PEG hydrogen binds extensively to water and due to its molecular structure fits well into the structure of bulk water. Protein adsorption would lead to unfavourable disruption of the hydrogen bonding. Secondly, the free energy of the polymer-water interface is minimal, decreasing the driving force of protein adsorption. Thirdly, a dense PEG brush has high volume exclusion properties due to high conformational entropy [65]. In the case of end-point grafted PEG, it has been found that the PEG coating provides an interfacial barrier that prevents proteins from interacting with the underlying substrate. Therefore, the molecular weight and interfacial graft density of PEG chains are important parameters to enable non-fouling properties of the coating [66, 67].

The production of alternative low-fouling surfaces is limited. Kleinfeld et al., [68] devised a strategy to control the attachment and outgrowth of neuronal cells on silanised silicon patterned by photolithography to have regions of alkyl silanes and amino functionalised silanes. Interestingly, the alkyl-silanes were able to resist the attachment of cells, leaving the cells to grow only on the amino functionalised regions. The low-fouling ability of this surface is presumably a result of the denaturation of secreted proteins that cells use to attach to the surface. The use of blocking proteins such as bovine serum albumin (BSA) or casein has also been used

to produce low-fouling surfaces [69]. By saturating a surface with these 'sticky' proteins, the subsequent adsorption of other proteins can be prevented.

1.2. Surface micro- and nano-patterning

The formation of micro- and nano-patterns of biomolecules on surfaces has been widely explored and enables the production of sophisticated biomaterials [6, 70, 71], the exploration of biomimetics [72], and the formation of advanced microarrays [41, 73]. Spatial control of biomolecules on solid substrate materials can be achieved using a variety of approaches to patterning. Specific strategies for the surface patterning of biomolecules include microfluidics, microcontact printing (μCP), microelectronics, photolithography, soft-lithography, laser ablation and robotic spotting [33, 74-79]. A detailed technical review of patterning techniques has recently been published [66]. Furthermore, effective spatial control of cell-surface interactions is also possible indirectly via spatially controlling biomolecule attachment to surfaces. Some of the methods that have been used with success are listed below, and a table of their advantages, disadvantages and applications is shown in Table 1.2 (see section 1.4.4.2).

1.2.1. Photolithography

Photolithography involves the irradiation of a surface by a high-energy beam, typically ultraviolet (UV) light, through a photomask. Surface alterations can include the ablation of a photoresist layer, breaking of a chemical bond resulting in the release of an attached molecule, initiation of polymerisation or initiation of formation of a chemical bond resulting in the grafting of a molecule [53, 78, 80]. Photolithography is also utilised for patterning of surfaces to create topographical

cues to control cell growth. This technique has been widely used and is able to pattern surfaces down to sub-micron dimensions, but suffers from the requirement for rigorous laboratory protocols and high setup and maintenance costs.

Photolithography has also been particularly useful for the patterning of proteins [81]. A number of approaches have been employed, but the general approach consists of coating a surface with a photoresist that is subsequently patterned by photolithography to re-expose the underlying material at specific locations. This material is functionalised, often by the use of silanes or self-assembled monolayers (SAMs) with a functional group that either adsorbs protein or is able to covalently link protein such as arylazide derivatives. The rest of the photoresist is subsequently removed and the remaining re-exposed surface is functionalised with a low-fouling material [81].

Falconnet et al., [78] produced a chemically patterned platform for spatially directed cell growth based upon the spontaneous adsorption of PLL grafted PEG to negatively charged surfaces, including oxides of niobium, titanium, silicon and indium tin as well as PS. A photoresist layer was coated onto niobium oxide coated silicon and patterned by photolithography using UV illumination. PLL-grafted-PEG functionalised with the RGD peptide was adsorbed onto the patterned surface, and the remaining photoresist was subsequently removed by washing with an organic solvent that did not disrupt the PLL-grafted-PEG layer. A pattern of functionalised PLL-grafted-PEG remained on a surface of bare niobium oxide. The bare niobium oxide was subsequently coated with non functionalised PLL-grafted-PEG, leaving a patterned surface with cell adhering regions separated by non-cell adhering regions. A pattern of human foreskin fibroblasts was successfully realised on this surface.

Otsuka et al., [80] developed a platform for spatially controlled cell growth by formation of a PEG/PLA block copolymer layer by spin coating on glass silanised with [3-(methacryloyl-oxy)-propyl]trimethoxysilane. Etching through a photomask with a nitrogen and hydrogen plasma removed the PEG/PLA layer and exposed the silanised glass. On this platform, Otsuka et al., [80] were able to demonstrate spatial control of bovine aortic endothelial cells (BAEc), which grew on the exposed glass regions that readily adsorbed proteins including ECM proteins, but not on the PEG/PLA regions where the PEG blocks were effective in resisting protein adsorption. Interestingly, rat primary hepatocytes were able to grow on both the PEG/PLA and the glass regions. Upon prior seeding and attachment of BAEc, spatial control of hepatocytes was achieved and hepatocyte spheroids grew on the etched regions carrying an underlying endothelial cell monolayer. A minimum centre-to-centre spacing between etched regions of 200 μm was also determined as sufficient to prevent bridging between colonies.

Spatially directed cell attachment has also been achieved using a vitronectin mediated, photolithographically formed, patterned *N*-(2-aminoethyl)-3-aminopropyltrimethoxysilane (EDS) and dimethyldichlorosilane (DMS) substrate. Spatially directed cell attachment was driven by the preferential adsorption of vitronectin to the EDS over the DMS [53]. The vitronectin acted as a promoter of cell growth in the regions it was adsorbed upon. This system sustained cell viability and attachment for at least 2 hr using human bone-derived cells.

Another application of photolithography is for on-chip DNA synthesis on DNA microarrays. In this technique a light source passes through a mask to direct light onto localised areas cleaving a photo-labile group and activating the site for the grafting of the next DNA nucleotide building block. By changing the photomask and

by controlling the addition of a particular nucleotide after each activation step, a high-density array of tailored sequences can be grown at the surface. This approach has also been achieved with inkjet technology, enabling probe growth without the rigorous protocols required of the photolithography strategy [82, 83]. *In situ* DNA growth enables the formation of an array with millions of probes per cm^2, however, probes are limited to 25 bases due to low synthesis yields at higher lengths. This approach also requires clean rooms and specialised equipment [82].

Laser ablation is another useful approach for micropatterning and can be considered a specialised case of photolithography. Here, a high-energy laser beam is directed on a surface through a patterned mask which leads to ablation of the surface underneath the transparent regions of the photomask. This method suffers from the same limitations as all photolithographic techniques, but is able to produce highly resolved patterns of controlled depth at a fast rate, thus, being applicable to the production of patterned surface topographies as well as patterned surface chemistries. Thissen, et al. utilised laser ablation with the development of a plasma polymer based system that was shown to spatially confine cell growth [33, 35]. A schematic of the approach is shown in Figure 1.3. An allylamine plasma polymer (ALAPP) with amine functionality was formed and aldehyde terminated PEG was grafted to the surface by reductive amination. Subsequent laser ablation produced micron resolution patterned PEG and ALAPP regions (Figure 1.3A and B). Cells were shown to be confined to the ALAPP region to micron resolution over a four day period using a bovine corneal epithelial cell line (BCEp) (Figure 1.3C) [33]. This system was expanded to include a human embryonic kidney cell (HEK) line [35], and has recently been shown to spatially control protein adsorption [84].

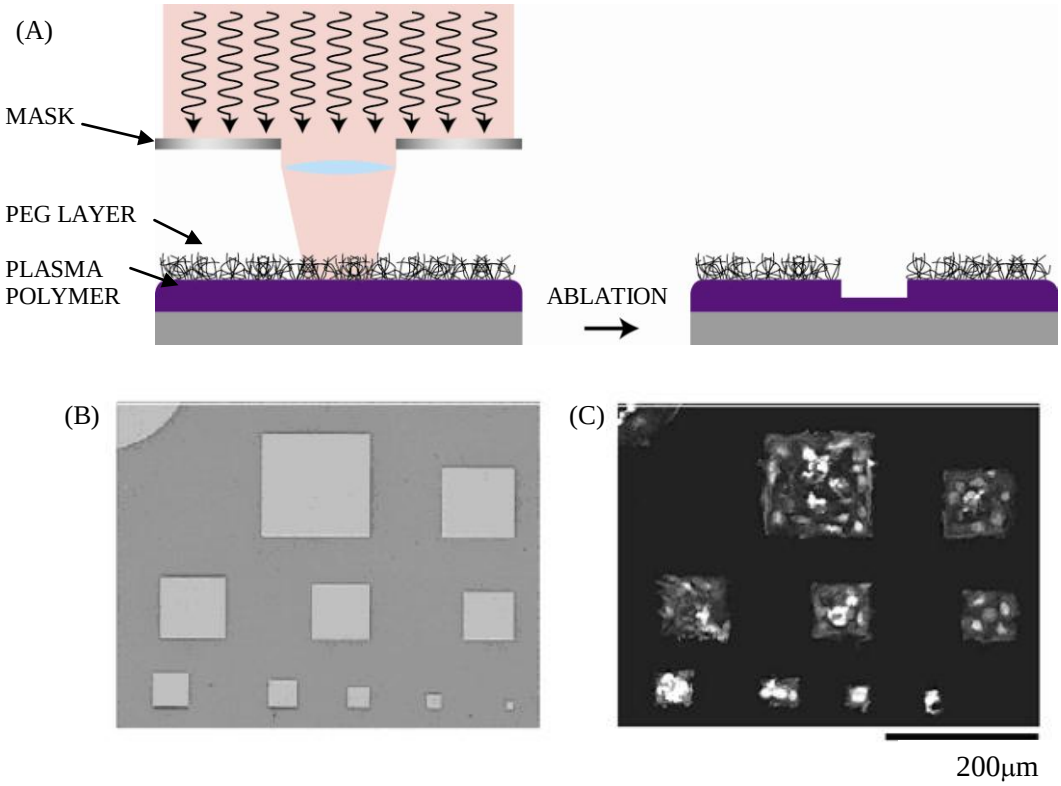

Figure 1.3. *(A) Schematic of two-dimensional patterning of the surface chemistry via excimer laser ablation. (B) Light microscopy image of laser ablated Si-ALAPP sample and (C) confocal scanning laser microscopy image of laser ablated Si–ALAPP–PEG sample after BCEp cell attachment and staining with PicoGreen®. From [33].*

1.2.2. Soft lithography

μCP is a soft lithography technique developed out of a need to pattern surfaces without the experimental difficulties and high costs of photolithography. Typically, this approach involves the once-off production of a mould, using photolithographic methods, that is patterned as the negative of the design of interest. This mould is then used to form a patterned stamp, typically composed of a crosslinked elastomeric polymer, like poly(dimethylsiloxane) (PDMS). The stamp is used to transfer a patterned image of an 'ink' molecule onto the desired substrate surface. The reusability of the photomask and low cost of the PDMS stamp make this technique an extremely cost effective and potentially high-throughput patterning alternative. Currently, this method is primarily used for the patterning of SAMs onto gold or silanes onto glass or silica surfaces. Thus, μCP suffers from a limited number of substrate surfaces and 'ink' molecules [85].

Zhang et al., [76] produced cell patterns using μCP of SAMs. A (11-mercaptoundec-1-yl)-hexa-(ethylene glycol) was printed onto gold coated silicon using a PDMS stamp with a topographical pattern. After SAM pattern transfer and washing, the surface was exposed to an engineered peptide strand containing an anchoring cysteine residue, an alanine linker and a Arg-Ala-Asp-Ser (RADS) cell adhesion motif linker group, which is based upon the recognition motif of ECM proteins and has been found to promote cell attachment [76]. This resulted in the spontaneous attachment of the peptide to the bare gold regions. Using this chemical pattern, cell patterns of micron resolution were formed using BAEc and human epidermal carcinoma cells. The use of normal mouse fibroblast (NIH3T3) cells,

however, demonstrated the ability of this cell type to grow over the ethylene glycol regions.

Hyun et al., [86] attempted to broaden the scope of μCP by developing surface chemistries that covalently react with the printed molecules. This was achieved by initially functionalising the surface of carboxylic acid functional polymers. The carboxylic acid groups were activated by reaction with pentafluorophenol to form pentafluorophenyl esters. Stamping of an amine functionaised molecule with biotin functionality resulted in its covalent attachment; thus, a patterned surface of biotin groups was produced. Subsequent addition of streptavidin modified molecules enabled the patterning of these molecules at the surface with micron resolution [86]. Tween 20 or BSA were adsorbed to the surface in order to saturate the surface with protein thereby minimising non-specific binding in between the printed regions. A similar technique was also used to initiate free radical polymerisation of PS by modifying a gold plated surface with thiols with terminal carboxylic acid functionality, subsequently converted to a pentafluorophenyl ester, and then printing a radical polymerisation initiator with a terminal amine. The initiator attached covalently to the SAM by formation of an amide bond. This enabled the spatially confined free radical polymerisation of PS at the surface upon addition of the polymerisation solution [87]. Here, cells preferentially attached to the SAM rather than the surface grafted PS layer.

In order to pattern cells upon a biodegradable surface, Kumar et al., [88] patterned a biocompatible chitosan substrate by μCP of random copolymers of methacrylic acid (MAA) and oligo(ethylene glycol) methacrylate (OEGMA). This polymer not only shows low fouling characteristics but, being an anionic polyelectrolyte, also binds through multivalent electrostatic interactions to the positively charged chitosan

substrate. A copolymer ratio for OEGMA/MA of 0.8 was found to be optimal composition for both ensuring strong polymer adsorption and cell resistance. Spatially controlled cell attachment with micron resolution was demonstrated using human microvascular endothelial cells.

1.2.3. Microfluidics

Microfluidics is a different approach to surface patterning whereupon biomolecule manipulation and spatial control is achieved by limiting the surface of the substrate that is accessible to the solvent carrying the biomolecule of interest. Microfluidic systems can be complicated, however, for a simple patterning experiment a patterned PDMS stamp, formed in a similar fashion to typical μCP experiments, has been shown to be very useful. The PDMS stamp is typically topographically patterned with grooves that form sealed channels when the stamp is pressed onto a hard, flat substrate surface.

Microfluidics often represents a cheaper and simpler solution than other patterning techniques and has the unique advantage of being able to separate and contain the reaction solution, enabling different solutions to be exposed to different locations on a particular surface. A further advantage is the gentler processing conditions in comparison to lithographical methods. This enables patterning over pre-attached cells or over proteins, which would be destroyed by harsher treatment conditions. However, there are limited number of channel geometries available and the resolution limit is generally lower than for lithographical approaches.

A multi-phenotype cell array was formed by encapsulating living cells within a hydrogel matrix, formed inside of a microfluidic channel made of PDMS [52]. Various cell lines in a hydrogel precursor solution were injected into parallel

channels flowing over a substrate surface. Cells were then trapped by irradiation of the channels with UV light through a photomask which resulted in cross-linking of the hydrogel. Subsequent removal of the microfluidic assembly left a patterned array of a multi-phenotype cell array. This system was able to sustain cell separation of murine fibroblast, murine hepatocytes and murine macrophages, keeping different cell types apart down to micron-size separation distances.

Patel et al., [74] produced a patterned culture of BAEc and pheochromocytoma (PC12) using microfluidics. A PDMS mould was formed containing grooves which formed microchannels when put in contact with a substrate. This enabled the spatial control of solvent flow over the surface. The substrate used was a film of PLA-PEG block copolymer modified with biotin. Flow of avidin over the film through the microchannels produced spatially activated regions on the substrate. Biotinylated peptides containing the RGD peptide or a laminin fragment were subsequently flowed through the microchannels to produce a surface conducive to cell attachment. Removal of the PDMS mould and seeding of the cells on the activated surface resulted in preferential attachment of the cells to the modified regions.

Takayama et al., [75] developed a method of cell patterning using combined laminar flows through capillary networks. In one experiment *Escherichia coli* (*E-coli*) was patterned to a surface by prepatterning a surface with a mannose containing protein (Figure 1.4A). Mannose was chosen because the cell membrane of *E-coli* is decorated with mannose-binding proteins. Subsequent incubation of *E-coli* with the patterned surface caused the adsorption of *E-coli* to the mannose-coated regions (Figure 1.4B). This technique also enabled the surface patterning of eukaryotic cells and proteins.

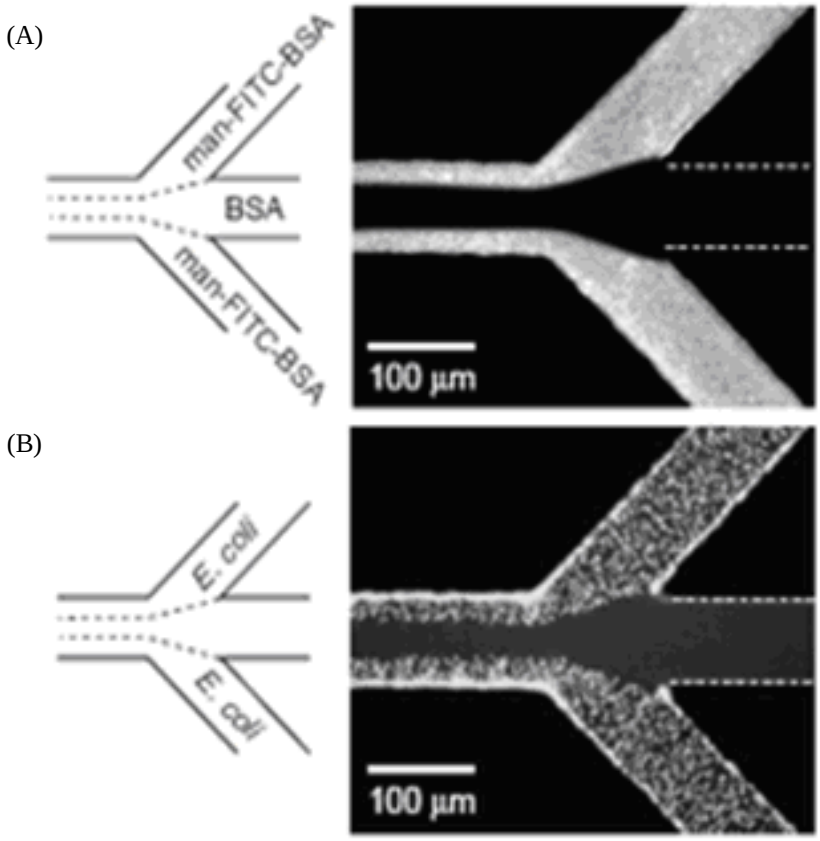

Figure 1.4. *Schematic representation of a laminar flow patterning experiment. Flow is from right to left. (A) Patterns of adsorbed protein created by laminar flow. Solutions of α-D-mannopyranosyl phenylisothiocyante,fluorescein isothiocyanate (FITC)–BSA (0.5 mg/ml in PBS) and BSA (10 mg/ml in PBS) were allowed to flow from the designated inlets into the main channel for 15 min under gentle aspiration, and the system was washed for 3 min with PBS. (B) The channels shown in (A) were filled with a suspension of E-coli RB 128 and allowed to stand for 10 min to allow adhesion; nonadherent cells were removed by washing with PBS. Cells were visualised with a fluorescent nucleic acid stain (Syto 9, 15 mM in PBS). Both micrographs were taken from the top of the capillary network looking through the PDMS. White dotted lines identify channels not visible with fluorescence microscopy. From [75].*

Finally, the Whitesides group has extensively investigated methods of cell patterning including μCP, microfluidics and laminar flow patterning. Much of this research has been previously reviewed [4, 85, 89-91].

1.2.4. Microelectronics

Microelectronics is a new field that exploits microcircuitry to manipulate biomolecules and cells. This technique has been developed by Huang et al., [77] to separate monocytic white blood cells and human T cells transformed with the oncogene Tax from human peripheral blood mononuclear cells as well as neuroblastoma cells from glioma cells on the basis of the distinct dielectric properties of the different cell types. Using a microelectronic chip array, effective separation and sorting of different cell types was demonstrated (Figure 1.5) by stepwise addition of cells (Figure 1.5A), separation by dielectrophoresis (Figure 1.5B), and then washing by buffer (Figure 1.5C and D). Microelectronic chips have also been shown to effectively control DNA adsorption and surface diffusion [92, 93]. This method is limited by the electrode pattern that can be fabricated. However, this approach does combine spatial control with switchability. Furthermore, as well as having the ability to pattern cells, it has the unique capability to control surface diffusion of cells, which adds a new dimension to advanced cellular manipulation.

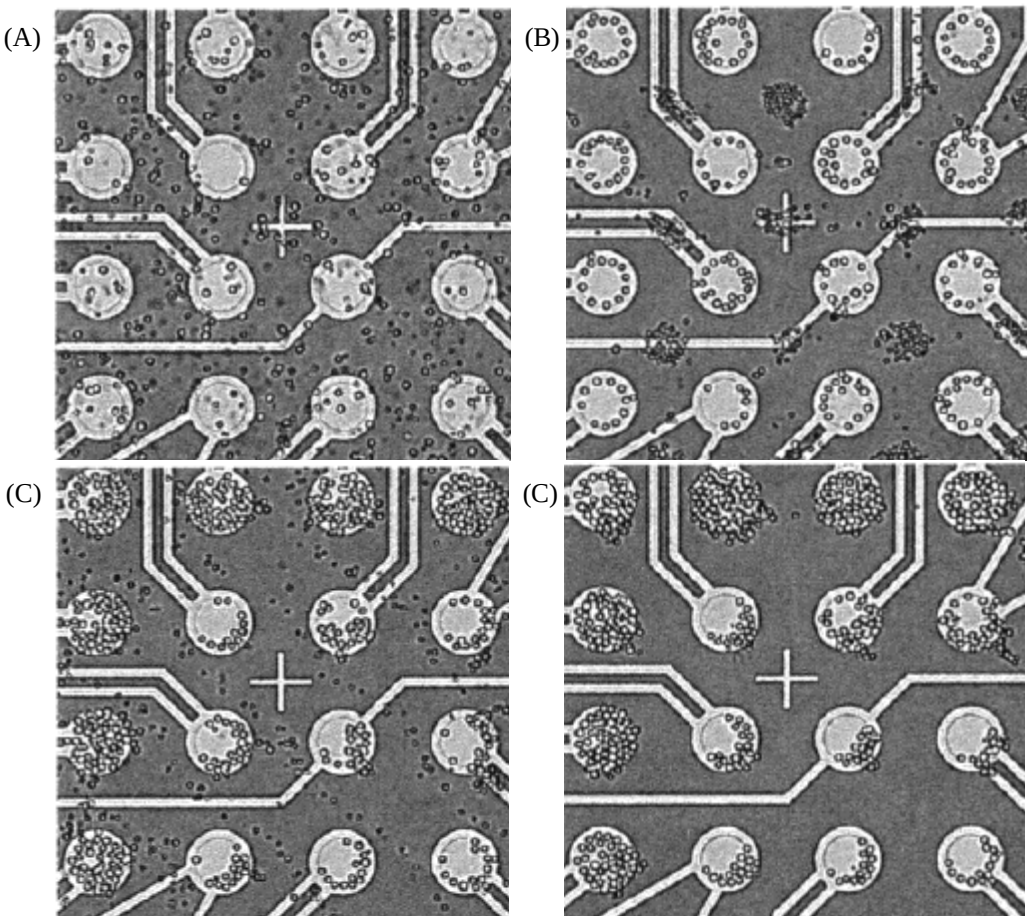

Figure 1.5. *The procedure of dielectrophoretic separation for a monocytic cell and peripheral blood mononuclear cell mixture. (A) The mixture is introduced to the array. (B) Monocytic cells are separated from peripheral blood mononuclear cells on array by dielectrophoresis 5 min after an ac voltage of 500 kHz frequency and 7 V amplitude is applied. Monocytic cells are collected on the electrodes and peripheral blood mononuclear cells are accumulated at the space between the electrodes. (C) Buffer is introduced from a reservoir to the array by fluid flow of 40 μL/min while the voltage is kept on. Peripheral blood mononuclear cells are carried away with the fluid stream. (D) Peripheral blood mononuclear cells are washed off from the array and monocytic cells are retained on the electrodes after 10 min of washing. From [77].*

1.2.5. Robotic contact and non-contact microprinting

Formation of micron resolution arrays is routinely achieved by robotic contact and non-contact microprinting. Robotic contact printing is achieved using a robotic spotter that first dips a pin with microscale diameter into a desired solution then spots the sample onto the substrate surface at a specified location. Two types of pins are typically used. First, a solid pin, which is commonly used for transferring proteins and other sticky molecules because of their ease of cleaning and second, a quilled pin that has a hollow centre that is able to draw up the solution and act as a reservoir allowing repeated spotting without re-dipping. Although, this increases the rate of microarray formation, these pins are much more difficult to keep clean and are, therefore, only suitable for 'non-sticky' molecules. Robotic non-contact printing is achieved by ejecting nano-litre volumes of the desired solution from a microcapillary onto specified positions on a surface. The advantage of this strategy is that common problems with pins, such as the risk of contamination if the pins are insufficiently cleaned, inhomogeneous spot geometry and variations in the dispensed volume, can be avoided [94], however, this approach typically suffers from 'splattering' of ejected volumes. Such strategies can be used to form DNA and protein microarrays and more recently also cell microarrays [8, 15, 82, 94-99].

This form of patterning is very effective at quickly and reproducibly producing micron resolution patterns that can be used for the cost effective, high-throughput analysis of proteins and DNA products using very little reagents on, typically, a single microscope slide. Microarrays were key to the success of the human genome project and will underpin further genomic analysis. The development of cell microarrays will further advance genomic analysis, and as the investigation of more

complex genomic questions proceeds, advanced surface chemistries for microarrays are required.

For example, one of the limitations with contact and non-contact printing is that although patterned arrays of DNA, proteins and other molecules are easy to form, there are very limited procedures to prevent cross-contamination or surface migration of arrayed species. One such strategy was developed by Yamauchi et al., [100], who spatially confined droplets of DNA solution at the surface by using a patterned SAM with regions of varied hydrophilicity produced using alkanethiols with different end-groups. Spots containing amine, hydroxyl and carboxylic acid groups separated by methyl terminated alkanethiols were shown to readily confine DNA containing water droplets. Baghdoyan et al., [101] sought to confine DNA by adding gelatin to the DNA mixture spotted onto a glass slide in the form of a microarray. This microarray was subsequently used for reverse transfection with the highest transfection efficiency occuring at 0.25-0.5% gelatin concentration. Addition of the gelatin was hoped to increase spatial control of DNA, however, this was not clearly demonstrated.

Spotted material can also be held in place by introducing various attractive interactions between the surface and the spotted material. For example, DNA is typically immobilised to a surface by either covalent interactions, such as immobilisation of thiolated ssDNA to gold surfaces, or non-covalent interactions such as adsorption of DNA to amine functionalised surfaces where electrostatic interactions dominate or interactions of biotin labelled ssDNA with avidin-presenting surfaces.

1.3. Surfaces with switchable properties

The development of switchable surfaces is a key enabling advancement for biodevice applications, including biomaterials and in particular tissue engineering and cell microarrays. Switchability, in essence, enables temporal control, adding another dimension to controlled biomolecular manipulation. These types of surfaces have already been instrumental in gaining a better understanding of biomolecular surfaces at the solid-liquid interface. Typically, DNA adsorption and desorption is temporally controlled by electrochemistry due to the polycationic nature of this biomolecule. On the other hand, a number of strategies to reversibly control cell and protein adhesion have been investigated and typically involve the use of hydrogels and switching of these polymers from a hydrophobic to hydrophilic state by temperature shifts about the lower critical solution temperature (LCST). Other triggers such as pH, specific ligand-receptor interactions and light have been investigated to evoke changes in hydrogel properties, including optical and density changes [70, 102-104].

1.3.1. Switchable DNA adsorption and desorption

Of great interest in terms of DNA surface manipulation are surfaces that can switch between a positive and negative surface charge, instigating temporal control over DNA adsorption and desorption. This is particularly important for TCMs whereupon adsorbed DNA must be released in order to be internalised by cells [1]. The ability to electro-stimulate the desorption of DNA has been studied extensively on gold [18, 105-108]. Wang et al., [105] demonstrated small amounts of DNA were released at voltages as low as -0.2 V, however, maximised DNA release was observed at -1.2 V. Jiang et al., [109] demonstrated by AFM analysis that the surface

morphology of adsorbed dsDNA could be changed by application of an increased magnitude of positive voltage.

Heller et al., [92] utilised the electro-responsive nature of DNA to form switchable checkerboard patterns of fluorescently labelled DNA on a microelectronic chip (Figure 1.6). By application of the appropriate positive and negative voltages DNA became spatially confined and a pattern was formed (Figure 1.6B). The inverse checkerboard pattern was formed by reversing the polarity of the applied voltage, and this reorientation was complete after 7 s (Figure 1.6D). Analysis of the stringency of DNA hybridisation was also achieved by controlling the surface diffusion of DNA oligonucleotides to move, on demand, over different regions functionalised with complementary or slightly mismatched oligonucleotides. Gilles et al., [93] used this technology to study single point mutations along the encoding a human mannose binding protein. Point mutations on genes are stable and can contribute to genetic disorders. Detection of a single point mutation is difficult considering the vast number of base pairs within any given genome. Gilles et al., [93] immobilised a number of different single stranded 123 bp oligonucleotide fragments of the allele of a mannose binding protein gene that differed by single point mutations at different sites on a 5 x 5 microelectronic chip array by streptavidin-biotin interactions. Application of a positive voltage at a particular site directed the immobilisation of each strand to a desired location. 21 or 22 bp oligonucleotide probes specific for the wild type allele or specific for a particular single point mutation were injected into the system and allowed to hybridise with immobilised DNA strands. By application of a negative voltage at a specific site the mismatched probe DNA could be driven away, whereas complementary probes would stay

behind. This strategy enabled the differentiation of the wild type and single point mutation oligonucleotides.

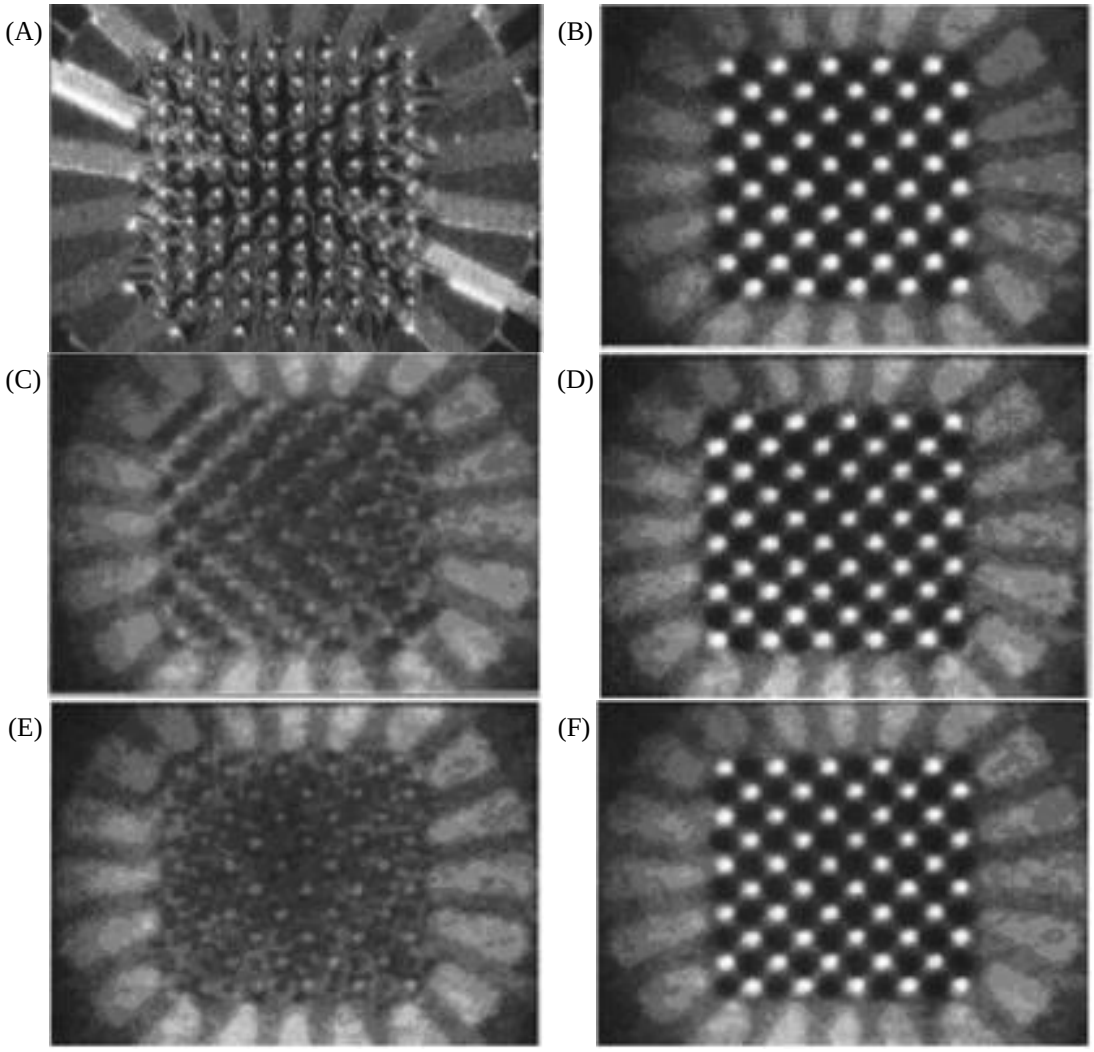

Figure 1.6. *DNA checkerboarding on 100 test site microelectronic array. In this experiment, all the microelectrodes on an agarose permlayer-coated 100 test site chip are biased positive or negative in a checkerboard pattern, with the polarity being reversed every 7 s. White light and fluorescent images are acquired in real-time using a charge coupled detector (CCD) camera and digital tape recorder. (A) 100 test site chip under white light and the 100 test site array with its 80 μm diameter microlocations. (B) Fluorescent image of the rapid accumulation of fluorescent probe at the positively (+) biased microlocation (white spots), and repulsion of the DNA probes from the negatively biased microlocation (black spots). Note that the fluorescent DNA over the unactivated counter-electrodes on the perimeter of the device is not influenced during the checkerboard experiment. (C) Fluorescent DNA in rapid transport as the polarity is reversed after 7 s. (D) Fluorescent probes now accumulating on the newly biased negative microlocations. (E) Transport after polarity reversal. (F) Accumulation of the fluorescent probes on the newly biased positive microlocations. From [92].*

1.3.2. Switchable surfaces for the control of proteins and cells

Controlling the behaviour of cells firstly requires the ability to manipulate the proteins that cells use to mediate their attachment to surfaces. Since a major driving force for protein adsorption is the surface dehydration associated with hydrophobic interactions, a focus for switching protein and cell attachment has been the production of surfaces that are able to alter their wettability when stimulated appropriately.

Okano's research group has developed a switchable polymeric surface for cell attachment using poly(*N*-isopropylacrylamide) (P*N*IPAAm), which switches from a hydrophilic state to a hydrophobic state by increasing the temperature above its LCST of 32 °C. Mammalian cells grew on the hydrophobic polymer, but not the hydrophilic polymer enabling cell adhesion to be turned on and off [110]. A pattern of the P*N*IPAAm was formed on a surface by UV-initiated polymerisation of the polymer through a metal photomask (Figure 1.7A) in direct contact with the surface such that P*N*IPAAm was only formed where the UV was not blocked. Using this technique, Yamato et al., [73] were able to produce an array of 1 mm diameter circular domains of P*N*IPAAm on a background of tissue culture grade PS. Seeded rat hepatocytes grew on both the P*N*IPAAm and the PS (Figure 1.7B), however, upon lowering the temperature, the cells detached from the P*N*IPAAm regions (Figure 1.7C). Upon raising the temperature to 37 °C seeded endothelial cells then attached to the P*N*IPAAm, generating a patterned cell co-culture (Figure 1.7D). Alternatively, Yamato et al., [64] seeded rat hepatocytes on the patterned P*N*IPAAm at 20 °C, below the LCST, such that cells only attached to the unmodified tissue culture grade PS. Subsequently seeded human fetal lung fibroblasts at 37 °C, above

the LCST, adhered to the P*N*IPAAm regions resulting in the formation of a heterotypic cell pattern. This approach has the advantage that cell detachment is not required. These methods are in principle adaptable to different cell types; theoretically any patterned co-culture of two cell types could be realised.

Extending the above approach, Edahiro et al., [104] developed a photoresponsive, switchable surface for cell attachment. The surface was composed of P*N*IPAAm with a photoresponsive chromophore that underwent isomerisation upon exposure to UV, and reversed upon exposure to light in the visible spectrum. A Chinese hamster ovary cell line (CHO-K1) was shown to have preferential attachment to the isomerised chromophore once exposed to UV, although the mechanism for this was not understood. This surface was patterned by irradiation of UV through a photomask to produce regions that cells preferentially attached to. Use of P*N*IPAAm enabled the bulk regeneration of the surface by reducing the temperature below P*N*IPAAm's LCST, causing the cells to detach.

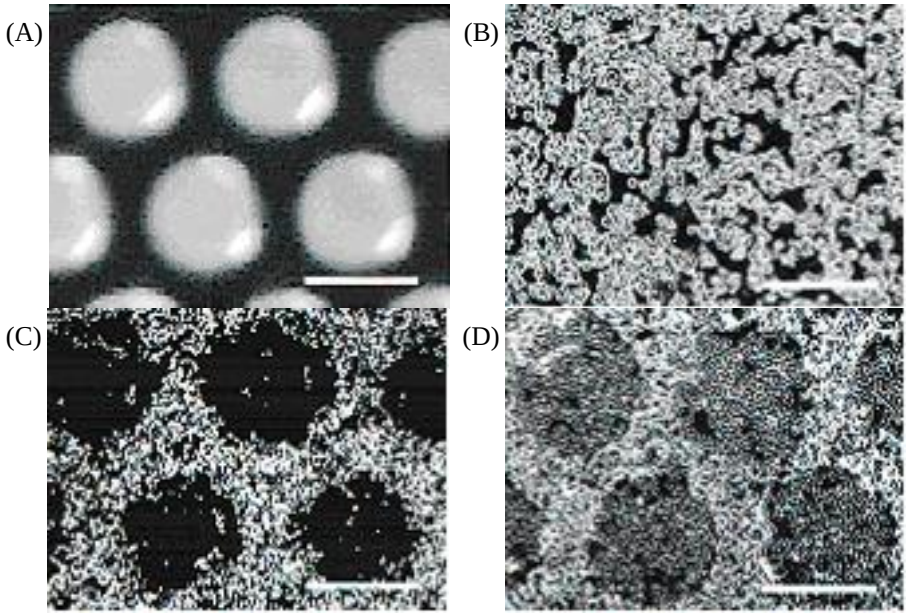

Figure 1.7. *A patterned co-culture of hepatocytes and endothelial calls. (A) The patterned metal mask with holes (1-mm diameter) used for surface patterning of PNIPAAm and PS. (B) Hepatocytes were seeded and adhered homogeneously on the whole surfaces at 37 °C. (C) By reducing the temperature, hepatocytes detached spontaneously and selectively from PNIPAAm -grafted domains. (D) Endothelial cells were seeded and cocultured with formerly seeded hepatocytes at 37 °C, forming a co-culture. Scale bars = (A, C, D) 1 mm and (B) 200 μm. From [73].*

Hyun et al., [111] developed a strategy for the switchable attachment of peptides modified with an elastin-like polypeptide moiety based upon the pentapeptide sequence of Val-Pro-Gly-X-Gly, where X is any amino acid other than proline. First, a patterned SAM with carboxylic acid functionality was formed by dip-pen nanolithography (DPN). An elastin-like polypeptide was then immobilised on the surface by 1-ethyl-3-(diethylamino)propyl carbodiimide (EDC) – *N*-hydroxysuccinimide (NHS) coupling. The elastin-like polypeptide is able to switch between a soluble and insoluble state at its LCST, which is tunable within the temperature range of 0-100 °C [111]. The LCST of the polypeptide could be reduced by increasing the ionic strength. Proteins could be adsorbed onto this surface in the collapsed state and released by reducing the temperature or the ionic strength.

Miyata et al., [103] developed a smart hydrogel that swelled 10% in the presence of an antigen. The creation of an antigen responsive hydrogel adds an important and more specific stimulus ligand-receptor interactions, to the toolbox for switchable surfaces. This hydrogel was formed by copolymerisation of acrylate derivatives of antigen and its corresponding antibody with acrylamide (AAm), such that the antibody-antigen interaction produced extensive crosslinking of the formed hydrogel. Addition of free antigen resulted in competitive binding of the free and immobilised antigen for the immobilised antibody, resulting in the breakdown of some of the hydrogel crosslinks and a concurrent swelling of the polymer. Miyata et al., [103] used a rabbit immunoglobulin (IgG) antibody as the antigen and a goat anti-rabbit IgG antibody. The swelling was reversible, antigen specific and occurred within a time scale of approximately 1 hr. This switchable swelling may be useful for certain cell culture applications, but it is of great interest for drug delivery on demand.

1.3.3. Alternative switchable surfaces

Switchability is not only limited to hydrogel systems. There is no lack of other, alternative strategies for the development of switchable surfaces with biodevice applications.

Lahann et al., [112] developed a surface coating on gold that transduced conformational changes in a low density SAM initiated by a voltage bias into wettability changes. The SAM was formed by attaching a large, cleavable head-group onto the alkanethiol used (16-mercapto)hexanoic acid (MHA), which limited the packing density of the SAM. After cleavage of the head group, a low density SAM remained. By application of a voltage bias, the ionised carboxylic acid group was attracted to the surface, producing a conformational change in the MHA backbone that exposed a hydrophobic loop at the solid liquid/interface, producing a reversible change in hydrophilicity, which was observed as a change in contact angle. Development of these self assembled surfaces offers exciting opportunities when applied to the manipulation of biomolecules.

Gillies et al., [113] developed a one-off switchable system using pH sensitive micelles. Linear-dendritic block copolymers containing hydrophobic head groups and PEG tails were formed, which spontaneously formed micelles in aqueous conditions. The hydrophobic head group contained a cyclic acetal linker that, upon hydrolysis at lower pH, decomposed, releasing trimethoxy benzene and producing a diol end group. This reaction increased the hydrophilicity of the head group and essentially removed the driving force for micelle formation, which led to their breakdown. The micelles were stable at physiological pH, however, lowering the pH to 5 caused the hydrolysis of the acetal group, initiating the destabilisation of the

micelles. This pH switch was used to deliver a hydrophobic dye encapsulated within the micelles on demand.

Ionov et al., [114] developed a mixed polyelectrolyte brush consisting of poly(acrylic acid) (PAA) and poly(2-vinyl pyridine) (PVPI) chains with pKa values of 6.7 and 3.2, respectively, whereupon PAA is negatively charged above pH=6.7 and PVPI is positively charged below pH=3.2. Switching of the pH from 3 to 9 caused a switching of the surface chemistry from a positive surface charge to negative. This change also instigated a rearrangement of the surface bound polymer, whereupon, at low pH PVPI was extended and, thus, dominated the surface character, whilst PAA was collapsed, hidden beneath the PVPI layer. At high pH this was reversed, with the PVPI collapsing and PAA extending. Concurrently, changing the pH altered the contact angle of the mixed polymer brush surface, whereupon the surface exhibited hydrophilic properties at high and low pH, but was more hydrophobic over the pH range of 4-8, where the surface had a near neutral surface charge.

Winkelmann et al., [115] produced a patterned surface with conductive and non-conductive regions of titanium and silicon, respectively by photolithographic microfabrication using a patterned photoresist. Surfaces with regions of different metals were also formed using this technique, enabling the study of protein and cell adhesion to a variety of metal interfaces [116]. Using this substrate, the controlled removal of adsorbed PLL-g-PEG at conductive regions was demonstrated by application of +1800 mV voltage bias, which enables further adsorption of functional molecules, in the present case human fibrinogen was adsorbed, to the re-exposed titanium layer [117].

1.4. Application of patterned and switchable surfaces – Microarrays

Recent years have seen the development of many advanced biomedical devices that have been useful for the study, advanced manipulation and application of biomolecules. Such devices have proved to be valuable tools for solving many biologically based problems, particularly in the field of medicine. Examples include microarrays, advanced drug delivery systems, biosensors and scaffolds for tissue engineering [3, 4, 6, 8]. Advanced manipulation of biomolecules requires surfaces or materials with the ability to adsorb, desorb, bind or prevent adsorption of biomolecules in localised regions combined with the ability to switch between these processes on demand or upon activation by a defined stimulus. A number of studies have been conducted in this field, with the main interest being in high-throughput DNA or protein manipulation and concurrently in controlling cell adhesion on microarray substrates. [15, 17, 66, 99]. With the completion of the human genome project has come the challenge of elucidating the function of the vast amount of genomic information within any single person's genotype. This has led to the emergence of three primary types of genomic analysis tools: protein microarrays, DNA microarrays and cell microarrays. The key advantage of microarray technology is the ability to conduct high-throughput studies with small amounts of analyte, enabling the rapid, inexpensive examination of genomics, proteomics or gene expression [118]. Cell microarrays offer an additional advantage in their ability to analyse the expression of genes and the function of proteins in a living cell where all the machinery is present to ensure correct function enabling the high-throughput validation of tens of thousands of gene and protein targets [119].

1.4.1. DNA microarrays

Vast amounts of research have been conducted with DNA microarrays and have proven to be of paramount importance in the areas of cancer research and other genetic based diseases. In fact, DNA microarray based research is an integral part of many physiological based research and has revolutionised genomic studies, which pertains not only to oncology but also neurology, pathology, psychology, pharmacology, pharmacogenomics and toxicogenomics, to list a few.

There are three methodologies utilised for DNA microarray formation. The first method is contact printing, achieved by dipping an array of pins into defined sample solutions and then, by use of high precision robotics, bringing the pins in contact with a substrate, with the formation of spots as sample solution is transferred from the pin to the substrate (see section 1.2.5). DNA is typically immobilised to a surface by either covalent interactions, such as immobilisation of thiolated ssDNA to gold surfaces, or non-covalent interactions such as adsorption of DNA to amine functionaised surfaces or interactions of biotin labelled ssDNA with surface immobilised avidin. Various studies have sought to control the density of immobilised DNA in order to optimise DNA hybridisation whilst seeking to minimise non-specific DNA adsorption [120-122]. The surface energy of the substrate material is an important factor determining how the surface wets, spreads and dries. Although microarray formation is commonly done on glass, lack of reproducibility in spot formation has led to efforts attempting to produce varied surfaces with desirable surface energies that produce more reproducible spots [123]. One such method is the formation of a mixed SAM containing different ratios of alcohol and methyl terminated alkanethiols. SAMs are well known for their ability to produce regular, reproducible, defect free films [124]. Optimisation of surface energy

by tuning the alcohol:methyl ratio enabled the successful formation of spots of Cy5 dye in dimethylsufoxide (DMSO) with reproducible size and shape [123].

As an alternative to contact printing, non-contact printing has been utilised for injecting preformed DNA onto a surface at specific locations with high precision. This method is commonly achieved by utilising inkjet technology. The advantage of this strategy is that problems with pin transfer, such as risk of transfer of materials, variation in spot formation and the influence of metallic pins, can be avoided [94].

Furthermore, the development of an on chip DNA growth technique has also been successful achieved (see section 1.2.1).

DNA microarrays have previously been reviewed in detail [14-16, 82, 96, 125-130].

1.4.2. Protein microarrays

Protein microarrays are predominately used to investigate the abundance of specific proteins, usually achieved by the use of an antibody microarray, and how proteins interact with each other or with small molecules [3]. Protein microarrays are formed by adsorbing or covalently binding a number of different proteins in an array format. Washing with a labelled target molecule or a number of differently labelled targets, consisting of other proteins or small molecules, can result in the determination of the protein-protein or protein-small molecule interactions. Protein microarrays have been extended to include peptide microarrays, which, like protein arrays, are a series of small peptides immobilised onto a surface in an array format. Peptide arrays are advantageous over protein arrays in that peptides can be synthetically made and are, thus, easier to purify and enable the study of protein fragments, specifically the reactive sites [3].

A major problem with protein microarrays is the ability to attach the protein whist maintaining its functionality. Various methods of attachment are used including physioadsorption, metal complexation, covalent attachment, electrostatic attraction or by biological interaction (biotin-avidin) (see section 1.2.5) [79, 131, 132]. The common problem is that the attachment is either weak, enabling protein to be washed away or replaced with another protein, or the binding denatures or sterically hinders the binding site. One strategy to combat this was achieved by the production of a PLA-PEG film containing biotin [133]. Addition of avidin as a linker molecule enabled the potential attachment of biotin modified proteins, where if correctly modified, would result in correctly orientated proteins that are strongly attached. Another similar strategy is the use of His-proteins, which form a chelate complex with Ni^{2+}. Surfaces modified with carboxylic functionality are able to form such Ni^{2+} complexes and effectively immobilise His-proteins, which can be subsequently removed by addition of either EDTA that chelates Ni^{2+}, thus, breaking apart the complex formed with the his-protein, or imidiazole that competitively binds to the Ni^{2+} comples in place of the his-proteins. Such strategies are often used in protein purification. This and similar strategies involving protein modification and controlled attachment currently provide the means of effective protein microarray formation without compromising on protein activity.

Another problem associated with protein microarrays is storage, handling and purification of an array of proteins. Formed microarrays may have limited temperature ranges and often have short shelf lives. Ramachadran at al., [134] have developed a technique for the production of proteins *in situ* on the microarray on demand by utilising *in vitro* DNA transcription and translation. Complementary DNA (cDNA), which is DNA reverse transcribed from mRNA whereupon the RNA

has undergone post-transcriptional processing including gene shuffling and intron excision, is spotted onto the surface. cDNA libraries are usually constructed to include every gene within a genome and the genes are often inserted into plasmid DNA form. Once spotted and immobilised by a biotin-avidin interaction, use of cell-free *in vitro* transcription and translation machinery produces the encoded proteins *in situ* at addressed location. Addition of C-terminal glutathione *S*-transferase tag and surface-tethered glutathione *S*-transferase antibody enabled the immobilisation of the proteins *in situ*. Protein arrays produced in this fashion were used to perform typical protein microarray analysis, including protein recognition with antibodies and protein-protein interactions where the probe protein was also translated *in vitro*, but without a tag to prevent immobilisation [134].

Protein microarrays have previously been reviewed in depth and further information can be found in the following reviews [97-99, 135-142].

1.4.3. Polymer microarrays

Polymer microarrays are a recently developed microarray format that primarily allows for the screening of cell-material interactions and are a key enabling device for the development of new materials for specific biomaterial applications. Typically an array of polymer materials is formed on a low-fouling coating and subsequently exposed to cell culture conditions [143, 144]. Polymer spots inducing desirable behaviour to attached cells can be readily identified.

Anderson et al., [145] developed a method for the *in situ* polymerisation of polymer materials in an array format. Various combinations of acrylate monomers were deposited with a radical initiator in an array format on a low-fouling poly(hydroxyethyl methacrylate) coating. Upon UV irradiation rigid polymer spots

attached to the coating were formed that could be used for subsequent assay of cell-material interactions. Automated X-ray photoelectron spectroscopy (XPS), contact angle and time of flight secondary ion mass spectroscopy (ToF-SIMS) analysis allows for the rapid characterisation of the formed polymer array and the ability to match observed cellular behaviour with particular chemical or structural properties of individual polymer spots [146].

1.4.4. Cell microarrays

A number of different approaches to cell microarrays have been explored enabling the investigation of gene expression, cell surface interactions particularly with antibodies, ECM composition, cell migration and proliferation, the effects of drugs on cellular activity and a number of other areas [45]. A review of cell microarrays in general has been recently published [45]. Of great interest has been the development of TCMs [8]. A schematic representation of the TCM formation is shown in Figure 1.8. TCM formation consists of four key steps. Firstly, a nucleic acid microarray is formed using typical DNA microarray formation techniques, which have previously been reviewed in detail [15, 16, 82, 96]. Secondly, cells are seeded and attach onto the surface. Thirdly, DNA detaches from the surface and is taken up by the cells and finally overexpressed within the cells or, when using RNA interference (RNAi), the target gene is silenced. Various genomic studies have been undertaken utilising TCMs, such as the determination of the cellular position of expressed proteins, detection of gene products involved with apoptosis and the screening of agonists and antagonists of G-protein coupled receptors (GPCRs) [8, 147, 148]. A list of current applications of cell microarrays using transfection is shown in Table 1.1.

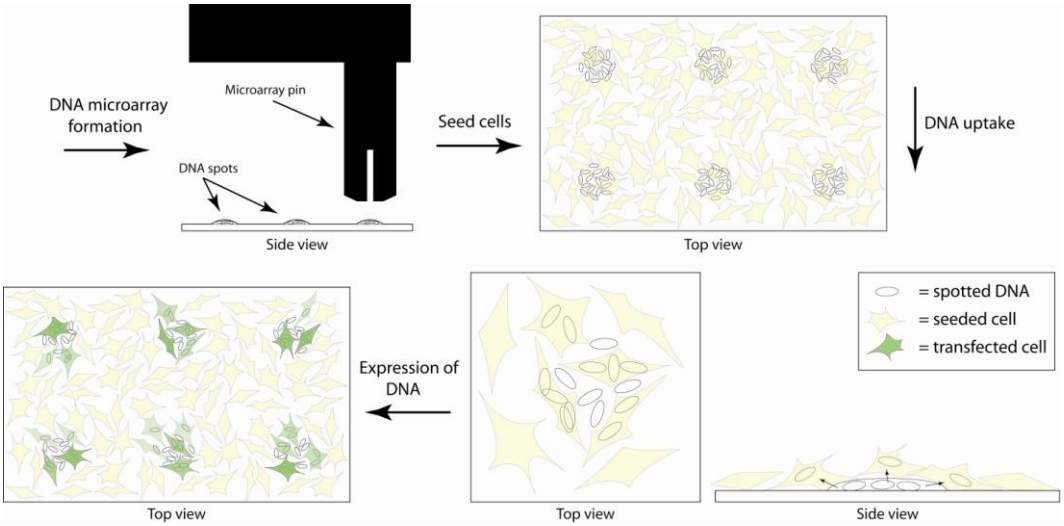

Figure 1.8. *Schematic of the formation of a transfected cell microarray. DNA is transferred to a solid surface using a robotic transfer device. Cells are then seeded and attach to the surface. Cells that attach to the regions where DNA was deposited will firstly uptake and then express the DNA [149]. Schematic not drawn to scale.*

Table 1.1. *Outline of the applications of transfected cell microarrays.*

Application	References
Screening of siRNAs and shRNAs for effective silencing of target genes by RNAi. Use of RNAi for gene function determination.	[150-154]
Development of a reporter system for monitoring the expression of proteins associated with signalling pathways.	[155, 156]
Assignment of the position of subcellular localised proteins.	[147, 157]
Automated analysis of nuclear area, cell area and number of cells.	[158]
Screening for agonists and antagonists of GPCRs.	[148]
Screening for gene products that are involved with kinase signalling pathways, stimulation of apoptosis or cell-cell adhesion.	[8]
Monitoring the interaction of receptor molecules with membrane-bound signal proteins.	[8, 159]
Use of linear polymerase chain reaction (PCR) products for TCM format.	[155]

Overexpressing a defined cDNA is useful for the genomic analysis of proteins of interest that are functioning within their natural environments. Receptor proteins have been a focus of these studies and, in particular, the screening of activators and inhibitors of GPCRs [148]. As GPCRs are currently the target of 40% of commercial drugs, determining the functionality and binding properties of unstudied GPCRs will likely determine other potential drug targets. Furthermore, microarray analysis of these receptors in a microarray format enables the high-throughput examination of the selectivity of drugs and identification of any side-reactions.

Recently, RNAi has been demonstrated on TCMs [150, 152-154]. RNAi for mammalian cells involves the use of either short (<30 nucleotides) interfering RNA molecules or the transfection of DNA constructs that induce the expression of short hairpin RNAs that interfere with the homologous messenger RNA to specifically silence the corresponding gene [160]. Double-stranded RNA strands longer than 30 nucleotides activate the interferon response within mammalian cells and are, therefore, not only useful for gene silencing assays in prokaryotic cells. Combined with TCMs, RNAi enables the high-throughput determination of the function of genes by observing the phenotypic effects of gene silencing. RNAi can be of even greater use for determining gene function than the over-expression of cDNAs, since the latter can give misleading results through the formation of unnatural phenotypes.

TCMs have three primary limitations. Firstly, an appropriately patterned substrate material that allows spatial control over both DNA and cells in order to effectively separate adjacent cell and DNA sites must be developed. This is important, not only for stringent confinement of DNA and cells to localised and addressable locations, but also for ease of analysis, whereupon, the lawn of non-transfected cells does not need to be discerned from transfected cells [45]. Secondly, low transfection

efficiencies are reported for reverse transfection experiments [29, 35, 101, 159]. Low transfection efficiencies are detrimental as each colony may consist of as little as 30 cells, thus, in order to gain statistically credible data close to 100% transfection efficiency is desirable. This is often not observed, limiting the technique to cell lines such as HEK and monkey kidney fibroblasts (COS) where relatively high transfection efficiencies are easily obtained [161], thus restricting the ability to study genes in the desired cell lines. Lastly, the requirement to accurately observe phenotypic changes within tens of thousands of cell colonies in a high-throughput fashion imposes a formidable challenge for TCM assay development.

1.4.4.1. Methods to generate DNA microarrays

The first step for TCM construction is the spatially controlled deposition of DNA in a microarray format. This is typically achieved by either contact printing or non-contact printing with a robotic spotter, μCP or on-chip DNA synthesis [15, 82, 94, 162]. DNA-gelatin mixtures are often utilised to ensure spatial confinement of DNA by physical entrapment [8, 101]. This can also be achieved by producing a surface with variations in hydrophilicity that effectively confine a DNA droplet to the hydrophilic regions, enabling DNA adsorption only in confined regions [100].

Spatial control of DNA has also been achieved utilising the electro-responsive nature of DNA to form switchable patterns of DNA on a microelectronics chip [92]. By application of the appropriate positive and negative voltages DNA can be spatially confined. The advantage of this system is the ability to induce surface diffusion of DNA by reversing the polarity of the applied voltage. This technique is limited by the pattern of the electrodes but combines spatial control with switchability for advanced DNA surface manipulation.

Although currently not utilised for TCM applications, the development of an on-chip DNA growth method enables high-density, spatially controlled DNA arrays to be formed that could be advantageous for TCMs provided this DNA could be taken up and successfully expressed by cells (see section 1.2.1).

For TCM applications obtaining high DNA surface concentrations is essential for enhancing transfection efficiencies. It is unlikely that DNA deposited at a particular location is taken up entirely by the cells seeded upon it, thus, one must ensure an excess of DNA by producing surface chemistries with the ability to sustain high DNA surface concentrations. However, DNA immobilisation must also be reversible so that the DNA can be subsequently taken up by cells [34]. Indeed, transfection efficiency has been shown to vary significantly with varying surface chemistries [29], demonstrating the importance of optimising DNA-surface interactions for TCM applications. In order to achieve this various surface chemistries and their interactions with DNA have been studied.

Generally, the adsorption of DNA onto a given surface is based upon two binding interactions, attractive electrostatic forces governed by the negative charge of the DNA phosphate groups and oppositely charged functional groups on the substrate surface as well as hydrophobic effects in aqueous medium associated with the interactions of nucleobases and nonpolar surface-bound moities (see section 1.1.2) [18, 19]. Hydrophobic effects are more significant for ssDNA as compared with dsDNA due to the role of nucleobases, which are imbedded within the core of a helical dsDNA strand but comparatively exposed within ssDNA.

Electrostatic interactions of surfaces with DNA have been the primary focus for enabling high DNA surface concentrations; thus, formation of positively charged surfaces is often desirable for DNA adsorption experiments. This is commonly

achieved by the production of amine rich surfaces, which are typically protonated at physiological pH. Common strategies for the formation of aminated surfaces are silanisation of glass, the adsorption of cationic molecules such as PEI and plasma polymerisation of amine containing monomers [24, 34, 42]. The use of cationic polymers is particularly useful for TCM applications as complexes formed between DNA and unbound cationic polymers can efficiently permeate the cellular membrane [163].

1.4.4.2. Cell seeding and attachment

Successful seeding and attachment of cells requires an adherent cell line and a biocompatible surface. There are many suitable surfaces for cell microarray formation including glass, silicon and tissue culture polystyrene, all of which are amenable to a variety of surface modifications. Furthermore, a method has been developed whereupon non-adherent cell lines are immobilised on a surface, increasing the scope of cell lines applicable for the TCM method [164]. This was achieved by modifying a glass surface with oleyl poly(ethylene glycol) ether, which acts as an anchor for subsequent membrane attachment.

TCMs can benefit from advanced cell patterning techniques if these methods can restrict cell attachment to regions where DNA has been deposited previously and prevent the migration of DNA or transfected cells. Research on cell patterning has focussed on producing 'black-and-white' patterned surfaces containing both bioactive regions that support protein and cell attachment, and non-adhesive regions that resist biomolecule attachment. As cells attach to a surface by the production of surface adhering proteins the manipulation of protein adsorption and cell attachment are closely related. A technical review of the various approaches to modifying surfaces for patterned cell growth has been recently published [66]. Strategies for

surface patterning are varied and include microfluidics, μCP, ultramicroelectronics, photolithography, soft lithography, laser ablation and robotic contact and non-contact printing (see section 1.2) [33-35, 52, 53, 74, 76-78, 80, 86, 88, 95, 165]. An outline of the various surface patterning techniques, their advantages and disadvantages and their application to TCMs is given in Table 1.2. Utilising methods including microfluidics and photolithography, the resolution of cell microarrays has been reduced to single-cell microarrays and these microarrays have been used for biological analysis such as monitoring Ca^{2+} mobilisation [165, 166].

A common strategy for promoting cell attachment is the functionalisation of a surface with proteins such as collagen, fibronectin, vitronectin or the immobilisation of integrin binding peptides such as RGD, a peptide representing a cell adhesion mediating sequence within fibronectin [33, 52-54].

Apart from effects based on the surface chemistry, the effects of topographical cues to initiate and control the attachment, proliferation, orientation and migration of cells and tissue samples on surfaces have been investigated (see section 1.1.3) [47, 56, 57, 62].

Table 1.2. *Description of various surface patterning techniques for spatially controlled cell attachment.*

Technique	Advantages	Disadvantages	Typical procedures	Cell microarray application	References
Photolithography	Sub-micron resolution pattern formation.	Rigorous laboratory procedures. Expensive maintenance costs. Clean environment required.	Deposition of a photoreist or a photoactive layer. Subsequently irradiate, typically with UV light, through a photomask.	Formation of patterned bioactive or non-fouling regions for spatially controlled cell attachment. Formation of topographical cues for directed cell attachment and outgrowth.	[53, 78, 80]
Laser ablation	Sub-micron resolution pattern formation. Controlled depth and rate of ablation. Adaptable to any ablatable surface.	Rigorous laboratory procedures. Expensive maintenance costs. Clean environment required.	Formation of an ablatable layer with subsequent laser irradiation, either thorough a mask or by a focussed layer.	Formation of patterned bioactive or non-fouling regions for spatially controlled cell attachment. Formation of topographical cues for directed cell attachment and outgrowth.	[33-35]
Microcontact printing	Lower costs and relative experimental ease. Micron resolution pattern formation.	Limited number of molecules and substratum that can be used.	Formation of a photomask for the formation of a patterned stamp. Stamp is then used to transfer thiolated SAMs onto gold or silanes onto glass.	Deposition of either bioactive or non-fouling molecules for spatially directed cell attachment	[76, 86, 88]
Microfluidics	Relative experimental ease. Ability to separate reaction solution.	Poor resolution. Limited patterns.	Formation of a PDMS mask from a mold contining grooves. Sealing of mask onto surface creates channels. Solution containing desired molecules or cells is flowed through channels.	Formation of single-cell microarrays and arrays of various cell lines by controlled delivery of cells to localised regions.	[52, 74, 165]
Microelectronics	Separates various cell types. Induces surface migration of cells. Effectively positions and holds cells spatially.	Poor resolution. Limited to the dimensions of the microelectronic s chip. Only applicable to limited cell lines.	Use of microelectronics chip containing an array of individual electrodes is used to apply specific voltages to localised regions.	Application of appropriate voltages leads to cell separation on the basis of distinct dielectric properties between different cell types.	[77]
Robotic contact and non-contact printing	Quick and simple pattern formation. Micron resolution.	No mechanism for spatial confinement once patterning completed. Patterned shape limited to pin (contact printing). Uneven adsorption of biomolecules in each spot.	Spotting of biomolecules onto localised addressable regions.	Cell microarrays have been formed spotting cell patterns by robotic arms.	[94, 95]

Several strategies have demonstrated the ability to reduce protein adsorption, including the surface immobilisation of carbohydrates. However, by far the most commonly used and most effective strategy for the formation of non-fouling surfaces available today is the surface grafting of PEG [66]. A number of surface modification methods designed to reduce non-specific protein adsorption based on PEG coatings have been discussed previously [66].

1.4.4.3. DNA uptake

The third step in the fabrication of a TCM is the uptake of DNA by cells from the surface. This step includes three primary processes, release of DNA from the surface, diffusion of DNA to the cell surface and transportation of DNA across the cellular membrane and, typically, into the nucleus. Low transfection efficiencies are likely due to a failure in one of these processes.

As previously discussed, DNA adsorbs to surfaces by hydrophobic or electrostatic interactions (see section 1.1.2). Therefore, releasing the DNA from the surface is achieved by reversing these interactions. Switching the hydrophobicity at a surface can be achieved using hydrogels that respond to temperature changes at their lower critical solution temperature by altering between hydrophobic and hydrophilic states. This system is readily used for producing switchable cell attachment [64, 73], but has not been demonstrated for DNA interactions. Hydrophobicity can also be altered by solvent changes, however, this is unsuitable for cell cultures. The easiest means of effecting DNA release from a surface is by changing the surface charge, typically achieved by application of a voltage. Temporal control of DNA adsorption and desorption has been extensively studied by electrochemical techniques [18, 106, 108].

Once released from the surface, DNA is able to diffuse in solution, soon contacting the surface of cells that are growing above the DNA loaded patches. From here, the polyanionic DNA must permeate the cell membrane, which typically also has an overall negative charge. From the methods usually used to facilitate transfection, only few can be used in a solid phase transfection scenario.

Commonly, transfection reagents such as the commercially available Effectene and Lipofectamine^{TM} reagents, are used to assist transfection in TCMs [8, 35, 101]. The transfection reagent is either mixed with DNA before spotting or afterwards, added on top of the DNA spots. Alternatively, inclusion of cationic polymers into the substratum enhances transfection due to the increased capacity for the surface binding of DNA resulting in an increased DNA concentration at the surface of attached cells and increased membrane permeability of DNA-cationic polymer complexes, which have a lower surface charge than bare DNA [163, 167].

A limited number of transfection methods have also been described for TCM applications as alternatives to the use of cationic polymers. Lentiviruses have been utilised for the transfection of a number of primary and transformed mammalian cells in a cell microarray format for both the overexpression of a particular gene and RNAi studies [168, 169]. Lentiviruses are advantageous over other transfection techniques in their ability to transfect a wide variety of cell types with a high efficiency. Another method developed to enhance DNA uptake is the use of electroporation [170]. The advantages of this approach is its ability to initiate both DNA release from the surface and subsequent uptake into the cells through transient pores in response to the application of a voltage.

Of particular interest have been studies showing that the interactions of ECM proteins enhance transfection efficiency [171-173]. The particular type of ECM

protein that will enhance transfection efficiency depends on the cell line used. For example, the use of collagen IV as a surface coating improved transfection efficiency up to 8-fold in PC12, where fibronectin showed little effect [172]. This contrasts with previous studies done with HEK cells, human mesenchymal stem cells, Henrietta Lack (HeLa) cells, normal mouse fibroblasts and human hepatocellular liver carcinoma where high solid state transfection efficiencies were achieved with the addition of fibronectin [173]. The postulated mechanism for ECM proteins promoting transfection efficiency is the mechanical stress that these proteins inflict upon the cellular membrane, easing the uptake of DNA through the stressed cell membrane.

A number of proteins such as transferrin, adenoviral penton protein and human immunodeficiency virus Tat protein have also been shown to improve transfection efficiency and have been applied to TCM applications successfully [155]. Of all proteins used, inclusion of the adenoviral penton protein has achieved the highest transfection efficiencies. The mechanism for this is unknown.

1.4.4.4. DNA expression

The final step in the formation of a TCM is the expression of the uptaken DNA by the cell. This process is complex and beyond the scope of this chapter.

Green fluorescing protein (GFP) is often used as a reporter protein to ensure that a particular plasmid has been taken up and is being expressed intracellularly. Interestingly, a variance in the intensity of fluorescence of cells transfected by a GFP encoding gene has been noted and the fluorescence intensity seems to correlate with the number of plasmids or DNA fragments taken up by a cell.

One of the challenges for TCMs is the analysis of potentially thousands of individual cell colonies each displaying a different phenotype, often requiring

imaging not only of cell clusters, but also of single cells and at the subcellular level. Fluorescent microarray scanners are useful for the quick production of an image of the entire array, however, the development of fluorescence scanning microscopes, which are able to automatically locate, focus and acquire images of individual cells, enables high-resolution, subcellular imaging. Considering the vast number of images potentially generated an automated, high-throughput, reproducible strategy for subsequent analysis is important. A number of software programs have been developed for this purpose. One such approach enabled survey analysis of nuclear area, total cell area and number of cells by software analysis of the red, blue and green channels from fluorescence images taken of cells stained with various subcellular localised dyes enabled the [158]. The automated accrual of images of transfected cells has also been used to generate an automated classification system whereupon. By reference to a set of assigned images, the subcellular position of expressed GFP tagged proteins was detected and assigned [147].

1.5. Conclusion and future perspectives

The development of mechanisms and devices for the advanced surface manipulation of biomolecules is an exciting field of research that promises valuable tools for scientists pursuing sophisticated biological studies or developing advanced biodevices. Surface manipulation of biomolecules currently permits spatial control over biomolecule placement via patterned surface chemistry or topography and temporal control over the attachment, adsorption or association and detachment, desorption or dissociation events via switchable surfaces. Limited research has also demonstrated control over surface diffusion of biomolecules, which is an exciting new dimension to the manipulation of biomolecules on a surface. A number of

techniques have been developed to achieve these various abilities, however, the most interesting and useful systems are those that combine patterns on the micro- or even nano-scale and switchable architectures to achieve both temporal and spatial control over biomolecule surface interactions.

Recent studies have shed some light on understanding the processes involved with the adsorption and desorption of DNA at the solid/liquid interface. As a stable polyelectrolyte with in-built molecular recognition properties, DNA is an interesting and unique biomolecule, and owing to its biological importance it is an ideal focus for the development of biodevices. The manipulation of DNA on a surface requires control over electrostatic and hydrophobic interactions, the driving force for DNA adsorption. Typically, low pH and high salt concentrations enhance DNA adsorption. These principles have been utilised recently to improve DNA based biodevices for example TCMs.

The manipulation of cells at surfaces has been an area of significant recent research interest. Chemical, biological and topographical cues have been all shown to be effective in controlling cell surface interactions. Generally, the control of cell attachment is achieved via the manipulation of the proteins that the cells themselves produce to mediate their attachment to surfaces. Protein adsorption, driven largely by hydrophobic forces, has also attracted much interest, and the ability to pattern surfaces with proteins enables cell patterning. Key discoveries have led to patterned cultures of cells with micron resolution using a wide variety of cell types and substrate materials. The development of switchable systems for cell attachment has enabled formation of patterned co-cultures of cells and opens up exciting possibilities for applications in tissue engineering and stem cell research.

A number of biodevice applications will benefit from the further development of biomolecules manipulation and an advanced understanding of the underlying phenomena. In particular, the recently developed transfected cell microarray method will be optimised and its scope expanded to a wide range of cell lines and primary cells. Already key steps have been taken to confine cell colonies to localised regions, to improve transfection efficiency, to adapt the approach to cells that are notoriously difficult to transfect or even non-adherent. One can easily envisage systems being developed where cells and DNA are delivered with high precision and speed for formation of high-density cell co-cultures that will not only be useful for genomic and proteomic analysis, but also for stem cell differentiation experiments and tissue engineering.

The development of TCMs is both an exciting and important development for the high-throughput determination of gene function, which is important for combating genetic based disorders such as cancer and for the identification of potential drug pathways. The increased understanding of DNA-surface interactions and the development of advanced material surfaces with the ability to temporally and spatially control biomolecule manipulation, formed by the use of high-resolution patterning techniques, provides the means to develop highly functional and reliable platforms for advanced genomic analysis. The continued development of RNAi on TCMs for high-throughput loss-of-function studies and the development of methods enabling highly resolved subcellular phenotypic examination will enable more in-depth studies, not only into gene function but also into the machinery involved in gene expression. The means to optimise the DNA microarray formation, cell seeding, DNA uptake and expression are within grasp and no doubt will result in the implementation of an advanced genomic analysis tool that is adaptable to a wide

variety of gene functions and cell lines. Furthermore, the development of cDNA and RNAi genome wide libraries would enable the high-throughput, rapid and inexpensive analysis of entire genomes, with each gene either overexpressed or silenced at defined cell clusters, all upon a single glass slide.

However, a number of key issues must be resolved before TCMs can become the high-throughput tool that is desired. Methods to manage low transfection efficiencies and effective colony separation needs to be developed. Recent developments discussed in this chapter point to a solution of these problems. The greatest foreseeable challenge is the ability to process tens of thousands of colonies, all potentially with a varied phenotype. A number of automated fluorescence systems are being developed, and further progress in this area is essential for the successful implementation of TCMs. The use of fluorescence tags and GFP as a reporter gene are pivotal to this analysis and have been used successfully for a number of gene function studies. However, the further development of other screening methods that infer gene function would broaden the scope of TCM applications to study phenotypes where fluorescence tagging or staining is not viable.

II

CHAPTER 2. SPATIALLY CONTROLLED ELECTRO-STIMULATED DNA ADSORPTION AND DESORPTION FOR BIODEVICE APPLICATIONS

The content of this chapter is based upon references [34, 174, 175].

2.1. Introduction

The development of biodevices, which includes systems for 'smart' drug delivery, tissue engineering, biosensing, biomimetics, implant biocompatibility and microarray technology [3-8] promises to provide solutions to a vast array of biomedical problems by enabling the manipulation and study of biomolecules and living cells in a controlled, high-throughput and/or application specific fashion. The development of DNA and protein microarray technology has been particularly successful in revolutionising the way scientists have been able to study gene expression by providing a high-throughput method of analysis where entire genomes can be studied on a single array [101, 176]. In recent years, the scope of microarray technologies has been broadened by the development of a transfected cell microarray (TCM) [8] consisting of complementary DNA (cDNAs) arrays spotted onto a glass slide at addressable locations. Human embryonic kidney (HEK) cells seeded onto this DNA array were observed to take up DNA creating regions of localised transfection within a lawn of non-transfected cells [8]. Despite the successful application of TCMs a number of inherent limitations remain unsolved. A successful mechanism for the prevention of cross-contamination of cells and DNA between adjacent colonies or DNA spots has not been achieved, which limits the effective density of these arrays. TCMs also suffer from low transfection efficiencies limiting their use to cell lines

that are easy to transfect. Furthermore, as potentially thousands of cell colonies can be produced all with a slightly different phenotype, processing of these cell arrays is time consuming, particularly when differences are subcellular and subtle, making it difficult to differentiate between transfected cells and the lawn of non-transfected cells Recently, a platform for a transfection chip using plasma polymerisation-based modification of substrate materials was developed [35]. Plasma polymerisation refers to the formation of highly crosslinked polymerised material by use of a monomer in the plasma state [38] and can be used to effectively modify surfaces with a thin, well adherent polymer layer that, by the choice of the monomer, contains the desired functional groups without altering the substrate's bulk properties. Plasma polymerisation has been achieved with monomers containing alcohol, amine and carbonyl functiona groups to produce plasma polymers with equivalent functionality [177-179]. This is also a solvent free process, which prevents the presence of potentially toxic residual solvent molecules, increasing the biocompatibility of this material. Allylamine has previously been used as a monomer to produce an amine-rich allylamine plasma polymer (ALAPP) and have used this surface for the subsequent high-density grafting of poly(ethylene glycol) (PEG) [35]. Excimer laser ablation was then used to produce regions of ALAPP, which sustains cell growth, and PEG, which has been shown to resist cell attachment [33]. Yet, the amine functionaities of ALAPP, in their protonated state, are of additional use as they undergo electrostatic interactions with the negatively charged phosphate backbone of DNA [36, 180]. ALAPP coated surfaces should, therefore, lend themselves to the surface-retention of DNA. The investigation of spatially controlled DNA adsorption on this substrate would aid in the development of a highly useful substrate surface

with application for biodevices in general and transfected cell microarrays in particular.

The effectiveness of transfected cell microarrays is hampered somewhat by the low transfection efficiencies previously documented when DNA undergoes endocytosis if adsorbed to a surface [35, 159], henceforth termed 'solid phase transfection'. The reasons for diminished solid phase transfection efficiency in comparison to transfection with vectors dispersed in an aqueous phase are not well understood. It is plausible that the 'stickiness' of DNA on the surface impedes or slows down cellular internalisation. Transfection efficiency could be enhanced by initiating the controlled release of DNA from a suitable substrate surface once a cell lawn has formed. The use of a voltage bias as the stimulus for controlled adsorption and desorption of DNA has been extensively studied on metal electrodes [105, 106].

In the present chapter, the production and characterisation of a chemically patterned surface that allows spatially controlled cell attachment and DNA adsorption was performed. The method is depicted in Figure 2.1. Here, highly doped p^{++} (low resistivity) silicon wafers have been used as a substrate material. After cleaning of the silicon wafer and ALAPP deposition, an aldehyde terminated PEG polymer was grafted onto the ALAPP layer using reductive amination [181]. Subsequent use of masked excimer laser ablation produced the desired patterned surface. This platform has also been investigated for TCM applications. Once the chemically patterned surface was formed, DNA was spotted onto the ALAPP regions, where protonated amine groups assisted in the adsorption of DNA, preventing desorption of the DNA into solution. Cells were then seeded onto this surface and only attached on the ALAPP regions. Finally, the cells were analysed for evidence of successful transfection.

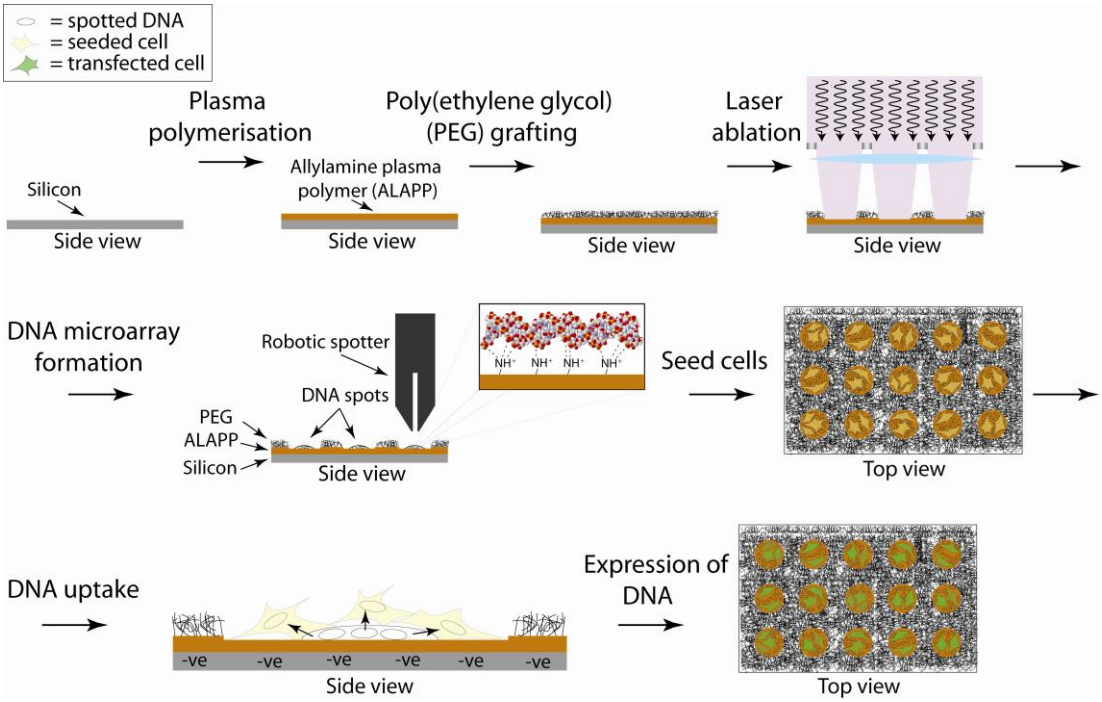

Figure 2.1. *Schematic of the formation of a TCM. Silicon was modified sequentially by plasma polymerisation and PEG grafting. Laser ablation was used to form ALAPP wells, a robotic arrayer was then used to spot DNA into these wells. Cells seeded onto this surface grew exclusively within the wells, on top of the DNA spots. Application of a negative voltage triggered the release of DNA from the surface, making it available for uptake by nearby, adhered cells. Transfected cells are depicted as green. Schematic not drawn to scale.*

The adsorption and desorption of oligonucleotides and plasmid DNA to ALAPP was manipulated by the application of an appropriate DC voltage to the semi-conducting silicon substrate in order to study the spatially controlled electro-stimulated manipulation of DNA. Furthermore, the subsequent growth and transfection of mammalian cells was conducted as depicted in Figure 2.1. Here, the enhancement of transfection efficiency by electro-stimulated DNA desorption was of particular interest.

The unique combination of patterned and switchable components of this device allows unprecedented control over the behaviour of cells and DNA in four dimensions. This approach is useful for overcoming the current limitations of TCMs and is promising for broader applications in advanced biodevices.

2.2. Materials and methods

2.2.1. Substrate preparation

Boron doped p^{++} silicon wafers (Virginia Semiconductors, Inc.) were cut into approximately 10 x 10 mm^2 pieces, cleaned by sonication for 30 min in a 5% surfactant (RBS 35, Pierce USA) solution and oxidised under UV light for 30 min.

2.2.2. Plasma polymerisation

Plasma polymerisation reactions were preformed in a custom-built reactor described elsewhere [182]. In short, the plasma reactor consisted of two circular electrodes separated by 125 mm in a cylindrical reactor being 350 mm high with a diameter of 170 mm. Allylamine (Aldrich, 98% purity) was used as a monomer.

Polymerisation conditions used were a frequency of 200 kHz, a power of 20 W and an initial monomer pressure of 0.188 mbar. Deposition time was 25 s.

2.2.3. Poly(ethylene glycol) grafting

PEG monoaldehyde (Shearwater Polymers, Huntsville AL, USA) with a molecular weight of 5000 was grafted onto freshly deposited ALAPP layers by reductive amination. Grafting was performed under 'cloud point' conditions in 20 ml of a 0.1 M sodium phosphate buffer containing K_2SO_4 (2.2 mg), $NaCNBH_3$ (60 mg) and PEG (50 mg) at pH 6.2. Freshly deposited ALAPP films were incubated in the PEG grafting solution at 60 °C for 16 hr.

2.2.4. Excimer laser ablation

Ablation experiments were conducted using a 248 nm KrF excimer laser Series 8000 (Exitech Limited, UK) equipped with a Lambda Physik LPX210i laser source. The beam delivery system contained beam shaping and homogenisation optics to create a uniform, square beam at the plane of a mask held on an open frame CNC controlled X-Y stage set. The square beam was passed through a chrome-on-quartz mask pattern. The beam was then passed through a 1:10 demagnification lens, NA of 0.3, a 1.5 mm diameter field with a theoretical resolution of 0.8 μm. PEG grafted ALAPP samples on silicon substrates were ablated at an energy density of 60 mJ/cm^2 and 4 pulses of 20 ns duration per area to form a spatially patterned substrate. The laser ablated pattern is shown in Figure 2.2. Light microscope images of the ablated pattern were taken with an Olympus SZ-STS light microscope and a charge coupled detector (CCD) colour video camera. Images were captured using Data translation, Inc. DT Acquire v3.3.0 software.

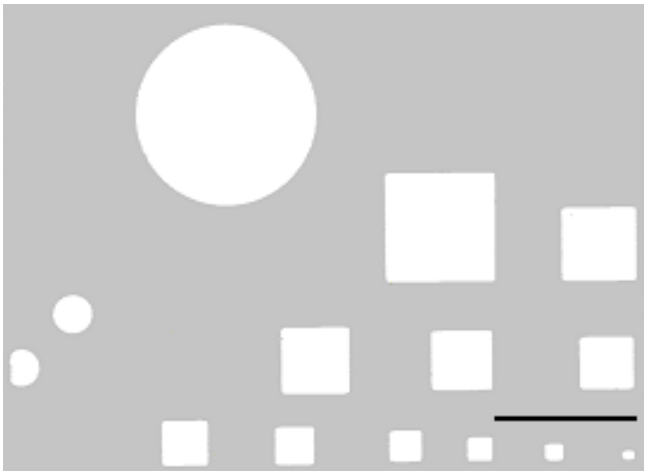

Figure 2.2. *Light microscope image of the pattern ablated onto the ALAPP coated, PEG grafted Si wafers. The scale bars equal 200 μm.*

2.2.5. X-ray photoelectron spectroscopy

X-ray photoelectron spectroscopy (XPS) was conducted on an AXIS His spectrometer (Kratos Analytical Ltd.) equipped with a monochromatised Al K_α source. The pressure during analysis was typically $5x10^{-8}$ mbar. The elemental composition of surfaces was determined from survey spectra, collected at a pass energy of 320 eV. High-resolution spectra were obtained at a pass energy of 40 eV. Binding energies were referenced to the aliphatic hydrocarbon peak at 285.0 eV. Peak fitting of high-resolution spectra was conducted with Vision 1.5 software, Kratos Analytical Ltd.

2.2.6. Fourier transform – infrared analysis

ALAPP samples were deposited onto KBr disks. Transmittance Fourier transform – infrared (FT-IR) analysis was conducted on a Nicolet Avatar 130 MLT, Thermo Electron Corporation.

2.2.7. Plasmid propagation

Plasmids pEGFP-N1 (4.7 kb) (Clontech), encoding the green fluorescing protein (GFP) (ex 470 nm, em 509 nm), were propagated in the JM109 *Escherichia coli* (*E-coli*) strain (Promega). Cells were transfected with plasmid using the heat shock method. Plasmid was isolated using the QIAprep® Miniprep Kit (Qiagen) according to the manufacturer's specifications. Isolated plasmid was characterised by UV-Vis quantification and restriction enzyme digest with Ssp1 and Sph1 (New England Biolabs) with subsequent agarose gel electrophoresis. Quantification of DNA bands

in the gel was achieved using the Molecular Dynamics FluorImager 595 and ImageQuant software 4.1, Molecular Dynamics.

2.2.8. DNA adsorption and desorption studies

DNA adsorption and desorption studies were initially conducted in a custom-built flow cell, as depicted in Figure 2.3, used in conjunction with a Leitz Fluorescence microscope. The flow cell consisted of a steel bottom plate that the substrate could be clamped to by placement of a moulded silicone rubber piece, cover slip and an acrylic top plate. A platinum counter electrode was clamped between the silicone rubber mould and the cover slip. The circular silicone rubber piece with a central square cavity was formed by curing Sylgard 184 silicone elastomer kit in a brass mould for 30 min at 280 °C after mixing of the elastomer components and extensive degassing in vacuum. Polypropylene tubes (diameter = 1 mm) were positioned in the mould before curing. The final volume of the flow cell chamber was 100 μl. Patterned ALAPP modified PEG grafted samples were clamped into the flow cell and 200 μl of ultra pure water was injected. After washing, 10 μl of 290 ng/μl 6-carboxyfluorescein (6-FAM) labelled (ex 497 nm, em 514 nm) 16-mer oligonucleotide (5'-FAM-GCCAGAAGCCAGTACT-3') (Geneworks) solution in ultra pure water was injected into the flow chamber and adsorption was observed. Positive voltage (0 – 2 V) was applied to the surface with a platinum wire counter electrode for typically 2 min to investigate electro-induced DNA adsorption. Likewise, negative voltage (0 – -2 V) was applied to the surface with a platinum wire counter electrode for typically 2 min to investigate electro-induced DNA desorption. Ultra pure water was injected to remove unbound DNA at various stages and for final washing.

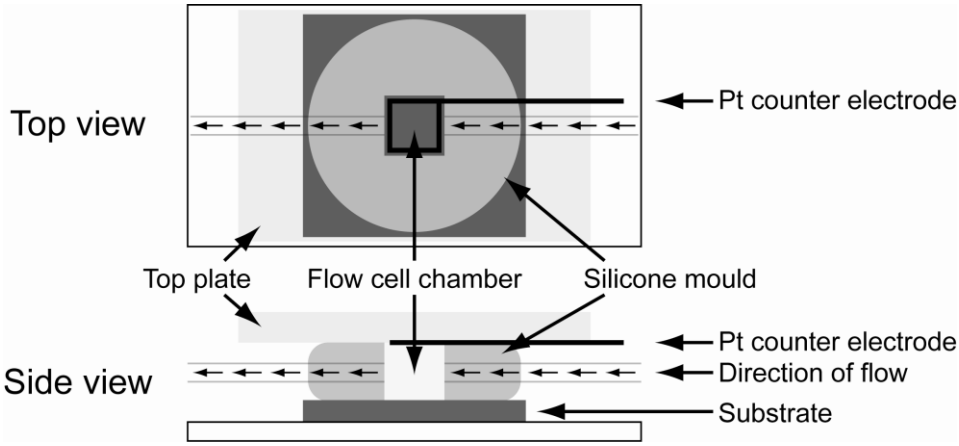

Figure 2.3. *Schematic of the flow cell used for DNA adsorption and desorption studies. The flow cell was formed by the consecutive stacking of a steel base plate, the substrate, a moulded silicone rubber piece with tubing to allow the flow of solvent to a central cavity that formed the flow cell chamber, a platinum counter electrode, a cover slip and an acrylic top plate.*

Quantitative studies were conducted in a custom-built electrochemical cell as described previously [124]. ALAPP samples were clamped into the cell and 2 ml of 200 ng/ml pEGFP-N1 solution in saline (0.1 M NaCl) 0.01 M phosphate buffer (PBS), pH = 7.4 was added over the sample. After 24 hr incubation at room temperature, a voltage was applied in a stepwise fashion (+1.5 V – -2V) over consecutive 2 min intervals with the substrate as the working electrode, an Ag/AgCl/saturated KCl reference electrode and a platinum auxiliary electrode. The DNA concentration of the solution was measured using PicoGreen® (ex 502 nm, em 523 nm) (Molecular Probes) according to the manufacturer's specifications before and after each voltage application. Solution removed for DNA concentration analysis was replaced with fresh PBS. Fluorescence was detected using a Perkin Elmer Instruments Luminescence Spectrometer LS 55.

2.2.9. Solid phase transfection

ALAPP substrates used for transfection and cell growth experiments were sterilised by incubation in ethanol (70%) for 15 min after which they were washed in sterile ultra pure water and allowed to air dry in a sterile laminar flow hood. Other consumables were sterilised by autoclaving for 15 min at 120 °C. Human embryonic kidney cells (HEK 293) were cultured in Dulbecco's modified eagle media (DMEM) containing 10% serum, penicillin and streptomycin and incubated at 37 °C, 5% CO_2 and 60-70% humidity. Identical incubation conditions were used for transfection experiments. Transfections were conducted on ALAPP substrates with the plasmid pEGFP-N1. 0.5 μl of a 240 ng/μl pEGFP-N1 solution was spotted onto the substrate surface with a typical area of 1.7 mm^2 and allowed to air dry in a sterile laminar flow hood. After drying, the DNA spots were rehydrated with 1 μl sterile ultra pure

water to ensure even DNA dispersion. Effectene Transfection Kit (Qiagen) was used to enhance transfection efficiency. To prepare the transfection solution, 4 μl enhancer was added to 37 μl DNA condensation buffer (EC buffer) and incubated at room temperature for 10 mins. 6 μl effectene was then added and after vortexing, 0.5 μl of the complete transfection solution was dispensed over the bound DNA and allowed to air dry. Patterned ALAPP/PEG surfaces were arrayed with DNA using a Perkin Elmer Piezoarray. Typically 300 pl of solvent was dispensed per spot. pEGFP-N1 was spotted at a concentration of 0.1 mg/ml. Prepared transfection reagent was diluted 4x and spotted on top of the DNA. Samples were then washed with PBS, pH = 7.4 and placed in a custom-built transfection cell. The cell was machined from Teflon to produce a cube-shaped incubation chamber with dimensions of 2x2x2 cm^3. Samples placed in the cell were clamped into position by stainless steel screws. Contact of the screws with the sample enabled the application of a voltage to the samples. HEK 293 cells were seeded at $1.0x10^5$ cells/cm^2 to the transfection cell and DMEM media was added to a total volume of 4 ml. After 4 hr incubation, -750 mV was applied for 0, 0.5, 1 and 5 min with the substrate as the working electrode, an Ag/AgCl/saturated KCl reference electrode and a platinum auxiliary electrode. Cells were incubated for further 20 hr before being characterised microscopically. HEK 293 cells were counterstained using the Hoechst 33342 dye (ex 350 nm, em 460 nm) (Molecular Probes), which is incorporated into the nucleus of all living cells, enabling the visualisation of the total cell population. Cells were incubated in 10 μg/ml Hoechst solution for 10 min, after which cells were washed with PBS, pH = 7.4. Cells growing over DNA spots were visualised with a Leitz fluorescence microscope and images were captured using a Nikon Digital Sight DS-L1 and a Nikon Digital Sight DS-SM camera head. The total number of cells

expressing pEGFP-N1 and the total cell population was calculated and the transfection efficiency was determined by dividing the number of transfected cells by the total number of cells.

2.3. Results and discussion

2.3.1. Characterisation of polymer films

Chemical characterisation of untreated and surface modified p^{++} Si wafers was carried out by XPS analysis. The elemental composition of each surface was determined from survey spectra (Table 2.1). High-resolution XPS spectra of the C 1s peak are shown in Figure 2.4. Both C 1s spectra could be de-convoluted into four components. In order of ascending binding energy, the four peaks correspond to aliphatic (C-H and C-C) carbon at 285.0 eV, C-O and C-N groups at 286.5 eV, amide and carbonyl groups at 288.0 eV, and ester and carboxylic acid groups at 289.0 eV. The quantification of the C 1s high-resolution spectra is summarised in Table 2.2.

Table 2.1. *Surface elemental composition (in atomic %) and nitrogen/carbon and oxygen/carbon elemental ratios for samples used in this chapter as determined by XPS.*

	C	N	O	Si	N/C	O/C
Si	12.9	0.0	34.2	50.8	0.00	2.66
Si-ALAPP	80.0	11.0	9.0	0.0	0.14	0.11
Si-ALAPP-PEG	73.1	5.7	21.0	0.0	0.08	0.29

Table 2.2. *Quantification of components fitted to high resolution C 1s spectra seen in Figure 2.4.*

Binding Energy (eV)	285.0	286.5	288.0	289.0
Si-ALAPP (%)	68.4	23.8	6.1	1.7
Si-ALAPP-PEG (%)	36.3	61.8	1.6	0.3

The absence of a Si signal on the Si-ALAPP surfaces (Table 2.1) strongly suggests that pinhole-free films with a thickness of more than 10 nm (the approximate penetration depth of XPS for polymers) were formed. The oxygen content of this film is due to the uptake of oxygen once it is re-exposed to air by reaction with long-lived reactive species in the polymer film such as free radicals [183, 184]. Upon subsequent grafting of PEG to the amino groups of the ALAPP coating, a significant decrease in the nitrogen content (11.0% to 5.7%) and an accompanying rise in the oxygen content (9.0% to 21.0%) was observed. Furthermore, the C 1s spectrum in Figure 2.4B shows a large increase in the C-O/C-N component and a relative decrease in the aliphatic carbon peak and higher oxidised carbon components as compared with the ALAPP film (Figure 2.4A; Table 2.2). These results suggest not only that PEG was successfully grafted to the ALAPP, but also that amino groups were indeed present on the ALAPP surface. The presence of a nitrogen signal for the PEG grafted surface suggests that this layer is less than 10 nm thick. The theoretical length of a fully extended PEG chain with a molecular weight of 5000 is approximately 42 nm [65]. The large difference between this theoretical value and the observed value is due both to the low persistence length of PEG random coils and to the fact that the XPS measurements were taken in the dry state where the grafted polymer is collapsed. A recent study by Zdryko et al., 2003 [65] reports a greater than 3 fold swelling of the PEG layer in an aqueous environment as compared to a dry sample.

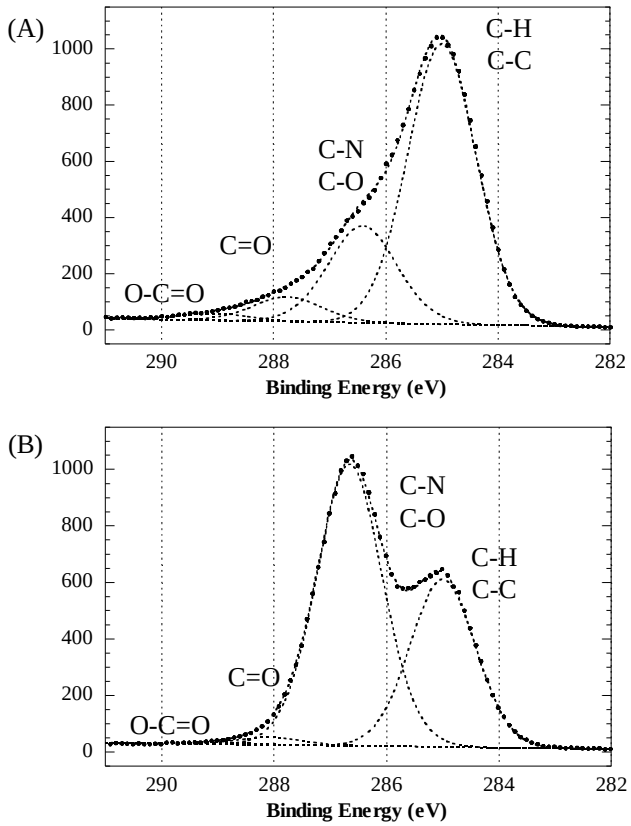

Figure 2.4. *High-resolution C 1s spectra for Si modified with A) ALAPP, B) PEG grafted onto ALAPP. Curves fitted with four components.*

To further characterise the chemical functionality of the plasma polymer films, ALAPP films were analysed by FT-IR. A typical spectrum for an ALAPP film deposited on a KBr disk is shown in Figure 2.5. The large width of adsorption bands is characteristic of the highly cross-linked plasma polymer [183]. An assignment of peaks is given in Table 2.3. Of significance are the large amine signals observed at 1100 cm^{-1} and 3040-3500 cm^{-1} whilst the minimal imide and amide signal seen at 1550-1750 cm^{-1} and the absence of a nitrile signal at 2100 cm^{-1}, suggesting that the nitrogen present with the ALAPP is predominantly in an amine form. However, conclusive quantitative results for FT-IR results are difficult due to the uncertainty of absorbance coefficients, thus, although FT-IR does further confirm the presence of amine functionality, it does not conclusively show the extent to which imine and amide functionalities can be found on the ALAPP film. A much lower imine, amide and nitrile signal is reported compared to previously reported studies [180, 185, 186]. Significant differences between the present procedure and previously used procedures include an alteration in the radio-frequency used to generate the plasma, 200 kHz as compared with 13.56 MHz, and a much lower input power of 20 W as compared with 200 W. This may result in less fragmentation of the monomer and a greater preservation of functional groups as well as the reduced production of reactive species that can result in post-deposition alterations to the film.

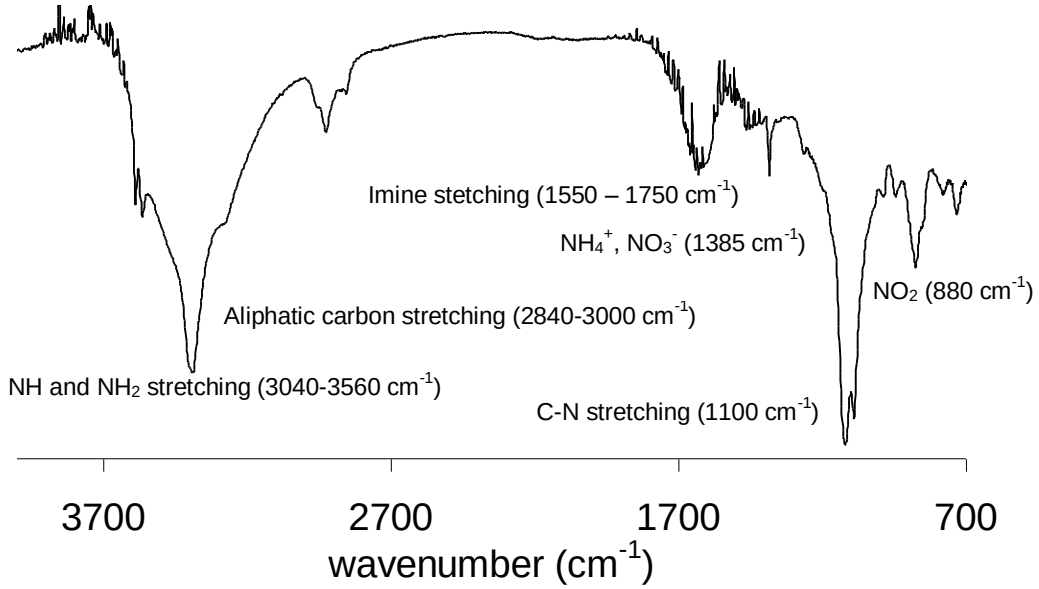

Figure 2.5. *FT-IR spectrum of ALAPP deposited onto KBr disk.*

Table 2.3. *Assignment of the vibrational bands of ALAPP observed by FT-IR analysis.*

Wavenumber (cm^{-1})	Assignment
880	NO_2
1100	C-N primary amine stretching
1385	NH_4^+, NO_3^-
1550-1750	C=N imine stretching, bending amides
2840-3000	Aliphatic carbon stretching
3040-3500	Bonded NH or NH_2 stretching
3390	Free NH_2 stretching
3560	Independent N-H stretch

2.3.2. DNA adsorption and desorption studies

DNA adsorption and desorption from the Si-ALAPP-PEG ablated surfaces was initially studied using a custom-built flow cell. Initially, short (16mer) oligonucleotides labelled with 6-FAM at the 5' end were used.

Oligonucleotide solution was injected over the Si-ALAPP-PEG patterned surface and analysed microscopically. The preferential adsorption of the DNA to the ALAPP regions (green regions) as opposed to the PEG regions (dark regions) was observed (Figure 2.6A), demonstrating the spatially controlled adsorption of DNA [187]. It is suggested that the mechanism for this adsorption is due mainly to electrostatic interactions of surface tethered, protonated amino groups with the negatively charged backbone of DNA. Electrostatic interactions between DNA and cationic polymers has been demonstrated (Appendix 2). The presence of amino groups in the ALAPP film was demonstrated by N 1s high resolution XPS spectra (results not shown), and indirectly by the successful grafting of PEG to the ALAPP film as confirmed by XPS (Table 2.1; Figure 2.4B). As experiments were conducted at a pH 7.4, and given the typical isoelectric point of aliphatic amines is 10.6 [43] the amino groups present on the ALAPP film were expected to be protonated. However, it cannot be said conclusively from the fluorescent images as to whether the PEG coating quantitatively prevents DNA adsorption. Figure 2.6A and Figure 2.6B both show a green background on the PEG regions that could be due to oligonucleotide adsorbing to the PEG surface, to free oligonucleotide in solution or to autofluorescence effects.

The flow cell design allowed the microscopic observation of the surface whilst applying an electrical bias. Spatially controlled DNA adsorption was observed on the ALAPP-PEG surface by visualisation of the green pattern after injection of the

oligonucleotide solution (Figure 2.6A). After the application of a positive voltage (Figure 2.6B), and subsequent washing (Figure 2.6C) the pattern persisted, whilst the pattern disappeared after applying a negative bias (Figure 2.6D) suggesting the complete removal of oligonucleotide. These results can be taken as evidence that the application of a positive or negative voltage stimulated the adsorption or desorption of DNA. However, additional factors such as the stringency of the washings and background adsorption at 0 V bias needed to be considered. A fading of the fluorescence was observed upon successive rinsing, even at +1.5 V bias (data not shown), suggesting that the washing protocol could influence the results of the fluorescence studies. Therefore, to independently investigate voltage bias induced DNA adsorption, an experiment was conducted without washing. Oligonucleotide was injected over the patterned surface (Figure 2.6E) and a higher fluorescence intensity was observed on the ablated ALAPP regions. Once +1.5 V was applied to the surface, an increased fluorescence intensity was observed on the chip surface, suggesting an increase in the amount of DNA adsorbed to the surface due to bias-enforced adsorption of the oligonucleotide to the surface (Figure 2.6F). However, adsorption in this case was not discriminative between ALAPP and the PEG surfaces, suggesting that prevention of DNA adsorption by the PEG layer was overcome by the application of a positive voltage. A similar electrostatic effect has been documented for proteins [84]. Furthermore, the application of -1.5 V resulted in the release of oligonucleotide from the surface as witnessed by a decrease in fluorescence (Figure 2.6G) both on ALAPP and PEG regions, suggesting that the attractive interactions between the DNA and ALAPP are overcome by the application of the negative voltage. However, a faint contrast remains in Figure 2.6G

indicating that a small amount of DNA remains adsorbed to the surface despite the application of a negative bias (-1.5 V).

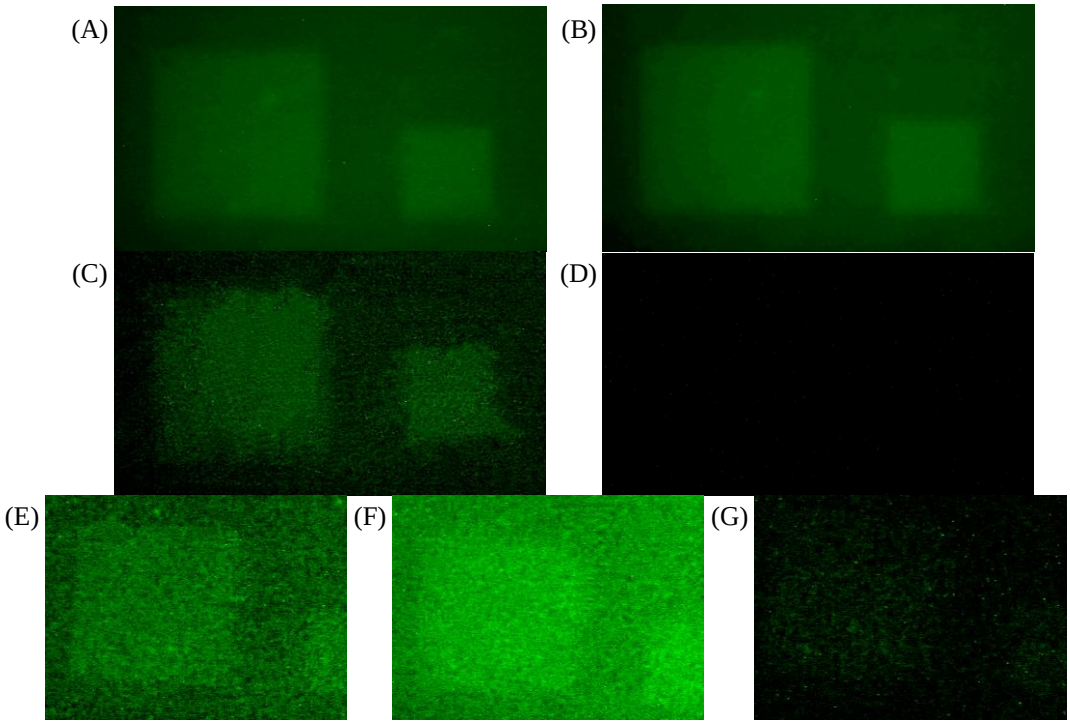

Figure 2.6. *Fluorescence microscopy images of 6-FAM labelled oligonucleotide adsorption on a patterned ALAPP-PEG surface detected through a 450-490 nm excitation filter and a 515 nm suppression filter. Images A) - D) and E) - G) represent two separate experiments. A) 10 μl of 290 ng/μl oligonucleotide solution injected over patterned surface and incubated for 5 min. B) +2 V applied to substrate and incubated for 5 min. C) Surface washed with 100 μl ultra pure water whilst still applying +2 V. D) Surface washed whilst 100 μl ultra pure water whilst applying –2 V. E) 10 μl of 290 ng/μl oligonucleotide solution injected over patterned surface and incubated for 5 min. F) +1.5 V applied to substrate and incubated for 5 min. G) -1.5 V applied to substrate and incubated for 5 min. Images A) and B) have identical exposure times. Images C) and D) have identical exposure times. Images E), F) and G) have identical exposure times. The scale bar equals 100 μm.*

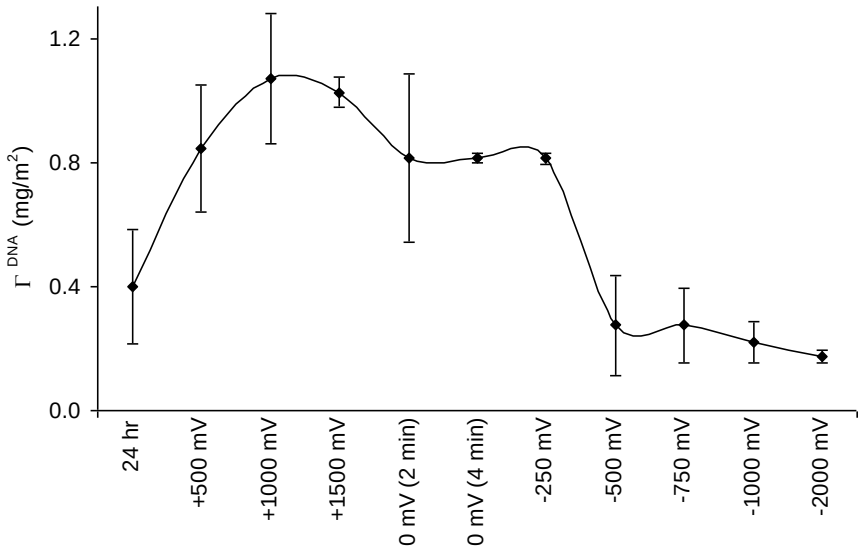

Figure 2.7. *Measurements of the DNA surface concentration (I^{DNA}) on the ALAPP surface. Initially the surface was incubated in DNA solution for 24 hr (no voltage applied), then DC voltages were applied as indicated. The amount of DNA was quantified in a fluorescence assay using PicoGreen® reagent. Results of three separate experiments have been averaged. Error bars are to 95% confidence.*

The adsorption and desorption of DNA to ALAPP was quantified by experiments where ALAPP surfaces were exposed to pEGFP-N1 solution in a custom built electrochemical cell. Initially the ALAPP sample was incubated with the plasmid DNA solution for 24 hr, after which a positive voltage was applied, further stimulating DNA adsorption. Subsequently, the bias was reversed and a negative voltage was applied, stimulating DNA desorption. The concentration of DNA in supernatant was quantified using the minor groove binder PicoGreen®, enabling the calculation of DNA surface concentration (Γ^{DNA}). The results are shown in Figure 2.7.

After 24 hr incubation, an increase in Γ^{DNA} on the ALAPP from 0.0 mg/m^2 to 0.4 mg/m^2 was observed (Figure 2.7), corresponding to the 'spontaneous' adsorption of DNA to the ALAPP surface. In identical control experiments, conducted with Teflon samples, no adsorbed DNA was detected. Electrophoretic analysis of the DNA adsorbed to the ALAPP surface showed three distinct DNA bands (results not shown) corresponding to the plasmid existing in three forms. Quantification of these bands determined that 85% of the plasmid DNA was in the supercoiled form whilst the remaining 15% were distributed between the linear and relaxed circular forms.

Assuming the spontaneous adsorption of DNA to ALAPP went to saturation (time taken for saturation of adsorbed DNA to occur on other substrates is typically 10-60 min [23, 30]), the surface concentration of DNA at saturation (Γ^{sat}) was 0.4 mg/m^2. If double-stranded DNA is considered as a cylinder with diameter 2 nm, as determined by the crystal structure of B-DNA, then the predicted Γ^{sat} value for a monolayer of linear DNA would be 1.7 mg/m^2. Thus, 25% surface coverage for spontaneous adsorption was observed. This result is similar to the Γ^{sat} reported for pUC18 DNA adsorbed onto silica by Melzak et al., 1996 [20]. The thermodynamic driving force

for the adsorption of DNA to a surface has been previously studied [20] where the driving force for adsorption was proposed as the entropically favourable dehydration of the surface. However, for the ALAPP surface, electrostatic interactions also need to be considered.

The adsorption of DNA was enhanced by the application of a positive voltage (Figure 2.7), where an increase in Γ^{DNA} from 0.4 mg/m^2 for spontaneously adsorbed DNA to 1.0 mg/m^2 for the electro-stimulated adsorption of DNA was observed. Maximum Γ^{DNA} was typically attained at +1 V, whereupon the application of higher voltages showed no further increase in DNA adsorption, suggesting that saturation was reached. The increase in Γ^{DNA} observed (0.4 mg/m^2 to 1.0 mg/m^2) implies that a rearrangement of the adsorbed DNA has taken place in order to accommodate a higher DNA coverage. The existence of two or more different configurations of the absorbed DNA layer is also consistent with the observed decrease in Γ^{DNA} from 1 mg/m^2 to 0.8 mg/m^2 once the voltage was no longer applied (Figure 2.7), suggesting that the formed DNA layer was, at least in part, unstable, and could revert to a lower density configuration. The process of DNA adsorption onto ALAPP may be driven by the electrostatic repulsion between adjacent DNA strands. This result also demonstrates the DNA constraining properties of a positively biased surface. The resulting DNA layer had a greater Γ^{DNA} of 0.8 mg/m^2 than after spontaneous adsorption, further suggesting that the application of the positive voltage bias rearranged the initial DNA layer to a high density configuration.

A decrease in Γ^{DNA} as a result of the fast electro-stimulated desorption of DNA from the surface, where desorption occurred within 2 min, was observed with the application of negative voltages above -250 mV (Figure 2.7). The initial application of -250 mV did not alter the Γ^{DNA}, implying that the attractive electrostatic

interactions between the ALAPP and the adsorbed DNA must be overcome by a suitable potential before the DNA can be released into solution. A plateau in the release of DNA was observed for increased negative voltages above -500 mV (Figure 2.7), thus, for subsequent experiments -750 mV was selected as a suitable voltage to stimulate the desorption of adsorbed DNA in order to minimise the voltage required to desorb the DNA whilst ensuring DNA desorption was maximised. In total, 85% of the adsorbed plasmid DNA was released by application of the negative voltage, with a final Γ^{DNA} of 0.18 mg/m^2. Once conditions for the controlled adsorption and desorption of surface-bound plasmid DNA were established, experiments were designed to test for its bioavailability. This was done by carrying out transfection assays.

2.3.3. Transfection experiments

The ultimate test of the concept investigated here was the ability of the surface to allow solid phase transfection with reasonable efficiencies. HEK 293 cells were grown on ALAPP films after adsorption of plasmid DNA (pEGFP-N1) in the presence of a transfection agent (Effectene). In order to mimic the transfected cell microarray plasmid DNA was manually spotted onto the ALAPP surface, as opposed to incubating the ALAPP in plasmid solution for 24 hr. Transfected cells showed green fluorescence. The total cell population was visualised using Hoechst 33342 by the blue fluorescence of the minor groove binder, which is incorporated into the nucleus of all living cells, non-transfected and transfected. Transfection efficiencies were determined by dividing the number of transfected cells by the total number of cells present. In order to study the effect of applying a negative voltage and electro-stimulating the desorption of DNA on transfection efficiency, first 0, -250, -500, -

750 and -1000 mV was applied for 2 min to samples after 4 hr preincubation with plasmid to allow cell attachment. Transfection efficiencies were measured after a further 20 hr incubation and are shown in Figure 2.8. When -250 mV was applied no improvement in transfection efficiency was observed as compared to when no voltage was applied (Figure 2.8A). However, an increase in transfection efficiency above 13% (transfection efficiency when no voltage was applied) was observed when voltages greater than -250 mV were applied with a maximum of 21% transfection efficiency attained upon application of -750 mV. Previous electro-stimulated DNA desorption experiments (Figure 2.7) suggested that -250 mV was not sufficient to overcome DNA-ALAPP interactions and, thus, drive DNA desorption, which only resulted at the application of higher voltages (Figure 2.7). This result strongly suggests that the key mechanism to enhanced transfection efficiency by application of a voltage bias to the DNA-constraining substrate in the range of -500 mV to -750 mV is a result of the increased availability of DNA for uptake by nearby cells due to the electro-stimulated desorption of otherwise bound DNA from the surface overcoming DNA-surface interactions. This is clearly shown by the failure of -250 mV to enhance transfection efficiency whereupon this voltage also does not electro-stimulate DNA desorption. Transfection efficiency was seen to decrease back to 12% when -1000 mV was applied. Presumably, this was caused by a decrease in the viability of cells as a result of the higher voltage application. As -750 mV was observed to cause the highest increase in transfection efficiency it was selected for further studies. -750 mV voltage was applied for 0, 0.5, 1 and 5 min to samples after 4 hr preincubation with plasmid with a subsequent 20 hr incubation before analysis. An increase in transfection efficiency was observed when the length of time -750 mV was applied for was increased from 0-1 min (Figure 2.8B). No

further increase in transfection efficiency was observed by increasing the voltage time beyond 1 min.

Thus, a large increase in transfection efficiency was demonstrated with the application of -750 mV from 13% to 30% (Figure 2.8). These values, although still below the reported efficiency in the liquid phase (40-60% according to the Effectene manufacturer) are an improvement over previous solid phase transfection studies of 5-15% [35, 159].

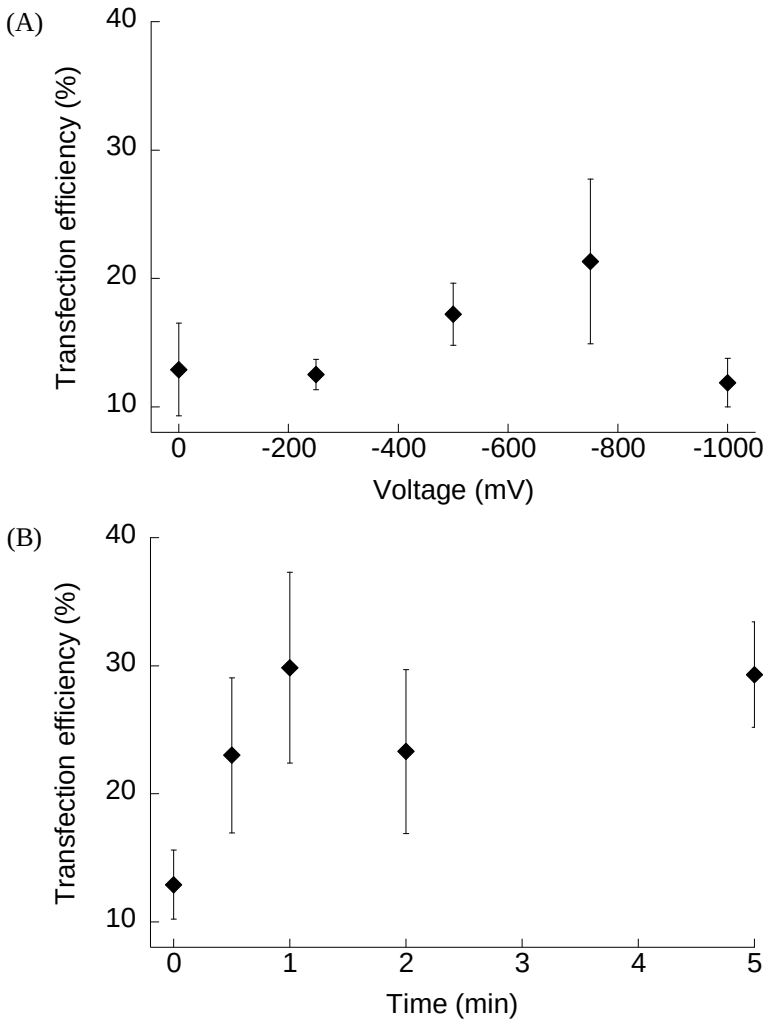

Figure 2.8. *Transfection efficiency of HEK 293 cells expressing pEGFP-N1 on ALAPP substrate after 24 hr culture period; (A) with the application of various voltage magnitudes for 2 mins, (B) with the application of -750 mV for various lengths of time. Error bars are to 95% confidence.*

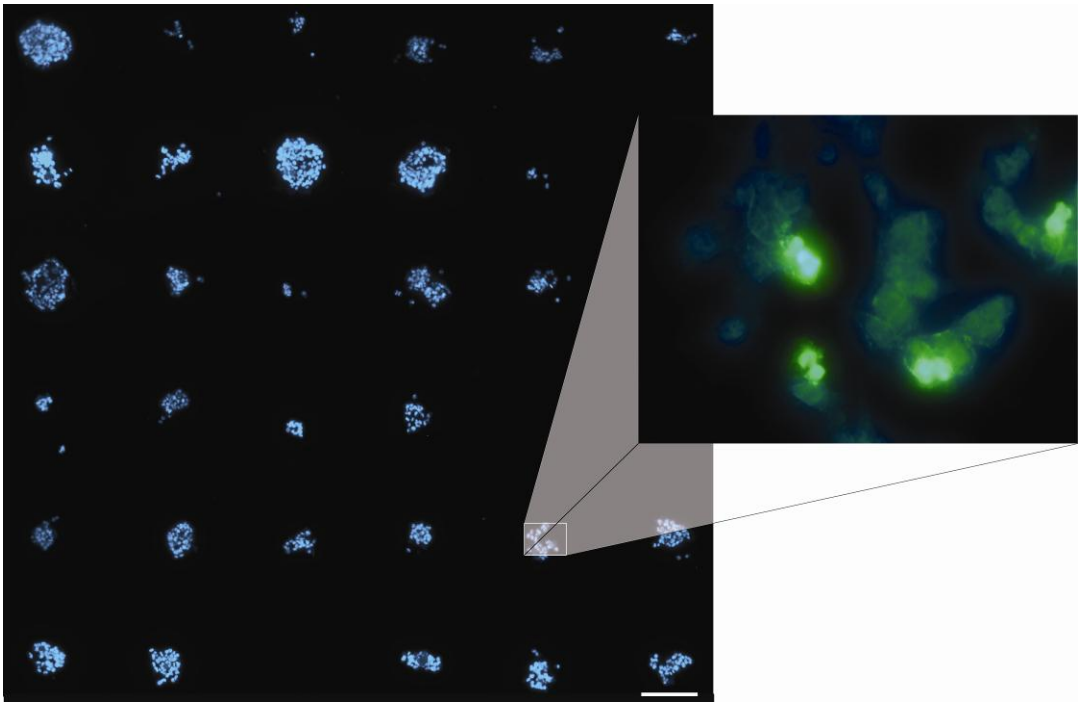

Figure 2.9. *Fluorescence microscopy image of the formation of a TCM with HEK 293 cells on an ALAPP/PEG patterned surface. Surfaces were patterned by laser ablation and DNA was deposited onto spots by a robotic arrayer. Cells were stained with Hoechst 33342. The main image was taken through a 270-380 nm excitation filter and a 410-580 nm suppression filter. The inset shows an overlay of the Hoechst 33342 fluorescence and fluorescence due to the expression of GFP, taken through a 450-490 nm excitation filter and a 515 nm suppression filter. Scale bar is 150 μm.*

2.3.4. Formation of a transfected cell microarray

Utilising the ALAPP/PEG surfaces, patterned by laser ablation, for TCM applications was of interest. After surface patterning pEGFP-N1 plasmid with Effectene transfection reagent was spotted onto the ALAPP regions using a piezoelectric non-contact printer. The surface was then seeded with HEK 293 cells and allowed to incubate for 24 hr. A fluorescence microscopy image of the formed cell array is shown in Figure 2.9. Here the cells were stained with Hoechst dye, which stains the nucleus of all cells present. Cells attaching to different ALAPP regions are clearly separated from each other. The absence of a lawn of cells could be enormously beneficial for detecting subtle, subcellular phenotypic changes within transfected cells, as there would be no need to differentiate between transfected and non-transfected cells, provided that near 100% of cells within each spot are transfected. Furthermore, as there is a migration barrier there is no way that transfected cells or adsorbed DNA can migrate from one cell cluster to another. This could allow for cell colonies to be positioned closer together allowing for the creation of high-density arrays.

The inset of Figure 2.9 shows an overlayed image of the fluorescence due to the Hoechst dye and also GFP fluorescence due to the expression of the pEGFP-N1 plasmid from a single cell cluster. As can be seen from the inset, some cells appear green, whilst others remain only blue, showing that 100% of cells were not transfected. Typically, a transfection efficiency of 20% was achieved. Further improvement to this transfection efficiency is possible by application of a voltage after cell attachment and by optimising the amount of DNA and transfection reagent

added. However, this approach currently suffers from difficulties aligning the ALAPP/PEG pattern with the DNA array deposited using the non-contact printer.

2.4. Conclusion

The formation and characterisation of two-dimensional chemical patterns on p^{++} silicon substrates using plasma polymerisation of allylamine in conjunction with PEG surface grafting and subsequent patterning by mask-assisted excimer laser ablation was demonstrated. The preferential adsorption of DNA onto the ALAPP regions on an ALAPP-PEG patterned surface was noted, showing that the PEG film repels not only proteins and cells, as shown before, but also nucleic acids and, therefore, provides a general non-biofouling coating. Furthermore, voltage bias-stimulated adsorption and desorption of DNA on ALAPP coated surfaces was demonstrated by fluorescence measurements. Solid phase transfection on ALAPP was shown to be enhanced by electro-stimulated desorption of DNA. The increase in transfection efficiency from 13% to 30% compares favourably with literature values and is an important step in improving solid phase transfection. The formation of a TCM on a chemically patterned substrate was also shown to be possible.

III

CHAPTER 3. COMPARISON OF THE BINDING MODE OF PLASMID DNA TO ALLYLAMINE PLASMA POLYMER AND POLY(ETHYLENE GLYCOL) SURFACES

The content of this chapter is based upon reference [188].

3.1. Introduction

Nucleic acid probes have been used extensively in recent years for applications such as biomimetics, 'smart' drug delivery, biosensing and tissue engineering [3, 4, 6] and for tasks such as DNA purification and gene therapy [1, 8, 14, 127]. During these applications the nucleic acid probes are often bound or associated to the surface of a biomaterial, thus, in order to increase the scope and capabilities of these devices advanced control over DNA manipulation at surfaces is required. Insight into the mode of DNA association with a particular surface of interest is, thus, pivotal in order to maximise DNA-surface interactions and allow for advanced manipulation of DNA at a surface such as switchable binding.

Double-stranded DNA can generally be regarded as a coiled rod with a purine/pyrimidine core and a phosphate and pentose sugar exterior. The negative charges of the phosphate groups endow DNA with the characteristic feature of an anionic polyelectrolyte. For this reason, the production of surfaces with a positive surface charge, often achieved by the incorporation of amine functionality, has been investigated and achieved by a number of strategies with the basic aim to increase DNA surface adsorption via electrostatic interactions [27]. As well as commonly utilised wet chemical silanisation strategies [9, 30] and coating formation with polyamines [29, 78], aminated surfaces have been produced by plasma

polymerisation [33-35, 38]. The key advantage of plasma polymerisation over wet chemical procedures is the ability to produce pinhole free, adherent films on almost any substrate with the ability to incorporate a desired functionality by the judicious choice of monomer. However, plasma polymer films exhibit complicated, cross-linked chemistries that are difficult to characterise and often change over time due to aging processes [183, 189]. Allylamine has been used extensively for the formation of plasma polymer films with amine functionality [180, 186, 190-193] and has been employed in a number of studies where DNA immobilisation/hybridisation [34, 36, 37] and mammalian cell attachment was desired [33, 35, 192, 194-197]. The success of the allylamine plasma polymer (ALAPP) to interact favourably with both DNA and cells makes this polymer a highly attractive surface for biodevice applications requiring biomolecule manipulation [1]. Despite the interest in ALAPP, the mechanism of DNA binding to this surface has not been studied in depth.

In general terms, it has been observed that higher salt concentrations and lower pH increase the propensity for DNA adsorption and vice versa [20, 23]. This effect has been studied for a number of different surfaces including glass, modified glass, mica, various minerals, silica particles, silica wafers, modified silica and latex particles and is generally assumed to be driven by a shielding of the anionic charges of the DNA [20, 22, 23, 30, 43, 198-200]. This is also useful for the purpose of DNA purification [198]. Apart from the influence of pH or ionic strength on DNA adsorptivity, fundamental studies of the driving forces of DNA adsorption to various surfaces are limited. Adsorption studies of DNA to silica surfaces modified with both anionic and cationic moieties suggest that DNA adsorption is driven by more than just electrostatic interactions [27]. Melzak et al. [20] undertook an in-depth study of the driving forces of DNA to silica wafers in perchlorate solutions and determined

that the most significant thermodynamic force for the adsorption of DNA is entropically favourable surface dehydration, whilst hydrogen bond formation also contributed to the interfacial interaction. Kang et al. [201] were able to visualise in real-time the adsorption of individual DNA molecules on silica using total internal reflection fluorescence microscopy. Interestingly, the report revealed the importance of hydrophobic interactions. DNA adsorption was only observed at a pH below 4.5, where the DNA surface concentration increased with decreasing pH. The hydrophobic interactions were more significant for single stranded DNA, suggesting interactions of the surface with the nucleobases [22]. Adsorption of DNA to negatively charged surfaces has also been observed due to the formation of cationic bridges often by the use of cations such as Mg^{2+} [43]. Furthermore, Saoudi et al. [27] reported the adsorption of DNA to aminated polypyrrole silica particles, which had a near-zero surface charge where the charge contribution from protonated amine groups was balanced by anionic silanol groups, suggesting that isolated positively charged groups and not a net positive surface charge is sufficient to stimulate DNA adsorption. DNA adsorption to polypyrrole is also closely related to dopant-phosphate ion exchange at the DNA/polypyrrole interface [202].

The low protein 'fouling' behaviour of poly(ethylene glycol) (PEG) layers as well as their ability to reduce cell attachment has been well studied [67, 203-206]. However, the use and performance of PEG coatings in conjunction with DNA binding has not been widely studied, despite evidence suggesting PEG is able to resist non-specific adsorption of DNA [207, 208]. Studies are limited to the adsorption of short, single-stranded oligomers, thus, investigation to longer and double-stranded DNA would be of interest, particularly for applications involving

both proteins and DNA whereupon it would be useful to have a surface coating that is able to universally reduce biomolecular adsorption.

PEG layers grafted to a surface are highly effective at preventing protein adsorption when the surface density of the grafted polymer is sufficiently high such that a 'brush' regime is reached, whereupon adjacent grafted chains repel one another causing the chains to extend away from the surface. A relatively dense PEG brush formed has high exclusion properties due to high conformational entropy. Furthermore, as the hydrophilic PEG hydrogen binds extensively to water, protein adsorption would lead to unfavourable disruption of the hydrogen bonding. In addition, the free energy of the polymer-water interface is minimal, decreasing the driving force of protein adsorption [65]. As cell attachment is regulated almost entirely by proteins, reduced protein adsorption concurrently leads to a decrease in cell attachment.

Hook et al. (See CHAPTER 2) [34], combined these two surfaces by demonstrating the spatially controlled adsorption of DNA on an amine rich ALAPP film by sequential deposition of an ALAPP film then grafting of PEG by reductive amination. Subsequent laser ablation produced a patterned surface that was able to direct DNA adsorption to the regions where the underlying plasma polymer was re-exposed. The ability to spatially direct DNA adsorption was of interest, however, a more detailed study of the binding mode of DNA on both the ALAPP and PEG surfaces is of interest. In particular, the complex chemistry of the ALAPP film presents considerable challenges for predicting the DNA-ALAPP interactions occurring at the solid/liquid interface. An increased understanding of this system could further promote advanced biomolecular manipulation, which is useful for the development of biodevices.

The same study also demonstrated the electro-stimulated adsorption and desorption of DNA from the ALAPP surface, whereupon the DNA surface concentration (Γ^{DNA}) was increased from 0.4 mg/m^2 to 1.0 mg/m^2 by application of a positive voltage and decreased to 0.2 mg/m^2 after application of a negative voltage (see section 2.3.2) [34]. The ability to electro-stimulate the adsorption and desorption of DNA has also been studied extensively on gold [18, 105-107].

In the present chapter, the adsorption of DNA to ALAPP and PEG layers was investigated to achieve an in-depth understanding of the biomolecule-surface interactions using a range of surface analytical methods including X-ray photoelectron spectroscopy (XPS), ζ-potential, contact angle and quartz crystal microbalance (QCM) measurements. Furthermore, studies into the electro-stimulated adsorption and desorption of DNA on these substrates were conducted.

3.2. Materials and methods

3.2.1. Substrate preparations

Boron doped p^{++} silicon wafers (Virginia Semiconductors, Inc.) were cut into approximately 10 x 10 mm^2 pieces, cleaned by sonication for 30 min in a 5% surfactant (RBS 35, Pierce USA) solution and oxidised under UV light for 30 min.

Plasma polymerisation reactions onto prepared substrates were performed in a custom-built reactor described elsewhere [182]. In short, the plasma reactor consisted of two circular electrodes separated by 125 mm in a cylindrical reactor being 350 mm high with a diameter of 170 mm. Allylamine (Aldrich, 98% purity) was used as a monomer. Polymerisation conditions used were a frequency of 200 kHz, a power of 20 W and an initial monomer pressure of 0.200 mbar. Deposition time was 25 s

resulting in a film thickness of approximately 30 nm as determined by atomic force microscopy (data not shown). After deposition samples were exposed briefly to air before storage under a N_2 atmosphere.

PEG monoaldehyde (Shearwater Polymers, Huntsville AL, USA) with a molecular weight of 5000 was grafted onto freshly deposited ALAPP films by reductive amination. Grafting was performed under 'cloud point' conditions in 20 ml of a 0.1 M sodium phosphate buffer containing K_2SO_4 (2.2 mg), $NaCNBH_3$ (60 mg) and PEG (50 mg) at pH 6.2. Freshly deposited ALAPP films were incubated in the PEG grafting solution at 60 °C for 16 hr.

3.2.2. Substrate characterisation

Contact angle measurements were performed by injecting 100 μl of 0.2 μm filtered MilliQ water (18.2 MΩ.cm) onto the surface of interest. Advancing contact angles were measured. Three measurements were taken for each sample. Images were taken using a Panasonic CCTV camera (WV-BP550) and processed using ImageJ software.

X-ray photoelectron spectroscopy (XPS) was conducted on an AXIS HSi spectrometer (Kratos Analytical Ltd.) equipped with a monochromatised Al K_α source. The pressure during analysis was typically $5x10^{-8}$ mbar. The elemental composition of surfaces was determined from survey spectra, collected at a pass energy of 320 eV. High-resolution spectra were obtained at a pass energy of 40 eV. Binding energies were referenced to the aliphatic hydrocarbon peak at 285.0 eV. Peak fitting of high-resolution spectra was conducted with Vision 1.5 software, Kratos Analytical Ltd. Two areas of each surface were analysed, and each sample preparation was prepared and analysed in duplicate.

ζ-potential measurements were taken of various surfaces using a ZetaCAD (CAD Instrumentation) using the streaming potential technique. Two identical surfaces were placed facing each other with a separation of 100 μm, which is large compared with the double thickness layer. A 0.01 M phosphate buffer of pH 5-7.4 or a 0.01 M acetate buffer of pH 4-5.5 was streamed between the two surfaces at various pressures ranging from 0-500 mbar in a stepwise fashion with pressure increments of 5 mbar. The flow was reversed after each measurement to avoid electrode asymmetry. For each pressure the temperature, conductivity, viscosity and dielectric constant of the solution was measured as well as the potential difference between the two ends of the surfaces using a multimeter (Keithley 2000) and silver electrodes placed at either end of the samples. A graph of the voltage difference was plotted against pressure to calculate the ζ-potential of the surface according to the Helmholtz-Smoluchowski formula shown as equation 3.1, where ζ is the ζ-potential, λ is the conductivity of the solution, η is the viscosity of the solution, ε is the permittivity of the solution, E is the measured potential across the surface and P is the pressure at which the solution is applied across the surface.

$$\zeta = \frac{\lambda \eta E}{\varepsilon P} \qquad (3.1)$$

3.2.3. Plasmid preparation

Plasmids pEGFP-N1 (4.7 kb) (Clontech), encoding the green fluorescing protein (GFP) (excitation 488 nm, emission 509 nm), were propagated using the JM109 *Escherichia coli* (*E-coli*) strain (Promega). Cells were transfected with plasmid using the heat shock method. Plasmid was isolated using the Promega® Maxiprep Kit (Promega) according to the manufacturer's specifications. Isolated plasmid was

characterised by UV-Vis quantification and restriction enzyme digestion with Ssp1 and Sph1 (New England Biolabs) with subsequent agarose gel electrophoresis.

3.2.4. DNA adsorption

The adsorption of plasmid DNA to ALAPP surfaces in various buffers was performed in cuvettes by analysing the depletion of solution fluorescence. 0.01 M phosphate buffer containing 100 ng/ml pEGFP-N1 was varied to have a pH in the range of 5-9, [NaCl] 0.01-3 M and ethanol content 0-50% (v/v). For thermodynamic studies, 0.01 M phosphate buffer containing 50-500 ng/ml pEGFP-N1 at a pH of 7.4, [NaCl] 0.5 M was utilised. For kinetic studies, 0.01 M phosphate buffer containing 50, 100 and 500 ng/ml pEGFP-N1 at a pH of 7.4, [NaCl] 0.5 M was utilised. Picogreen® (excitation 502 nm, emission 523 nm) (Molecular Probes) was added to the working solution at a 400x dilution to monitor [DNA] throughout. Standard curves of Picogreen® fluorescence versus [DNA] were formed for each solution used. Fluorescence measurements were performed using a LS 55 Luminescence Spectrometer (Perkin Elmer Instruments). Samples were initially incubated at room temperature overnight to allow adsorption of DNA to the cuvette walls. ALAPP coated silicon wafers of known area were then added to the cuvette and the solution was allowed to incubate again for 8 hr. A decrease in solution fluorescence after the addition of ALAPP films was related to the adsorption of DNA to the film. The mass of the solution was monitored throughout the experiment in order to take into account the effects of solvent evaporation. DNA adsorption studies excluding thermodynamic studies were conducted with a single batch of Si-ALAPP samples with an identical ageing period (1 day) to exclude differences in surface chemistry

due to post-deposition alterations. Thermodynamic studies were conducted with two different batches of Si-ALAPP samples.

Quartz crystal microbalance (QCM) measurements were taken using an Electrochemical Nanobalance EQCN-701 (Elchema). 9 V Quartz crystals (International Crystal Manufacturing Company) with gold electrodes were used for all measurements. The frequency of the crystal was measured and processed using Voltscan and Master Windows software. Frequency changes were converted to mass changes using the Sauerbrey equation, shown as equation 3.2, where Δf is the change in frequency, Δm is the change in mass, a is a constant related to the crystal used and A is the area.

$$\Delta f = -a\frac{\Delta m}{A} \qquad (3.2)$$

All measurements were conducted in a Faraday cage under N_2 at room temperature. For DNA adsorption studies, one side of the quartz crystal was coated with an ALAPP film according to the procedure described previously. The coated side was incubated in a 0.01 M phosphate buffer, pH 7.4, 0.5 M NaCl whilst the uncoated side was exposed to N_2 throughout. After 24 hr incubation, to allow for swelling of the polymer film and any post-deposition rearrangements and after ensuring the crystal had stabilised, a 300 μg/ml plasmid solution was added to make a final DNA concentration of 200 ng/ml and the change in mass was measured.

3.2.5. Data analysis

The adsorption of plasmid DNA to ALAPP and PEG films was modelled using the Langmuir model. The change in surface concentration of a species was related to the bulk concentration by equation 3.3, where Γ_s corresponds to the surface

concentration of the adsorbed species, K is the equilibrium constant, $\Gamma_{s\infty}$ is the surface concentration of the adsorbed species at saturation and C is the concentration of the adsorbing species in the bulk solution.

$$\Gamma_s = \frac{KC\Gamma_{s\infty}}{1+KC} \tag{3.3}$$

Equation 3.3 was used to model the system and for the determination of values of K and Γ_s using KaleidaGraph 4.0. Equation 3.3 can be rearranged to equation 3.4 by plotting the reciprocal of Γ_s against the reciprocal of C, whereupon a linear result suggests compliance with the Langmuir model [22].

$$\frac{1}{\Gamma_s} = \frac{1}{K\Gamma_{s\infty}C} + \frac{1}{\Gamma_{s\infty}} \tag{3.4}$$

3.2.6. Electrostimulated DNA adsorption and desorption

Quantitative studies of DNA adsorption were conducted in a custom-built electrochemical cell as described previously [124]. ALAPP or PEG samples were clamped into the cell and 2.4 ml of 100 ng/ml pEGFP-N1 solution in 0.01 M phosphate buffer containing 1.0 M NaCl, pH = 7.4 was added over the sample. After 24 hr incubation at room temperature, a voltage was applied in a stepwise fashion (+1.50 V, 0.00 V, -0.75 V) over consecutive 2 min intervals with the substrate as the working electrode, an Ag/AgCl/saturated KCl reference electrode and a platinum auxiliary electrode. The voltages used were optimised previously on ALAPP films [34]. The DNA concentration of the solution was determined using the fluorescent Picogreen® probe according to the manufacturer's specifications before and after each voltage application. Solution removed for DNA concentration analysis was replaced with fresh PBS. Fluorescence measurements were performed using a LS 55 Luminescence Spectrometer (Perkin Elmer Instruments).

Table 3.1. *Water contact angle measurements on bare silicon (Si), silicon modified with ALAPP (Si-ALAPP) and silicon modified with ALAPP and grafted with PEG (Si-ALAPP-PEG). Error shown is to 95% confidence.*

	Si		Si-ALAPP		Si-ALAPP-PEG	
Contact angle	36°	±3°	70°	±2°	12°	±2°

Table 3.2. *Atomic concentration in % on silicon substrate materials as determined by XPS. Value range shown to 95% confidence.*

	C		N		O		Si	
Si	11.6	± 0.5	0.9	± 0.2	36.0	± 1.0	50.5	± 1.3
Si-ALAPP	76.5	± 1.2	12.0	± 0.6	11.5	± 1.8	0.0	± 0.0
Si-ALAPP-PEG	70.0	± 0.7	6.4	± 0.3	23.6	± 0.6	0.0	± 0.0

3.3. Results and discussion

3.3.1. Surface characterisation

Surfaces used for DNA adsorption and desorption studies were initially characterised by contact angle, XPS and ζ-potential measurements. Results from contact angle measurements are shown as Table 3.1. ALAPP deposition on silicon gives rise to an increase in contact angle from 36° to 70°. This increase in hydrophobicity is a result of the deposition of a crosslinked organic polymer film containing moderately polar functional groups (e.g. amines and imines). Notably a large decrease in contact angle from 70° to 13° is observed when the high density PEG coating is grafted onto the ALAPP layer, corresponding to a significant increase in hydrophilicity.

XPS atomic percentages for bare silicon and ALAPP and PEG films are shown in Table 3.2. The absence of a silicon signal on the Si-ALAPP surfaces strongly suggests that pinhole-free ALAPP films with a thickness of more than 10 nm (the approximate penetration depth of XPS for polymers) were formed. The oxygen content of this film is due to the reactions of atmospheric oxygen with reactive species in the polymer film such as free radicals resulting in the incorporation of oxygen, which occurs once the film is exposed to air [183, 184, 189]. The inclusion of oxygen within the ALAPP film also suggests the formation of anionic groups on the polymer surface. Upon subsequent grafting of PEG to the amine groups of the ALAPP coating, a significant decrease in the nitrogen content (12.0% to 6.4%) and an accompanying rise in the oxygen content (11.5% to 23.6%) was observed, confirming the successful grafting of a high density PEG layer. High-resolution XPS spectra of the C 1s peak are shown in Figure 2.4 and discussed in section 2.3.1. The

presence of a small amount of carboxyl (O=C-O) carbon on the ALAPP film, which would contribute to the anionic properties of the film, is suggested by the presence of a C 1s component at 289.1 eV (Figure 2.4A, Table 2.2).

ζ-potential measurements of bare silicon, ALAPP and PEG films over a pH range from 4-7.5 are shown in Figure 3.1. Initially, the ζ-potential of bare silicon was measured. This surface had a negative charge (≈-15 mV), likely due to the silicate groups on the silicon surface, which did not significantly alter over the pH range measured. Initially, when the ζ-potential was measured for ALAPP coatings after short storage (2 days), a dynamic surface charge was observed, and an isoelectric point of approximately 5.5 was determined. This compares closely to work by Muir et al. [193], who reported an isoelectric point of 5.2 for an ALAPP film prepared and treated under similar conditions. Typically, aliphatic primary amines tend to have a pKa of 9-11, thus this low pI suggests the presence of additional anionic functionalities such as carboxylic acids.

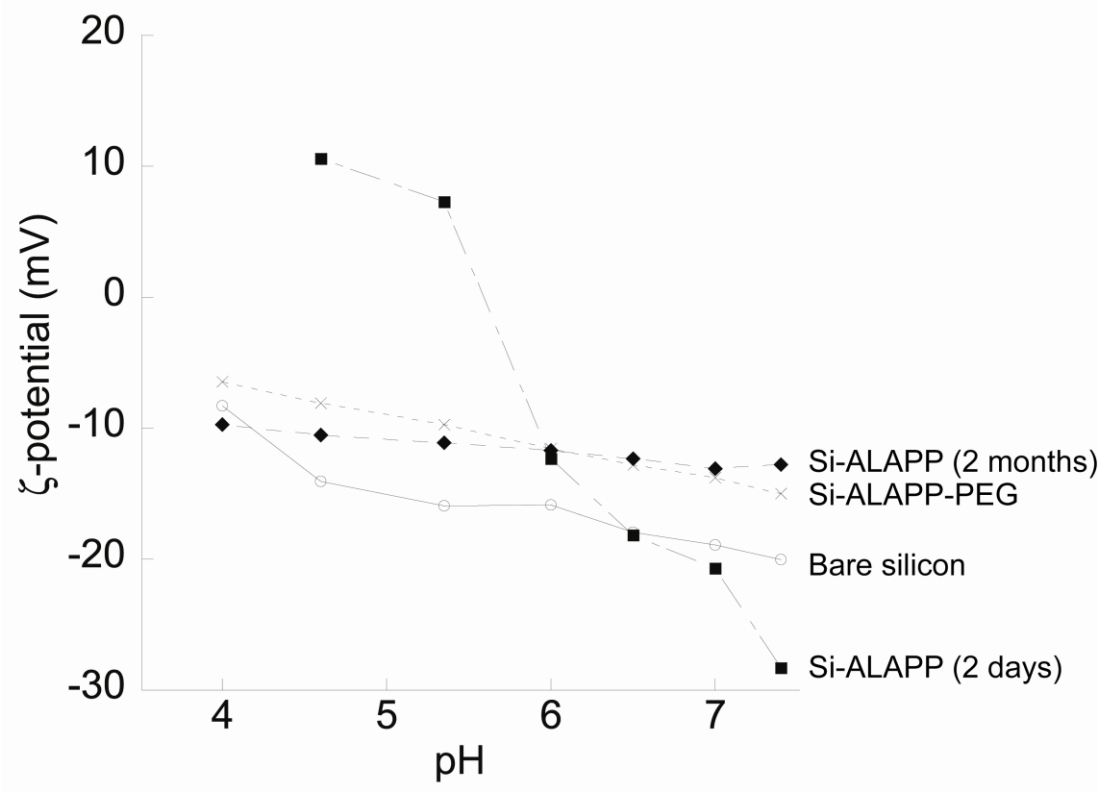

Figure 3.1. *ζ-potential versus pH for different modified substrates in 0.01 M phosphate buffer (0.14 M NaCl);(—○—) Si, (- -■- -) Si-ALAPP 2 days, (- -◆- -) Si-ALAPP 2 months, (- -×- -) Si-ALAPP-PEG.*

The known adsorption of DNA to negatively charged surfaces by formation of cationic bridges with solvated cations [43] suggests that the adsorption of DNA to ALAPP by electrostatic contacts could still proceed even in the presence of some negative surface charge due to anionic functionality. Nevertheless, it is expected that in solutions of pH less than 5.5 DNA adsorption to ALAPP films should be enhanced. Interestingly, when identical ζ-potential measurements were conducted on ALAPP films that were left in air for 2 months, a negative surface charge (-10 mV) resulted, which remained unchanged over the pH range measured, suggesting that these films undergo considerable aging over this time period and that the relative amine content of the film is greatly reduced. For this reason, all subsequent DNA adsorption studies were conducted on fresh ALAPP films after short storage times (<1 week) in N_2. A negative and non-dynamic ζ-potential was observed for the PEG film (≈-10 mV). Similar ζ-potential measurements have been previously reported for PEG films [209-212]. This suggests that the amine functionality of the ALAPP film is effectively removed by the PEG grafting, resulting in a negative surface charge that is not responsive to pH changes results.

3.3.2. Comparison of in situ QCM analysis and depletion of solution fluorescence

The adsorption of unlabelled plasmid DNA to the ALAPP film was initially monitored *in situ* by the use of QCM and compared with measurements of the depletion of solution fluorescence. An ALAPP coated QCM crystal was exposed to a 200 ng/ml DNA solution after stabilisation of the crystal in phosphate buffer. The observed change in mass due to DNA addition is shown in Figure 3.2. 3. The initial spike in the signal trace is due to the injection of the DNA solution, which causes sufficient disturbance of the thermal and kinetic equilibrium reached in the

crystal/solution system to alter the sensitive frequency of the crystal. A Γ^{DNA} of 1.02 mg/m^2 was reached after approximately 2000 s (Figure 3.2). According to the *K* and $\Gamma_{s\infty}$ values for DNA adsorption to ALAPP determined under equivalent pH, salt concentration and DNA concentration (200 ng/ml) by measurements of the depletion of solution fluorescence, a Γ^{DNA} of 1.20 mg/m^2 is predicted, which is slightly greater than the Γ^{DNA} measured by QCM. The reason for this difference could be the result of a second slow step in the adsorption of DNA not measured over the time course of the QCM experiment.

The QCM measurements also enable the analysis of the kinetics of DNA adsorption onto the ALAPP surface. The adsorption trace shown in Figure 3.2 display simple Langmuir kinetics with an initial exponential increase in DNA adsorption, plateauing off to a maximum value that is achieved after about 2000 s. A similar result has been previously reported by Zhang et al., for DNA adsorption to ALAPP achieved by surface plasmon resonance studies [36]. For comparison, kinetic measurements of DNA adsorption were also undertaken by measurements of the depletion of solution fluorescence. The results are shown in Figure 3.3. The shape of the adsorption time curve is similar to the time curve obtained from QCM measurements for low concentrations of DNA. An initial sharp increase in Γ^{DNA} was observed followed by a much slower rise. These results suggest a two-step DNA adsorption process; an initial fast DNA uptake followed by a slower rearrangement of surface bound DNA allowing for further, but kinetically much slower, DNA adsorption. The negative charge of DNA would mean that once a DNA strand had adsorbed, further DNA adsorption on this site would be unfavourable due to electrostatic repulsion. A two-step process would fit with this model. Such a process has been previously reported [22].

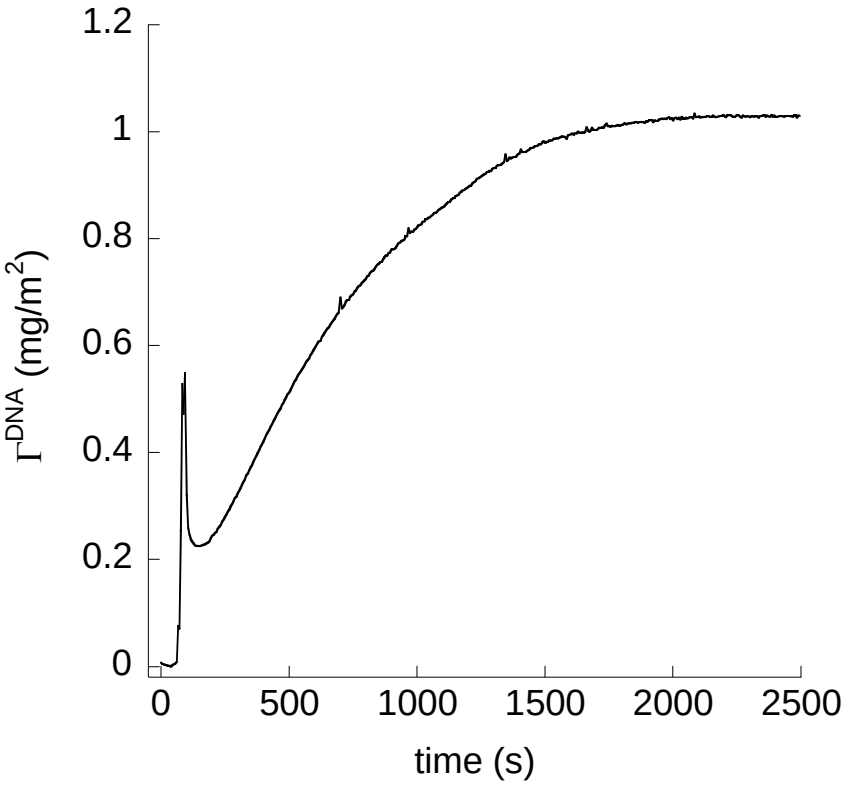

Figure 3.2. *Kinetics of the adsorption of 200 ng/ml plasmid DNA in 0.01 M phosphate buffer, pH 7.4, [NaCl] 0.5 M to an ALAPP film monitored by QCM.*

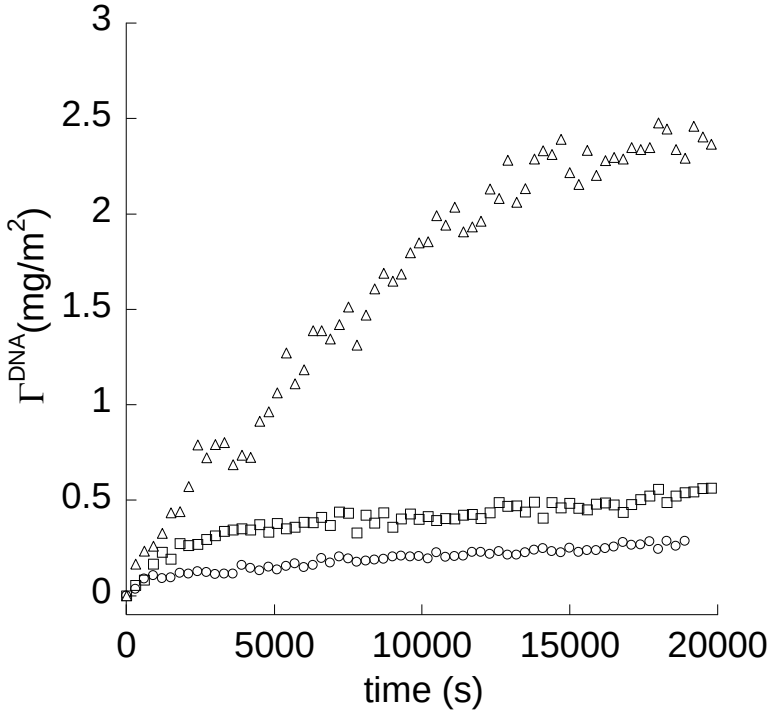

Figure 3.3. *Kinetics of DNA adsorption as determined by measurements of the depletion of solution fluorescence for 500 ng/ml (△), 100 ng/ml (□) and 50 ng/ml (○) plasmid DNA solutions in 0.01 M phosphate buffer, pH 7.4, [NaCl] 0.5 M.*

However, at a higher DNA solution concentration of 500 ng/ml, there seems to be a disparity arising between the two methods of analysis. Notably, the initial sharp increase in DNA adsorption did not plateau until 15000 s, which is at least 5 times longer than measurements taken with QCM. The reason for this disparity may be due to diffusion limitations in the fluorescence study, that is, the DNA that adsorbs to the surface is taken from the solution near the surface, forming a DNA depleted layer close to the surface that DNA from the bulk must diffuse into. A time delay would hence be expected between the change of DNA concentration in a near-surface layer and the translation of this change to a concentration change in the bulk, which was measured by the depletion method. Thus, although the measurements of the depletion of solution fluorescence was accurate for thermodynamic studies of DNA adsorption, this disparity suggests that at higher DNA concentration (>200 ng/ml) it is not accurate for kinetic analysis.

3.3.3. DNA adsorption.

Langmuir adsorption is widely used for the modelling of biological adsorption processes. In order to minimise the electrostatic repulsion between adsorbed DNA and DNA in solution that is approaching the surface, which would cause a deviation from the Langmuir model, lower concentrations of DNA (<1 μg/ml) in the bulk solution were used. The adsorption of DNA to the ALAPP and PEG surfaces was measured for different concentrations of plasmid DNA ([DNA]) to obtain a binding isotherm in 0.01 M phosphate buffer at a pH of 7.4 containing 1M NaCl using measurements of the depletion of solution fluorescence of Picogreen® intercalated with DNA (Figure 3.4A). $1/\Gamma^{DNA}$ was plotted against $1/C$ for both the ALAPP and PEG surfaces (Figure 3.4B and C). A pH of 7.4 was chosen for these studies since

the surface behaviour of DNA was of most interest at physiological pH. At this pH, the ALAPP and PEG modified surfaces gave ζ-potentials of -28 mV and -20 mV respectively. As predicted by equation 3.4, a linear relationship was observed with good correlation (Figure 3.4B and C), suggesting that this model is appropriate over the concentration range studied.

The DNA adsorption characterised in Figure 3.4 was conducted at a pH of 7.4, whereupon the ALAPP film had a measured ζ-potential of approximately -20 mV. As DNA adsorption was able to proceed despite the negative surface charge, the binding of DNA to ALAPP must depend on more than just electrostatic interactions. By application of the Langmuir model (equation 3.3) to the data sets shown in Figure 3.4, $\Gamma_{s\infty}$ and K for DNA adsorption to ALAPP were found to be 4.96 mg/m^2 and 1600 ml/mg respectively, suggesting a high affinity of the ALAPP film for DNA. For comparison, at an equivalent pH Elaissari et al., reported a $\Gamma_{s\infty}$ and K for the adsorption of polyadenylic acid onto latex particles of 1.21 mg/m^2 and 90 ml/mg respectively [22]. At an optimised pH (4.4), whereupon the latex particles had a positive charge of +60 mV, the reported $\Gamma_{s\infty}$ and K for the adsorption of polyadenylic acid was 2.62 mg/m^2 and 3630 ml/mg respectively [22]. Although correlation with the Langmuir model fits well with the data presented, deviation from this model at higher Γ^{DNA} would be expected as a result of the electrostatic repulsion between adjacent adsorbed DNA molecules.

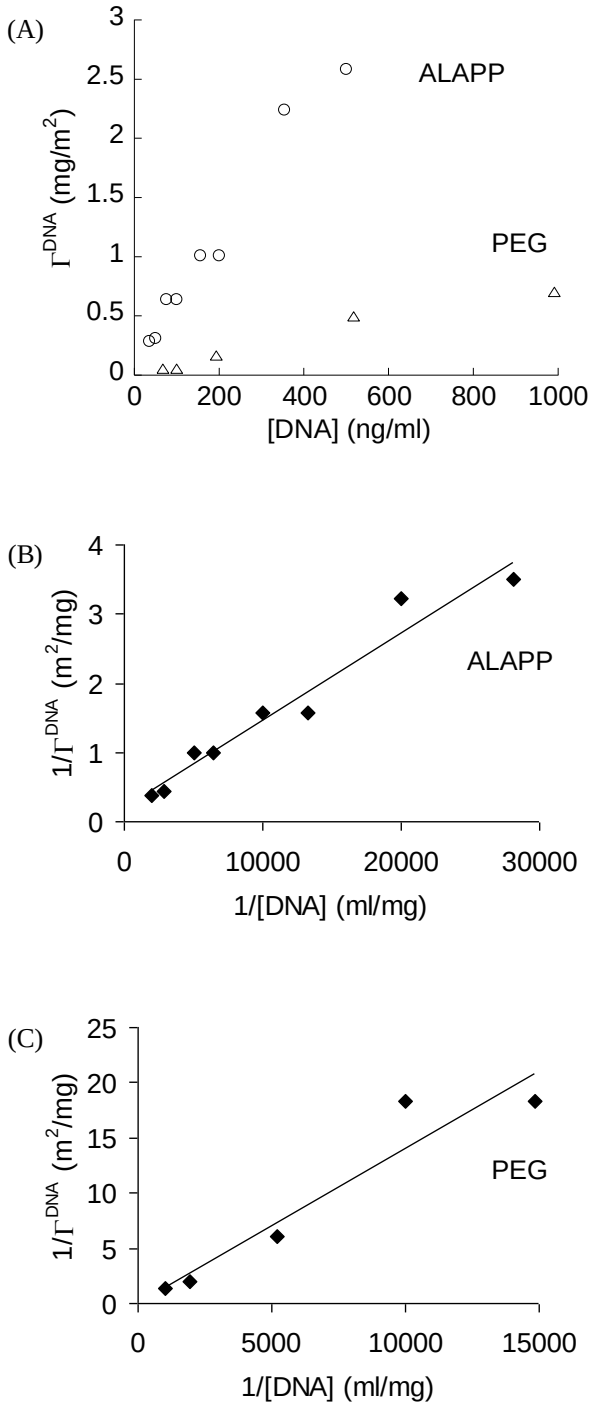

Figure 3.4. *(A) Binding isotherm for DNA adsorption to ALAPP (○) and PEG (△) and (B) and (C) inverse of DNA surface concentration against the inverse of the DNA concentration determined on (B) an ALAPP film and (C) PEG grafted onto ALAPP, in 0.01 M phosphate buffer, pH 7.4, [NaCl] 0.5 M obtained from measurements of the depletion of solution fluorescence. A linear correlation fit is shown; (B) R^2 = 0.954, (C) R^2 = 0.908.*

The Γ^{DNA} on PEG was found to be significantly lower than for ALAPP over the bulk DNA concentration range studied (Figure 3.4A) confirming that, as expected, PEG resists adsorption of DNA as compared with the ALAPP film. By applying the Langmuir model to the data sets shown in Figure 3.4, the $\Gamma_{s\infty}$ and K for DNA adsorption to PEG were found to be 1.75 mg/m^2 and 680 ml/mg respectively, which is significantly lower than the equivalent values of 4.96 mg/m^2 and 1600 ml/mg measured for ALAPP. The small amount of DNA adsorption observed on the PEG films is presumably due to weak Van der Waals interactions or hydrogen bonding.

At pH 7.4 a more negative ζ-potential was measured for ALAPP than for PEG. As such, electrostatic interactions with the ALAPP film should be less favourable than for the PEG film. Significantly, a contact angle difference of 57° was measured for the two films, with the PEG film being more hydrophilic, an important disparity between these two films at a pH of 7.4. Thus, rather than the stabilisation of a DNA on an ALAPP film being predominantly due to electrostatic interactions, hydrophobic effects between the hydrophobic nucleobases and hydrophobic functionalities within the ALAPP film were suspected to contribute significantly [18, 19]. It is suspected that the brush character of the PEG film, as discussed previously, also contributes to the low Γ^{DNA} seen on the PEG films.

To further investigate how DNA interacts with ALAPP surfaces, a series of experiments monitoring DNA adsorption in various solvents of varying pH, ion concentration and hydrophobicity were conducted. The results are shown in Figure 3.5-Figure 3.8. Entropically, the adsorption of DNA is driven by surface dehydration, that is, the removal of water molecules from the surface [20]. However, in order for this thermodynamically favourable process to occur, the DNA molecules must diffuse close enough to the surface to displace water molecules at the solid/liquid

interface. Being a polyelectrolyte, any charge at the surface would play a significant role in DNA adsorption due to long range electrostatic interactions. ζ-potential (Figure 3.1) and XPS (Table 3.2) measurements of freshly formed ALAPP suggest the presence of both anionic and cationic functionalities. The presence of cations and anions is thought to influence DNA adsorption in three ways. Firstly, the cations in solution should shield the anionic charge of the DNA, minimising any electrostatic repulsion from the surface [25, 26]. This is important as ALAPP has a net ζ-potential of $\approx$-20 mV at pH of 7.4. It is thought that there would be localised positive charge at the surface that could stabilise DNA on the surface. Secondly, the presence of cations should shield anionic functionalities on the DNA from adjacent charges on nearby DNA strands or on the same strand. This should allow the DNA to form a denser layer on the surface [25, 26]. Thirdly, and more apparent for higher valency cations, the presence of cations in solution can act as bridging ions between anionic charges on the surface and on the DNA strands. This has been observed particularly for DNA adsorption onto silica and mica [20, 23, 43]. To investigate whether the charged surface functionalities contribute to DNA adsorption via attractive electrostatic interactions, a plasmid solution was incubated with ALAPP samples and the resulting Γ^{DNA} was measured at varied [NaCl]. As expected, when the [NaCl] was increased, an increase in Γ^{DNA} was observed (Figure 3.5). The Γ^{DNA} increased up to 3 M salt solutions. Higher salt concentrations interfered with Picogreen® fluorescence. This result suggests that electrostatic interactions play a significant role in DNA adsorption to ALAPP. However, the pathway by which this enhanced DNA adsorption occurs is not clear, and all three above mentioned effects, the shielding of repulsive electrostatic DNA-surface interactions, compaction of DNA allowing higher density DNA layers and formation of bridging ions between the surface and

DNA, may contribute to the observed behaviour. To look more closely at the electrostatic forces occurring at the surface, the solution pH was varied between 4 and 9 whilst keeping the salt concentration constant. This should only alter the surface charge of the ALAPP surface whilst not altering the charge of the DNA molecule, which is negatively charged over most of the pH range [20]. Interestingly, the Γ^{DNA} was constant over the pH range of 6-8, but increased suddenly when the pH dropped to 5 and decreased slightly when the pH was increased to 9 (Figure 3.6). This corresponds well to the changes in ζ-potential measured for the freshly deposited ALAPP film. To demonstrate this, the Γ^{DNA} was plotted against ζ-potential over pH of 5-9, shown as Figure 3.7. A linear relationship is seen over the surface charge range. This result strongly suggests that DNA is interacting with the ALAPP electrostatically, however, this results also implies that the net negative charge of the polymer surface does, in part, inhibit the adsorption of DNA. The significant amount of DNA adsorption occurring at a ζ-potential of zero (0.2 mg/m^2), whereupon DNA adsorption is governed primarily by hydrophobic binding, further suggests the important role hydrophobic interactions play for DNA adsorption to ALAPP films.

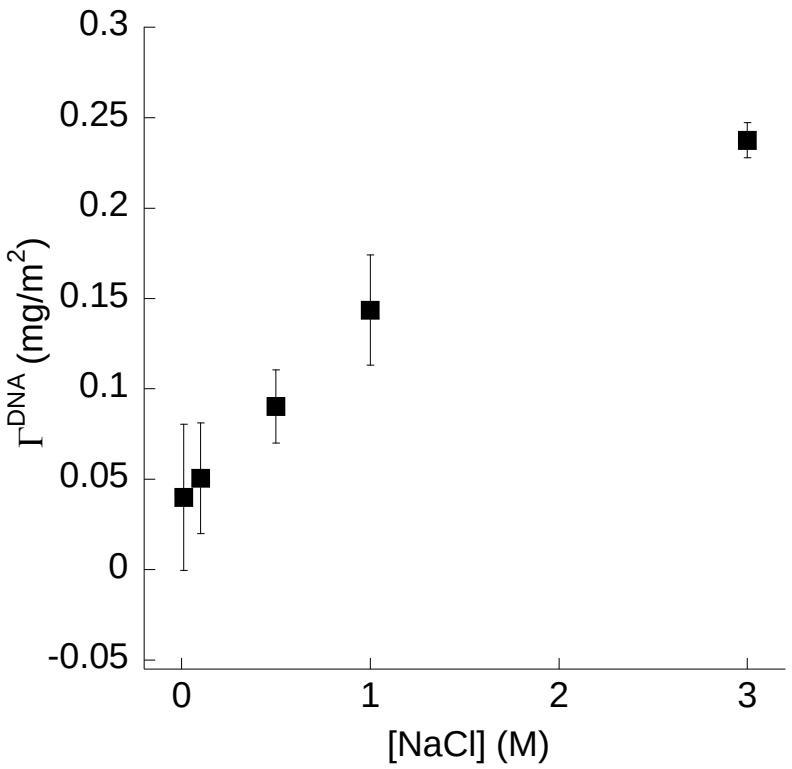

Figure 3.5. *DNA surface concentration as detected by measurements of the depletion of solution fluorescence on ALAPP against increasing [NaCl] in 0.01 M phosphate buffer, pH 7.4. Each DNA adsorption experiment was repeated three times. Error reported to 95% confidence.*

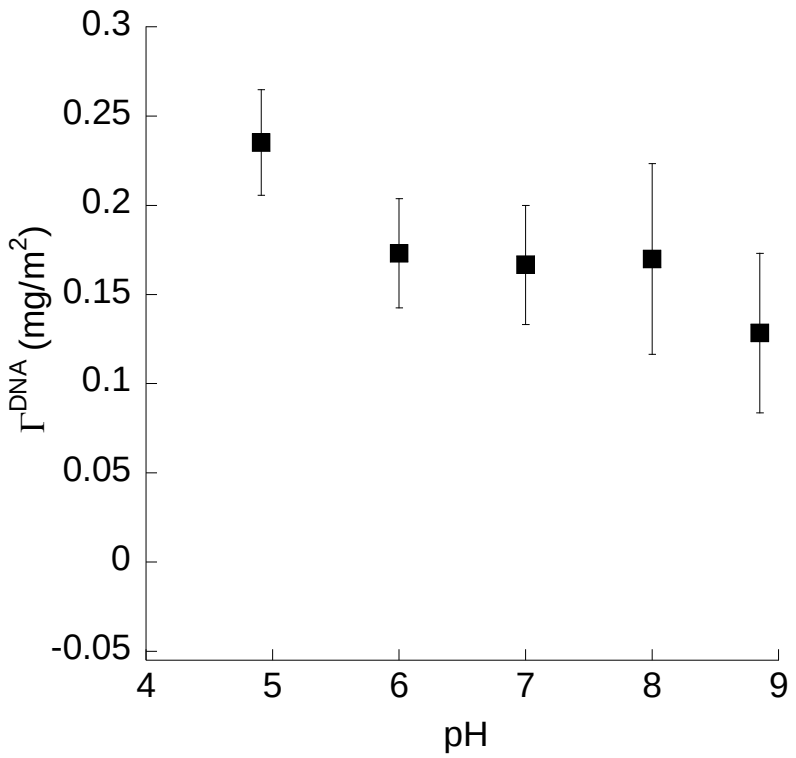

Figure 3.6. *DNA surface concentration as detected by measurements of the depletion of solution fluorescence on ALAPP against increasing solution pH in 0.01 M phosphate buffer, [NaCl] 0.5 M. Each DNA adsorption experiment was repeated three times. Error reported to 95% confidence.*

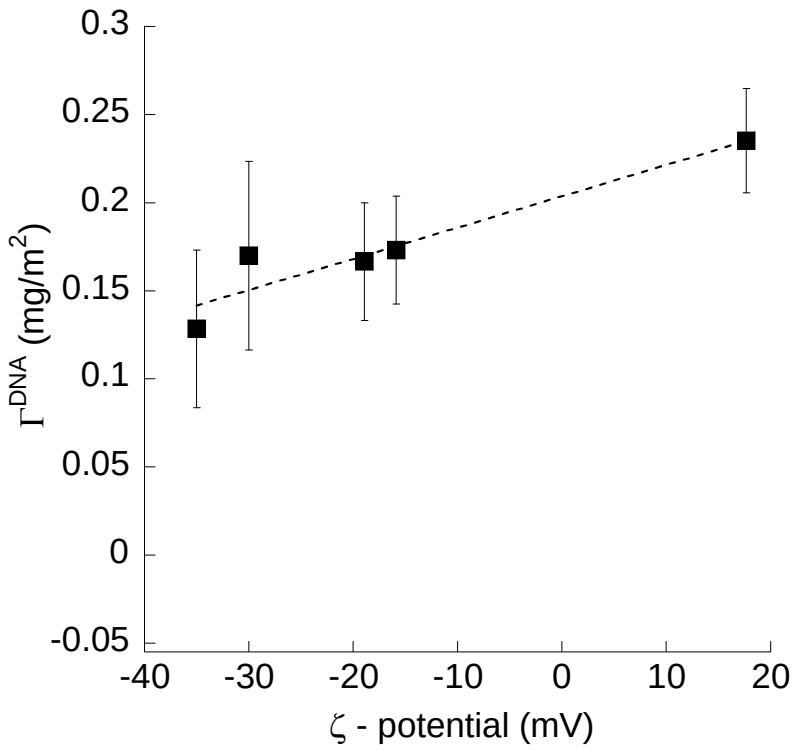

Figure 3.7. *Correlation of DNA surface concentration as detected by measurements of the depletion of solution fluorescence on ALAPP and ζ-potential in 0.01 M phosphate buffer, [NaCl] 0.5 M. A linear correlation fit is shown with R^2 = 0.904. Error reported to 95% confidence.*

To observe the influence of hydrophobic forces on the interaction of DNA with ALAPP, DNA adsorption was observed in solutions containing varied amounts of ethanol, from 0-50% (v/v). Higher ethanol content could not be measured because of quenching of Picogreen® fluorescence and high evaporation rates. The added ethanol decreases the free energy of the liquid/solid interface by decreasing the thermodynamic penalty for having a polar solvent exposed to hydrophobic moieties on the surface [213]. Thus, increasing ethanol content should decrease the driving force for DNA adsorption if hydrophobic interactions play a role. Electrostatic interactions on the other hand should remain unchanged. Interestingly, Γ^{DNA} decreased with increasing ethanol content (Figure 3.8) suggesting that hydrophobic interactions indeed contribute to DNA adsorption to ALAPP.

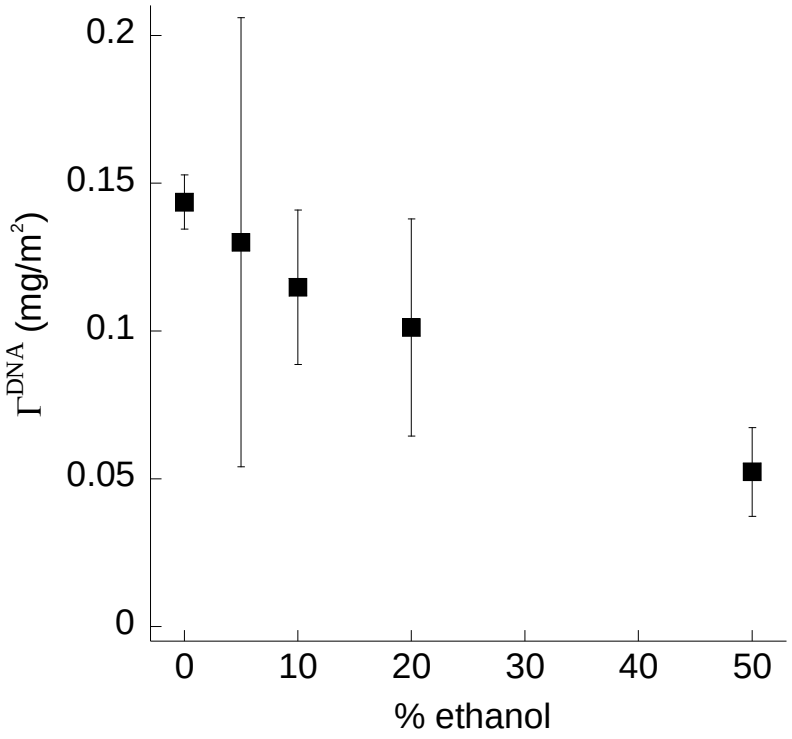

Figure 3.8. *DNA surface concentration after adsorption on ALAPP from aqueous solutions with increasing % ethanol as detected by measurements of the depletion of solution fluorescence. Each DNA adsorption experiment was repeated three times. Error reported to 95% confidence.*

3.3.4. Electro-stimulated DNA adsorption and desorption

As a final study, the electro-stimulated adsorption and desorption of DNA to both the ALAPP and PEG films was studied using measurements of the depletion of solution fluorescence. Initially the films were incubated in DNA solution overnight. Subsequently, +1.50 V was applied for 2 min to promote further DNA adsorption. After stabilisation for 4 mins, whereupon no voltage was applied, the polarity of the voltage was reversed and -0.75 V was applied for 2 min in order to trigger DNA desorption. After each voltage application, the DNA concentration of the bulk solution was determined by fluorescence spectroscopy and related to changes in the Γ^{DNA}. Delamination of the ALAPP or ALAPP-PEG films was not observed after voltage application.

The results are shown as Figure 3.9. Notably, very low Γ^{DNA} (<0.17 mg/m^2) were observed on the PEG film even with the application of a positive voltage, suggesting that PEG is very effective at resisting DNA adsorption, further proposing PEG films as highly robust non-fouling layers. However, the Γ^{DNA} on ALAPP was improved from 0.40 mg/m^2 to 1.33 mg/m^2 with the application of positive voltage. This increase in Γ^{DNA} was maintained at 0.90 mg/m^2 after the removal of voltage. Application of negative voltage was able to reduce the Γ^{DNA} down to 0.54 mg/m^2, clearly showing that the electro-stimulated DNA adsorption and desorption is possible on the ALAPP film. Similar results for ALAPP have been previously reported [34].

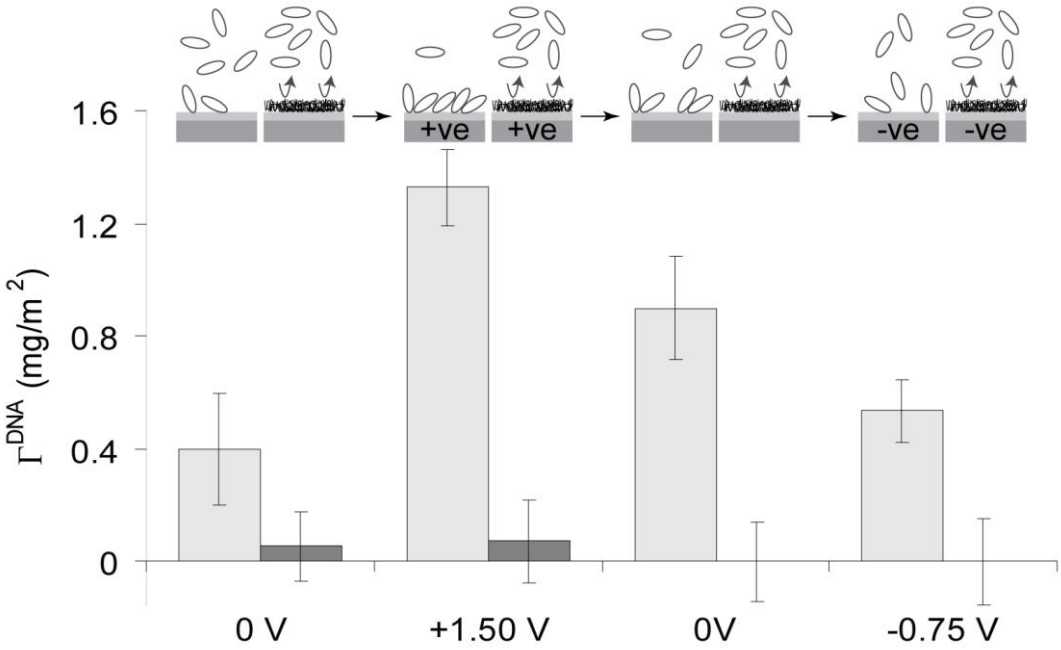

Figure 3.9. *The electro-stimulated adsorption and desorption of DNA on ALAPP (light grey) and PEG (dark grey) as detected by measurements of the depletion of solution fluorescence in 0.01 M phosphate buffer, [NaCl] 1.0 M, pH 7.4. ALAPP and PEG films were initially incubated for 24 hr in 100 ng/ml DNA solution before the stepwise application of +1.50 V, 0.00V and -0.75 V. Error reported to 95% confidence.*

3.4. Conclusion

Plasmid DNA adsorption has been characterised on ALAPP and PEG coatings using contact angle measurements, XPS, ζ-potential measurements, QCM and fluorescence measurements. These results provide new insights into the nature of DNA-surface interactions on the surfaces studied, suggesting that ALAPP coatings display electrostatic as well as hydrophobic functionalities that both contribute to DNA adsorption, allowing for the adsorption of DNA to ALAPP at a pH where the surface is negatively charged. Furthermore, under the conditions used the $\Gamma_{s\infty}$ and K for DNA adsorption to ALAPP were found to be 4.96 mg/m^2 and 1600 ml/mg respectively, suggesting a high DNA binding capacity. Time course studies of DNA adsorption showed that adsorption to both PEG and ALAPP surfaces followed simple Langmuir behaviour across the DNA concentration range studied, with ALAPP proving to be a superior DNA immobilisation matrix and PEG having a lower affinity for DNA. These results suggest that ALAPP coatings are suitable as substrate surfaces for applications where DNA immobilisation is desired, whilst PEG surfaces effectively reduce adsorption of double-stranded DNA. Given these findings, there is scope to produce two-dimensionally controlled DNA adsorption patterns on spatially controlled regions displaying ALAPP and PEG chemistries. Furthermore this chapter demonstrates that the adsorption and desorption of DNA to ALAPP surfaces can be stimulated by a positive or negative voltage, respectively. In comparison, identical voltages applied to a PEG surface did not have an effect on the amount of DNA adsorbed.

IV

CHAPTER 4. ADVANCED SUBSTRATE FABRICATION FOR CELL MICROARRAYS

The content of this chapter is based upon references [214, 215].

4.1. Introduction

The elucidation of complex biological relationships, such as genomic function, cellular development, molecular biological pathways as well as many other applications such as drug discovery require the analysis of biological data in a high-throughput, cost-effective manner in order to account for the large diversity, scope and multiplexicity demanded by current research. Microarrays have become standard tools for the highly parallel analysis of biological processes [97, 99, 125, 127, 216], requiring only minute amounts of probe molecules of interest, typically DNA, proteins or small biomolecules, to be deposited onto addressable locations on a surface conducive to biomolecular adsorption or covalent attachment [1, 15, 139]. Arrays of living cells are a relatively new addition to microarray technology and have shown promise in advancing the understanding of cellular processes and cell behaviour in terms of gene function, cell-cell signalling and cellular response to changes in environmental conditions [45].

Typically, cell arrays have been implemented by either of two approaches: printing arrays of cells onto a substrate [95, 217] or allowing cells to attach to an array-patterned substrate [45]. This second approach has been applied in the formation of polymer microarrays for the screening of cell-material interactions [143, 218], which enables the identification and development of new materials for specific biomedical applications. However, the arrayed polymers were not covalently linked

to the underlying surface. Another study arrayed monomers of interest with an initiator that upon UV irradiation instigates the *in situ* polymerisation of polymer material to form rigid polymer spots cross-linked to the substrate surface [145, 146]. This polymer microarray has been utilised to study the influence of surface chemistry on transfection [219]. However, this approach is limited to the formation of highly crosslinked, randomly ordered polymer networks, the structure of which may be difficult to characterise and replicate at a larger scale.

Cell microarrays have also been widely utilised for the formation of transfected cell microarrays (TCM), which utilise reverse transfection to form locally transfected cells within a lawn of cells seeded onto a microarray of DNA vectors of interest [1, 8]. Typically, a TCM is formed by firstly forming an array of DNA or RNA vectors of interest. Cells are then seeded onto the array for the formation of a lawn of cells such that cells attached onto arrayed spots will take up the arrayed vectors and express or silence the genes of interest. Recently, use of recombinant adenovirus based transfection systems allows for the use of primary cells with TCMs [169]. A significant challenge for this type of cell array is the prevention of cross-contamination between the spots and the outgrowth of cells from spots of interest. Therefore, researchers desire cell attachment to be limited to the arrayed spots, whilst the area in between the spots prevents cell attachment. This can only be achieved by surface patterning, introducing cell adhesive regions within a background that prevents protein adsorption and concurrently cell attachment, termed ‘low fouling’ [67]. A chemical or physical pattern regulating the growth of cells can be generated using a range of lithographic techniques including photolithography, soft lithography, microfluidics and microelectronics (see section 1.2) [66]. However, all of these techniques require microfabrication tools that are not always readily

accessible to life science laboratories, and whilst soft lithography has been adopted by life science researchers for surface patterning, methods such as microcontact printing or micromolding are not conducive to the production of an array of chemically or biologically diverse spots. Moreover, additional deposition of biomolecular arrays on top of the cell growth regulating patterns would typically occur in a different instrument, e.g. a microarray printer, such that pattern alignment issues arise and have to be overcome (see section 2.3.4) [174].

Here, the formation of a chemical pattern using photoreactive polymers is reported. Photoreactive crosslinkers have previously been investigated for covalently immobilising peptides, proteins and other biomolecules for the formation of biomolecular microarrays [220]. Typically, the underlying surface chemistry can be modified to contain photoactivatable groups that upon irradiation with a light source produce a highly reactive functional group that readily forms covalent bonds with biomolecules printed onto the layer [220]. This approach has been utilised to alter surface chemistry by immobilising polymer molecules to a surface [221], however, this is limited to surface coatings that can be functionalised, which may present a conflicting requirement to that of low fouling properties and also requires a blocking step in order to prevent binding to unreacted sites. Alternatively, the biomolecules themselves can be modified to contain a photoactivatable group. Peptides containing the Arg-Gly-Asp sequence have been immobilised to a surface by this method in order to promote cell attachment [222]. Furthermore, stable polymer surface coatings have been generated by functionalising a polymer of interest with a photoactivatable group [223]. This approach has also been adapted for modifying the surface of nanoparticles [224]. By utilising robotic contact printing, this approach could easily be adapted for development of a patterned substrate for formation of a cell

microarray. Such an approach was demonstrated, as illustrated in Figure 4.1, and allows the facile patterning of almost any base surface chemistry with a large variety of different polymer chemistries.

In this chapter, polymers of interest were modified with a crosslinker containing a photoactivatable phenylazide group. The modified polymers were then arrayed onto a low fouling coating and UV irradiated to crosslink the arrayed polymers to the underlying surface coating (Figure 4.1). The low fouling background was formed by initially coating a glass substrate with a thin plasma polymer film utilising allylamine as a monomer to introduce amine functionality that could subsequently be used to graft a high density poly(ethylene glycol) (PEG) brush to the surface. In the case of end-point grafted PEG, it has been found that the PEG coating provides an interfacial barrier that prevents proteins from interacting with the underlying substrate, which is concomitant with resistance to cell attachment. Therefore, the molecular weight and interfacial graft density of PEG chains are important parameters to enable low fouling properties of the coating [66, 67]. The resultant PEG coatings have been shown to resist protein adsorption, DNA adsorption and cell attachment [84, 188, 197].

Specifically, this approach enables the formation of a surface pattern consisting of islands, where cell attachment is promoted, on a low fouling background surface. This method further allows the formation of a library of polymers in an array format. Moreover, since patterning is readily achieved using a robotic spotting device, the surface patterns formed can be used for the subsequent deposition of biomolecule arrays, thus, enabling chip-based, high density cell assays.

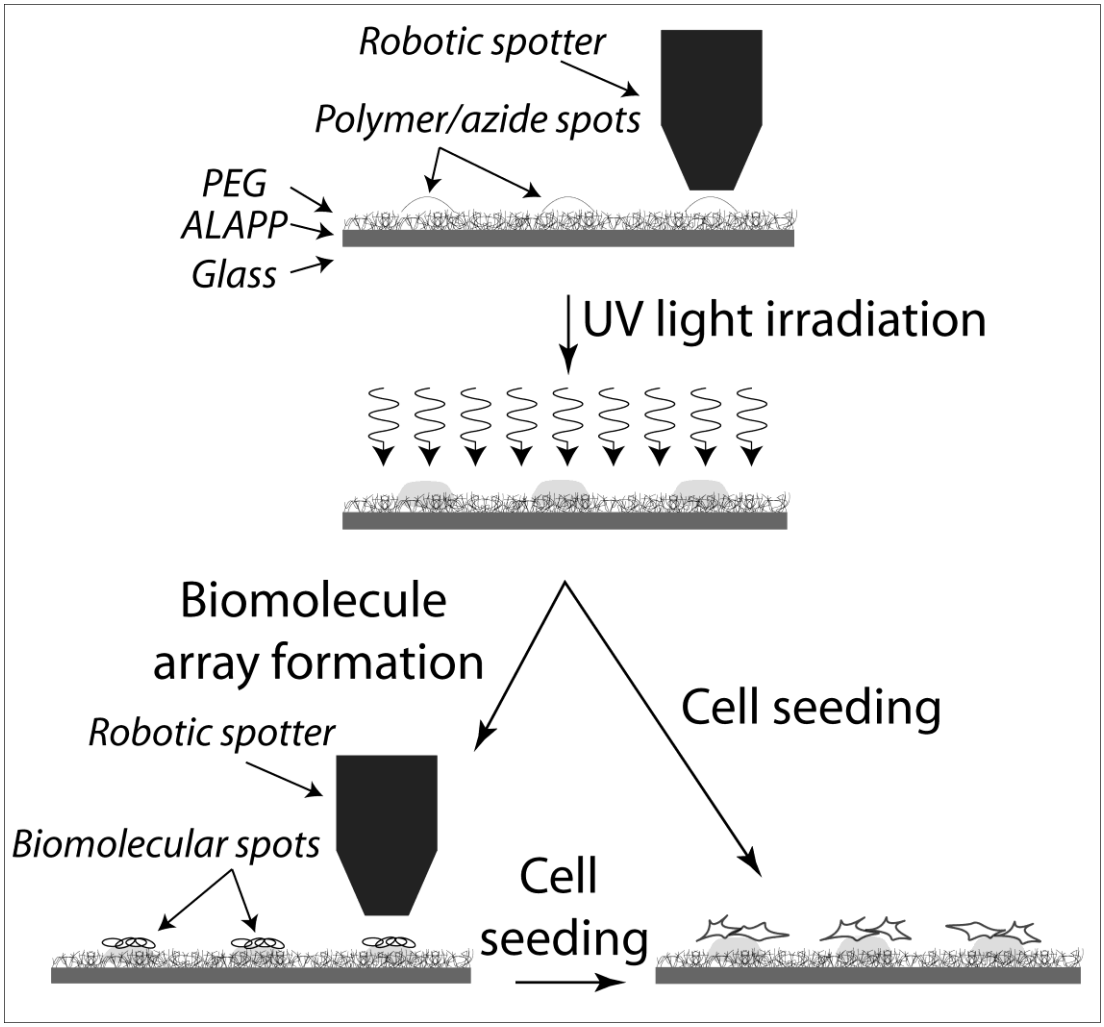

Figure 4.1. *Schematic of the formation of a chemically patterned surface for cell microarray applications. A polymer functionalised with a photoreactive phenylazide group is arrayed onto a PEG surface using a robotic spotter. Subsequent irradiation with UV covalently links the polymer to the PEG surface, resulting in the formation of a patterned surface, which can subsequently be used as a base substrate for the additional formation of a DNA, protein or small molecule array formed by the same robotic spotter that was utilised for the polymer array formation. When cells are seeded to these patterned surfaces, cell attachment follows the crosslinked polymer pattern while attachment on the PEG surface between printed spots is prevented. Schematic not drawn to scale.*

4.2. Materials and methods

4.2.1. Substrate preparation

Allylamine plasma polymer (ALAPP) depositions onto glass slides were performed in a custom-built reactor described elsewhere [182]. In short, the plasma reactor consisted of two circular electrodes separated by 125 mm in a cylindrical reactor being 350 mm high with a diameter of 170 mm. Allylamine (Aldrich, 98% purity) was used as a monomer. Polymerisation conditions used were a frequency of 200 kHz, a power of 20 W and an initial monomer pressure of 0.188 mbar. Deposition time was 25 s. PEG monoaldehyde (Shearwater Polymers, Huntsville AL, USA) with a molecular weight of 5000 was grafted onto freshly deposited ALAPP layers by reductive amination. Grafting was performed under 'cloud point' conditions in 20 ml of a 0.1 M sodium phosphate buffer containing K_2SO_4 (2.2 mg), $NaCNBH_3$ (60 mg) and PEG monoaldehyde (50 mg) at pH 6.2. Freshly deposited ALAPP films were incubated in the PEG grafting solution at 60 °C for 16 hr.

4.2.2. Array formation

For optimisation of polymer printing, a 1 mg/ml poly(ethyleneimine) (PEI) (MW 70,000, Fluka) solution was arrayed onto a (PEG) surface using a BioOdyssey Calligrapher MiniArrayer (Bio-Rad) with a 375 µm diameter solid pin (ArrayIt) delivering approximately 4.0 nL/spot. Initially, the formation of the PEI array on the PEG surface was optimised by altering the humidity in the range of 57-65% and the temperature in the range of 3-37 °C. 65% humidity and 25 °C were determined to produce optimum spot size and uniformity and were used for subsequent formation

of polymer arrays. PEI arrays were scanned using a GenePix 4000A microarray scanner. PEI spots were analysed using ImageQuant V 5.2 software.

Poly(acrylic acid) (PAA) (Aldrich, MW 90,000), PEI, poly(L-lysine) (PLL) (Sigma, MW 70,000) and poly(vinyl pyrrolidone) (PVP) (Fluka, MW 380,000) were spotted onto ALAPP-PEG coated glass. Before spotting, polymer samples were prepared to 4.0 mg/ml solutions in ultra pure water containing 2.0 mg/ml (6.6 mM), 1.00 mg/ml (3.3 mM), 0.50 mg/ml (1.6 mM) or 0.00 mg/ml (0.0 mM) N-succinimidyl-5-azido-2-nitrobenzoate (NSANB) (Fluka) and polymer-NSANB solutions were incubated at 25 °C for 10 min before array formation. Alternatively, PAA (8.0 mg/ml) was prepared in 50 µl of ultra pure water containing 150 mM N-hydroxy succinimide (NHS) (Sigma) and 60 mM 1-ethyl-3-(3-dimethylaminopropyl) carbodiimide hydrochloride (EDC) (Fluka) and incubated for 1 hr at 37 °C. 50 µl of 4.0 mg/mL (13.2 mM), 2.0 mg/mL (6.6 mM), 1.0 mg (3.3 mM) or 0.0 mg (0.0 mM) NSANB in ultra pure water containing 14.0 mM ethylenediamine (Merck) at 25 °C was incubated for 10 min before adding to the 50 µl of activated PAA, to make a final volume of 100 µl, and incubating for a further 10 min before array formation. For analysis by profilometry, arrays were prepared from initial polymer concentrations of 2.00, 1.00, 0.50, 0.25, 0.10 or 0.00 mg/ml containing 1.0 mg/ml (3.3 mM) NSANB solution. Spotting was conducted using a BioOdyssey Calligrapher MiniArrayer (Bio-Rad) using a 375 µm diameter solid pin (ArrayIt) at a humidity of 65% and a temperature of 25 °C. The approach speed of the pin and the dwell time of the pin in contact with the surface were set to 20 mm/s and 15 ms respectively. All polymer spotting and solution preparation was conducted in the dark. All solutions used for spotting were made to a final volume of 50 µl. After array formation samples were exposed to UV (25 W) for at least 10 mins, which was

sufficient time to ensure complete reaction of the crosslinker. This resulted in the formation of crosslinked PEI and PLL spots ((PEIc) and (PLLc) respectively). In this case, PAA and PVP were used as negative controls. The UV lamp (multiband source, 254-365 nm) was held 1 cm from the sample. Resultant polymer arrays were washed overnight in 0.05% Tween20 (Aldrich) solution at 37 °C with stirring before rinsing with MilliQ water and drying under nitrogen. For preparation of a polymer array with subsequent DNA array formation, the initial PLLc polymer array was deposited using a 1000 µm diameter solid pin (ArrayIt). This pin was also used for subsequent spotting of DNA and transfection reagent. After formation of the polymer array the chips were removed from the MiniArrayer, exposed to UV and washed in MilliQ water before being dried under a nitrogen stream and placed back in the MiniArrayer. Positioning blocks within the MiniArrayer were used to ensure exact re-positioning of removed slides. Plasmids pEGFP-N1, encoding for the green fluorescence protein (GFP), and pDsRed2, encoding for the red fluorescence protein (RFP), were then arrayed onto the polymer spots in a checkerboard pattern at a concentration of 100 µg/ml in nuclease free water at a humidity of 65% and a temperature of 15 °C. DNA spots were reprinted thrice to increase surface coverage. Effectene transfection agent (QIAGEN) was spotted directly on top of the DNA array at the same atmospheric conditions. Effectene transfection reagent was prepared as follows. 4 µl enhancer was added to 37 µl DNA condensation buffer (EC buffer) and incubated at room temperature for 10 mins. 6 µl Effectene was then added and all reagents were vortexed before printing. Arrays were washed with MilliQ water to remove unbound DNA before cell culture.

4.2.3. Characterisation of polymer crosslinking

Arrays were imaged before and after washing using a GenePix 4000A microarray scanner (Axon Instruments) using a 17 mW 532 nm laser for excitation and a 570 nm suppression filter. The thickness and profile of the arrayed spots was determined by profilometry using a Dektak 6M Stylus Profiler (Veeco). A diamond stylus of radius 12.5 µm was moved over the surface at a resolution of 0.25 µm/sample and a stylus force of 5 mg. Each spot was measure 3 times. The rims of spots were ignored for height measurements.

4.2.4. Cell culture

SK-N-SH neuroblastoma and human embryonic kidney (HEK-293) cell lines were used for cell attachment experiments. Cells were cultured in Dulbecco's modified eagle media (DMEM) containing 10% fetal bovine serum, 5 mM Glutamax and penicillin and streptomycin and incubated at 37 °C, 5% CO_2 and 60-70% humidity. For cell attachment studies, SK-N-SH cells were seeded onto surfaces at a seeding density of $5x10^4$ cells/cm^2 and allowed to attach to the surface after which they were incubated at 37 °C, 5% CO_2 and 60-70% humidity for 24 hr. Cells were then stained by incubation in Hoechst 33342 dye (10 mg/ml) for a further 5 min before analysis by fluorescence microscopy. Cells were visualised with an IX81 Olympus fluorescence microscope and analysed using analySIS LS Research v2.5 software using a 360-370 nm excitation filter and a 420 nm suppression filter to detect Hoechst 33342 fluorescence. Formation of a TCM was achieved by seeding HEK-293 cells onto the pEGFP-N1 and pDsRed2 checkerboard pattern. Cells were seeded onto surfaces at a seeding density of $5x10^4$ cells/cm^2 and allowed to attach to the surface after which they were incubated at 37 °C, 5% CO_2 and 60-70% humidity

for 48 hr. Cells were visualised by fluorescence microscopy. GFP fluorescence was taken through a 470-495 nm excitation filter and a 510 nm suppression filter. RFP fluorescence was observed through a 530-550 nm excitation filter and a 575 nm suppression filter.

4.3. Results and discussion

4.3.1. Optimisation of polymer printing

Initially the optimised formation of PEI arrays was of interest, thus, PEI printing was conducted at varied temperature, humidity, approach speed of the pin to the surface and dwell time of the pin in contact with the surface. Fluorescence images of PEI spots formed under these varied conditions are shown in Figure 4.2. The diameter and variability of the pixel height, calculated as the standard deviation of the height of the total number of pixels for each spot, was calculated and also graphed in Figure 4.2. It should be noted that Figure 4.2A and Figure 4.2B were obtained on separate days such that the pixel intensity values are not quantitatively comparable. A number of key conclusions can be determined from Figure 4.2. Firstly, printed PEI spots always have a rim as a result of mass transport effects as the spot dries [225]. Formation of this rim results in an increased variability across the spots. It can be seen from Figure 4.2A that decreasing both temperature and humidity increases the variability as a result of increasing the thickness and height of the rim. Altering humidity does not have any affect on the spot diameter. However, decreasing temperature increases the spot size. In order to minimise variability, a humidity of 65 % and a temperature of 30 °C was selected for further PEI array formation.

In order to further optimise the formation of PEI spots, the approach speed and dwell time of the pin to the surface where altered. The PEI spots formed as a result of altering these parameters are shown as Figure 4.2B. Interestingly, altering dwell time appeared to have little effect on the size or morphology of spots, however, increasing the approach speed from 5 to 20 mm/s was observed to decrease the spot diameter from 580 µm to 490 µm and also decreased the spot variability, presumably by minimising the formation of the polymer rim. Thus, an approach speed of 20 mm/s and a dwell time of 10 ms were selected for subsequent PEI printing.

4.3.2. Polymer microarray formation

Initially, a low fouling polymer film was formed on a clean glass slide. Plasma polymerisation [38] using allylamine as a monomer was used to deposit a thin film displaying amine functional groups, which were used to subsequently graft aldehyde terminated PEG chains by reductive amination under cloud point conditions [67]. Plasma polymerisation was used here as it is able to produce a pin-hole free, well adherent film on almost any base substrate, allowing this approach to readily be adapted to almost any material of choice.

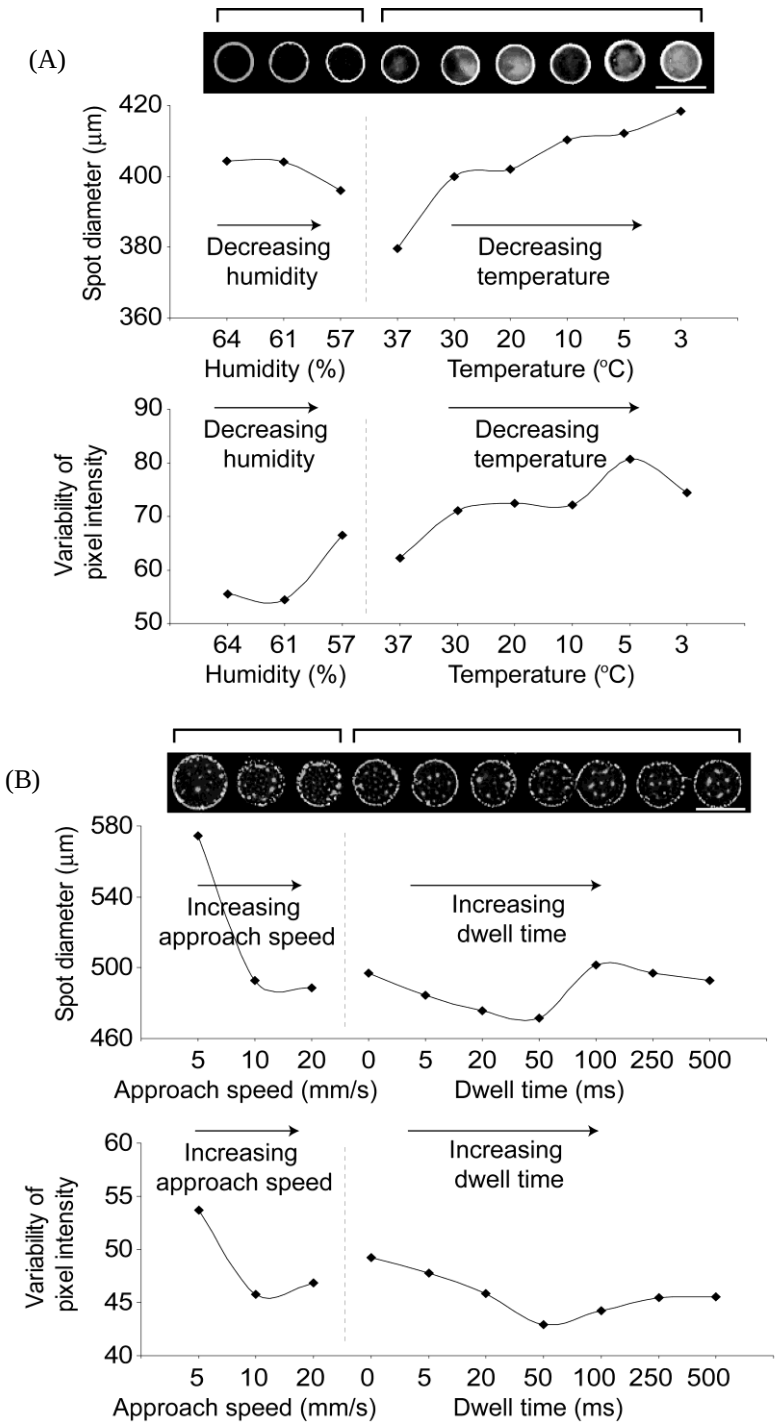

Figure 4.2. *Characterisation of the spotting of PEI onto an ALAPP-PEG surface. (A) 1 mg/ml PEI spots spotted at varied humidity and temperature. From left to right, the first three spots correspond to humidity of 64%, 61% and 57%. The next six spots correspond to temperatures of 37 °C, 30 °C, 20 °C, 10 °C, 5 °C and 3 °C. (B) 1 mg/ml PEI spots spotted at varied approach speed and dwell time. From left to right, the first three spots correspond to approach speeds of 5 mm/s, 10 mm/s and 20 mm/s. The next seven spots correspond to dwell times of 0 ms, 5 ms, 20 ms, 50 ms, 100 ms, 250 ms and 500 ms. The spot diameter and the variability of pixel intensity for each spot is graphed underneath each spot. The scale bars equal 500 µm.*

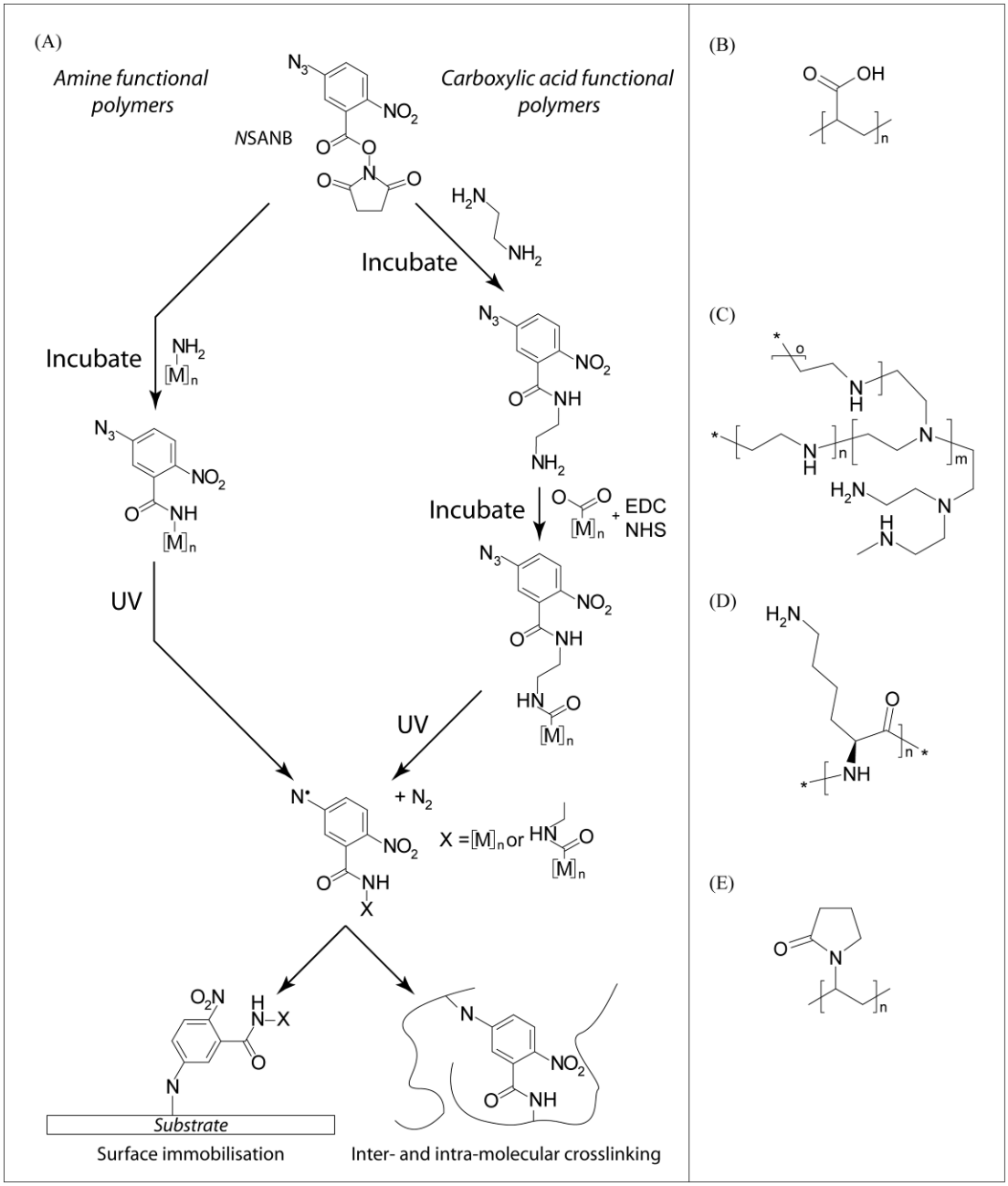

Figure 4.3. *(A) Chemical schematic of an amine or carboxylic acid functional polymer $[M]_n$ functionalised with phenylazide functional groups by incubating with NSANB and its activation for surface immobilisation and inter- and intra-molecular crosslinking. For carboxylic functional polymer the NSANB was initially amine functionalised by a reaction with ethylenediamine. (B-E) structures of polymers used; (B) PAA, (C) PEI, (D) PLL, (E) PVP.*

NSANB was reacted with amine functional synthetic polymers in aqueous media in order to produce phenylazide modified polymers, as shown in Figure 4.3A [220, 226]. Two amine functional polymers were used, PEI and PLL (Figure 4.3C and D). In addition, two polymers without amine groups were used as negative controls; PAA and PVP (Figure 4.3B and E). The NSANB concentration was altered from 0 to 2 mg/ml, resulting in molar ratios of cross-linker to amine groups for the amine functional polymers of 0.24, 0.12, 0.06 and 0.00. In order to functionalise the PAA with NSANB, the NSANB was initially incubated with ethylenediamine before being covalently linked to PAA in the presence of EDC and NHS. This approach will also result in the formation of some diazide crosslinker, whereupon a NSANB molecule links to both ends of the ethylenediamine, however, this side reaction should assist in the surface immobilisation and inter- and intra-molecular crosslinking of PAA spots. NSANB concentrations were altered from 0 to 2 mg/ml, resulting in molar ratios of cross-linker to carboxylic acid groups for the PAA of 0.12, 0.06, 0.03 and 0.00, assuming the functionalisation reaction went to completion. This process is shown schematically in Figure 4.3A. After reaction with the crosslinker, the polymers were spotted onto the PEG coated glass slide surfaces in an array format using a robotic contact spotter. This was done in a dark room. Once an array of polymer spots was formed, the slide was irradiated with UV light for 10 min to form highly reactive nitrene species that readily insert into nearby C-H bonds, enabling the formation of covalent bonds between the printed polymer and the underlying PEG coating as well as inter- and intra-molecular crosslinking (Figure 4.3A). The advantage of this approach is that the underlying surface chemistry is not limited to the PEG surface described, but can be readily applied to other organic surface coatings such as self-assembled monolayers of PEGylated-thiols on a gold substrate. After washing to

remove any unbound polymer, the resultant surface pattern was available for subsequent formation of an additional microarray deposited on top of the polymer spots or for the seeding of cells that readily attach to the regions modified with amine functional polymers, while cell attachment on the underlying PEG coating is prevented. This technique is not limited exclusively to amine functional polymers. By choice of suitable photoreactive crosslinkers, microarrays containing a wide variety of synthetic polymers with diverse chemistries could be formed.

4.3.3. Polymer microarray characterisation

Initial experiments were aimed at demonstrating that amine functional polymers reacted with NSANB can indeed be covalently bound to the PEG coating in the form of an array of polymer spots. A polymer array set of PAA, PEI, PLL and PVP was initially incubated with NSANB at a concentration of 2, 1, 0.5 and 0 mg/ml for 10 min. As a negative control, PAA and PVP were also included. The phenylazide derivatised polymers was arrayed onto the PEG coating and subsequently irradiated with UV. The array was then subjected to overnight washing in 0.05% Tween20 solution at 37 °C with constant stirring to remove unbound polymer. Fluorescence microscopy images were taken of the array before and after washing and are shown in Figure 1. The polymer spots are approximately 400 µm in diameter due to the use of a 375 µm diameter spotting pin. Here the fact that these polymers show autofluorescence is utilised [227]. PEI shows strong autofluorescence whilst PAA showed only weak fluorescence (Figure 4.4A). After washing, the PAA and PVP arrays were removed, judging by the absence of fluorescence (Figure 4.4C). This was expected as NSANB was not able to react with these polymers due to the absence of amine groups, thus preventing the formation of covalent linkages between polymers

and the surface. Furthermore, no difference was observed between PAA and PVP spots with and without NSANB after washing (Figure 4.4C), suggesting the NSANB did not directly link this polymer to the surface utilising amine functionality on the plasma polymer layer, which should be shielded by the dense PEG coating. This contrasts with PAA functionalised with NSANB, which showed equivalent autofluorescence before washing irrespective of the amount of NSANB present (Figure 4.4B). However, after washing all the PAA spots were removed, judging by the absence of fluorescence (Figure 4.4D), except for the polymer spot containing the highest concentration of NSANB of 2.0 mg/ml (Figure 4.4D). This suggests that by introducing amine functionality to the NSANB prior to incubating with PAA a covalently immobilised PAA array on the PEG coating can be formed. Furthermore, the PEIc and PLLc that were covalently immobilised to the surface could be observed even after extensive washing (Figure 4.4C). Spots printed from polymer solutions without crosslinker were removed almost completely (the column of spots on the right of each array set) (Figure 4.4C). This confirms that the spots formed from the derivatised polymers are covalently cross-linked to the surface and are able to withstand extensive washing.

The polymer spots were further analysed by profilometry before and after washing in order to quantitatively observe the removal of unbound polymer. The heights of spots formed on a PEG coating from polymer concentrations of 2, 1, 0.5, 0.25, 0.1 and 0 mg/ml containing 1 mg/ml NSANB were measured. All polymers exhibited an increase in height with increasing polymer solution concentration (Figure 4.5). However, after washing the height of PAA and PVP spots at all initial polymer concentrations was reduced to near zero (Figure 4.5A and D), whilst the height of PEIc and PLLc remained statistically indistinguishable after washing from

the height before washing (Figure 4.5B and C). This further confirms the photoinduced formation of covalent crosslinks between the phenylazide modified polymer and the PEG surface.

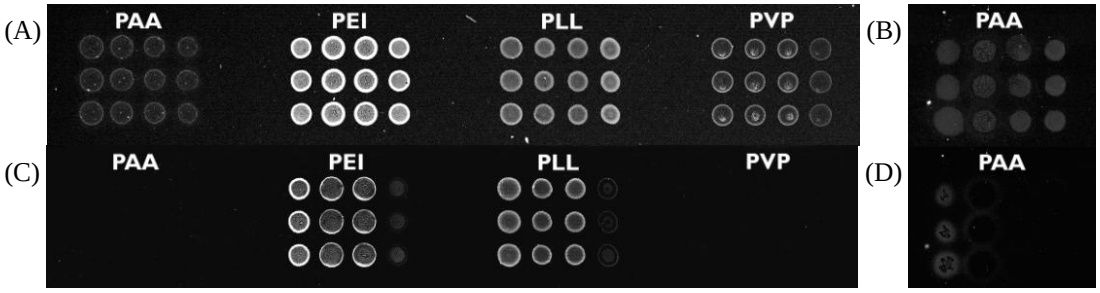

Figure 4.4. *Fluorescence images of polymer arrays before (A and B) and after (C and D) overnight washing. For (A) and (C), from left to right each array set corresponds to PAA, PEI, PLL and PVP printed onto a PEG coating at an initial polymer concentration of 4 mg/mL. Across each row from left to right in each array set the concentration of NSANB incubated with the polymer before spotting is altered between 2.0, 1.0, 0.5 and 0.0 mg/mL. Each column is a set of three replicates. For (B) and (D), each array set is of PAA functionalised with NSANB printed onto a PEG coating at an initial polymer concentration of 4 mg/mL. Across each row from left to right in each array set the concentration of NSANB incubated with the polymer before spotting is altered between 2.0, 1.0, 0.5 and 0.0 mg/mL. Each column is a set of three replicates. The centre-to-centre distance between spots is 750 μm.*

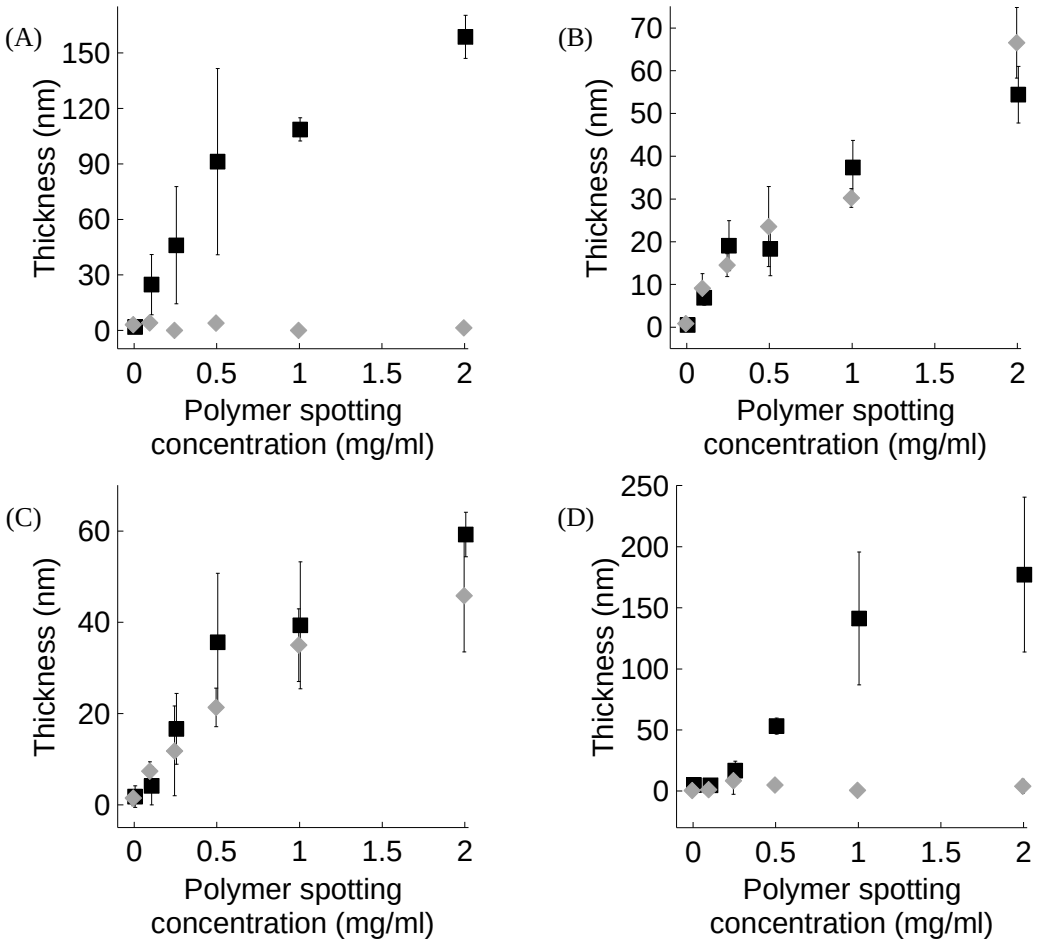

Figure 4.5. *Height measurements of UV irradiated polymer spots determined from profilometry before (■) and after (◆) washing of polymer spots of PAA (A), PEIc (B), PLLc (C) and PVP (D) printed from polymer solutions of varied concentration, all containing 1 mg/ml NSANB solution.*

4.3.4. Cell microarray formation

In order to test the suitability of the polymer microarrays for subsequent formation of a cell microarray, PLLc on a PEG background were incubated with SK-N-SH neuroblastoma cells. This cell line was used as these cells are known to be adherent on many different surfaces, thus, presenting a good model for studying cell adhesive properties [228]. Cell array formation was visualised by fluorescence staining with Hoechst 33342 after overnight attachment. The resulting fluorescent images are shown in Figure 4.6A and B.

Cells were found to adhere well to PLLc as seen by the high numbers of cells attached to these regions. Typically, 1400 cells were found on each PLLc with a diameter of approximately 400 µm given an average cell area of 90 μm^2. The cell pattern formed aligns perfectly with the underlying polymer pattern with the resultant cell adhesive areas being well defined (Figure 4.6B). PEG is well known in its ability to resist cell attachment and protein adsorption [65, 67, 84], whilst, PLL is known to promote the attachment of many different cell types [229]. Thus, this surface chemistry is universal in nature, being applicable to most adherent cell lines. This was demonstrated by repeating the same experiment using HEK-293 cells, a different cell line which also formed clear cell patterns matching the underlying polymer pattern (Figure 4.6C). The PEG background showed significantly less cell attachment for both cell lines, enabling the formation of a well defined surface pattern containing both low fouling and cell adhesive regions. The general approach of a low fouling background coating combined with a photocrosslinked polymer can be readily adapted to other low fouling background coatings, polymers and crosslinker chemistries.

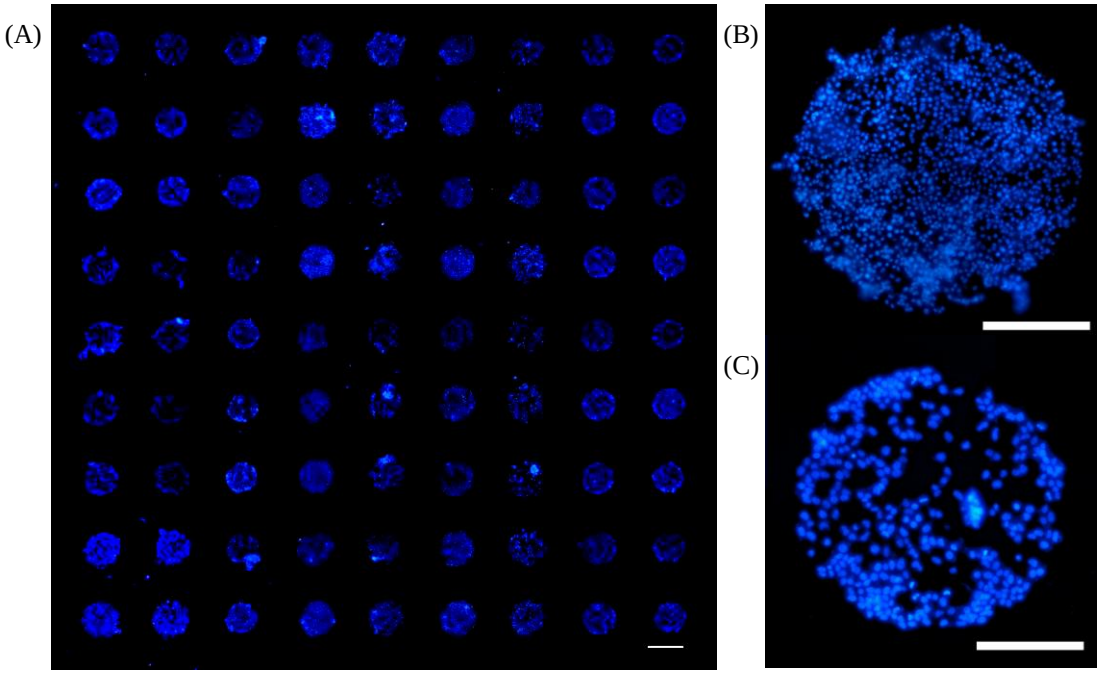

Figure 4.6. *Fluorescence microscopy images of Hoechst 33342 stained mammalian cells grown on a PLLc array with (A) image of a SK-N-SH neuroblastoma cell microarray, 4x magnification, scale bar equals 500 µm, (B) 20x magnification of a single spot, scale bar equals 200 µm and (C) single spot of a HEK-293 cell microarray, 20x magnification, scale bar equals 200 µm.*

However, the key advantage of this approach is the integration of the cell adhesion regulating pattern with the subsequent formation of a small-molecule, protein, DNA or RNA microarray. By way of a demonstration, a TCM was prepared by first spotting an array of DNA vectors using pEGFP-N1, a plasmid encoding for a GFP, and pDsRed2, a plasmid encoding for a RFP, along with Effectene transfection agent on top of the already prepared PLLc polymer array. Since surface patterning and microarray formation are carried out on the same instrument, alignment of the two surface patterns was easily achieved. At neutral pH, PLL is positively charged, thus stabilising electrostatically the deposited DNA. The interactions between DNA and PAA, polyallylamine (PALA), PEI, PLL and PVP surface coatings was assessed by atomic force microscopy force measurements (Appendix 2). This demonstrated the electrostatic nature of interactions between DNA and PALA, PEI and PLL. The PEG surface has previously been shown to restrict DNA adsorption, hence preventing surface diffusion of the DNA spots on the surface [188, 207]. HEK-293 cells were subsequently seeded onto the array and were visualised by fluorescence microscopy after 48 hr incubation at 37 °C to check for reverse transfection. A checkerboard pattern of red and green cells resulted (Figure 4.7A), whereupon cells fluorescing green were localised to regions where pEGFP-N1 had been spotted on PLLc (Figure 4.7B) whilst cells fluorescing red were localised to regions where pDsRed2 had been deposited on PLLc (Figure 4.7C), confirming that reverse transfection had occurred. There were no fluorescent cells found outside the PLLc regions. Furthermore, green and red fluorescing cells were not observed on the same spot, demonstrating the absence of cross-contamination. Typically, transfection efficiencies of 15-20% were observed, which is similar to previously reported efficiencies [29, 35].

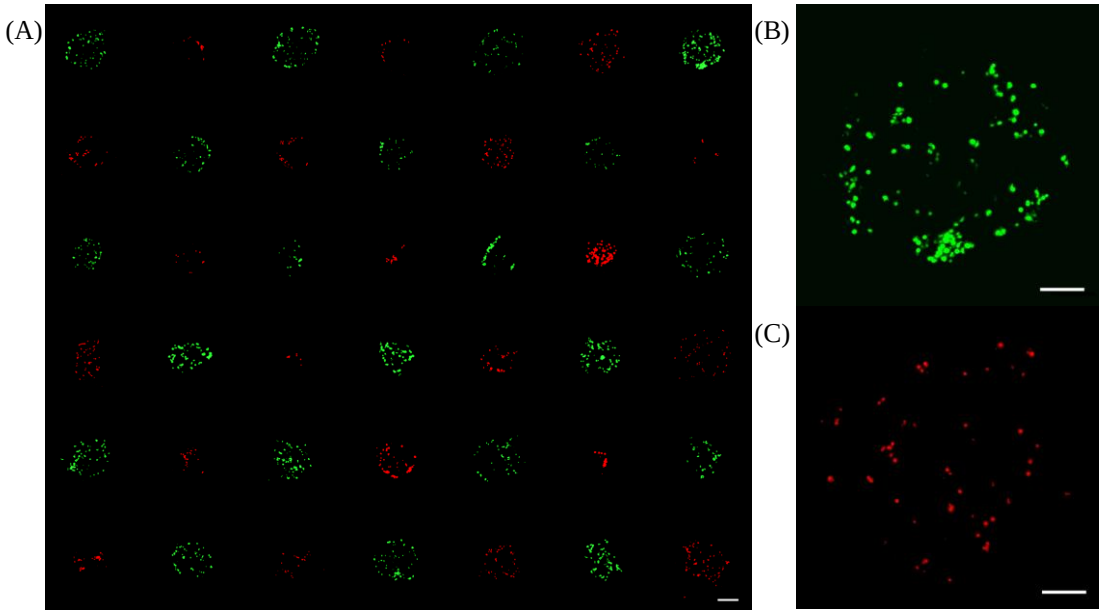

Figure 4.7. *Fluorescence microscopy images of HEK-293 cells grown on a PLLc pattern on a PEG background with a checkerboard DNA vector array pattern. (A) 4x magnification of entire checkerboard array with red and green fluorescence combined. Scale bar equals 500 μm. (B) 20x magnification of a single spot containing a plasmid encoding for GFP. Green fluorescence is due to the presence of GFP within cells. Scale bar equals 200 μm. (C) 20x magnification of a single spot containing a plasmid encoding for RFP. Red fluorescence is due to the presence of RFP within cells. Scale bar equals 200 μm. GFP fluorescence taken through a 470-495 nm excitation filter and a 510 nm suppression filter. RFP fluorescence taken through a 530-550 nm excitation filter and a 575 nm suppression filter.*

This result effectively demonstrates the successful formation and alignment of a DNA microarray on top of a prepared surface pattern that is able to influence adhered cells in two ways. Firstly, the presence of the synthetic polymer pattern directs cell attachment and, secondly, the spotted DNA vectors alter the gene expression profile of the cell, imparting a significant improvement to current cell microarray technology.

4.4. Conclusion

This chapter demonstrates the ability of the BioOdyssey Calligrapher microarrayer to successfully form a polymer microarray that can subsequently be used for cell attachment studies. Tuning the printing parameters, such as humidity and temperature, enables the altering of the printed spots to an idealised state.

Additionally, this chapter demonstrates the formation of stable, covalently linked polymer microarrays using a robotic spotting device. Utilising a highly reactive crosslinker to activate soluble synthetic polymers enables the covalent linkage of the resultant arrays to a broad range of organic substrate materials, including low fouling PEG coatings. In the present chapter PEI and PLL were covalently linked to surfaces, however, by judicious choice of a crosslinker a wide range of polymers can be used following this approach. In addition, polymer patterns can also be generated by means other than robotic printing, for example using micromolding, microfluidics, dip-pen nanolithography and microcontact printing.

Furthermore, polymer microarray formation enables the pre-patterning of microarray substrates for the formation of biomolecule microarrays. Seeding of cells onto such microarrays enables the high-throughput study of cellular responses to a library of biomolecules of interest. In the present case a TCM was successfully

formed on a pre-patterned substrate. Here, cell attachment is limited to specific regions, making this platform suitable for high density cell assays such as those for use in functional genomics.

V

CHAPTER 5. SURFACE PLASMON RESONANCE IMAGING OF POLYMER MICROARRAYS

5.1. Introduction

Polymer microarrays are an emerging key enabling technology for the identification and development of new polymer materials for specific biomaterial applications. Typically, a polymer microarray consists of an array of different polymers with varied properties in order to assess the biological response, including cell attachment, proliferation or differentiation in response to a particular polymer chemistry or topography [143, 145, 218]. In one approach to creating a polymer microarray, different ratios of 24 different monomers were arrayed in the presence of an initiator on an epoxy coated glass substrate [145]. UV irradiation was used to initiate the *in situ* polymerisation of polymer material to form rigid, cross-linked polymer spots. Polymer-cell interactions were assessed on this array [219, 230]. However, this technique is limited to the formation of highly crosslinked polymer networks, the structure of which may be difficult to characterise and replicate at a larger scale. Polymers arrays may also be formed by arraying pre-fabricated polymers to a substrate surface by a method such as robotic contact printing [143, 144], allowing for the analysis of polymer materials fabricated by means of advanced polymerisation techniques, such as atom transfer radical polymerisation or radical addition-fragmentation chain transfer polymerisation [231, 232]. Copolymers including block-copolymers are also available for printing, further increasing the combinatorial space. Moreover, the polymers can be characterised extensively by conventional techniques before being arrayed. An array of 120 polyurethanes formed

by this method was used to identify polymers that promoted the attachment of dendritic cells, which is an important step in the development of phagocytosis assays [144]. Polymers containing poly(tetramethylene glycol) and 4,4'methylene bis(phenylisocyanate) were found to be suitable for this application [144]. This approach has been further developed by incorporating a switchable cross-linker activated by UV exposure into the polymer arrays, resulting in the formation of covalently linked, rigid, stable polymer spots suitable for long incubation time cell growth analysis (See CHAPTER 4)[215]. This technique also benefits protein and cell microarrays by enabling the formation of adhesive areas on a low-fouling polymer background. Pattern formation using the same apparatus as is used to array proteins or cells avoids misalignment between surface patterns and enables surface patterning and biomolecule deposition in a one step procedure.

The high-throughput, expeditious characterisation of the resultant polymer microarrays is imperative for assessment of cell-material interactions. Water contact angle measurements, X-ray photoelectron spectroscopy (XPS) and time-of-flight secondary ion mass spectroscopy (Tof-SIMS) measurements of a polymer microarray have been achieved in a rapid format to successfully characterise the properties of each individual spot [146, 233]. Of interest is the correlation of these surface properties with cell attachment and outgrowth. However, when considering cell-material interactions, a range of surface properties must be factored in including topography, chemistry, elastic modulus and charge [234].

As cell-material interactions are closely linked to biomolecule-material interactions, the high-throughput analysis of the interactions of a polymer library with biomolecules of interest can be studied as a first step to deconvolute cell-material interactions. Biomolecular targets are typically fitted with a label, including

radioisotopes, fluorophores, enzyme substrates or haptens [235, 236]. However, the requirement for a label can result in adverse effects to biomolecules, such as blocking of active epitopes and steric hindrance, as well as altering kinetic properties and affinity constants [118, 235, 237]. Imaging ellipsometry allows the highly sensitive, label-free detection of surface-binding events with high spatial resolution; however, incorporation of a flowthrough system for real-time analysis is not currently possible [238-240]. Surface Plasmon Resonance imaging (SPRi), in comparison, enables spatially resolved, surface sensitive, label-free, real-time analysis of surface-biomolecule interactions in a parallel format. Formation of patterned surfaces by microfluidics, robotic spotting and photolithography has been utilised for the observation of spatially directed bimolecular adsorption by SPRi [237, 241-244]. However, the surface patterning in these studies resulted in homogeneous surface coatings with comparable refractive index. To enable the simultaneous surface plasmon resonance (SPR) analysis of a diverse polymer library containing many different polymer chemistries with a broad range of dielectric properties, densities and 3-D structures, careful considerations must be given to adequate procedures for obtaining quantitative comparisons of SPR measurements on these diverse spots [245, 246].

In the present chapter, three polymers with disparate chemistries were investigated for their interaction with biomolecules of interest. These polymers were arrayed using a robotic spotting device, which is readily available to life science laboratories interested in cell-material interactions. Moreover, use of this device enables the facile incorporation of subsequent biomolecular arrays on top of the polymer microarrays whilst avoiding misalignment (section 4.3.4). However, the resulting polymer spots did not exhibit uniform thickness and possibly presented an

inhomogeneous refractive index. A method was, therefore, devised to comparably and simultaneously conduct SPR measurements of a polymer microarray, containing spots of varied thickness and refractive index. This approach was used to investigate the kinetics and thermodynamics of bovine serum albumin (BSA), fibronectin (FN) and collagen (CN) type I adsorption on the polymer microarray spots. In addition, cell attachment to the polymer spots was also investigated.

5.2. Theory behind surface plasmon resonance imaging

SPR reflectivity measurements enable the determination of the thickness or refractive index (η) of a thin organic or biopolymer film in real-time with a high degree of surface sensitivity [247, 248]. This has allowed for measurements in changes in the refractive index or thickness of the film, which in turn has permitted the monitoring of biological interactions such as antibody-antigen binding, DNA hybridisation and protein-DNA interactions [248]. A typical SPR experiment is conducted by illuminating a noble metal coating (silver, gold or copper) by *p*-polarised light (electric field vector oscillating parallel to the plane of incidence) to excite surface plasmons (charge-density waves that propagate parallel to an interface) when the sign of the real part of the dielectric constant of the two materials at the interface is opposite, for instance, a metal and a dielectric [248-250]. The excitation of surface plasmons results in a loss of energy from the incident beam and a decrease in the intensity of the reflected light, which can be monitored [247].

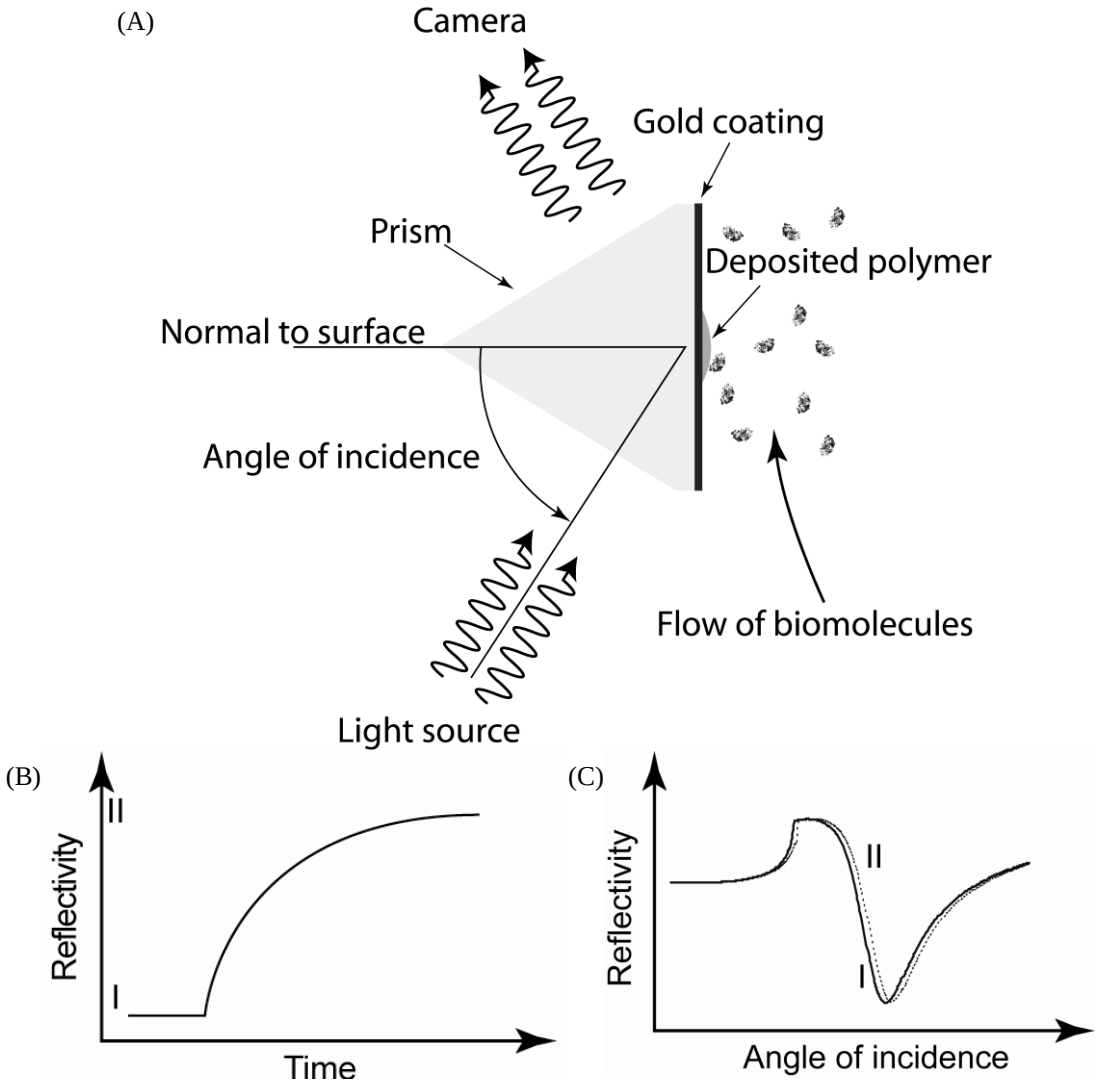

Figure 5.1. *(A) The Kretschmann configuration for SPR measurements. Light is coupled at a specific angle of incidence into a glass prism, which has one face coated by a metal. The evanescent light wave produced at the total internal reflectance event excites surface plasmons at the metal/dielectric interface. This event can be detected by measuring changes in the intensity of the reflected light. Changes in the dielectric properties of the dielectric material in contact with the metal surface, such as the adsorption or desorption of a biomolecule, alter the excitation of the surface plasmons producing a change in the intensity of the reflected light. Conducted at a fixed angle over time, this allows the measurement of biomolecular adsorption in real-time, producing a sensorgram of reflectivity over time as shown in (B). Here a biomolecular adsorption event resulted in a shift in reflectivity from* ***I*** *to* ***II****. If reflectivity measurements were taken for varied angle of incidence before and after the adsorption event a shift in the resonance angle, at which reflectivity is minimised, would be observed, as shown in (C) with a shift in the reflectivity versus angle of incidence curve from* ***I*** *to* ***II****.*

Momentum matching conditions are not satisfied when light illuminates a planar metal/dielectric interface, requiring the Kretschmann configuration [251] to be adopted whereby attenuated total internal reflectance through a glass prism is used to excite surface plasmons by the resultant evanescent wave. A typical Kretschmann configuration is shown in Figure 5.1A. One face of the Kretschmann glass prism is coated with a metal. The evanescent light wave produced when light is directed at a specific angle of incidence through the prism and reflected off the glass/metal interface excites surface plasmons when the wave vector of the evanescent light (K_{ev}) equals the wave vector of the surface plasmon (K_{sp}). The excitation of surface plasmons is maximised at a specific resonance angle. K_{ev} is given by equation 5.1 where w_0 is the frequency of the incident light, c is the speed of light in vacuum, η_g is the refractive index of the glass prism and θ is the angle of incidence of the light [247].

$$K_{ev} = \frac{w_0}{c}\eta_g \sin\theta \qquad (5.1)$$

K_{sp} is given by equation 5.2 where ε_m is the dielectric constant of the metal film and η_s is the refractive index of the dielectric [247].

$$K_{sp} = \frac{w_0}{c}\sqrt{\frac{\varepsilon_m \eta_s^2}{\varepsilon_m + \eta_s^2}} \qquad (5.2)$$

By the criterion of equality of equation 5.1 and 5.2, it can be seen that changes in the refractive index of the dielectric, the angle of incidence or the wavelength of the incident light impacts greatly on the excitation of surface plasmons [247]. SPR experimental setups endeavour to measure changes in SPR reflectivity with wavelength or angle of incidence.

The resulting surface plasmons are evanescent waves that have an intensity maximum at the metal/dielectric interface that decays exponentially into the dielectric to a penetration depth of about 200 nm. Thus, changes in the dielectric properties within 200 nm of the dielectric material in contact with the metal coating will alter the excitation of the surface plasmons, the change of which can be detected by changes in the intensity of the reflected light [248]. In a typical experiment, light is coupled into the prism at a fixed angle of incidence, whereupon, for a plot of reflectivity against angle of incidence the absolute value of the differential of reflectivity versus angle of incidence is maximised. This is typically at an angle slightly lower than the resonance angle. The intensity of the reflected light is monitored. The reverse side of the metal coating is then primed with a suitable buffer before a molecule of interest is flowed over the metal surface (Figure 5.1A). The detection of an adsorption event, as injected molecules of interest replace buffer molecules associated with the surface, can be detected by a sudden increase in the reflected light intensity (Figure 5.1B) as a result of a shift in the resonance angle (Figure 5.1C) associated with a change in the refractive index of the dielectric. This increase will reach a plateau as the surface is saturated with the molecule of interest, and will finally decrease with washing of buffer to remove loosely bound molecule of interest. Thus, the difference in the initial and final intensity of the reflected light is a result of the adsorption of the molecules of interest and, when a monochromatic light source is used, can be related to the shift in the resonance angle required to fulfil $K_{ev} = K_{sp}$ (Figure 5.1C) [247].

SPRi, or SPR microscopy, is achieved by coupling SPR with imaging [252, 253]. Typically, the reflected light from an SPR experiment is detected by a camera or viewed through a microscope, enabling spatial measurements of changes in the

thickness or refractive index at a particular surface. This feature of SPRi allows the rapid, parallel SPR analysis of the adsorption of a particular biomolecule to an array of microscale spots under identical environmental conditions. The lateral resolution of SPRi is limited by the propagation length of the excited surface plasmons, which is dependent on ε_m, η_s and w_0 [244]. Under optimised conditions a resolution less than 2 μm can be achieved [249]. SPRi has been used to monitor many different patterned surfaces and analyte behaviour including DNA hybridisation [254-256], protein-material interactions [257], protein-DNA interactions [258], avidin-biotin binding [259], self-assembled monolayer (SAM) formation [242], protein-carbohydrate interactions [260], antibody-antigen interactions [261, 262], electropolymerisation of organic films [263] and small molecule-protein interactions [245]. However, presently SPRi is limited to imaging uniform surface coatings [245, 246].

5.3. Materials and methods

5.3.1. Substrate preparation

SPR chips (SPR-1000-050, GWC Technologies) with a gold coating of 45 nm on SF10 glass were used as received.

Poly(ethylene glycol) (PEG) coatings were prepared as follows. Initially, SPR chips or glass slides were coated by plasma polymerisation in a custom-built reactor described elsewhere [182]. In short, the plasma reactor consisted of two circular electrodes separated by 12.5 cm in a cylindrical reactor being 35 cm high with a diameter of 17 cm. Allylamine (Aldrich, 98% purity) was used as a monomer. Allylamine plasma polymer (ALAPP) deposition conditions used were a frequency of 200 kHz, a power of 20 W and an initial monomer pressure of 0.200 mbar. The

deposition time was 5 s. Freshly deposited ALAPP samples were left overnight in hexamethylene diisocyanate (HDI) at room temperature while excluding the presence of water. Subsequently, samples were washed thrice for 10 mins in acetonitrile (Merck, 99.9% purity). HDI-modified samples were incubated overnight at 45 °C in a solution of hydroxyl-terminated star-PEG (MW 116,000, 24 arms, Shearwater Polymers, USA) in acetonitrile (3 mg/ml). Subsequently samples were washed in MilliQ water (18.2 MΩ.cm) three times for 1 hr and finally air dried.

5.3.2. Polymerisation of poly(N-isopropylacrylamide)

Poly(*N*-isopropylacrylamide) (P*N*IPAAm) was prepared as previously described [264]. *N*-isopropylacrylamide (*N*IPAAm) (97 %, Sigma) was purified by recrystallisation in distilled *n*-hexane. Purified *N*IPAAm monomer was dissolved to a concentration of 7 % (w/v) in ultrapure MilliQ water (18.2 MΩ.cm) along with 0.1 % (w/v) 4,4'-azobis(4-cyanopentanoic acid) (ACPA, 98%, Fluka). Polymerisation was carried out at 55 °C under a nitrogen atmosphere for 45 min. Purification of P*N*IPAAm was achieved by dialysis (MW cutoff 124,000 Da) in MilliQ water (18.2 MΩ.cm) for 3 days followed by freeze drying.

5.3.3. Array formation

Poly(acrylic acid) (PAA) (Aldrich, MW 90000, η = 1.527), poly(ethylene imine) (PEI) (MW 70000, η = 1.48) and poly-L-lysine (PLL) (Sigma, MW 70000, η = 1.37) were spotted onto either gold coated SPR chips or gold coated SPR chips that were further coated with PEG. Arrays for cell growth studies were spotted onto PEG coated glass slides.

Before spotting polymer samples were prepared to 2, 1, 0.5, 0.25, 0.1, 0.05 and 0.01 mg/ml solutions in ultra pure water. A solution of pure water was also spotted as a negative control. For studies with switchable polymers, P*N*IPAAm was spotted onto gold coated SPR chips at a concentration of 1.5, 0.75, 0.37 and 0.18 mg/ml in water. Spotting was conducted using a BioOdyssey Calligrapher MiniArrayer (Bio-Rad) using a 375 μm diameter solid pin (ArrayIt), a humidity of 65% and at a temperature of 25 °C. The approach speed of the pin and the dwell time of the pin in contact with the surface were set to 20 mm/s and 15 ms respectively. All spots formed were reprinted thrice directly after initial spot formation to minimise variation in spot formation.

For formation of covalently crosslinked PEI and PLL polymer spots ((PEIc) and (PLLc) respectively), PEI and PLL were spotted onto PEG-modified SPR chips. Before spotting, polymer samples were prepared to 50 μl of 0.5 mg/ml solutions in ultra pure water containing 1.0 mg/ml (3.3 mM) *N*-succinimidyl-5-azido-2-nitrobenzoate (NSANB) (Fluka). Polymer-NSANB solutions were incubated at 25 °C for 10 min before array formation. For the formation of covalently crosslinked PAA spots (PAAc), PAA (4.0 mg/ml) was prepared in 50 μl of ultra pure water containing 75 mM N-hydroxy succinimide (NHS) (Sigma) and 30 mM 1-ethyl-3-(3-dimethylaminopropyl) carbodiimide hydrochloride (EDC) (Fluka) and incubated for 1 hr at 37 °C. 50 μl of 2.00 mg/mL (6.6 mM) NSANB in ultra pure water containing 7.0 mM ethylenediamine (Merck) at 25 °C was incubated for 10 min before adding to the 50 μl of activated PAA, to make a final volume of 100 μl, and incubating for a further 10 min before array formation. After array formation, samples were exposed to UV irradiation (25 W) for at least 10 mins, which was sufficient time to ensure

complete reaction of the crosslinker. Here, the UV lamp (multiband source, 254-365 nm) was held at 1 cm distance from the sample.

5.3.4. SPR imaging

SPR imaging was conducted using a SPRimagerII (GWC Technologies Inc.). A collimated polychromatic polarised light source was impinged onto a gold film sample through a prism assembly at a specific angle of incidence. The light reflected from the sample passed through a narrow band-pass filter (800 nm) and was detected by a charge coupled detector (CCD) camera, which was able to capture an image of the entire optical field of the chip surface. Images were analysed using V++ Precision Digital Imaging System (V.4).

SPR signal standardisation studies were conducted by initially forming a polymer array onto a gold coated glass SPR chip. The surface was initially washed with 0.05 M phosphate buffer at a flow rate of 3 μl/s. The SPR signal for each spot was then measured against the angle of incidence of the impinging light beam and an optimal angle for subsequent fixed angle SPR measurements was selected. 0.1% (v/v) ethanol in water was then injected over the array until equilibrium was reached at a flow rate of 3 μl/s. Subsequently, the SPR signal for each spot was again measured against the angle of incidence of the impinging light beam. This allowed for the measurement of the shift in the resonance angle as a result of a change in the refractive index of the buffer. A similar approach was taken for all SPR measurements.

Biomolecular adsorption experiments were conducted by priming the polymer microarray initially in 0.05 M phosphate buffer at pH 7.4. Once a stable background was reached the SPR signal for each spot was measured against the angle of incidence of the impinging light beam before 10 μg/ml, 5 μg/ml, 2 μg/ml or 1 μg/ml

albumin (from bovine serum, Sigma), FN (from bovine plasma, Sigma) or CN type I (from rat tail, Sigma) in 1 mM acetic acid was injected at a flow rate of 5 μl/s until SPR signal had plateaued. This slightly higher flow rate was used to ensure kinetic measurements were not limited by mass transport of the adsorbant from the bulk solution. The 1 mM acetic acid present with CN type I, required for dissolution of CN type I, reduced the pH from 7.4 to 7.35. The surface was then washed with 0.05 M phosphate buffer at 5 μl/s to allow desorption of weakly bound biomolecules, before the SPR signal for each spot was measured against the angle of incidence of the impinging light beam. The surface was subsequently regenerated by washing with 0.1% Tween solution at a flow rate of 3 μl/s for 60 s and 0.1 M NaOH solution at a rate of 3 μl/s for 60 s or 0.1 M HCl solution at a rate of 3 μl/s for 60 s. The surface was then washed with 0.05 M phosphate buffer at a flow rate of 3 μl/s until baseline was again reached. Measurements were taken over an angle of incidence range of 48-57° while the temperature was held constant at 25 °C.

SPR signal intensity versus angle of incidence curves measured for varied polymer spots before and after biomolecular interaction events were modelled by Fresnel equations using Winspall V 3.01 software. Simulation parameters used were a 60° triangular prism using *p*-polarised light of wavelength 800 nm. Refractive index values used were SF10 glass η = 1.71129, gold η = 0.16 + 4.84*i* [265, 266], biopolymer layer η = 1.45 [248] and water η = 1.32908 [267]. For curve fitting, only the position of the resonance angle was considered.

5.3.5. Study of switching of PNIPAAm by SPR imaging

P*N*IPAAm spots printed from a 1.5 mg/ml protein solution were selected for studying temperature switching. 0.05 M phosphate buffer was injected over the

P*N*IPAAm array at 3 μl/s and then reduced to 1 μl/s whereupon the system was setup to recirculate the buffer. The temperature was then altered between 25 °C and 40 °C in order to observe the swelling and collapse of the P*N*IPAAm hydrogel spots.

5.3.6. Cell growth

A SK-N-SH neuroblastoma cell line was used for cell attachment experiments. Cells were cultured in Dulbecco's modified eagle media (DMEM) containing penicillin and streptomycin and incubated at 37 °C, 5% CO_2 and 60-70% humidity. For attachment studies of cells, SK-N-SH cells were seeded onto surfaces at a seeding density of $5x10^4$ cells/cm^2 and allowed to attach to the surface after which they were incubated at 37 °C, 5% CO_2 and 60-70% humidity for 24 hr. Cells were then stained with Hoechst 33342 dye (10 mg/mL) for a further 5 min before analysis by fluorescence microscopy. Cells were visualised with an IX81 Olympus fluorescence microscope and analysed using analySIS LS Research v2.5 software using a 360-370 nm excitation filter and a 420 nm suppression filter to detect Hoechst 33342 fluorescence. Captured images were modified using Adobe Photoshop software.

5.3.7. Kinetic analysis

Assuming a one-step kinetic process whereupon the protein in bulk solution (*P*) adsorbs to a surface binding site (*B*) to form a surface bound complex (*PB*), the rate of adsorption of a given protein is given by equation 5.3, where k_a is the association constant, k_d is the dissociation constant, [*P*] is the concentration of free protein in solution, [*B*] is the number of free binding sites at the surface and [*PB*] is the concentration of surface bound protein [247].

$$\frac{d[PB]}{dt} = k_a[P][B] - k_d[PB] \qquad (5.3)$$

The surface concentration of the adsorbed species at saturation ($\Gamma_{s\infty}$) is proportional to the total number of surface binding sites ([*B*] + [*PB*]), thus, [*B*] is proportional to the difference of $\Gamma_{s\infty}$ and [*PB*] (let [*PB*] = Γ_s). As protein adsorption experiments are conducted under flow, [*P*] can be considered as a constant (*C* = concentration of bulk solution). Thus, equation 5.3 can be rewritten as equation 5.4 and 5.5 [247].

$$\frac{d\Gamma_s}{dt} = k_a C(\Gamma_{s\infty} - \Gamma_s) - k_d\Gamma_s \qquad (5.4)$$

$$\frac{d\Gamma_s}{dt} = k_a C\Gamma_{s\infty} - (k_a C + k_d)\Gamma_s \qquad (5.5)$$

From equation 5.5 a plot of $d\Gamma_s/dt$ against Γ_s would produce a straight line with slope equal to $-(k_aC + k_d)$ (γ). By producing this plot for a range of *C*, a plot of γ against *C* produces a straight line with slope equal to k_a and a y-intercept of k_d. The binding constant (*K*) can be found as k_a/k_d [247].

$\Gamma_{s\infty}$ can by determined by assuming Langmuir binding between *P* and *B*. In this case, Γ_s is related to *C* by equation 5.6, which can be rearranged to give equation 5.7.

$$\Gamma_s = \frac{KC\Gamma_{s\infty}}{1 + KC} \qquad (5.6)$$

$$\frac{1}{\Gamma_s} = \frac{1}{K\Gamma_{s\infty}C} + \frac{1}{\Gamma_{s\infty}} \qquad (5.7)$$

Thus, $\Gamma_{s\infty}$ can be determined from the y-intercept of the plot of the inverse of Γ_s against the inverse of *C*, and is given in units of mg/m^2 assuming a protein density of 1.35 g/cm^3 [268].

Curve fitting was conducted using Prism V 4.0c software.

5.4. Results and discussion

5.4.1. SPR imaging of a PNIPAAm microarray

Initially, SPRi was utilised for studying the switchable nature of P*N*IPAAm. Surface plasmons were excited using the Kretschmann configuration (Figure 5.1A). The reflectivity of light at a wavelength of 800 nm was selected for probing the excitation of surface plasmons. A longer wavelength was utilised in this case, as compared to commonly used light of wavelength 635 nm [248, 269], due to the higher sensitivity attained due to the smaller angle shifts and sharper minima, which also allows for measurements with thicker films [248]. However, the excited surface plasmons have a longer propagation length, thus, decreasing the lateral resolution to approximately 25 μm [248]. However, for the typical dimensions of surface features being investigated (spot diameter of 400 μm) this resolution was adequate to resolve surface patterns.

An array of P*N*IPAAm from solutions of varied concentration was formed for SPRi analysis. A typical SPR image of the resultant array is shown as Figure 5.2. Spots of equivalent thickness were selected (Figure 5.2, 4th column), thus, fixed angle analysis with the SPR instrument was possible. P*N*IPAAm is an interesting material for biomaterial applications due to its high water content and switchability between a collapsed state, which sustains biomolecular adsorption, and a swollen state, which resists biomolecular adsorption, about its lower critical solution temperature (LCST) [270]. For P*N*IPAAm this is approximately 32 °C [70]. Production of a patterned P*N*IPAAm surface would allow for both spatial and temporal control of biomolecular surface adsorption. Hydrogel surfaces have frequently been patterned using photolithographic techniques [271-273]. However,

of interest is the facile integration of P*N*IPAAm patterns with protein and cell microarrays, which can be achieved by forming a P*N*IPAAm array using a contact printer [215]. Thus, the formation and behaviour of a P*N*IPAAm microarray printed using a robotic spotter was assessed, with a particular focus on its ability to switch between a swollen and collapsed state about its LCST whilst in an arrayed format.

SPR signal intensity was set up to look spatially at a P*N*IPAAm spot and simultaneously at uncoated gold as a negative control. The resulting reported change in SPR signal intensity is the difference between the signal measured at the P*N*IPAAm spot and the uncoated gold.

Initially, the array was allowed to reach a stable background with constant buffer flow at 1 μl/s at an initial temperature of 20 °C. The temperature was then increased to 40 °C. The resulting sensorgram is reported as Figure 5.3. The initial spike is due to inhomogeneous sample heating resulting in localised differences in temperature. Upon the temperature reaching the polymers LCST (ca. 32 °C), the intensity of the reflected light was enhanced due to a displacement of the resonance angle to higher angles as a result of a local increase in the refractive index (Figure 5.3) [263]. This can be explained by a net increase in polymer at close proximity to the surface and a net rise in the polymer's refractive index as a result of the polymer transitioning from a well-solvated random coil state to a densely packed globular state, with the expulsion of water allowing for intermolecular hydrophobic interactions [274]. This switchable behaviour, above the polymers LCST, is an effect of the entropic penalty dominating over the exothermic enthalpy for the hydrogen bonding between water molecules and the polymer's polar groups, resulting in the solvation of the polymer becoming thermodynamically unfavourable [275].

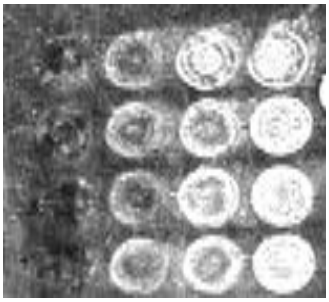

Figure 5.2. *SPR image of PNIPAAm array, spotted at a concentration of 0.18, 0.37, 0.75 and 1.5 mg/ml from left to right (each column is four replicates of each concentration), used for temperature switching experiments. Spot diameter is approximately 400 μm.*

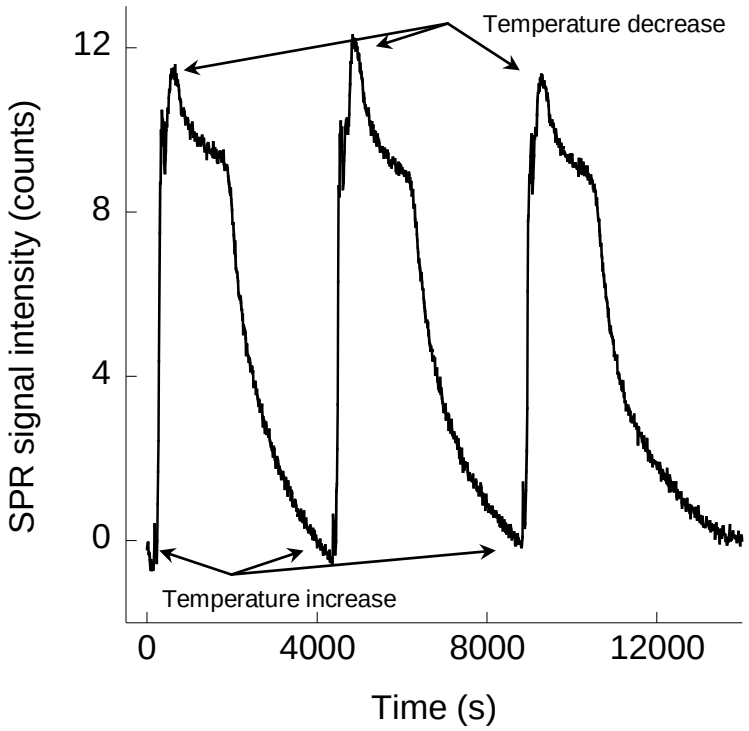

Figure 5.3. *SPR sensorgram for a PNIPAAm array spot switching between 20-40 °C over three cycles to observe the swelling and collapse about the LCST.*

Upon the cooling of the microarray below the LCST, a gradual decrease in the intensity of the reflected light was observed as the polymer spots swell and take on more water (Figure 5.3), whereupon exothermic enthalpy is the thermodynamic driving force for hydrogen bond formation between water molecules and the polymer's polar groups. This continued until the SPR signal intensity declined to the baseline level. Therefore, the change in P*N*IPAAm morphology was reversible and could be repeated over three heating and cooling cycles in succession (Figure 5.3). Similar results for P*N*IPAAm coatings have been observed previously by SPR [276-278].

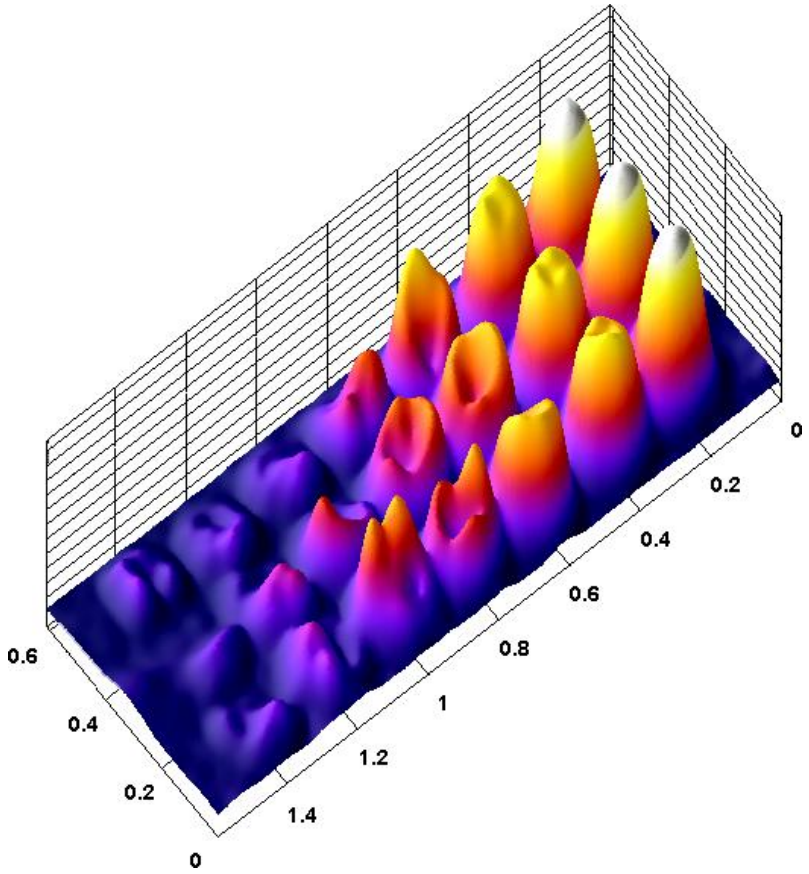

Figure 5.4. *Surface plot of reflectivity taken from an array of PLL spotted onto bare gold over a concentration series of 2.0, 1.0, 0.5, 0.25, 0.1, 0.05 and 0.01 mg/ml. Each concentration was repeated in triplicate. The angle of incidence was set such that the bare gold background was in resonance. The intensity of the reflected light is enhanced at the PLL spots from the higher concentrations due to the displacement of the resonance angle to higher angles as a result of the local increase in the refractive index. Each spot is approximately 400 μm in diameter, with a centre-to-centre distance of 500 μm.*

5.4.2. Standardising SPR signal on a polymer microarray

PLL was arrayed onto bare SPR gold chips from a concentration series ranging from 0-2 mg/ml. A surface plot of the resultant SPR signal intensity obtained of the array formed from such a concentration series is shown as Figure 5.4. Formation of polymer arrays of PAA, PEI, PLL and polyvinylpyrrolidone (PVP) has previously been characterised (see section 4.3.3). No method was devised for crosslinking PVP to the surface, which limits the 'shelf life' of this polymer array, thus, PVP, used for polymer arrays in CHAPTER 4, was excluded from SPRi measurements.

For the polymer array formed in Figure 5.4, the polymer spots range in thickness from 0-54 nm as determined by profilometry (Figure 4.5). At a given angle, this results in differences in the attenuation of a light beam impinging upon the surface as compared with the uncoated regions, which allows each spot to be spatially resolved by SPR imaging. The reflectivity is enhanced at the PLL spots formed from the higher concentrations due to the displacement of the resonance angle to higher angles as a result of the local increase in the refractive index. For thicker spots formed from higher polymer concentrations the shift in resonance angle is greater resulting in a larger increase in reflectivity.

A fixed angle SPR adsorption experiment is conducted at an angle at which the greatest absolute value of the differential of SPR reflectivity occurs for the surface being studied (Figure 1.1C) [248]. This is obtained from the reflectivity against angle of incidence curve for the surface. However, for a polymer array of varied thickness or refractive index, for instance taking an array of PLL of thickness ranging from 0 – 200 nm, described theoretically in Figure 5.5A by 4-phase Fresnel equations using Winspall software [248, 279] (Fresnel reflectivity calculations were based on a four-

layer system of a glass prism (η = 1.71129), a 45 nm gold layer (η = 0.16 + 4.84i) [265, 266], a PLL polymer layer of varied thickness (η = 1.37) and an infinite water layer (η = 1.32908) [267]).and in Figure 5.5B as the change in reflectivity against the angle of incidence, it can be seen from Figure 5.5B that the angles at which each spot reaches the greatest absolute value for the differential of SPR reflectivity occurs over a range of 49.3° to 53.5°. 49.3° was selected for subsequent fixed angle theoretical calculations. For formation of a polymer microarray consisting of varied polymer materials of different refractive index properties this problem is further amplified. Furthermore, each polymer spot formed by robotic spotting will have non-ideal, rough topography. It is, thus, difficult to select one single angle at which the SPR intensity will be of equivalent sensitive to changes in refractive index for all spots.

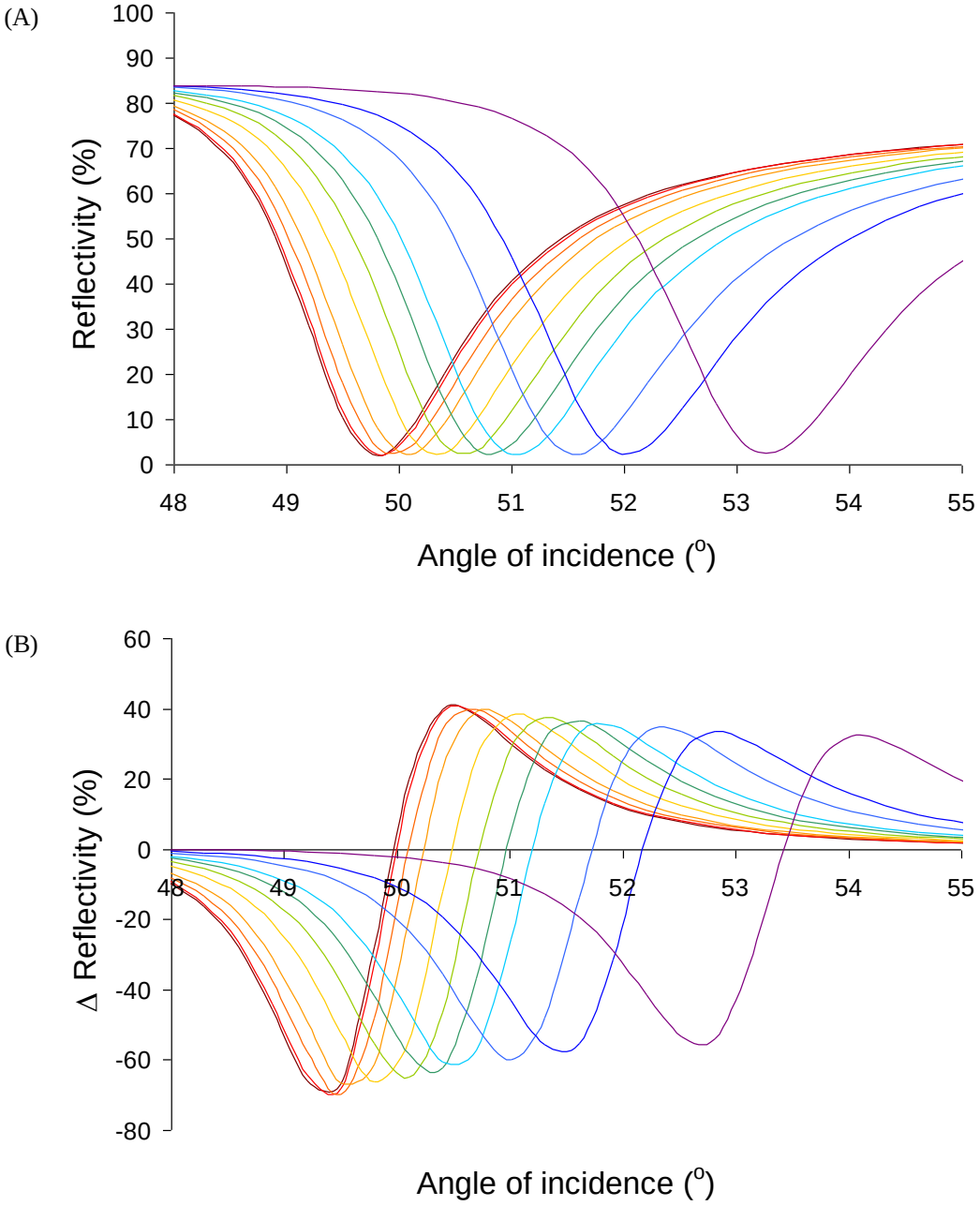

Figure 5.5. *Theoretical (A) SPR reflectivity (%) and (B) change in SPR reflectivity (%) against angle of incidence as modelled by Fresnel equations using Winspall software based on a four-layer system of a glass prism (η = 1.71129), a 45 nm gold layer (η = 0.16 + 4.84i), a PLL polymer layer of varied thickness; (■) uncoated, (■) 1 nm, (■) 5 nm, (■) 10 nm, (■) 20 nm, (■) 30 nm, (■) 40 nm, (■) 50 nm, (■) 75 nm, (■) 100 nm, (■) 200 nm (η = 1.37) and an infinite water layer (η = 1.32908).*

The ultimate application of SPR is for probing interactions of biomolecules. Thus, if investigating the adsorption of a 5 nm thick biopolymer layer onto a PLL array of thickness varied from 0-200 nm a resonance angle shift to higher angles is expected as shown in Figure 5.6, where the theoretical reflectivity versus angle of incidence is shown both with (dotted) and without (solid) a biopolymer layer. Real-time biomolecule adsorption experiments are typically achieved using a fixed angle approach, thus, the change in reflectivity at the optimised angle from Figure 5.5B of 49.3° for each polymer spot after the addition of a 5 nm biopolymer layer is shown in Figure 5.7A. An equivalent response of approximately 23 units is measured for spots over a range of thicknesses of 0 – 5 nm, however, this response decreases rapidly for polymer spots thicker than 10 nm and almost no change is observed at this fixed angle for the spot with a thickness of 200 nm. This exemplifies the difficulty faced when measuring SPR signal changes for inhomogeneous surfaces.

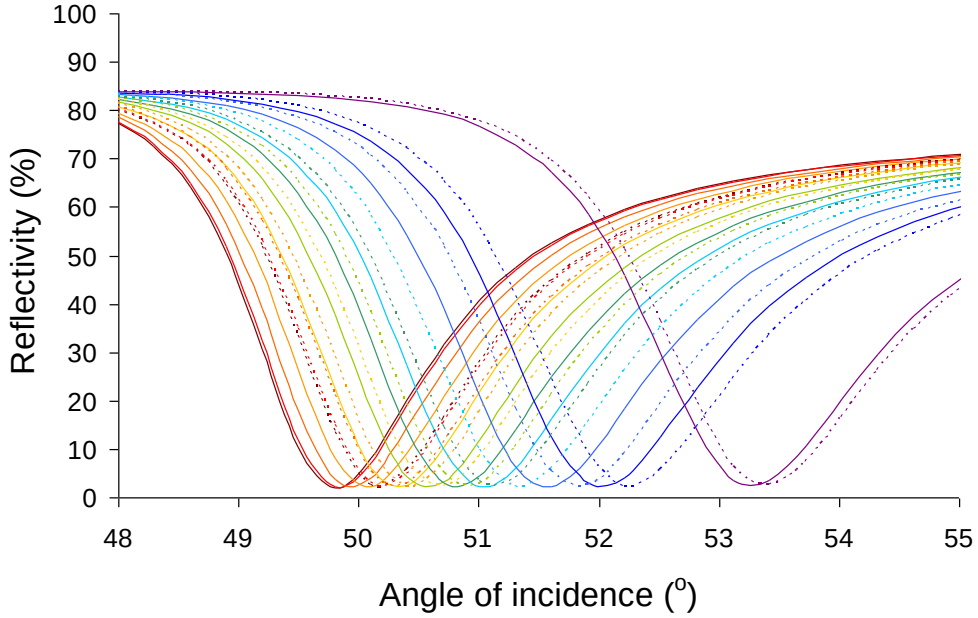

Figure 5.6. *Theoretical SPR reflectivity (%) against angle of incidence as modelled by Fresnel equations using Winspall software based on a five-layer system of a glass prism (η = 1.71129), a 45 nm gold layer (η = 0.16 + 4.84i), a PLL polymer layer of varied thickness; (■) uncoated, (■) 1 nm, (■) 5 nm, (■) 10 nm, (■) 20 nm, (■) 30 nm, (■) 40 nm, (■) 50 nm, (■) 75 nm, (■) 100 nm, (■) 200 nm (η = 1.37), with (dotted) and without (solid) a 5 nm biopolymer layer (η = 1.45) and an infinite water layer (η = 1.32908).*

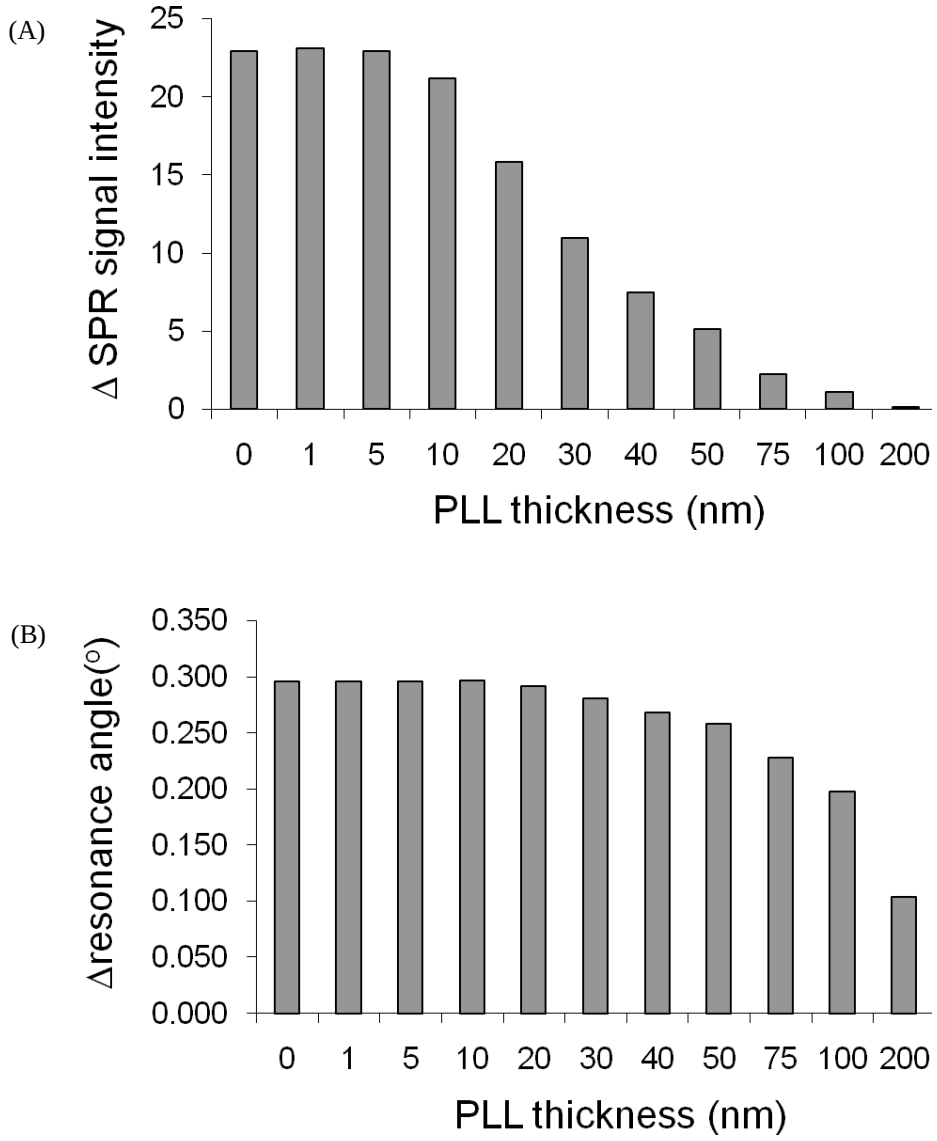

Figure 5.7. *Measured change in (A) reflectivity and (B) resonance angle shift for PLL coatings of varied thickness with the addition of a 5 nm thick biopolymer layer as modelled by Fresnel equations using Winspall software.*

However, if the shift in the resonance angle after the addition of a 5 nm biopolymer layer is measured for each spot (shown as Figure 5.7B) an equivalent response of approximately 0.3° is measured up to a thickness of 20 nm. A slight decrease in the measured value is seen for polymer spots of thicknesses above 30 nm. A response of approximately 0.1° was measured for the polymer spot of thickness 200 nm. This result suggests that a larger spot thickness range can be used, when replacing the measurement of change in signal intensity at constant angle with the shift in the resonance angle. For the PLL array discussed, equivalent measurements could be taken over a thickness range of 0-30 nm. This is a significant improvement over the 0-5 nm thickness range that currently limits fixed angle experiments.

In order to obtain real-time measurements by SPRi reflectivity measurements at a fixed angle must be taken, despite the advantages of exclusively measuring shifts in the resonance angle. However, knowing the relationship between the reflectivity against angle of incidence for a particular spot at the fixed angle used for real-time biomolecular adsorption experiments, the changes in reflectivity measured during such an experiment can be converted to a shift in the resonance angle using the total change in resonance angle measured as a result of biomolecular adsorption, as depicted in Figure 5.8.

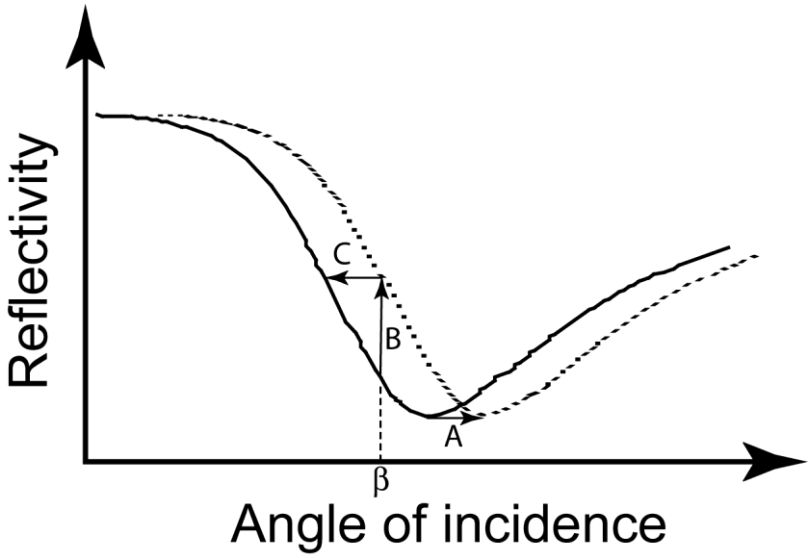

Figure 5.8. *Schematic depicting the method used to normalise a measured change in reflectivity to the shift in the resonance angle. On a given SPR chip surface an adsorption event would result in a shift in the reflectivity versus angle of incidence curve from the solid to the dotted curve, resulting in a shift in the resonance curve corresponding to the arrow labelled* A*. However, for a fixed angle SPR measurement, at an angle of incidence* β*, the change in reflectivity, corresponding to the arrow labelled* B*, is measured. Using the initial (solid) reflectivity versus angle of incidence curve the corresponding shift in resonance angle* C *can be determined, whereupon* C *is found to be equal to* A*. Using this approach every change in reflectivity measured during a fixed angle experiment can be converted to the corresponding shift in resonance angle.*

As a proof of principle approach a PAAc array spotted from polymer solutions with a concentration of 1.0, 0.5 and 0.25 mg/ml was prepared corresponding to average thicknesses of 4.2, 3.4 and 2.2 nm respectively, determined from the measured shift in resonance angle after formation of the polymer spot using the Winspall modelling software. An SPR image of the array is shown as Figure 5.9. Reflectivity and the change of reflectivity versus angle of incidence for each of the spots as well as the unmodified bare gold background were measured after priming the array in phosphate buffer as shown in Figure 5.10.

The resonance angle for the PAAc was higher than for unmodified gold (50.4°, 50.2° and 50.1° for spots from polymer concentrations of 2.0 mg/ml, 1.0 mg/ml, 0.5 mg/ml, respectively, compared to 49.8° for uncoated gold) (Figure 5.10A). This is due to the introduction of inhomogeneities in the surface coating by the addition of PAA. Peak minimums for the differential of the reflectivity were found in the range of 48.9°-49.4° (Figure 5.10B). An angle of 48.9° was selected for subsequent fixed angle measurements.

After a stabilising phase in phosphate buffer for 1000 s, a solution of 1% ethanol in water was injected into the SPR flowcell at 3 μl/s and the SPR signal intensity was measured over time for the PAAc array (Figure 5.11A). The exchange of phosphate buffer for 1% ethanol would result in an equivalent change in refractive index across the entire surface, thus, an equivalent SPR response was desired at each spot. A decrease in the reflectivity was observed corresponding to a negative shift in the resonance angle. Notably, however, the change in reflectivity was significantly different for the different spots, ranging from -13 – -27 units. Clearly, the inhomogeneities and thickness differences between each spot prevent measuring a constant change in reflectivity for a constant change in refractive index for each spot.

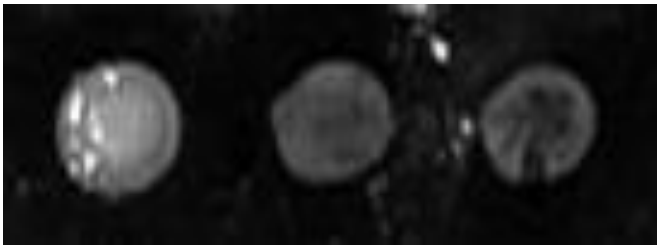

Figure 5.9. *SPR image of an array of PAAc spotted at initial polymer concentrations of 1.0, 0.5 and 0.25 mg/ml. The centre-to-centre distance between spots is 750 μm.*

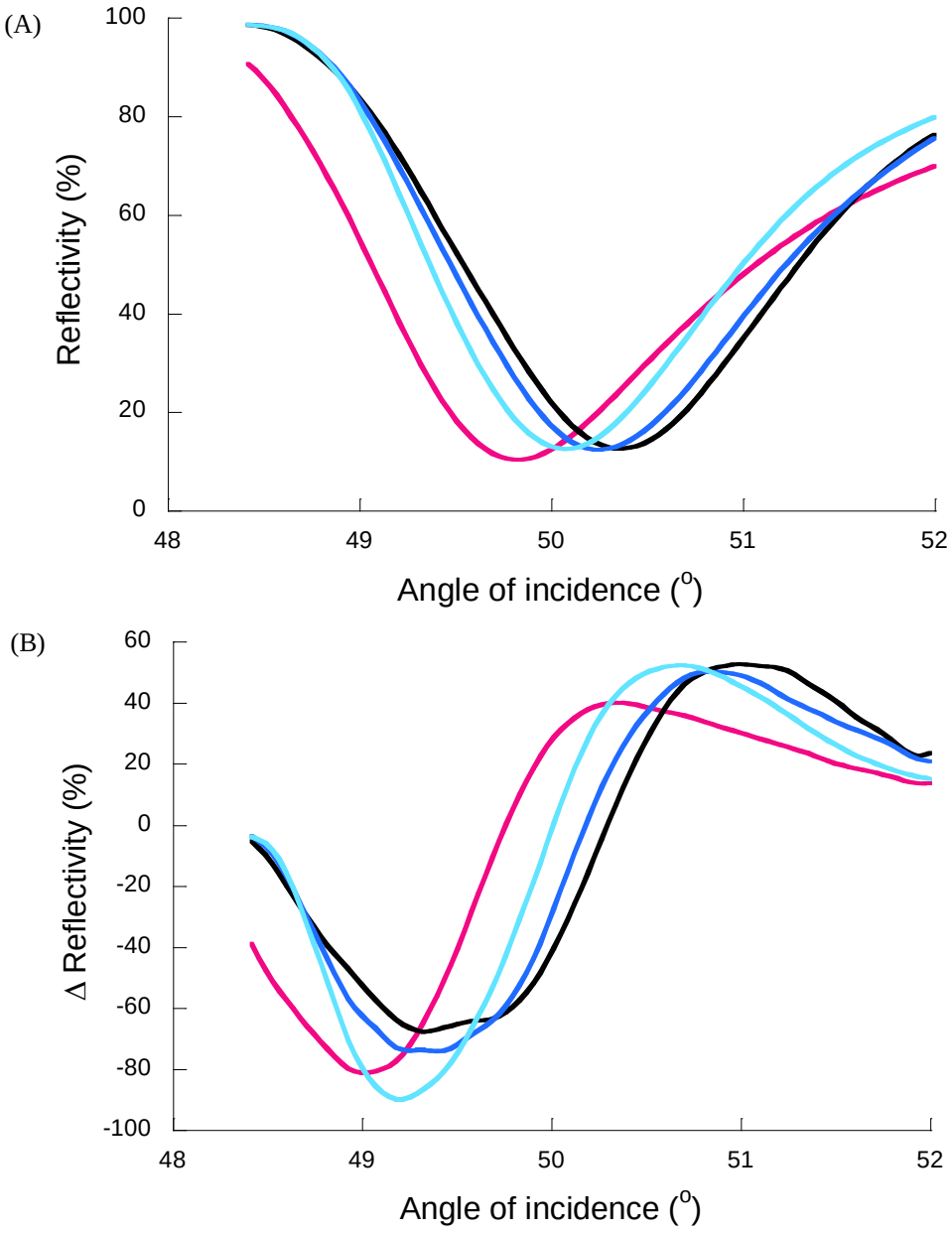

Figure 5.10. *(A) reflectivity (%) and (B) change in reflectivity (%) versus angle of incidence spectra for PAAc spotted at (■) 2.0 mg/ml, (■) 1.0 mg/ml, (■) 0.5 mg/ml and (■) uncoated in phosphate buffer.*

Reflectivity versus angle of incidence curves were measured before and after addition of ethanol (Figure 5.11C) allowing the determination of the total shift in the resonance angle. Furthermore, determining the slope of this curve for every angle of incidence gives the relationship between a change in reflectivity and a change in resonance angle. This enabled the conversion of the change in reflectivity, measured during a fixed angle measurement, to the corresponding shift in resonance angle, as depicted in Figure 5.8. For simplicity, where the relationship between resonance angle and reflectivity was found to be linear the ratio of the total shift in resonance angle to the total change in reflectivity was used to convert each change in reflectivity measurement from a fixed angle experiment to a shift in resonance angle. However, when the relationship was not linear each change in reflectivity measurement was converted independently using the method outlined in Figure 5.8. The resultant kinetic curves showing changes in resonance angle are shown in Figure 5.11B, and here all four spots measure equivalent responses with an average value of -0.147°. As determined by SPR measurements, the phosphate buffer solution used has a η = 1.3355. A 1% ethanol solution has a refractive index of 1.3336, thus, the change in refractive index was 0.0019. This should correspond to a resonance angle shift of -0.141°. This value is very close to the experimentally determined value of -0.147°, well within the limits of the experimental error.

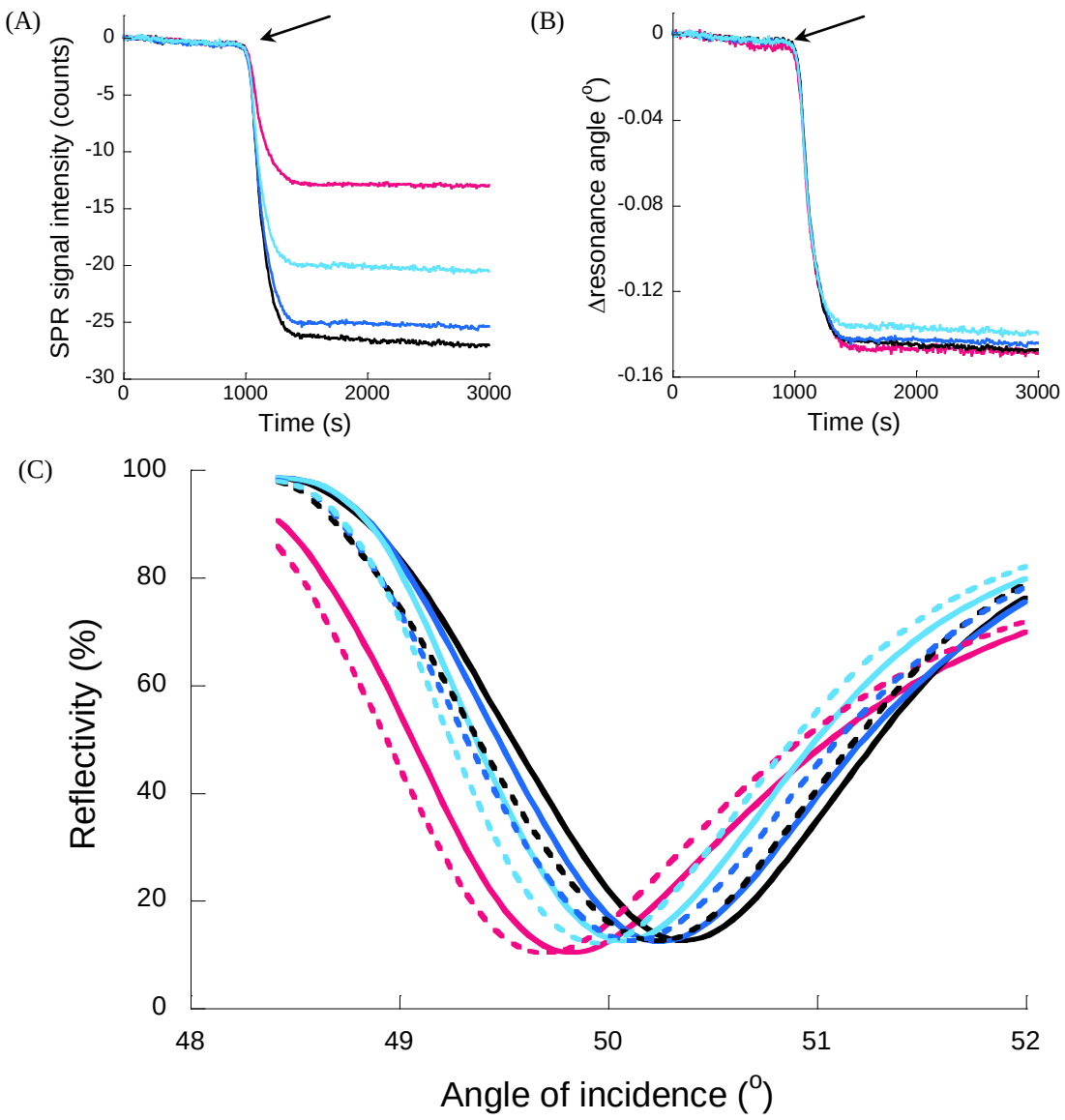

Figure 5.11. *SPRi measurements of a PAA array spotted at (■) 2.0 mg/ml, (■) 1.0 mg/ml, (■) 0.5 mg/ml and (■) uncoated upon the addition of 1% ethanol; (A) SPR signal intensity for each spot over time upon the addition of 1% ethanol solution at 1000 s, (B) resultant Δ resonance angle versus time curve for the addition of 1% ethanol solution after converting the measured change in SPR signal intensity from (A) with the measured shift in the resonance angle in (C), (C) reflectivity (%) versus angle of incidence spectra for PAA spots before (solid) and after (dotted) the addition of 1% ethanol solution.*

This approach was conducted for a larger polymer array consisting of PAA, PEI, and PLL (for structures see Figure 4.3B-D) spotted at concentrations of 2.0, 1.0, 0.5, 0.25, 0.1, 0.05 and 0.01 mg/ml, resulting in an array of 21 polymer spots of varied thickness and refractive index. Similar to the experiment described above, this array was first equilibrated in phosphate buffer and the reflectivity for a range of angles of incidence was measured for each spot. Then a fixed angle experiment at 48.9° was conducted to monitor the change in SPR signal intensity versus time for the exchange of phosphate buffer with 1% ethanol. The resultant sensorgram is shown as Figure 5.12A. Subsequently, the measurement of reflectivity for a range of angles of incidence was repeated after ethanol injection and the measured change in the resonance angle was used to convert the change in SPR signal intensity measured for the fixed angle experiment (Figure 5.12A) to a change in resonance angle against time, shown as Figure 5.12B. Significantly, the resultant shift in resonance angle measured for the majority of spots converged to -0.141° as expected. Only four spots differed significantly from the expected value, which had thicknesses greater than 15 nm.

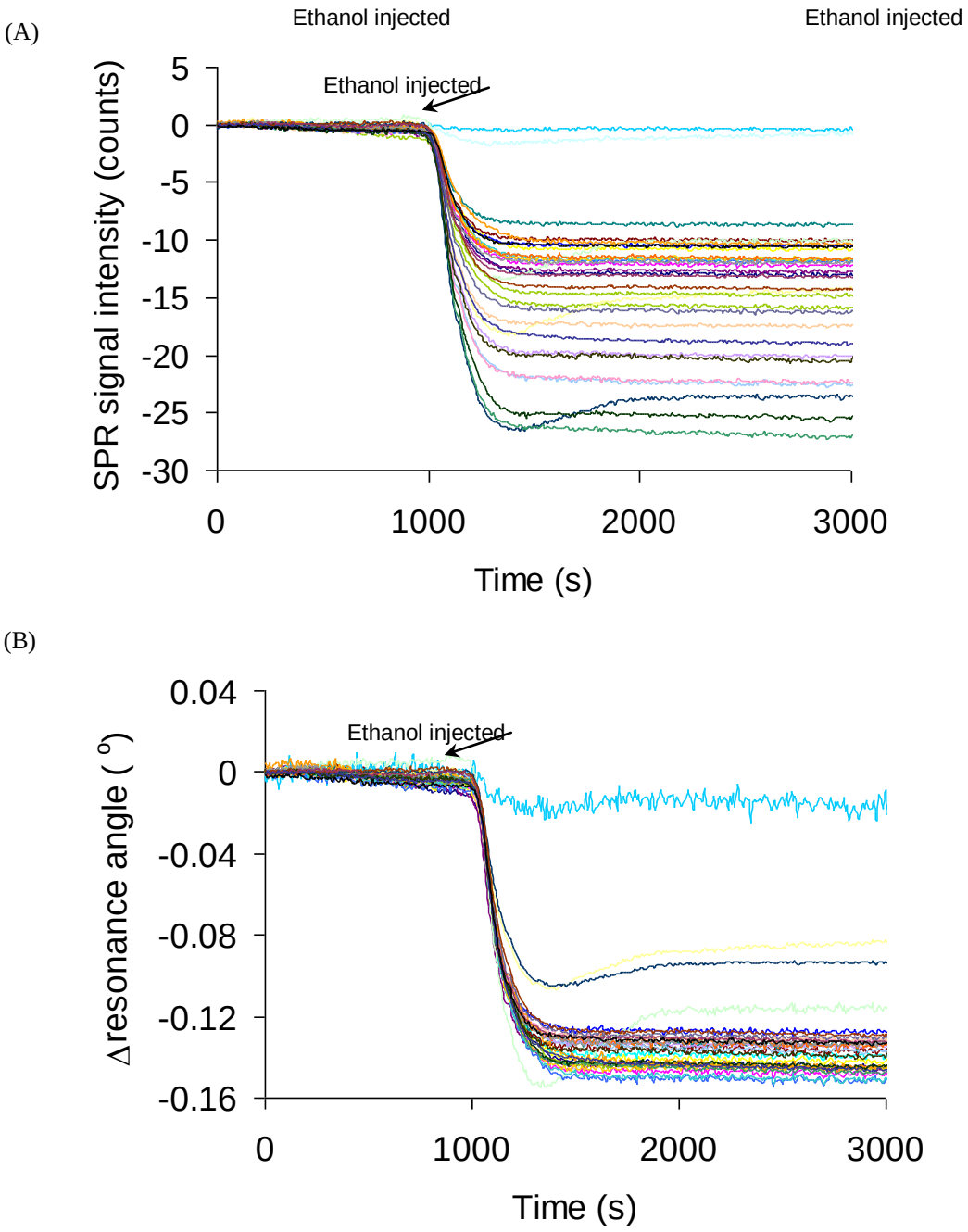

Figure 5.12. *SPRi measurements of a polymer array including PAA, PEI and PLL; (A) sensorgram for each spot. 1% ethanol solution was added at 1000 s, (B) resultant Δ resonance angle versus time curve for the addition of 1% ethanol solution after converting the measured change in SPR signal intensity from (A) into a shift in the resonance angle.*

5.4.3. Kinetic analysis of protein adsorption to polymer array

The adsorption to a polymer microarray of BSA, a globular serum protein present in cell culture media, FN, a globular extracellular matrix (ECM) protein that is important for cell attachment and contains the RGD cell adhesion mediating sequence, and CN type I, which is a protein also integral to the ECM and involved largely with the structural properties of the ECM, was studied by SPRi due to the important role played by these proteins for cell attachment in standard cell culture conditions. For these studies, a polymer microarray was first deposited on a HDI-PEG layer. Initially, experiments were attempted to coat the SPR chips with the ALAPP-PEG constructs previously described [34](section 2.2.2 and 2.2.3), however, the elevated temperature and use of the strong reducing agent $NaCNBH_3$ demanded by this approach led to the stripping of the gold layer from the glass SPR chips. To overcome this problem, a new approach was developed to deposit a thin PEG layer with relative ease. A thin ALAPP layer was deposited and incubated overnight with HDI. This activated the layer for subsequent grafting of a PEG brush layer with similar low fouling properties to the ALAPP-PEG layers previously described. This approach is advantageous over the use of a PEGylated alkanethiol [280] as it can also be used to coat almost any material of choice including glass or silicon, which allows this coating to be readily transferred from a SPR chip to a substrate for cell attachment and outgrowth assays. Thus, this approach provides an alternative to self-assembled monolayers of thiols or use of dextran for coating SPR chips.

After the HDI-PEG layer had been deposited a resonance angle shift of 1.14° was measured corresponding to a thickness of 10.6 nm assuming the layer has a refractive index of 1.5, as determined by Winspall curve fitting software. Initially, a polymer

array of PAAc, PEIc and PLLc was formed on the PEG coated substrate utilising photocrosslinking methods previously developed [215](CHAPTER 4). Fuctionalisation of the polymers with NSANB, which includes a photoresponsive phenylazide group, allowed for the surface immobilisation and intra- and inter-molecular crosslinking of the polymer spots upon UV irradiation (Figure 4.3A). Polymers were spotted at concentrations above 0.25 mg/ml to ensure complete coverage. Both PEI and PLL were spotted at 0.5 mg/ml whilst PAA was spotted at 2.0 mg/ml. The higher spotting concentration was chosen for PAA as these polymers were found to produce immeasurably thin layers at 0.5 mg/ml. A typical SPRi image of the polymer array is shown as Figure 5.13A. For the polymer array used the average thicknesses for PAAc, PEIc and PLLc were 2.2, 8.3 and 18.8 nm respectively, as determined from the reflectivity versus angle of incidence curves shown as Figure 5.13B and Winspall curve fitting software. These results correspond well with previously measured spot thicknesses from profilometry of 1.4, 18.3 and 21.3 nm for PAA, PEI and PLL respectively (Figure 4.5). Differences between these measurements could arise from differences between the wet and dry state of the polymers and varied environmental conditions, such as humidity and temperature, during array formation.

This polymer array was investigated for the adsorption and desorption of FN, CN type I and BSA at various solution concentrations.

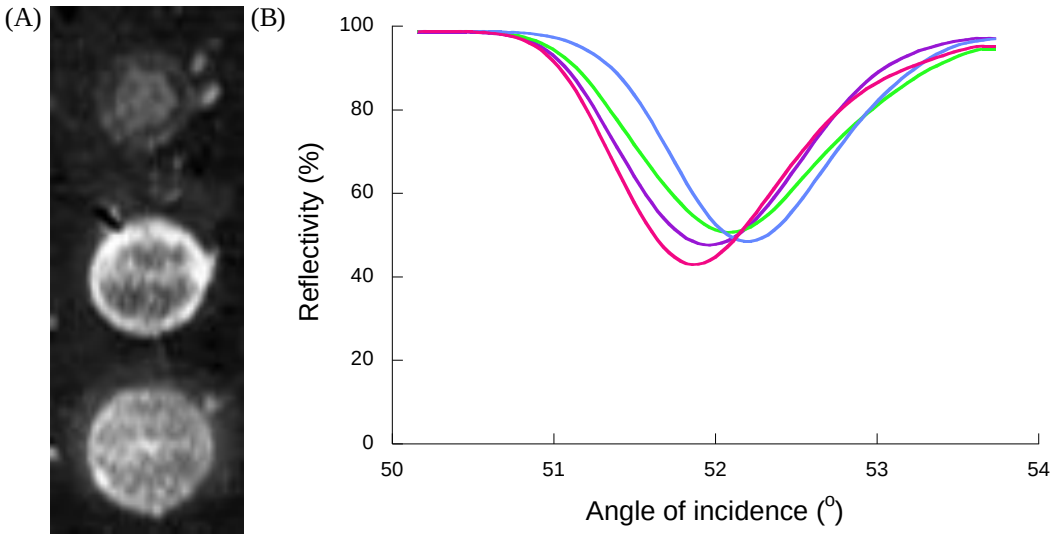

Figure 5.13. *(A) SPR image of representative polymer spots. From top to bottom, spots correspond to PAAc, PEIc, PLLc. Spot diameter is approximately 400 μm. (B) Reflectivity (%) versus angle of incidence spectra for (■) PAAc, (■) PEIc and (■) PLLc on (■) HDI-PEG coating.*

Kinetic plots for the adsorption of CN type I, FN and BSA to the polymer array are shown in Figure 5.14-Figure 5.16. In order for $\Gamma_{s\infty}$ to be quantitatively comparable the measured change in reflectivity must be converted to a shift in resonance angle, as discussed in section 5.4.2. Thus, immediately before and after sensorgrams were measured, reflectivity versus the angle of incidence was measured for each spot. This enabled the measurement of the shift in the resonance angle for each spot due to the biomolecular interactions and enabled the measured change in reflectivity to be correlated with a shift in the resonance angle. Using the Winspall analysis software, the shift in resonance angle from each spot could be converted to an increase in biomolecular thickness, assuming a refractive index of this layer of 1.45. Assuming a monolayer coverage with a density of 1.35 g/cm^3 [268], the biomolecular thickness was converted to units of mg/m^2. This approach enables the standardisation of the reported SPRi response for an inhomogeneous surface coating.

R^2 values for graphs of $d\Gamma_s/dt$ *against* Γ_s *for the adsorption of CN type I, FN and BSA from various bulk concentrations to a polymer array of PAAc, PEIc and PLLc.*

	CN type I				FN				BSA			
	1 μg/ml	2 μg/ml	5 μg/ml	10 μg/ml	1 μg/ml	2 μg/ml	5 μg/ml	10 μg/ml	1 μg/ml	2 μg/ml	5 μg/ml	10 μg/ml
PAA	0.526	0.991	0.993	0.991	0.975	0.986	0.944	0.998	0.463	0.954	0.803	0.935
PEI	0.831	0.948	0.890	0.959	0.441	0.227	0.974	0.990	0.797	0.987	0.989	0.985
PLL	0.787	0.967	0.897	0.978	0.905	0.944	0.993	0.986	0.372	0.994	0.993	0.994

Adsorption curves at varied protein concentration were analysed using a one-step kinetic process, as outlined in section 5.3.7. However, this model is simplistic for a protein adsorption process, which may include complex processes such as protein-surface interactions, changes in protein conformation, re-orientation of proteins and surface diffusion [281]. However, plots of $d\Gamma_s/dt$ against Γ_s produced a linear curve with high R^2 values, as shown for each biomolecular adsorption reaction in 0, with values typically >0.97, except when low Γ_s was measured such as when 1 μg/ml protein concentrations were used. This suggests that a one-step protein-adsorption process dominates kinetics over the initial time period, thus, for simplicity, this model was used to analyse the kinetic data further. The resultant k_a, k_d, K, and $\Gamma_{s\infty}$, as determined from equation 5.5 and equation 5.7, for each polymer with each protein is shown in Table 5.1. Assuming monolayer coverage, the area per biomolecule (A_{biomol}) can be calculated for each $\Gamma_{s\infty}$ using equation 5.8, where M is the molar mass of the protein and N_A is Avogadro's constant = 6.02214×10^{23}. The A_{biomol} measured for CN, FN and BSA adsorption onto the polymer array are shown in Table 5.2.

$$A_{biomol} = \frac{M}{\Gamma_{s\infty} N_A} \tag{5.8}$$

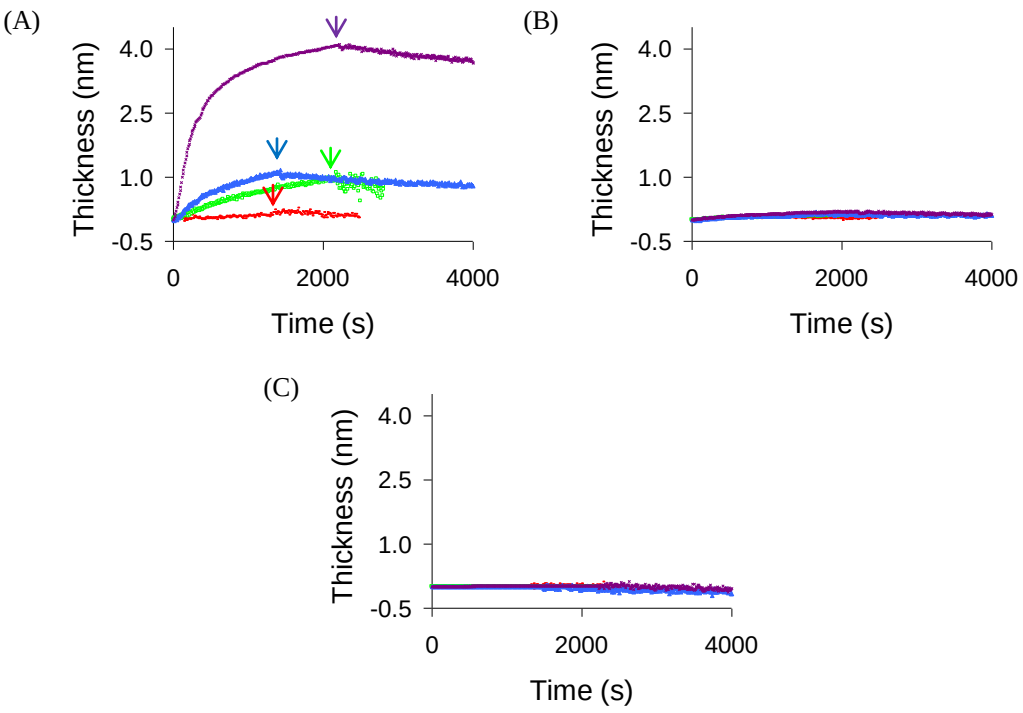

Figure 5.14. *SPR sensorgrams for the adsorption and desorption of CN type I to (A) PAAc, (B) PEIc and (C) PLLc at concentrations of (x) 10 µg/ml, (▲) 5 µg/ml, (□) 2 µg/ml and (-) 1 µg/ml at pH 7.4. All curves have had the background subtracted (SPR signal on the unmodified HDI PEG coating). Protein was injected once the surface had stabilised in phosphate buffer. Protein injection has been standardised to time=0 for ease of comparison. Buffer was injected as indicated by the arrows.*

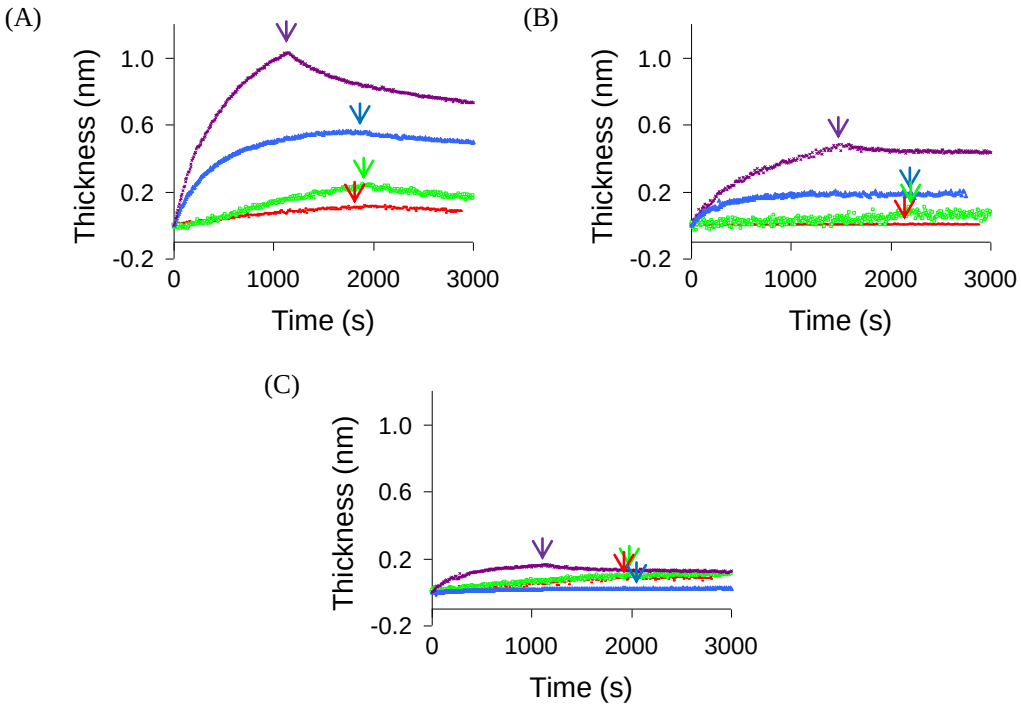

Figure 5.15. *SPR sensorgrams for the adsorption and desorption of FN to (A) PAAc, (B) PEIc and (C) PLLc at concentrations of (x) 10 µg/ml, (▲) 5 µg/ml, (□) 2 µg/ml and (-) 1 µg/m at pH 7.4. All curves have had the background subtracted (SPR signal on the unmodified HDI PEG coating). Protein was injected once the surface had stabilised in phosphate buffer. Protein injection has been standardised to time=0 for ease of comparison. Buffer was injected as indicated by the arrows.*

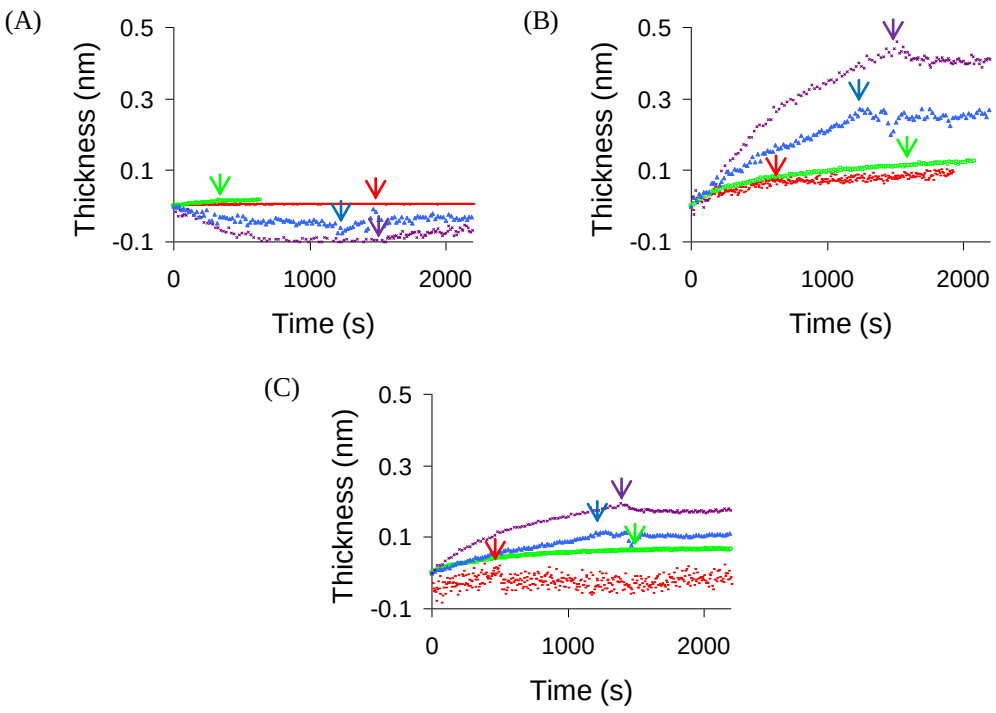

Figure 5.16. *SPR sensorgrams for the adsorption and desorption of BSA to (A) PAAc, (B) PEIc and (C) PLLc at concentrations of (x) 10 µg/ml, (▲) 5 µg/ml, (□) 2 µg/ml and (-) 1 µg/ml at pH 7.4. All curves have had the background subtracted (SPR signal on the unmodified HDI PEG coating). Protein was injected once the surface had stabilised in phosphate buffer. Protein injection has been standardised to time=0 for ease of comparison. Buffer was injected as indicated by the arrows.*

Table 5.1. *Association and dissociation rates, binding constant and total binding capacity of CN type I, FN and BSA to PAAc, PEIc and PLLc obtained by fitting a one step kinetic process to kinetic data obtained (Figure 5.14, Figure 5.15 and Figure 5.16) by SPRi of a polymer array.*

	CN type I				FN				BSA			
	k_a ($s^{-1}M^{-1}$) ($x10^3$)	k_d (s^{-1}) ($x10^{-4}$)	K (M) ($x10^6$)	$\Gamma_{s\infty}$ (mg/m^2)	k_a ($s^{-1}M^{-1}$) ($x10^3$)	k_d (s^{-1}) ($x10^{-4}$)	K (M) ($x10^6$)	$\Gamma_{s\infty}$ (mg/m^2)	k_a ($s^{-1}M^{-1}$) ($x10^3$)	k_d (s^{-1}) ($x10^{-4}$)	K (M) ($x10^6$)	$\Gamma_{s\infty}$ (mg/m^2)
PAA	102.40	0.401	2555.5	15.7	69.94	2.55	274.4	15.3	0.49	26.09	0.2	NA
PEI	15.33	2.999	51.1	0.5	35.87	8.67	41.4	3.2	17.38	12.68	13.7	3.8
PLL	8.32	3.546	23.5	0.1	88.60	3.55	249.9	0.3	5.81	4.61	12.6	3.2

Table 5.2. A_{biomol} (nm^2) *calculated from the* $\Gamma_{s\infty}$ *measured for CN type I, FN and BSA adsorption to PAAc, PEIc and PLLc.*

	CN	FN	BSA
PAA	43	49	NA
PEI	1352	234	30
PLL	6758	2490	35

A CN type I layer of average thickness of approximately 4 nm was observed to deposit on the PAAc after approximately 2000 s at a bulk concentration of 10 μg/ml (Figure 5.14A), however, almost no adsorption was observed on the PEIc and PLLc polymers (Figure 5.14B-C). This was confirmed by the high k_a, K and $\Gamma_{s\infty}$ of 102.4×10^3 $s^{-1}M^{-1}$, 2555.5×10^6 M and 15.7 mg/m^2 respectively and the low k_d value of 0.401×10^{-4} s^{-1} calculated for CN type I adsorption to PAAc as compared with PEIc with the next highest k_a, K and $\Gamma_{s\infty}$ of 15.3×10^3 $s^{-1}M^{-1}$, 51.1×10^6 M and 0.5 mg/m^2 respectively and the next lowest k_d value of 2.999×10^{-4} s^{-1} (Table 5.1). At physiological pH CN type I has a weak negative charge, with an isoelectric point (pI) of 5.5 [282, 283], however, positively charged domains along the fibrils, which are implicated to its structure and biological function [284, 285] can interact strongly with the negative charge on the PAAc polymer [286] allowing for the end point attachment of CN type I. The end point attachment of CN type I to PAAc is suggested by the low A_{biomol} of 43 nm^2 measured (Table 5.2) as compared with the size of CN type I of 450 nm^2 [287], suggesting only 9.6% of an adsorbed CN type I molecule is in contact with the surface. The measured $\Gamma_{s\infty}$ of 15.7 mg/m^2 is higher than the $\Gamma_{s\infty}$ of 6-7 mg/m^2 measured previously for CN type I adsorption onto poly(ethylene terephthalate) [287]. The end on adsorption regime of CN type I to PAAc proposed would allow for a higher binding capacity.

A FN layer was observed on PAAc of average thickness of 1.0 nm after adsorption for 1500 s at 10 μg/ml (Figure 5.15A), and smaller thicknesses of 0.5 nm and 0.2 nm were observed on PEIc and PLLc respectively (Figure 5.15B and C). The $\Gamma_{s\infty}$ for FN adsorption to PAAc, PEIc and PLLc were found to be 15.3, 3.2 and 0.3 mg/m^2, respectively (Table 5.1).

FN has a pI of 5.3 [288], thus at physiological pH this protein will possess a small negative charge. This suggests that electrostatic interactions may govern this interaction with the positively charged PEIc and PLLc [289, 290]. However, similar to the adsorption behaviour of CN type I, the measured $\Gamma_{s\infty}$ on PEIc and PLLc is significantly smaller than for adsorption to negatively charged PAAc. The $\Gamma_{s\infty}$ determined for FN adsorption to Au, Ti-oxide and Ta-oxide of 14.6, 10.6 and 11.0 mg/m^2 [291] are comparable with the FN adsorption measured to PAAc. The pKa of both PAA and Ta-oxide are both approximately 3, thus, would both have a similar negative charge [286, 291]. FN adsorption has also been reported onto other negatively charged surfaces including anionic phospholipids and silica [292]. The A_{biomol} measured for FN adsorption to PAAc of 49 nm^2 (Table 5.2) is significantly lower than the size of FN of 384 nm^2 as measured by scanning electron microscopy [288], suggesting that FN adsorbs end on, with only a 12.8% of the protein in contact with the surface. This allows for the formation of a dense biomolecular layer. A similar A_{biomol} for FN adsorption to gold of 45 nm^2 has been previously reported [291]. The A_{biomol} measured for FN adsorption to PEIc of 234 nm^2 (Table 5.2) is much closer to the size of FN, and suggests that FN adsorbs side on in this case. The A_{biomol} measured for FN adsorption to PLLc of 2490 nm^2 (Table 5.2) is large compared to the size of FN and suggests only 15% surface coverage of FN to PLLc is possible under the experimental conditions used here.

The counterintuitive adsorption of both CN and FN to PAAc, which should electrostatically repel both CN and FN, suggests the net charge of the protein must not be dominating its surface adsorption behaviour in this case. Contributing factors to FN adsorption may be electrostatic interactions between positively charged domains of the protein and negatively charge surface moieties, a specific interaction

between CN and FN with PAAc, an entropy effect as a result of protein rearrangement or conformational changes upon surface adsorption that may expose positively charged domains embedded with the protein resulting in a change in the protein pI upon adsorption [293].

The k_a measured for FN adsorption to PAAc, PEIc and PLLc were 69.9×10^3, 35.9×10^3 and 88.6×10^3 $s^{-1}M^{-1}$, respectively (Table 5.1). Interestingly, FN adsorption to PLLc had a higher k_a than to PEIc, despite both polymer being positively charged. Moreover, FN adsorption to PAAc also had a higher k_a than to PEIc. The reason for the relatively fast rate of adsorption of FN to PLL is unclear.

BSA adsorption was observed on both PEIc and PLLc, with adsorption for 1500 s at 10 mg/ml resulting in protein layers of thickness 0.4 and 0.2 nm, respectively (Figure 5.16B and C). Conversely, little to no BSA adsorption was measurable on the PAAc (Figure 5.16A). In fact, a negative change in mass was measured for PAAc (Figure 5.16A). Since the SPR sensorgrams shown in Figure 5.14-Figure 5.16 have had the signal from the unmodified HDI PEG background subtracted, this negative result is likely due to the PAAc resisting BSA adsorption more effectively than the PEG background. BSA has a pI of 4.7 [294] and is, thus, negatively charged at physiological pH. The resistance of BSA adsorption by PAAc is therefore likely to be due to the electrostatic repulsion of the overall negative charge of the protein with the negative charge of PAA. Likewise, the adsorption to PEIc and PLLc is likely due to electrostatic attraction between the overall negative charge of BSA and the positive charge of PEI and PLL. Adsorption of BSA has been previously shown to be electrostatically mediated [281, 295]. The $\Gamma_{s\infty}$ of BSA adsorption to PEIc and PLLc was found to be 3.8 and 3.2 mg/m^2, respectively (Table 5.1), which is significantly lower than the $\Gamma_{s\infty}$ of CN type I and FN adsorption to PAAc of 15.7 and 15.3 mg/m^2

respectively (Table 5.1). These lower values are likely due to the lower molecular weight of the adsorbed BSA of 68 kDa [296] as compared with 407 kDa for CN type I [297] and 450 kDa for FN [288]. Thus, the adsorption of a single BSA molecule will produce only 15% of the equivalent response of a FN molecule. Furthermore, a thicker layer would be expected for monolayer coverage of FN and CN type I as compared with BSA due to the larger size of FN and CN type I. The A_{biomol} of 30 and 35 nm^2 for BSA adsorption to PEIc and PLLc (Table 5.2), respectively, suggests that approximately 54% and 62% of the protein area (total size is 56 nm^2 [298]) is in contact with the surface at complete coverage. BSA adsorption to PLL has previously been studied given a Γ_s of 6.5 mg/m^2 [295]. This higher BSA adsorption is likely due to the lower pH of 5 at which the adsorption was conducted.

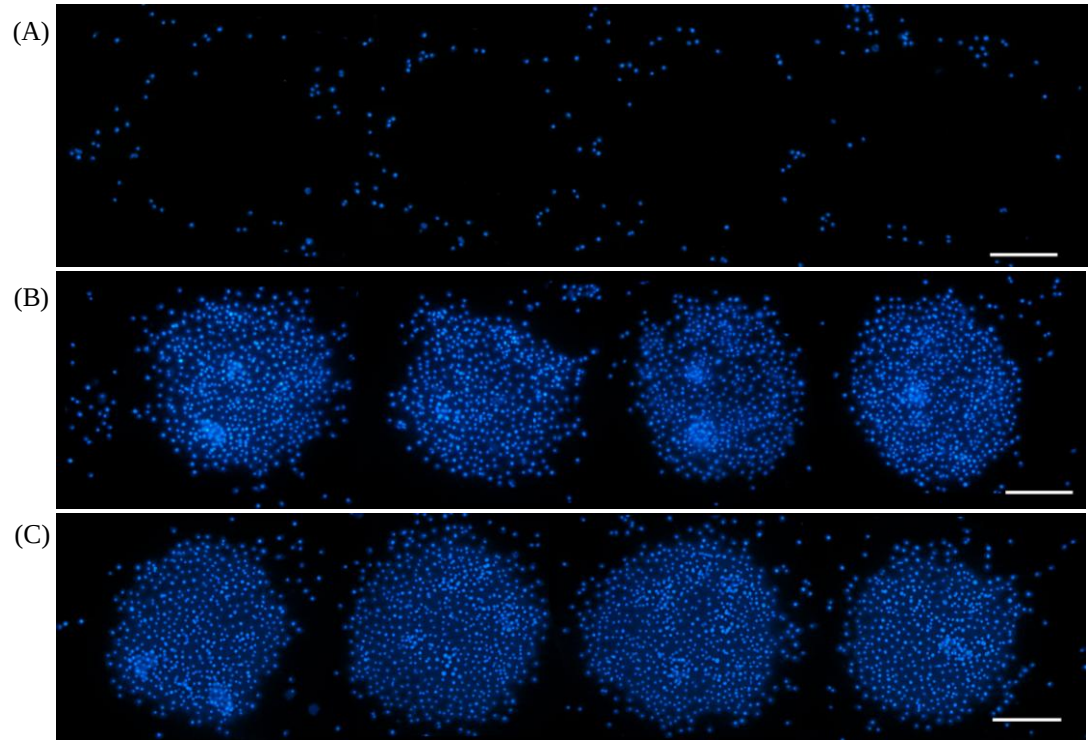

Figure 5.17. *Fluorescence microscopy images of SK-N-SH cells grown for 24 hr on (A) PAAc, (B) PEIc and (C) PLLc arrayed onto PEG coated surface. Scale bar is 250 μm.*

5.4.4. Assessment of cell attachment to polymer arrays

Further to the SPRi analysis of biomolecular adsorption to a polymer microarray, PAAc, PEIc and PLLc arrays on the HDI PEG coated surface were subjected to cell attachment assays. SK-N-SH neuroblastoma cells were seeded onto the polymer array and after 24 hr were stained using Hoechst 33342 and observed by fluorescence microscopy. This cell line was used as they are known to be highly adhesive to many different surfaces, thus, presenting a good model for studying cell adhesive properties [228]. The resultant cell patterns are shown as Figure 5.17. Cell attachment was observed on PEIc and PLLc as determined by the large number of cells aligning with the underlying polymer array as compared with the low cell numbers on the PEG background (Figure 5.17B and C). Thus, PEIc and PLLc promoted neuroblastoma cell attachment. PEG is well known in its ability to resist cell attachment and protein adsorption, thus, low cell attachment on this layer was expected [65, 67, 84], whilst, the presence of amine groups has previously been shown to promote cell attachment, particularly with neuronal cells [299]. Conversely, cell attachment was poor on the PAAc (Figure 5.17A). Interestingly, an even lower cell density was observed on these polymer spots as compared with the underlying PEG coating. Cell attachment inhibition by PAA has been previously reported for a number of different cell types [300-303]. This contrasts with the low-density grafting of PAA, which on some substrate surfaces is able to improve cell attachment by tuning the surface wettability to be more suitable for cell attachment [304, 305]. However, in the present case, PAA surface density is sufficiently high to repel cell attachment by electrostatic repulsion with the negative charge on the cell membrane [300-303].

Comparing cell attachment with the protein adsorption experiments (section 5.4.3), a clear correlation between cell attachment and BSA adsorption was observed. This may suggest that cell attachment is mediated by the adsorption of negatively charged serum proteins, which has previously been reported [306]. Under normal cell culture conditions in the presence of serum cell attachment is observed to occur over a period of a few hours, thus, the kinetics of BSA adsorption would suggest that protein is able to adsorb to the surface before cells attach, thus, would be present when cells are attaching to the surface. However, BSA adsorption, which is used to prevent cell attachment [307], is unlikely to mediate cell attachment. The correlation between BSA adsorption and cell attachment suggests that both processes occur by the same underlying mechanism, that is, electrostatic interactions; the overall negative charge of the cell membrane [308] will be electrostatically attracted to the positive surface charge of the PEI and PLL spots and likewise be repelled from the negatively charged PAA spots. However, determining clear correlations between protein-surface interactions and cell attachment behaviour is intrinsically difficult due to the complex nature of cell attachment, which can be influenced by surface properties such as chemistry, inclusion of biological cues, elastic modulus, wettability, charge and topography as well as cell culture conditions such as the cell line, the concentration of serum and the time period of incubation.

It is interesting to note that cell attachment did not occur on the PAAc despite this surface being suitable for the adsorption of ECM proteins whilst it did occur on PEIc and PLLc, which were seen to resist CN type I adsorption (Figure 5.14 and Table 5.1). This result may have implications for long term cell growth on these surfaces, whereupon, PEIc and PLLc may resist the formation of ECM about attached cells and PAAc may, over time, become susceptible to cell attachment by the adsorption

of secreted collagen fibrils. Moreover, the inclusion of FN and CN in the cell culture media may also promote cell attachment on the PAAc.

5.5. Conclusion

The characterisation of a polymer array containing non-uniform surface features using SPRi has been achieved, overcoming the requirement for homogeneous surfaces for comparative SPRi measurements. A method has been developed whereby changes in reflectivity measured during a typical fixed angle SPR experiment can be related to the corresponding shift in resonance angle. This process was shown to theoretically produce equivalent responses for microarray polymer spots of 0-30 nm thickness when exposed to an equivalent change in refractive index and was found to produce quantitatively comparable results in practice. This approach has been utilised to study the adsorption of CN type I, FN and BSA to a polymer array of PAA, PEI and PLL. For this, a novel approach to producing a low fouling background for SPR applications was developed by initially coating a SPR chip with a thin plasma polymer layer that was modified with HDI in order to attach a low-fouling PEG layer. BSA adsorption to the polymer array followed the expected trends assuming electrostatic interactions, however, CN type I and FN, despite having a negative charge, adsorbed on both positively and negatively charged surface chemistries. The end on adsorption of both these polymers to PAA was suggested. This result highlighted the complex behaviour of biomolecules at surfaces and, thus, the difficulty associated with correlating protein and cellular behaviour.

Comparison of protein adsorption studies with cell attachment assays conducted with SK-N-SH in serum over 24 hr suggest that cell attachment is largely driven by electrostatic interactions.

The results demonstrate the ability of the label-free technique SPRi to achieve useful kinetic and thermodynamic insights into the biomolecular behaviour within a polymer microarray format without the need for advanced fabrication approaches to ensure a homogeneous surface. Use of a larger polymer library would allow for the high-throughput determination of the suitability of particular materials for specific biomedical applications, including tissue engineering, drug delivery and implant development, and would engender insights into the underlying mechanisms of biomolecular adsorption and cell attachment.

VI

CHAPTER 6. OVERALL CONCLUSIONS

An increased understanding of the behaviour of biomolecules at surfaces coupled with the continued development of tools for the advanced surface manipulation of biomolecules is imperative for studying complex biological systems or developing advanced biomedical devices. One particularly useful approach to achieving advanced biomolecular surface manipulation is the production of patterned or switchable surfaces, which has been the focus of this thesis. A number of techniques have been developed to achieve these abilities, however, the most interesting and useful systems are those that combine patterns on the micro- or even nanoscale with switchable architectures to achieve both temporal and spatial control over biomolecule surface interactions concurrently.

Two examples of patterned and switchable systems have been described in this thesis. The first system, described in CHAPTER 2, included the formation of patterned surface chemistries, which were able to spatially organise the adsorption of DNA and cells for the formation of microarrays (section 2.3.2 and 2.3.4), combined with a switchable electrical bias generated on the application of a positive or negative voltage to the substrate surface. A negative electrical bias stimulated DNA desorption and enhanced solid phase transfection efficiency (section 2.3.2 and 2.3.3).

The second patterned and switchable system reported in this thesis was the formation of a P*N*IPAAm microarray (section 5.4.1). Here, surface patterning was achieved by robotic contact printing of P*N*IPAAm spots onto a low fouling coating. Switching was achieved by a temperature change exploiting the thermoreversible properties of P*N*IPAAm, which is adherent for biomolecules above its LCST and non-adherent below the LCST. Although not explored in great depth in this thesis,

this system has also been explored for cell attachment studies, as discussed in section 1.3.2, and promises to be a powerful approach to constructing intricate cell architectures, which is particularly relevant for tissue engineering applications.

Concomitant with the importance of patterned and switchable elements for biomedical applications is a need to understand in detail the mechanisms of biomolecular behaviour at surfaces. This was the focus of CHAPTER 3 and CHAPTER 5, and was exemplified by the discovery of a number of unexpected mechanisms, consistent with the complex nature of biology at interfaces.

Initially, allylamine plasma polymer (ALAPP) coatings were utilised for TCM applications because of their amine functionality, which was thought to enable electrostatic interactions with negatively charged DNA and also with the plasma membrane of cells (section 2.3.2). However, in addition to electrostatic interactions playing a role, resulting in enhanced DNA adsorption at low pH and high salt concentration (section 3.3.3) (discussed in section 1.1.2), further investigation suggested hydrophobic interactions dominated DNA adsorption at physiological pH (section 3.3.3). This result suggested the partial denaturation of the DNA strand upon adsorption in order to expose the hydrophobic core to hydrophobic moieties on the ALAPP coating. DNA adsorption may also be stabilised by electrostatic interactions between isolated positive surface charges and the anionic charge on DNA despite the overall negative surface charge of ALAPP, as discussed in section 1.1.2. This highlights the need to consider specific domains of a biomolecule in addition to its overall properties in order to understand the adsorption behaviour of the biomolecule.

Counterintuitive behaviour was also observed for collagen (CN) type I and fibronectin (FN) adsorption to poly(acrylic acid) (PAA) coatings (section 5.4.3).

These molecules possess a negative charge at physiological pH, thus, should electrostatically repel each other. However, despite this a high binding capacity of CN type I and FN to PAA was observed that exceeded the binding capacity to cationic polymers (section 5.4.3). The mechanism of CN type I and FN adsorption to PAA, similar to DNA adsorption to ALAPP, may involve the adsorption of a positively charged domains of CN type I or FN to the PAA.

Microarrays have revolutionised genomic studies and are a key enabling tool for the identification and characterisation of new biomaterials. The formation of DNA, cell and polymer microarrays have all been explored in this thesis (section 2.3.4, 4.3.2, 4.3.4 and 5.4.1) and the ability to analyse various biological and chemical features in a high-throughput, cost-effective manner has been demonstrated. The development of TCMs is a particularly exciting and important development for high-throughput studies of genomics. The increased understanding of DNA-surface interactions and the development of advanced material surfaces combined with the ability to temporally and spatially manipulate biomolecules provide the means to develop highly functional and reliable platforms for advanced genomic analysis.

A novel approach was explored for the advanced substrate fabrication of cell microarrays, as discussed in CHAPTER 4. Here, surface patterning using robotic contact printing was combined with the photo-induced chemistry of phenylazide. The formation of stable surface patterns utilising a highly reactive crosslinker bound to soluble synthetic polymers enabled the covalent photo-induced linkage of the resultant polymer arrays to a broad range of organic substrate materials, including low fouling poly(ethylene glycol) (PEG) coatings. Furthermore, polymer microarray formation enabled the pre-patterning of microarray substrates for the formation of biomolecule microarrays, which was demonstrated by the formation of a cell

microarray (section 4.3.4). Use of robotic contact printing makes integrated polymer and biomolecular arrays accessible to life science laboratories for the first time, to whom this technology is of particular interest. Furthermore, this novel approach is of particular significance for TCM technology, whereby problems associated with cross-contamination between adjacent spots on the microarray by DNA surface diffusion and cell migration are alleviated, allowing for higher density arrays. Moreover, this approach may also reduce processing times associated with the analysis of arrays by removing the need to differentiate between transfected cells and the background of non-transfected cells encountered when no chemical pattern is present. The continued development of RNAi techniques on TCMs for high-throughput loss-of-function studies and the development of methods enabling highly resolved subcellular phenotypic examination will see more in-depth studies being undertaken, not only into gene function but also into the machinery involved in gene expression. Furthermore, the development of cDNA and RNAi genome wide libraries will enable the high-throughput, rapid and inexpensive analysis of entire genomes.

High-throughput, cost-effective studies of microarrays were also investigated in CHAPTER 5, where the high-throughput analysis of the interaction of CN type I, FN and bovine serum albumin (BSA) to a polymer microarray was explored by surface plasmon resonance imaging (SPRi). This approach is of interest as it has the potential to investigate the interaction of individual biomolecules with a polymer microarray without the need for fluorescent labelling in a high-throughput format. Such studies are complementary to the high-throughput studies of the cellular behaviour and chemical characterisation of polymer microarrays, which have previously been reported. These techniques are invaluable for the determination of the suitability of

new materials for specific biomedical applications, particularly since biomolecular and cellular interactions with material surfaces are complex and difficult to predict *a priori*.

In summary, a number of biodevice applications will benefit from the further development of biomolecular manipulation and an advanced understanding of the interface behaviour of biomolecules and cells. Here, it has been demonstrated that this can be achieved by introducing both patterned and switchable elements in order to both spatially and temporally control the complex biological systems that biodevices interact with, coupled with the development of tools to analyse in depth the surface behaviour of biomolecules and living cells.

APPENDIX 1. LIST OF ABBREVIATIONS

2D	Two dimensional
3D	Three dimensional
Γ^{DNA}	Surface coverage of DNA
$\Gamma^{protein}$	Surface coverage of protein
μCP	Microcontact printing
AAm	Acrylamide
ACPA	4,4'-azobis(4-cyanopentanoic acid)
AFM	Atomic force microscopy
ALAPP	Allylamine plasma polymer
AOLG	Amino-oligonucleotide
APTMS	3-aminopropyltrimethoxysilane
BAEc	Bovine aortic endothelial cells
BCEp	Bovine corneal epithelial cells
BSA	Bovine serum albumin
CCD	Charge coupled detector
cDNA	Complementary DNA
CHO-K1	Chinese hamster ovary cell line
CN	Collagen
COS	Monkey kidney fibroblasts
DC	Direct current
DMEM	Dulbecco's modified eagle media
DMS	Dimethyldichlorosilane
DMSO	Dimethylsufoxide
DNA	Deoxyribonucleic acid
DPN	Dip-pen nanolithography
dsDNA	Double stranded DNA
EC buffer	Condensation buffer
ECM	Extra cellular matrix
E-coli	*Escherichia coli*
EDC	1-ethyl-3-(diethylamino)propyl carbodiimide
EDS	*N*-(2-aminoethyl)-3-aminopropyltrimethoxysilane
EDTA	Ethylenediaminetetraacetic acid
FAM	Carboxyfluorescein
FDA	Fluorescein diacetate
FITC	Fluorescein isothiocyanate
FN	Fibronectin
FT-IR	Fourier transform – infrared
GFP	Green fluorescing protein
GPCRs	G-protein coupled receptors
HDI	Hexamethylene diisocyanate
HeLa	Henrietta Lack
HEK	Human embryonic kidney cell
IgG	Immunoglobulin
LCST	Lower critical solution temperature

MAA	Methacrylic acid
MHA	(16-mercapto)hexanoic acid
mRNA	Messenger RNA
NHS	*N*-hydroxysuccinimide
NIH3T3	Normal mouse fibroblast
NSANB	*N*-succinimidyl-5-azido-2-nitrobenzoate
OCT-1	Osteoblast-like cells
OEGMA	Oligo(ethylene glycol) methacrylate
PAA	Poly(acrylic acid)
PAAc	Covalently linked PAA spot
PALA	Polyallylamine
PBS	Phosphate buffer saline
PC12	Pheochromocytoma
PCR	Polymerase chain reaction
PDMS	Poly(dimethylsiloxane)
PEG	Poly(ethylene glycol)
PEI	Poly(ethyleneimine)
PEIc	Covalently linked PEI spot
pI	Isoelectric point
PLA	Poly(lactic acid)
PLL	Poly(L-lysine)
PLLc	Covalently linked PLL spot
P*N*IPAAm	Poly(*N*-isopropylacrylamide)
PS	Polystyrene
PVPI	Poly(2-vinyl pyridine)
PVP	Polyvinylpyrrolidone
QCM	Quartz crystal microbalance
RADS	Arginine-alanine-asparagine-serine
RFP	Red fluorescing protein
RGD	Arginine-glycine-asparagine
RNA	Ribonucleic acid
RNAi	RNA interference
SAMs	Self-assembled monolayers
SK-N-SH	Neuroblastoma
SPR	Surface plasmon resonance
SPRi	SPR imaging
ssDNA	Single stranded DNA
TCM	Transfected cell microarray
TE	Tris-EDTA
ToF-SIMS	Time of flight secondary ion mass spectroscopy
UV	Ultraviolet
XPS	X-ray photoelectron spectroscopy

APPENDIX 2. AFM FORCE CURVES OF CROSS-LINKED POLYMER ARRAYS

A2.1. Introduction

Surface modification has become of increasing importance for a wide range of applications. Techniques to modify the outer surface of a material whilst not compromising the materials bulk properties or integrity are of interest. Of particular interest are patterned surfaces that are able to offer spatial control over the behaviour of biomolecules at a particular surface. Surface patterning may incorporate both chemical and topographical features, and can be achieved by a wide range of approaches including photolithography, soft lithography, robotic printing, microfluidics and microelectronics [66, 74-77, 79, 133, 197, 214]. A significant outcome of the development of microfabrication is microarrays. DNA and protein microarrays have revolutionised genomic studies and continue to bring considerable insight ubiquitously in medical science [98, 127, 135, 309]. Development of patterned surface chemistry that precisely match the surface patterns of microarrays could increase microarray capabilities by allowing higher densities by minimising the required separation between adjacent spots, and higher signal to noise ratios by incorporating low-fouling surfaces that minimise non-specific binding. This is of particular interest for microarrays containing living cells [1, 45].

The formation of a patterned surface, as described in CHAPTER 4, is of particular suitability for DNA microarray applications. Initially a polycationic polymer having bioactive properties is functionalised with a phenylazide cross-linker then arrayed onto a low-fouling surface and UV cross-linked to form a covalently linked polymer

microarray that can be used as a base substrate for additional array formation. The array format allows for the parallel analysis of varied polymers with their performance as an immobilisation matrix for DNA microarrays, however, specific analysis of the interactions between various polymers and biomolecules is of interest. Force-distance (*F-D*) curves achieved by atomic force microscopy (AFM) are a powerful tool for the investigation of the adhesive, viscoelastic and stiffness properties of materials [310]. For this reason, *F-D* curves were performed on a DNA-modified tip and polymer array surfaces.

A2.2. Materials and methods

A2.2.1. Plasma polymerisation

Approximately 1 cm^2 glass samples, cleaned by sonication for 20 min in a 5% (detergent concentration) surfactant (RBS 35, Pierce USA) wash, followed with rinsing in water and drying in a laminar flowhood, were modified with an allylamine plasma polymer (ALAPP), preformed in a custom-built reactor described elsewhere [182]. In short, the plasma reactor consisted of two circular electrodes separated by 125 mm in a cylindrical reactor being 350 mm high with a diameter of 170 mm. Allylamine (Aldrich, 98% purity) was used as a monomer. Polymerisation conditions used were a frequency of 200 kHz, a power of 20 W and an initial monomer pressure of 0.188 mbar. Deposition time was 25 s.

A2.2.2. Polymer array formation

Poly(allylamine) (PALA) (Sigma, MW 70000), poly(acrylic acid) (PAA) (Aldrich, MW 90000), poly(ethylene imine) (PEI) (MW 70000), poly-L-lysine (PLL)

(Sigma, MW 70000) and polyvinylpyrrolidone (PVP) (Fluka, MW 380000) were spotted onto ALAPP coated glass. Before spotting polymer samples were prepared to 4, 2, 1, 0.5, 0.25, 0.1 and 0 mg/ml solutions in ultra pure water. 1 mg/ml *N*-succinimydl 5-azido-2-nitrobenzoate (Fluka) was also preadded and polymer-phenylazide solutions were incubated at 25 °C for 10 min before array formation. Spotting was conducted using a BioOdyssey Calligrapher MiniArrayer (Bio-Rad) using a 375 μm diameter solid pin (ArrayIt). Spotting was conducted at a humidity of 65% and at a temperature of 25 °C. The approach speed of the pin and the dwell time of the pin in contact with the surface were set to 20 mm/s and 15 ms respectively. All spots formed were reprinted once directly after initial spot formation to minimise variation in spot formation. All spotting and solution preparation was conducted in the dark. After array formation samples were exposed to UV for 10 mins. Arrays were then imaged using a GenePix 4000A microarray scanner.

A2.2.3. Polymer spin coating

As controls, polymer samples of PALA, PAA, PEI, PLL and PVP were prepared on bare silicon by spin coating. Highly doped, p++ silicon (Virginia semiconductors, Inc.) were cut into 1 cm^2 pieces and washed by sonication for 20 min in a 5% (detergent concentration) surfactant wash. Surfaces were then dried in a laminar flowhood. Spin coating was conducted on a WS-400B-6NPP/LITE Spin coater (Laurell Technologies). 166 μl of 10 mg/ml polymer solution (in water) was pipetted onto the sample such that the entire surface was covered. The sample was then spun at 3000 rpm for 10 s. After this an additional 166 μl was added and the sample was spun again for another 10 s. A further 166 μl of polymer solution was added and the sample was spun for 30 s.

A2.2.4. AFM tip modification

OTR8 and NP-20 tips were modified with a 27 mer, amino-oligonucleotide (AOLG) (5'-amino TTT AGT TGA TTT GTG CTT CAG TGT GCT, Geneworks). Tips were initially cleaned in piranha solution (3:1, H_2SO_4:30% H_2O_2) for 30 s before rinsing in water and drying under nitrogen. Tips were then incubated in mercaptobutyltrimethoxysilane (1% in toluene) for 10 mins under nitrogen at room temperature before washing with toluene, then water and drying under nitrogen. Complete reduction of the mercapto group was ensured by incubation of the tips with tris(2-carboxyethyl) phosphine hydrochloride (66.3 mM in PBS) for 5 min and then washing and drying under nitrogen. Tips were then added to 3-(maleimido)propionic acid N-hydroxysuccinimide ester (3.76 mM in 1:1 PBS:DMF) and incubated for 2 hr under nitrogen at room temperature with occasional irritation before washing with water and drying under nitrogen. Tips were then added to AOLG (1.1 pM in PBS) and incubated for 2 hr under nitrogen at room temperature before washing with water and drying under nitrogen. Finally, tips were added to ethanolamine (0.55 M in water) and incubated for 10 mins at room temperature under nitrogen to quench any non-reacted NHS groups, before extensive washing with water and drying under nitrogen.

A2.2.5. AFM force measurements

Force measurements were conducted between OTR8 and NP-20 AOLG modified and unmodified tips and the polymer array as well as control polymer surfaces. A Nanoscope IIIa scanning probe microscope was used in contact mode, with the initial vertical deflection set to -1.5 V, scan rate of 1 Hz, a ramp size of 1 μm. Force curves were taken under fluid in Tris-EDTA (TE) buffer supplemented with 10, 5, 1 and 0

% (v/v) ethanol. Images were taken with an unmodified NP-20 tip in contact mode with an initial vertical deflection of -2.7 V.

A2.3. Results

A2.3.1. Polymer spot characterisation

Five different polymers were chosen for formation of a polymer array. The distinctive feature of three, PALA, PLL and PEI, is their amine functionality, which allows formation of a covalent bond with the phenylazide cross-linker as well as introducing an overall positive charge at neutral pH; the isoelectric point of amines is typically >10. This positive charge was selected for the potential electrostatic interaction with the negative charges on the phosphate backbone of DNA. As a control, a negatively charged polymer in PAA was chosen, as well as a neutral and slightly hydrophobic polymer in PVP. The structure of each of these polymers is shown in Figure A1.0. Each of these polymers is also readily solubilised in water, which allows for the simple printing into an array without having to use organic solvents for printing or cleaning.

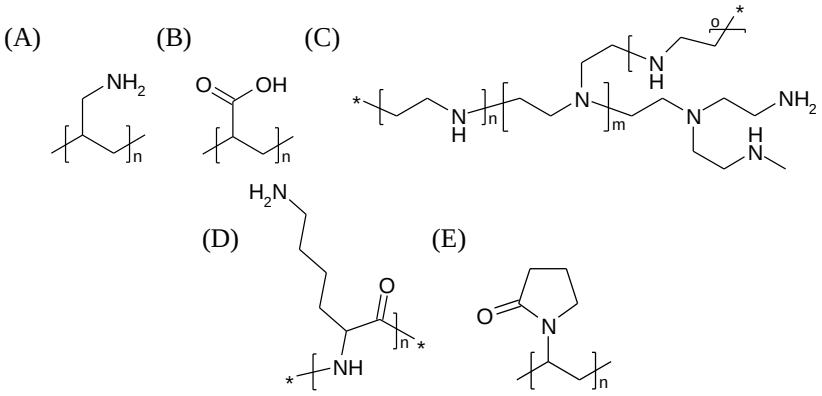

Figure A1.0. *Structures of (A) PALA, (B) PAA, (C) PEI, (D) PLL, (E) PVP.*

F-D curves were measured for all polymers and the control samples under fluid in TE buffer. Measurements on the control samples were identical to measurements done on individual spots, suggesting the preservation of polymer chemistry when using the arraying approach. As expected, a greater pull off force was seen for AOLG-modified tips with polycationic polymers than with unmodified tips or with modified tips with either PAA or PVP. Representative *F-D* curves are shown as Figure A1.1. Using the unmodified tip the *F-D* curve showed no distinctive feature for any of the polymers (Figure A1.1A, C and E). However, when using the modified tip a small repulsive force was observed for the interaction between the tip and PAA as compared with the unmodified tip (Figure A1.1A and B), whilst an attractive force was observed for PLL as a pull off force (Figure A1.1D). Similar results were also seen with PALA and PEI. The interaction with PVP was unchanged when comparing the modified and unmodified tip (Figure A1.1E and F).

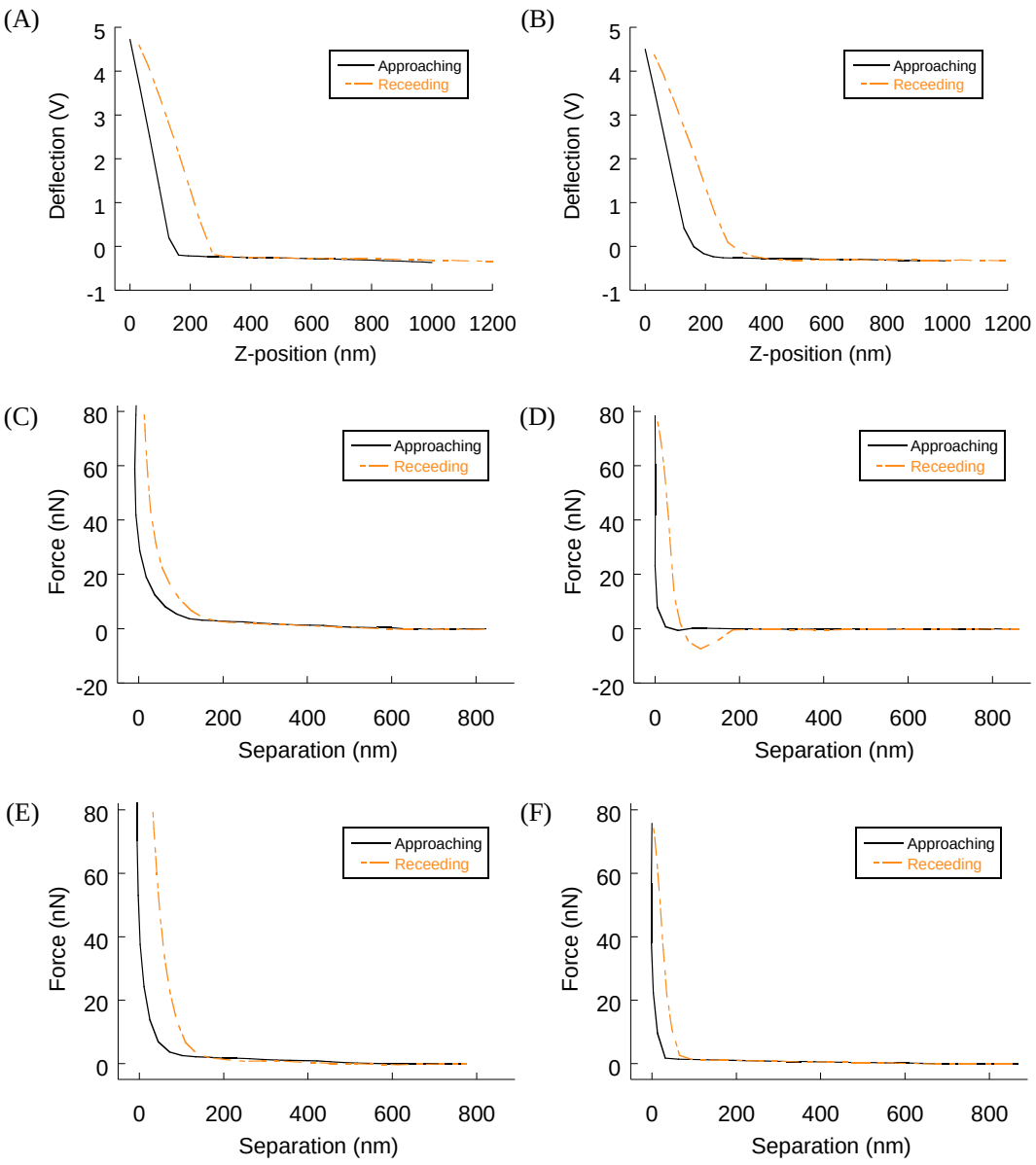

Figure A1.1. *F-D curve measurement for (A, C and E) unmodified and (B, D and F) DNA coated OT 28 tips approaching (A and B) PAA, (C and D) PLL and (E and F) PVP..*

In order to characterise the extent of hydrophobic interactions between the AOLG-modified tip and the polymer coatings *F-D* curves were conducted in TE buffer supplemented with different % (v/v) of ethanol. The added ethanol decreases the free energy of the liquid/solid interface by decreasing the thermodynamic penalty for having a polar solvent exposed to hydrophobic moieties on the surface [213]. Thus, increasing ethanol content should decrease the driving force for DNA adsorption if hydrophobic interactions play a role [188].

A summary of the pull off forces measured between the polymer samples and the DNA is shown as Figure A1.2. Interestingly, no polymer showed a decrease in the pull off force at higher ethanol concentrations, suggesting that hydrophobic interactions do not play a significant role for the interactions being studied. However, the force between the tip and PALA, PEI and PLL was observed to greatly increase at higher ethanol concentrations. Ethanol weakly solvates charge compared with water, thus, at higher ethanol concentrations it is entropically favourable for the formation of polar interactions. Thus, the increase in ethanol concentration enhanced the electrostatic interactions between the AOLG-modified tip and the polycationic polymers. This clearly demonstrates the presence of the strong electrostatic interactions possible between DNA and PALA, PEI and PVP, whilst the ability of PAA and PVP to repel DNA.

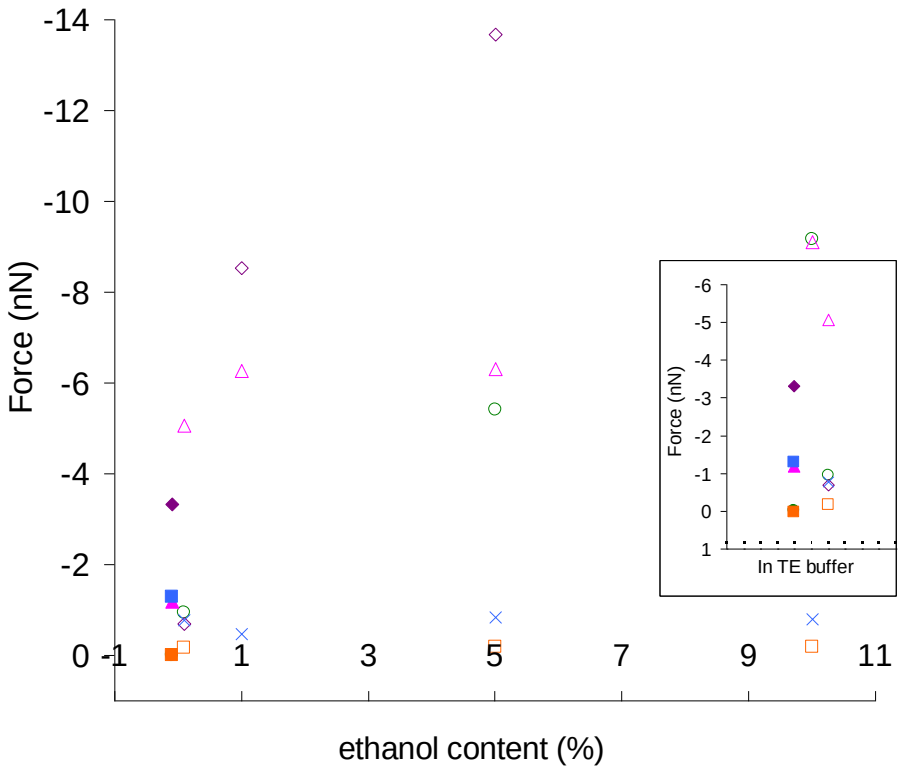

Figure A1.2. *Summary of pull off force for the interaction of DNA modified OT28 tip with variation in the content of ethanol in solution for polymer coatings; PALA (○), PAA (□), PEI (◇), PLL (△), PVP (x). Solid shapes represent interaction due to unmodified tip (see inset).*

BIBLIOGRAPHY

[1] Hook, A. L.; Voelcker, N.; Thissen, H. *Trends in Biotechnology* **2006**, *24*, 471-477.
[2] Hook, A. L.; Voelcker, N.; Thissen, H. *Progress in Surface Science* **2008**, *In Press*.
[3] Reimer, U.; Reineke, U.; Schneider-Mergener, J. *Current Opinions in Biotechnology* **2002**, *13*, 315-320.
[4] Kasemo, B. *Surface Science* **2002**, *500*, 656-677.
[5] Kim, J. J.; Park, K. *Journal of Controlled Release* **2001**, *77*, 39-47.
[6] Langer, R.; Peppas, N. A. *AIChE Journal* **2003**, *49*, 2990-3006.
[7] Situmorang, M.; Gooding, J. J.; Hibbert, D. B.; Barnett, D. *Electroanalysis* **2001**, *13*, 1469-1474.
[8] Ziauddin, J.; Sabatini, D. M. *Nature* **2001**, *411*, 107-110.
[9] Chan, V.; Graves, D. J.; Fortina, P.; McKenzie, S. E. *Langmuir* **1997**, *13*, 320-329.
[10] Tilton, R. D.; Robertson, C. R.; Gast, A. P. *Langmuir* **1991**, *7*, 2710-2718.
[11] Norde, W.; Lyklema, J. *Journal of Biomaterials Science-Polymer Edition* **1991**, *2*, 183-202.
[12] Gaspers, P. B., Robertson, C. R., Gast, A. P.,. *Langmuir* **1994**, *10*, 2699-2704.
[13] Chan, V.; McKenzie, S. E.; Surrey, S.; Fortina, P.; Graves, D. J. *Journal of Colloid and Interface Science* **1998**, *203*, 197-207.
[14] Hatfield, G. W.; Hung, S. P.; Baldi, P. *Molecular Microbiology* **2003**, *47*, 871-877.
[15] Heller, M. J. *Annual Review of Biomedical Engineering* **2002**, *4*, 129-153.
[16] Levicky, R.; Horgan, A. *Trends in Biotechnology* **2005**, *23*, 143-149.
[17] Wu, R. Z.; Bailey, S. N.; Sabatini, D. M. *Trends in Cell Biology* **2002**, *12*, 485-488.
[18] Wang, J.; Jiang, M.; Mukherjee, B. *Bioelectrochemistry* **2000**, *52*, 111-114.
[19] Zhao, Y.; Pang, D.; Hu, S.; Wang, Z.; Cheng, J.; Qi, Y.; Dai, H.; Mao, B.; Tian, Z.; Luo, J.; Lin, Z. *Analytica Chimica Acta* **1999**, *388*, 93-101.
[20] Melzak, K. A.; Sherwood, C. S.; Turner, R. F. B.; Haynes, C. A. *Journal of Colloid and Interface Science* **1996**, *181*, 635-644.
[21] Palecek, E. *Bioelectrochemistry and Bioenergetics* **1986**, *15*, 275-295.
[22] Elaissari, A.; Pichot, C.; Delair, T.; Cros, P.; Kurfurst, R. *Langmuir* **1995**, *11*, 1261-1267.
[23] Romanowski, G.; Lorenz, M. G.; Wackernagel, W. *Applied and Environmental Microbiology* **1991**, *57*, 1057-1061.
[24] Carre, A.; Lacarrriere, V.; Birch, W. *Journal of Colloid and Interface Science* **2003**, *206*, 49-55.
[25] Bloomfield, V. A. *Biopolymers* **1997**, *44*, 269-282.
[26] Teeters, M. A.; Root, T. W.; Lightfoot, E. N. *Journal of Chromatography, A* **2004**, *1036*, 73-78.
[27] Saoudi, B.; Jammul, N.; Chehimi, M. M.; McCarthy, G. P.; Armes, S. P. *Journal of Colloid and Interface Science* **1997**, *192*, 269-273.
[28] Lemeshko, S. V.; Powdrill, T.; Belosludtsev, Y. Y.; Hogan, M. *Nucleic Acids Research* **2001**, *29*, 3051-3058.
[29] Delehanty, J. B.; Shaffer, K. M.; Lin, B. C. *Biosensors and Bioelectronics* **2004**, *20*, 773-779.
[30] Balladur, V.; Theretz, A.; Mandrand, B. *Journal of Colloid and Interface Science* **1997**, *194*, 408-418.
[31] Horinaka, J.; Nakura, H.; Maeda, S. *Journal of Biochemical and Biophysical Methods* **2004**, *61*, 349-357.
[32] Shi, X. Y.; Sanedrin, R. J.; Zhou, F. M. *Journal of Physical Chemistry B* **2002**, *106*, 1173-1180.
[33] Thissen, H.; Hayes, J. P.; Kingshott, P.; Johnson, G.; Harvey, E. C.; Griesser, H. J. *Smart Materials and Structures* **2002**, *11*, 792-799.
[34] Hook, A. L.; Thissen, H.; Hayes, J. P.; Voelcker, N. H. *Biosensors and Bioelectronics* **2005**, *21*, 2137-2145.
[35] Szili, E.; Thissen, H.; Hayes, J. P.; Voelcker, N. *Biosensors and Bioelectronics* **2004**, *19*, 1395-1400.
[36] Zhang, Z.; Chen, Q.; Knoll, W.; Foerch, R.; Holcomb, R.; Roitman, D. *Macromolecules* **2003**, *36*, 7689-7694.
[37] Zhang, Z.; Knoll, W.; Foerch, R. *Surface and Coatings Technology* **2005**, *200*, 993-995.
[38] Yasuda, H. *Plasma Polymerization*, Academic Press: Orlando, Florida **1985**.

[39] Decher, G. *Science* **1997**, *277*, 1232-1237.
[40] Pei, R. J.; Cui, X. Q.; Yang, X. R.; Wang, E. K. *Biomacromolecules* **2001**, *2*, 463-468.
[41] Yamauchi, F.; Kato, K.; Iwata, H. *Langmuir* **2005**, *21*, 8360-8367.
[42] Messai, I.; Munier, S.; Ataman-Onal, Y.; Verrier, B.; Delair, T. *Colloids and Surfaces B-Biointerfaces* **2003**, *32*, 293-305.
[43] Bezanilla, M.; Manne, S.; Laney, D. E.; Lyubchenko, Y. L.; Hansma, H. G. *Langmuir* **1995**, *11*, 655-659.
[44] Hansma, H. G.; Laney, D. E. *Biophysical Journal* **1996**, *70*, 1933-1939.
[45] Angres, B. *Expert Review of Molecular Diagnostics* **2005**, *5*, 769-779.
[46] Puleo, D. A.; Kissling, R. A.; Sheu, M. S. *Biomaterials* **2002**, *23*, 2079-2087.
[47] Scheideler, L.; Geis-Gerstorfer, J.; Kern, D.; Pfeiffer, F.; Rupp, F.; Weber, H.; Wolburg, H. *Materials Science and Engineering C-Biomimetic and Supramolecular Systems* **2003**, *23*, 455-459.
[48] Elwing, H.; Welin, S.; Askendal, A.; Nilsson, U.; Lundstrom, I. *Journal of Colloid and Interface Science* **1987**, *119*, 203-210.
[49] Cha, T.; Guo, A.; Jun, Y.; Pei, D. Q.; Zhu, X. Y. *Proteomics* **2004**, *4*, 1965-1976.
[50] Cosnier, S. *Biosensors and Bioelectronics* **1999**, *14*, 433-456.
[51] Rao, S. V.; Anderson, K. W.; Bachas, L. G. *Mikrochimica Acta* **1998**, *128*, 127-143.
[52] Koh, W. G.; Itle, L. J.; Pishko, M. V. *Analytical Chemistry* **2003**, *75*, 5783-5789.
[53] McFarland, C. D.; Thomas, C. H.; DeFilippis, C.; Steele, J. G.; Healy, K. E. *Journal of Biomedical Materials Research* **2000**, *49*, 200-210.
[54] Kulkarni, G. V.; Chen, B.; Malone, J. P.; Narayanan, A. S.; George, A. *Archives of Oral Biology* **2000**, *45*, 475-484.
[55] Abrams, G. A.; Goodman, S. L.; Nealey, P. F.; Franco, M.; Murphy, C. J. *Cell and Tissue Research* **2000**, *299*, 39-46.
[56] Singhvi, R.; Stephanopoulos, G.; Wang, D. I. C. *Biotechnology and Bioengineering* **1994**, *43*, 764-771.
[57] Baac, H. W.; Lee, J. H.; Seo, J. M.; Park, T. H.; Chung, H.; Lee, S. D.; Kim, S. J. *Materials Science and Engineering C-Biomimetic and Supramolecular Systems* **2004**, *24*, 209-212.
[58] Zhu, B. S.; Lu, Q. H.; Yin, J.; Hu, J.; Wang, Z. G. *Journal of Biomedical Materials Research Part B-Applied Biomaterials* **2004**, *70B*, 43-48.
[59] Recknor, J. B.; Recknor, J. C.; Sakaguchi, D. S.; Mallapragadaa, S. K. *Biomaterials* **2004**, *25*, 2753-2767.
[60] Berry, C. C.; Campbell, G.; Spadiccino, A.; Robertson, M.; Curtis, A. S. G. *Biomaterials* **2004**, *25*, 5781-5788.
[61] Anselme, K.; Bigerelle, M.; Noel, B.; Iost, A.; Hardouin, P. *Journal of Biomedical Materials Research* **2002**, *60*, 529-540.
[62] Walboomers, X. F.; Croes, H. J. E.; Ginsel, L. A.; Jansen, J. A. *Biomaterials* **1997**, *19*, 1861-1868.
[63] Wan, Y. Q.; Wang, Y.; Liu, Z. M.; Qu, X.; Han, B. X.; Bei, J. Z.; Wang, S. G. *Biomaterials* **2005**, *26*, 4453-4459.
[64] Yamato, M.; Konno, C.; Utsumi, M.; Kikuchi, A.; Okano, T. *Biomaterials* **2002**, *23*, 561-567.
[65] Zdyrko, B.; Klep, V.; Luzinov, I. *Langmuir* **2003**, *19*, 10179-10187.
[66] Falconnet, D.; Csucs, G.; Grandin, H. M.; Textor, M. *Biomaterials* **2006**, *27*, 3044-3063.
[67] Kingshott, P.; Thissen, H.; Griesser, H. J. *Biomaterials* **2002**, *23*, 2043-2056.
[68] Kleinfeld, D.; Kahler, K. H.; Hockberger, P. E. *Journal of Neuroscience* **1988**, *8*, 4098-4120.
[69] Vogt, R. F.; Phillips, D. L.; Henderson, L. O.; Whitfield, W.; Spierto, F. W. *Journal of Immunological Methods* **1987**, *101*, 43-50.
[70] Miyata, T.; Jikihara, A.; Nakamae, K.; Hoffman, A. S. *Advanced Drug Delivery Reviews* **2002**, *54*, 79-98.
[71] Dikovsky, D.; Bianco-Peled, H.; Seliktar, D. *Biomaterials* **2006**, *27*, 1496-1506.
[72] Chen, C. S.; Mrksich, M.; Huang, S.; Whitesides, G. M.; Ingber, D. E. *Biotechnology Progress* **1998**, *14*, 356-363.
[73] Yamato, M.; Kwon, O. H.; Hirose, M.; Kikuchi, A.; Okano, T. *Journal of Biomedical Materials Research* **2001**, *55*, 137-140.
[74] Patel, N.; Padera, R.; Sanders, G. H. W.; Cannizzaro, S. M.; Davies, M. C.; Langer, R.; Roberts, C. J.; Tendler, S. J. B.; Williams, P. M.; Shakesheff, K. M. *FASEB Journal* **1998**, *12*, 1447-1454.

[75] Takayama, S.; McDonald, J. C.; Ostuni, E.; Liang, M. N.; Kenis, P. J. A.; Ismagilov, R. F.; Whitesides, G. M. *Proceedings of the National Academy of Sciences of the United States of America* **1999**, *96*, 5545-5548.
[76] Zhang, S. G.; Yan, L.; Altman, M.; Lassle, M.; Nugent, H.; Frankel, F.; Lauffenburger, D. A.; Whitesides, G. M.; Rich, A. *Biomaterials* **1999**, *20*, 1213-1220.
[77] Huang, Y.; Joo, S.; Duhon, M.; Heller, M.; Wallace, B.; X., X. *Analytical Chemistry* **2002**, *74*, 3362-3371.
[78] Falconnet, D.; Koenig, A.; Assi, T.; Textor, M. *Advanced Functional Materials* **2004**, *14*, 749-756.
[79] MacBeath, G.; Schreiber, S. L. *Science* **2000**, *289*, 1760-1763.
[80] Otsuka, H.; Hirano, A.; Nagasaki, Y.; Okano, T.; Horiike, Y.; Kataoka, K. *ChemBioChem* **2004**, *5*, 850-855.
[81] Blawas, A. S.; Reichert, W. M. *Biomaterials* **1998**, *19*, 595-609.
[82] Dufva, M. *Biomolecular Engineering* **2005**, *22*, 173-184.
[83] Lausted, C.; Dahl, T.; Warren, C.; King, K.; Smith, K.; Johnson, M.; Saleem, R.; Aitchison, J.; Hood, L.; Lasky, S. R. *Genome Biology* **2004**, *5*, R58.
[84] Cole, M. A.; Voelcker, N. H.; Thissen, H. *Smart Materials and Structures* **2007**, *16*, 2222-2228.
[85] Kane, R. S.; Takayama, S.; Ostuni, E.; Ingber, D. E.; Whitesides, G. M. *Biomaterials* **1999**, *20*, 2363-2376.
[86] Hyun, J.; Zhu, Y. J.; Liebmann-Vinson, A.; Beebe, T. P.; Chilkoti, A. *Langmuir* **2001**, *17*, 6358-6367.
[87] Hyun, J.; Chilkoti, A. *Macromolecules* **2001**, *34*, 5644-5652.
[88] Kumar, G.; Wang, Y. C.; Co, C.; Ho, C. C. *Langmuir* **2003**, *19*, 10550-10556.
[89] Alarcon, C. D. H.; Pennadam, S.; Alexander, C. *Chemical Society Reviews* **2005**, *34*, 276-285.
[90] Dillow, A. K.; Tirrell, M. *Current Opinion in Solid State and Materials Science* **1998**, *3*, 252-259.
[91] Sia, S. K.; Whitesides, G. M. *Electrophoresis* **2003**, *24*, 3563-3576.
[92] Heller, M. J.; Forster, A. H.; Tu, E. *Electrophoresis* **2000**, *21*, 157-164.
[93] Gilles, P. N.; Wu, D. J.; Foster, C. B.; Dillon, P. J.; Chanock, S. J. *Nature Biotechnology* **1999**, *17*, 365-370.
[94] Gutmann, O.; Kuehlewein, R.; Reinbold, S.; Niekrawietz, R.; Steinert Chris, P.; de Heij, B.; Zengerle, R.; Daub, M. *Biomedical Microdevices* **2004**, *6*, 131-7.
[95] Xu, C. W. *Genome Research* **2002**, *12*, 482-486.
[96] Forster, T.; Roy, D.; Ghazal, P. *Journal of Endocrinology* **2003**, *178*, 195-204.
[97] Lee, B. H.; Nagamune, T. *Biotechnology and Bioprocess Engineering* **2004**, *9*, 69-75.
[98] Stoll, D.; Templin, M. F.; Bachmann, J.; Joos, T. O. *Current Opinion in Drug Discovery and Development* **2005**, *8*, 239-252.
[99] Templin, M. F.; Stoll, D.; Schrenk, M.; Traub, P. C.; Vohringer, C. F.; Joos, T. O. *Trends in Biotechnology* **2002**, *20*, 160-166.
[100] Yamauchi, F.; Kato, K.; Iwata, H. *Biochimica et Biophysica Acta - General Subjects* **2004**, *1672*, 138-147.
[101] Baghdoyan, S.; Roupioz, Y.; Pitaval, A.; Castel, D.; Khomyakova , E.; Papine, A.; Soussaline, F.; Gidrol, X. *Nucleic Acids Research* **2004**, *32*, e77.
[102] Nakayama, D.; Takeoka, Y.; Watanabe, M.; Kataoka, K. *Angewandte Chemie - International Edition* **2003**, *42*, 4197-4200.
[103] Miyata, T.; Asami, N.; Uragami, T. *Nature* **1999**, *399*, 766-769.
[104] Edahiro, J.; Sumaru, K.; Tada, Y.; Ohi, K.; Takagi, T.; Kameda, M.; Shinbo, T.; Kanamori, T.; Yoshimi, Y. *Biomacromolecules* **2005**, *6*, 970-974.
[105] Wang, J.; Rivas, G.; Jiang, M.; Zhang, X. *Langmuir* **1999**, *15*, 6541-6545.
[106] Wang, J. *Electroanalysis* **2000**, *13*, 635-638.
[107] Wang, J.; Jiang, M. *Langmuir* **2000**, *16*, 2269-2274.
[108] Wang, J.; Zhang, X. J.; Parrado, C.; Rivas, G. *Electrochemistry Communications* **1999**, *1*, 197-202.
[109] Jiang, X. H.; Lin, X. Q. *Electrochemistry Communications* **2004**, *6*, 873-879.
[110] Okano, T.; Yamada, N.; Sakai, H.; Sakurai, Y. *Journal of Biomedical Materials Research* **1993**, *27*, 1243-1251.
[111] Hyun, J.; Lee, W. K.; Nath, N.; Chilkoti, A.; Zauscher, S. *Journal of the American Chemical Society* **2004**, *126*, 7330-7335.

[112] Lahann, J.; Mitragotri, S.; Tran, T. N.; Kaido, H.; Sundaram, J.; Choi, I. S.; Hoffer, S.; Somorjai, G. A.; Langer, R. *Science* **2003**, *299*, 371-374.
[113] Gillies, E. R.; Jonsson, T. B.; Frechet, J. M. J. *Journal of the American Chemical Society* **2004**, *126*, 11936-11943.
[114] Ionov, L.; Houbenov, N.; Sidorenko, A.; Stamm, M.; Luzinov, I.; Minko, S. *Langmuir* **2004**, *20*, 9916-9919.
[115] Winkelmann, M.; Gold, J.; Hauert, R.; Kasemo, B.; Spencer, N. D.; Brunette, D. M.; Textor, M. *Biomaterials* **2003**, *24*, 1133-1145.
[116] Scotchford, C. A.; Ball, M.; Winkelmann, M.; Voros, J.; Csucs, C.; Brunette, D. M.; Danuser, G.; Textor, M. *Biomaterials* **2003**, *24*, 1147-1158.
[117] Tang, C. S.; Schmutz, P.; Petronis, S.; Textor, M.; Keller, B.; Voeroes, J. *Biotechnology and Bioengineering* **2005**, *31*, 285-295.
[118] Seidel, M.; Niessner, R. *Analytical and Bioanalytical Chemistry* **2008**, *391*, 1521-1544.
[119] Mousses, S.; Kallioniemi, A.; Kauraniemi, P.; Elkahloun, A.; Kallioniemi, O. P. *Current Opinion in Chemical Biology* **2002**, *6*, 97-101.
[120] Herne, T. M.; Tarlov, M. J. *Journal of the American Chemical Society* **1997**, *119*, 8916-8920.
[121] Aqua, T.; Naaman, R.; Daube, S. S. *Langmuir* **2003**, *19*, 10573-10580.
[122] Hong, B. J.; Sunkara, V.; Park, J. W. *Nucleic Acids Research* **2005**, *33*, e106.
[123] Datwani, S. S.; Vijayendran, R. A.; Johnson, E.; Biondi, S. A. *Langmuir* **2004**, *20*, 4970-4976.
[124] Losic, D.; Gooding, J. J.; Shapter, J. G.; Hibbert, D. B.; Short, K. *Electroanalysis* **2001**, *13*, 1385-1393.
[125] Venkatasubbarao, S. *Trends in Biotechnology* **2004**, *22*, 630-637.
[126] Kumar, A.; Goel, G.; Fehrenbach, E.; Puniya, A. K.; Singh, K. *Engineering in Life Sciences* **2005**, *5*, 215-222.
[127] Choudhuri, S. *Journal of Biochemical and Molecular Toxicology* **2004**, *18*, 171-179.
[128] Leung, Y. F.; Cavalieri, D. *Trends in Genetics* **2003**, *19*, 649-659.
[129] Schulze, A.; Downward, J. *Nature Cell Biology* **2001**, *3*, E190-E195.
[130] Bowtell, D. D. L. *Nature Genetics* **1999**, *21*, 25-32.
[131] Lueking, A.; Horn, M.; Eickhoff, H.; Bussow, K.; Lehrach, H.; Walter, G. *Analytical Biochemistry* **1999**, *270*, 103-111.
[132] Zhu, H.; Bilgin, M.; Bangham, R.; Hall, D.; Casamayor, A.; Bertone, P.; Lan, N.; Jansen, R.; Bidlingmaier, S.; Houfek, T.; Mitchell, T.; Miller, P.; Dean, R. A.; Gerstein, M.; Snyder, M. *Science* **2001**, *293*, 2101-2105.
[133] Patel, N.; Bhandari, R.; Shakesheff, K. M.; Cannizzaro, S. M.; Davies, M. C.; Langer, R.; Roberts, C. J.; Tendler, S. J. B.; Williams, P. M. *Journal of Biomaterials Science-Polymer Edition* **2000**, *11*, 319-331.
[134] Ramachandran, N.; Hainsworth, E.; Bhullar, B.; Eisenstein, S.; Rosen, B.; Lau, A. Y.; Walter, J. C.; LaBaer, J. *Science* **2004**, *305*, 86-90.
[135] LaBaer, J.; Ramachandran, N. *Current Opinion in Chemical Biology* **2005**, *9*, 14-19.
[136] Dufva, M.; Christensen, C. B. V. *Expert Review of Proteomics* **2005**, *2*, 41-48.
[137] Espina, V.; Mehta, A. I.; Winters, M. E.; Calvert, V.; Wulfkuhle, J.; Petricoin, E. F.; Liotta, L. A. *Proteomics* **2003**, *3*, 2091-2100.
[138] Espina, V.; Woodhouse, E. C.; Wulfkuhle, J.; Asmussen, H. D.; Petricoin, E. F.; Liotta, L. A. *Journal of Immunological Methods* **2004**, *290*, 121-133.
[139] Korf, U.; Wiemann, S. *Expert Review of Proteomics* **2005**, *2*, 13-26.
[140] Lee, S. Y.; Lee, S. J.; Jung, H. T. *Journal of Industrial and Engineering Chemistry* **2003**, *9*, 9-15.
[141] Wilson, D. S.; Nock, S. *Angewandte Chemie-International Edition* **2003**, *42*, 494-500.
[142] Zhu, H.; Bilgin, M.; Snyder, M. *Annual Review of Biochemistry* **2003**, *72*, 783-812.
[143] Tourniaire, G.; Collins, J.; Campbell, S.; Mizomoto, H.; Ogawa, S.; Thaburet, J. F.; Bradley, M. *Chemical Communications* **2006**, 2118-2120.
[144] Mant, A.; Tourniaire, G.; Diaz-Mochon, J. J.; Elliott, T. J.; Williams, A. P.; Bradley, M. *Biomaterials* **2006**, *27*, 5299-5306.
[145] Anderson, D. G.; Levenberg, S.; Langer, R. *Nature Biotechnology* **2004**, *22*, 863-866.
[146] Urquhart, A. J.; Anderson, D. G.; Taylor, M.; Alexander, M. R.; Langer, R.; Davies, M. C. *Advanced Materials* **2007**, *19*, 2486-2491.
[147] Conrad, C.; Erfle, H.; Warnat, P.; Daigle, N.; Lorch, T.; Ellenberg, J.; Pepperkok, R.; Eils, R. *Genome Research* **2004**, *14*, 1130-1136.

[148] Mishina, Y. M.; Wilson, C. J.; Bruett, L.; Smith, J. J.; Stoop-Myer, C.; Jong, S.; Amaral, L. P.; Pedersen, R.; Lyman, S. K.; Myer, V. E.; Kreider, B. L.; Thompson, C. M. *Journal of Biomolecular Screening* **2004**, *9*, 196-207.
[149] Erfle, H.; Neumann, B.; Liebel, U.; Rogers, P.; Held, M.; Walter, T.; Ellenberg, J.; Pepperkok, R. *Nature Protocols* **2007**, *2*, 392-399.
[150] Erfle, H.; Simpson, J. C.; Bastiaens, P. I. H.; Pepperkok, R. *Biotechniques* **2004**, *37*, 454-+.
[151] Kumar, R.; Conklin, D. S.; Mittal, V. *Genome Research* **2003**, *13*, 2333-2340.
[152] Silva, J. M.; Mizuno, H.; Brady, A.; Lucito, R.; Hannon, G. J. *Proceedings of the National Academy of Sciences of the United States of America* **2004**, *101*, 6548-6552.
[153] Wheeler, D. B.; Bailey, S. N.; Guertin, D. A.; Carpenter, A. E.; Higgins, C. O.; Sabatini, D. M. *Nature Methods* **2004**, *1*, 127-132.
[154] Vanhecke, D.; Janitz, M. *Oncogene* **2004**, *23*, 8353-8358.
[155] Redmond, T. M.; Ren, X. M.; Kubish, G.; Atkins, S.; Low, S.; Uhler, M. D. *Molecular and Cellular Proteomics* **2004**, *3*, 770-779.
[156] Webb, B. L.; Diaz, B.; Martin, G. S.; Lai, F. *Journal of Biomolecular Screening* **2003**, *8*, 620-623.
[157] Hu, Y. H.; Vanhecke, D.; Lehrach, H.; Janitz, M. *Biochemical Society Transactions* **2005**, *33*, 1407-1408.
[158] Mousses, S.; Caplen, N. J.; Cornelison, R.; Weaver, D.; Basik, M.; Hautaniemi, S.; Elkahloun, A. G.; Lotufo, R. A.; Choudary, A.; Dougherty, E. R.; Suh, E.; Kallioniemi, O. *Genome Research* **2003**, *13*, 2341-2347.
[159] Delehanty, J. B.; Shaffer, K. M.; Lin, B. C. *Analytical Chemistry* **2004**, *76*, 7323-7328.
[160] Wheeler, D. B.; Carpenter, A. E.; Sabatini, D. M. *Nature Genetics* **2005**, *37*, S25-S30.
[161] Bailey, S. N.; Wu, R. Z.; Sabatini, D. M. *Drug Delivery Today* **2002**, *7*, s113-s118.
[162] Fujita, M.; Mizutani, W.; Gad, M.; Shigekawa, H.; Tokumoto, H. *Ultramicroscopy* **2002**, *91*, 281-285.
[163] Segura, T.; Shea, L. D. *Bioconjugate Chemistry* **2002**, *13*, 621-629.
[164] Kato, K.; Umezawa, K.; Miyake, M.; Miyake, J.; Nagamune, T. *Biotechniques* **2004**, *37*, 444-452.
[165] Thorsen, T.; Maerkl, S. J.; Quake, S. R. *Science* **2002**, *298*, 580-584.
[166] Yamamura, S.; Kishi, H.; Tokimitsu, Y.; Kondo, S.; Honda, R.; Rao, S. R.; Omori, M.; Tamiya, E.; Muraguchi, A. *Analytical Chemistry* **2005**, *77*, 8050-8056.
[167] Chang, F. H.; Lee, C. H.; Chen, M. T.; Kuo, C. C.; Chiang, Y. L.; Hang, C. Y.; Roffler, S. *Nucleic Acids Research* **2004**, *32*.
[168] Bailey, S. N.; Ali, S. M.; Carpenter, A. E.; Higgins, C. O.; Sabatini, D. M. *Nature Methods* **2006**, *3*, 117-122.
[169] Pirone, D. M.; Qi, L. X.; Colecraft, H.; Chen, C. S. *Biomedical Microdevices* **2008**, *10*, 561-566.
[170] Yamauchi, F.; Kato, K.; Iwata, H. *Nucleic Acid Research* **2004**, *32*, e187.
[171] Kopatz, I., Remy, J. S., Behr, J. P., . *Journal of Gene Medicine* **2004**, *6*, 769-776.
[172] Uchimura, E.; Yamada, S.; Uebersax, L.; Yoshikawa, T.; Matsumoto, K.; Kishi, M.; Funeriu, D. P.; Miyake, M.; Miyake, J. *Neuroscience Letters* **2005**, *378*, 40-43.
[173] Yoshikawa, T.; Uchimura, E.; Kishi, M.; Funeriu, D. P.; Miyake, M.; Miyake, J. *Journal of Controlled Release* **2004**, *96*, 227-232.
[174] Hook, A. L.; Thissen, H.; Hayes, J. P.; Voelcker, N. *Proceedings of SPIE* **2006**, *6413*, 1-11.
[175] Hook, A. L.; Thissen, H.; Hayes, J. P.; Voelcker, N. *Bio-medical materials and engineering* **2008**, *In press*.
[176] Pompeia, C.; Hodge, D. R.; Plass, C.; Wu, Y. Z.; Marquez, V. E.; Kelley, J. A.; Farrar, W. L. *Cancer Research* **2004**, *64*, 3465-3473.
[177] Meichsner, J.; Nitschke, R.; Rochotzki, R.; Zeuner, M. *Surface and Coatings Technology* **1995**, *74-75*, 227-231.
[178] Nihlstrand, A.; Hjertberg, T.; Johansson, K. *Journal of Adhesion Science and Technology* **1996**, *10*, 123-150.
[179] Shard, A. G.; Whittle, J. D.; Beck, A. J.; Brookes, P. N.; Bullett, N. A.; Talib, R. A.; Mistry, A.; Barton, D.; McArthur, S. L. *Journal of Physical Chemistry B* **2004**, *108*, 12472-12480.
[180] Chen, Q.; Forch, R.; Knoll, W. *Chemical Materials* **2004**, *16*, 614-620.
[181] Abdel-Magid, A. F.; Carson, K. G.; Harris, B. D.; Maryanoff, C. A.; Shah, R. D. *Journal of Organic Chemistry* **1996**, *61*, 3849-3862.
[182] Griesser, H. J. *Vacuum* **1989**, *39*, 485-488.

[183] Gengenbach, T. R.; Griesser, H. J. *Journal of Polymer Science Part A-Polymer Chemistry* **1999**, *37*, 2191-2206.
[184] Whittle, J. D.; Short, R. D.; Douglas, C. W. I.; Davies, J. *Chemical Materials* **2000**, *12*, 2664-2671.
[185] Li, M. L.; Timmons, R. B.; Kinsel, G. R. *Analytical Chemistry* **2005**, *77*, 350-353.
[186] van Os, M. T.; Menges, B.; Foerch, R.; Vancso, G. J.; Knoll, W. *Chemistry of Materials* **1999**, *11*, 3252-3257.
[187] Hook, A. L.; Thissen, H.; Hayes, J. P.; Voelcker, N. H. *Proceedings of SPIE* **2005**, *5651*, 418-426.
[188] Hook, A. L.; Thissen, H.; Quinton, J.; Voelcker, N. H. *Surface Science* **2008**, *602*, 1883-1891.
[189] Gengenbach, T. R.; Chatelier, R. C.; Griesser, H. J. *Surface and Interface Analysis* **1996**, *24*, 271-281.
[190] Beck, A. J.; Candan, S.; Short, R. D.; Goodyear, A.; Braithwaite, N. S. J. *Journal of Physical Chemistry B* **2001**, *105*, 5730-5736.
[191] Gancarz, I.; Pozniak, G.; Bryjak, M.; Tylus, W. *European Polymer Journal* **2002**, *38*, 1937-1946.
[192] Harsch, A.; Calderon, J.; Timmons, R. B.; Gross, G. W. *Journal of Neuroscience Methods* **2000**, *98*, 135-144.
[193] Muir, B. W.; Nelson, A.; Fairbrother, A.; Fong, C.; Hartley, P. G.; James, M.; McLean, K. M. *Plasma Processes and Polymers* **2007**, *4*, 433-444.
[194] Griesser, H. J.; Chatelier, R. C.; Gengenbach, T. R.; Johnson, G.; Steele, J. G. *Journal of Biomaterials Science-Polymer Edition* **1994**, *5*, 531-554.
[195] Griesser, H. J.; Johnson, G.; Steele, J. G. *Abstract of Papers of the American Chemical Society* **1990**, *199*, 828-832.
[196] Hamerli, P.; Weigel, T.; Groth, T.; Paul, D. *Biomaterials* **2003**, *24*, 3989-3999.
[197] Thissen, H.; Johnson, G.; Hartley, P. G.; Kingshott, P.; Griesser, H. J. *Biomaterials* **2006**, *27*, 35-43.
[198] Boom, R.; Sol, C. J. A.; Salimans, M. M. M.; Jansen, C. L.; Wertheim-van Dillen, P. M. E.; Van der Noordaa, J. *Journal of Clinical Microbiology* **1990**, *28*, 495-503.
[199] Poly, F.; Chenu, C.; Simonet, P.; Rouiller, J.; Monrozier, L. J. *Langmuir* **2000**, *16*, 1233-1238.
[200] Ganachaud, F.; Elaissari, A.; Pichot, C.; Laayoun, A.; Cros, P. *Langmuir* **1997**, *13*, 701-707.
[201] Kang, S. H.; Shortreed, M. R.; Yeung, E. S. *Analytical Chemistry* **2001**, *73*, 1091-1099.
[202] Saoudi, B.; Jammul, N.; Chehimi, M. M.; Jaubert, A. S.; Arkam, C.; Delamar, M. *Spectroscopy-an International Journal* **2004**, *18*, 519-535.
[203] Zhu, X. Y.; Jun, Y.; Staarup, D. R.; Major, R. C.; Danielson, S.; Boiadjiev, V.; Gladfelter, W. L.; Bunker, B. C.; Guo, A. *Langmuir* **2001**, *17*, 7798-7803.
[204] Ma, H. W.; Hyun, J. H.; Stiller, P.; Chilkoti, A. *Advanced Materials* **2004**, *16*, 338-341.
[205] Vacheethasanee, K.; Wang, S. W.; Qiu, Y. X.; Marchant, R. E. *Journal of Biomaterials Science-Polymer Edition* **2004**, *15*, 95-110.
[206] Kato, K.; Uchida, E.; Kang, E. T.; Uyama, Y.; Ikada, Y. *Progress in Polymer Science* **2003**, *28*, 209-259.
[207] Schlapak, R.; Armitage, D.; Saucedo-Zeni, N.; Hohage, M.; Howorka, S. *Langmuir* **2007**, *23*, 10244-10253.
[208] Schlapak, R.; Pammer, P.; Armitage, D.; Zhu, R.; Hinterdorfer, P.; Vaupel, M.; Fruhwirth, T.; Howorka, S. *Langmuir* **2006**, *22*, 277-285.
[209] Zahr, A. S.; Davis, C. A.; Pishko, M. V. *Langmuir* **2006**, *22*, 8178-8185.
[210] Emoto, K.; Nagasaki, Y.; Iijima, M.; Kato, M.; Kataoka, K. *Colloids and Surfaces B-Biointerfaces* **2000**, *18*, 337-346.
[211] Sanderson, L. A. W.; Emoto, K.; Van Alstine, J. M.; Weimer, J. J. *Journal of Colloid and Interface Science* **1998**, *207*, 180-183.
[212] Uchida, E.; Uyama, Y.; Ikada, Y. *Langmuir* **1994**, *10*, 481-485.
[213] Burghardt, T. P.; Axelrod, D. *Biophysical Journal* **1981**, *33*, 455-467.
[214] Hook, A. L.; Thissen, H.; Voelcker, N. H. *BioRAD Technote* **2007**, *Bulletin 5577*.
[215] Hook, A. L.; Thissen, H.; Voelcker, N. H. *Biomacromolecules* **2008**, *In press*.
[216] Onuki-Nagasaki, R.; Nagasaki, A.; Hakamada, K.; Uyeda, T. Q. P.; Fujita, S.; Miyake, M.; Miyake, J. *Lab on a Chip* **2008**, *8*, 1502–1506.
[217] Saunders, R. E.; Gough, J. E.; Derby, B. *Biomaterials* **2008**, *29*, 193-203.

[218] Anderson, D. G.; Putnam, D.; Lavik, E. B.; Mahmood, T. A.; Langer, R. *Biomaterials* **2005**, *26*, 4892-4897.
[219] Unciti-Broceta, A.; Diaz-Mochon, J. J.; Mizomoto, H.; Bradley, M. *Journal of Combinatorial Chemistry* **2008**, *10*, 179-184.
[220] Ito, Y. *Biotechnology Progress* **2006**, *22*, 924-932.
[221] Liu, L.; Yan, M. D. *Angewandte Chemie-International Edition* **2006**, *45*, 6207-6210.
[222] Sugawara, T.; Matsuda, T. *Journal of Biomedical Materials Research* **1995**, *29*, 1047-1052.
[223] Sugawara, T.; Matsuda, T. *Macromolecules* **1994**, *27*, 7809-7814.
[224] Pourcelle, V.; Devouge, S.; Garinot, M.; Preat, V.; Marchand-Brynaert, J. *Biomacromolecules* **2007**, *8*, 3977-3983.
[225] Deegan, R. D.; Bakajin, O.; Dupont, T. F.; Huber, G.; Nagel, S. R.; Witten, T. A. *Nature* **1997**, *389*, 827-829.
[226] Dankbar, D. M.; Gauglitz, G. *Analytical and Bioanalytical Chemistry* **2006**, *386*, 1967-1974.
[227] Shadpour, H.; Musyimi, H.; Chen, J.; Soper, S. A. *Journal of Chromatography A* **2006**, *1111*, 238-251.
[228] Khung, Y. L.; Barritt, G.; Voelcker, N. H. *Experimental Cell Research* **2008**, *314*, 789-800.
[229] Sartori, S.; Rechichi, A.; Vozzi, G.; D'Acunto, M.; Heine, E.; Giusti, P.; Ciardelli, G. *Reactive and Functional Polymers* **2008**, *68*, 809-821.
[230] Pernagallo, S.; Unciti-Broceta, A.; Diaz-Mochon, J. J.; Bradley, M. *Biomedical Materials* **2008**, *3*.
[231] Limer, A.; Haddleton, D. M. *Progress in Reaction Kinetics and Mechanism* **2004**, *29*, 187-241.
[232] McLeary, J. B.; Klumperman, B. *Soft Matter* **2006**, *2*, 45-53.
[233] Urquhart, A. J.; Taylor, M.; Anderson, D. G.; Langer, R.; Davies, M. C.; Alexander, M. R. *Analytical Chemistry* **2008**, *80*, 135-142.
[234] Zelzer, M.; Majani, R.; Bradley, J. W.; Rose, F.; Davies, M. C.; Alexander, M. R. *Biomaterials* **2008**, *29*, 172-184.
[235] Li, P. Y.; Bo, L.; Gerstenmaier, J.; Cunningham, B. T. *Sensors and Actuators B-Chemical* **2004**, *99*, 6-13.
[236] Taylor, M.; Urquhart, A. J.; Anderson, D. G.; Williams, P. M.; Langer, R.; Alexander, M. R.; Davies, M. C. *Macromolecular Rapid Communications* **2008**, *29*, 1298-1302.
[237] Wegner, G. J.; Lee, H. J.; Corn, R. M. *Analytical Chemistry* **2002**, *74*, 5161-5168.
[238] Asinovski, L.; Beaglehole, D.; Clarkson, M. T. *Physica Status Solidi a-Applications and Materials Science* **2008**, *205*, 764-771.
[239] Chamritski, I.; Clarkson, M.; Franklin, J.; Li, S. W. *Australian Journal of Chemistry* **2007**, *60*, 667-671.
[240] Jin, G. *Physica Status Solidi a-Applications and Materials Science* **2008**, *205*, 810-816.
[241] Mannelli, I.; Courtois, V.; Lecaruyer, P.; Roger, G.; Millot, M. C.; Goossens, M.; Canva, M. *Sensors and Actuators B-Chemical* **2006**, *119*, 583-591.
[242] Steiner, G.; Sablinskas, V.; Hubner, A.; Kuhne, C.; Salzer, R. *Journal of Molecular Structure* **1999**, *509*, 265-273.
[243] Kanoh, N.; Kumashiro, S.; Simizu, S.; Kondoh, Y.; Hatakeyama, S.; Tashiro, H.; Osada, H. *Angewandte Chemie-International Edition* **2003**, *42*, 5584-5587.
[244] Smith, E. A.; Corn, R. M. *Applied Spectroscopy* **2003**, *57*, 320A-332A.
[245] Kanoh, N.; Kyo, M.; Inamori, K.; Ando, A.; Asami, A.; Nakao, A.; Osada, H. *Analytical Chemistry* **2006**, *78*, 2226-2230.
[246] Lecaruyer, P.; Mannelli, I.; Courtois, V.; Goossens, M.; Canva, M. *Analytica Chimica Acta* **2006**, *573*, 333-340.
[247] Green, R. J.; Frazier, R. A.; Shakesheff, K. M.; Davies, M. C.; Roberts, C. J.; Tendler, S. J. B. *Biomaterials* **2000**, *21*, 1823-1835.
[248] Brockman, J. M.; Nelson, B. P.; Corn, R. M. *Annual Review of Physical Chemistry* **2000**, *51*, 41-63.
[249] Steiner, G. *Analytical and Bioanalytical Chemistry* **2004**, *379*, 328-331.
[250] Homola, J.; Yee, S. S.; Gauglitz, G. *Sensors and Actuators B-Chemical* **1999**, *54*, 3-15.
[251] Kretschmann, E. *Zeitschrift für Physik A Hadrons and Nuclei* **1971**, *241*, 313-324.
[252] Yeatman, E.; Ash, E. A. *Electronics Letters* **1987**, *23*, 1091-1092.
[253] Rothenhausler, B.; Knoll, W. *Nature* **1988**, *332*, 615-617.
[254] Thiel, A. J.; Frutos, A. G.; Jordan, C. E.; Corn, R. M.; Smith, L. M. *Analytical Chemistry* **1997**, *69*, 4948-4956.

[255] Nelson, B. P.; Grimsrud, T. E.; Liles, M. R.; Goodman, R. M.; Corn, R. M. *Analytical Chemistry* **2001**, *73*, 1-7.
[256] Bassil, N.; Maillart, E.; Canva, M.; Levy, Y.; Millot, M. C.; Pissard, S.; Narwa, W.; Goossens, M. *Sensors and Actuators B-Chemical* **2003**, *94*, 313-323.
[257] Jordan, C. E.; Corn, R. M. *Analytical Chemistry* **1997**, *69*, 1449-1456.
[258] Brockman, J. M.; Frutos, A. G.; Corn, R. M. *Journal of the American Chemical Society* **1999**, *121*, 8044-8051.
[259] Jordan, C. E.; Frutos, A. G.; Thiel, A. J.; Corn, R. M. *Analytical Chemistry* **1997**, *69*, 4939-4947.
[260] Smith, E. A.; Thomas, W. D.; Kiessling, L. L.; Corn, R. M. *Journal of the American Chemical Society* **2003**, *125*, 6140-6148.
[261] Kanda, V.; Kariuki, J. K.; Harrison, D. J.; McDermott, M. T. *Analytical Chemistry* **2004**, *76*, 7257-7262.
[262] Kyo, M.; Usui-Aoki, K.; Koga, H. *Analytical Chemistry* **2005**, *77*, 7115-7121.
[263] Szunerits, S.; Knorr, N.; Calemczuk, R.; Livache, T. *Langmuir* **2004**, *20*, 9236-9241.
[264] Cole, M.; Voelcker, N.; Thissen, H. *Proceedings of SPIE* **2005**, *5651*, 19-27.
[265] Schulz, L. G. *Journal of the Optical Society of America* **1954**, *44*, 357-362.
[266] Schulz, L. G.; Tangherlini, F. R. *Journal of the Optical Society of America* **1954**, *44*, 362-368.
[267] Schiebener, P.; Straub, J.; Sengers, J.; Gallagher, J. S. *Journal of Physical and Chemical Reference Data* **1990**, *19*, 677-717.
[268] Fischer, H.; Polikarpov, I.; Craievich, A. F. *Protein Science* **2004**, *13*, 2825-2828.
[269] Fiche, J. B.; Buhot, A.; Calemczuk, R.; Livache, T. *Biophysical Journal* **2007**, *92*, 935-946.
[270] Gil, E. S.; Hudson, S. A. *Progress in Polymer Science* **2004**, *29*, 1173-1222.
[271] Hu, Z. B.; Chen, Y. Y.; Wang, C. J.; Zheng, Y. D.; Li, Y. *Nature* **1998**, *393*, 149-152.
[272] Shin, H. *Biomaterials* **2007**, *28*, 126-133.
[273] Zourob, M.; Gough, J. E.; Ulijn, R. V. *Advanced Materials* **2006**, *18*, 655-659.
[274] Fujishige, S.; Kubota, K.; Ando, I. *J. Phys. Chem.* **1989**, *93*, 3311-3313.
[275] Chung, J. E.; Yokoyama, M.; Aoyagi, T.; Sakurai, Y.; Okano, T. *Journal of Controlled Release* **1998**, *53*, 119-130.
[276] Balamurugan, S.; Mendez, S.; Balamurugan, S. S.; O'Brien, M. J.; Lopez, G. P. *Langmuir* **2003**, *19*, 2545-2549.
[277] Hirata, I.; Okazaki, M.; Iwata, H. *Polymer* **2004**, *45*, 5569-5578.
[278] Sorrell, C. D.; Lyon, L. A. *Journal of Physical Chemistry B* **2007**, *111*, 4060-4066.
[279] Hansen, W. N. *Journal of the Optical Society of America* **1968**, *58*, 380-390.
[280] Holmlin, R. E.; Chen, X. X.; Chapman, R. G.; Takayama, S.; Whitesides, G. M. *Langmuir* **2001**, *17*, 2841-2850.
[281] Silin, V.; Weetall, H.; Vanderah, D. J. *Journal of Colloid and Interface Science* **1997**, *185*, 94-103.
[282] Barbani, N.; Lazzeri, L.; Cristallini, C.; Cascone, M. G.; Polacco, G.; Pizzirani, G. *Journal of Applied Polymer Science* **1999**, *72*, 971-976.
[283] Nezu, T.; Winnik, F. M. *Biomaterials* **2000**, *21*, 415-419.
[284] Hulmes, D. J. S.; Miller, A.; Parry, D. A. D.; Piez, K. A.; Woodhead-Galloway, J. *Journal of Molecular Biology* **1973**, *79*, 137-148.
[285] Hadley, J. C.; Meek, K. M.; Malik, N. S. *Glycoconjugate Journal* **1998**, *15*, 835-840.
[286] Katsuura, H.; Kawamura, H.; Manabe, M.; Kawasaki, H.; Maeda, H. *Colloid and Polymer Science* **2002**, *280*, 30-37.
[287] De Cupere, V. M.; Van Wetter, J.; Rouxhet, P. G. *Langmuir* **2003**, *19*, 6957-6967.
[288] Tooney, N. M.; Mosesson, M. W.; Amrani, D. L.; Hainfeld, J. F.; Wall, J. S. *Journal of Cell Biology* **1983**, *97*, 1686-1692.
[289] Murthy, V. S.; Cha, J. N.; Stucky, G. D.; Wong, M. S. *Journal of the American Chemical Society* **2004**, *126*, 5292-5299.
[290] Neu, M.; Fischer, D.; Kissel, T. *Journal of Gene Medicine* **2005**, *7*, 992-1009.
[291] Hemmersam, A. G.; Rechendorff, K.; Foss, M.; Sutherland, D. S.; Besenbacher, F. *Journal of Colloid and Interface Science* **2008**, *320*, 110-116.
[292] Malmsten, M. *Journal of Colloid and Interface Science* **1995**, *172*, 106-115.
[293] Malmsten, M. *Colloids and Surfaces B: Biointerfaces* **1995**, *3*, 371-381.
[294] Ghiggeri, G. M.; Ginevri, F.; Candiano, G.; Oleggini, R.; Perfumo, F.; Queirolo, C.; Gusmano, R. *Kidney International* **1987**, *32*, 547-553.

[295] Laos, K.; Parker, R.; Moffat, J.; Wellner, N.; Ring, S. G. *Carbohydrate Polymers* **2006**, *65*, 235-242.
[296] Weber, K.; Osborn, M. *Journal of Biological Chemistry* **1969**, *244*, 4406-4412.
[297] Diez, J.; Panizo, A.; Gil, M. J.; Monreal, I.; Hernandez, M.; Mindan, J. P. *Circulation* **1996**, *93*, 1026-1032.
[298] Squire, P. G.; Moser, P.; O'Konski, C. T. *Biochemistry* **1968**, *7*, 4261-4272.
[299] Stenger, D. A.; Pike, C. J.; Hickman, J. J.; Cotman, C. W. *Brain Research* **1993**, *630*, 136-147.
[300] Li, B.; Ma, Y. X.; Wang, S.; Moran, P. M. *Biomaterials* **2005**, *26*, 4956-4963.
[301] Bet, M. R.; Goissis, G.; Vargas, S.; Seliste-de-Araujo, H. S. *Biomaterials* **2003**, *24*, 131-137.
[302] Lee, J. H.; Jung, H. W.; Kang, I. K.; Lee, H. B. *Biomaterials* **1994**, *15*, 705-711.
[303] Li, B.; Ma, Y. X.; Wang, S.; Moran, P. M. *Biomaterials* **2005**, *26*, 1487-1495.
[304] Jung, H.; Kwak, B.; Yang, H. S.; Tae, G.; Kim, J. S.; Shin, K. *Colloids and Surfaces a-Physicochemical and Engineering Aspects* **2008**, *313*, 562-566.
[305] Vankooten, T. G.; Schakenraad, J. M.; Vandermei, H. C.; Busscher, H. J. *Biomaterials* **1992**, *13*, 897-904.
[306] Liu, S.; Vareiro, M.; Fraser, S.; Jenkins, A. T. A. *Langmuir* **2005**, *21*, 8572-8575.
[307] Taborelli, M.; Eng, L.; Descouts, P.; Ranieri, J. P.; Bellamkonda, R.; Aebischer, P. *Journal of Biomedical Materials Research* **1995**, *29*, 707-714.
[308] Escriou, V.; Ciolina, C.; Helbling-Leclerc, A.; Wils, P.; Scherman, D. *Cell Biology and Toxicology* **1998**, *14*, 95-104.
[309] Meloni, R.; Khalfallah, O.; Biguet, N. F. *Pharmacological Research* **2004**, *49*, 303-308.
[310] Wang, X. P.; Shi, Q. W.; Hu, H. L.; Zhang, K. *European Polymer Journal* **2004**, *40*, 2179-2183.